MPR-SAT-WF-61-8
December 14, 1961

SATURN

CCN

GEORGE C. MARSHALL SPACE FLIGHT CENTER

HUNTSVILLE, ALABAMA

SATURN SA-1 FLIGHT EVALUATION

TO - Available to NASA Offices and NASA Centers Only.

NATIONAL AERONAUTICS AND SPACE ADMINISTRATION

SECURITY NOTE

This document contains information affecting the national defense of the United States within the meaning of the Espionage Law, Title 18, U.S.C., Sections 793 and 794 as amended. The revelation of its contents in any manner to an unauthorized person is prohibited by law.

GEORGE C. MARSHALL SPACE FLIGHT CENTER

MPR-SAT-WF-61-8

SATURN SA-1 FLIGHT EVALUATION

By Saturn Flight Evaluation Working Group

(U) ABSTRACT

This report presents the results of the Early Engineering Evaluation of the Saturn SA-1 test flight. The performance of each major vehicle system is discussed with special emphasis on malfunction and deviations.

The test flight of SA-1 was very successful and all planned test objectives were achieved. No major malfunctions or deviations which could be considered a serious system failure or design deficiency occurred.

[redacted]

GEORGE C. MARSHALL SPACE FLIGHT CENTER

MPR-SAT-WF-61-8

December 14, 1961

SATURN SA-1 FLIGHT EVALUATION (U)

SATURN FLIGHT EVALUATION
WORKING GROUP

[redacted]

[redacted]

(U) TABLE OF CONTENTS

(U) TABLE OF CONTENTS (cont')

(U) TABLE OF CONTENTS (cont')

(U) TABLE OF CONTENTS (cont')

(U) LIST OF TABLES

(U) LIST OF ILLUSTRATIONS

(U) LIST OF ILLUSTRATIONS (cont')

(U) LIST OF ILLUSTRATIONS (cont')

[redacted]

GEORGE C. MARSHALL SPACE FLIGHT CENTER

MPR-SAT-WF-61-8

SATURN SA-1 FLIGHT EVALUATION (U)

By Saturn Flight Evaluation Working Group

1.0 (C) FLIGHT TEST SUMMARY

1.1 FLIGHT TEST RESULTS

Saturn space vehicle SA-1 was launched at 1006 EST on October 27, 1961. The flight was a complete success. The flight test did not reveal any malfunctions or deviations which could be considered a serious system failure or design deficiency.

SA-1 was launched approximately 10 weeks after arrival of the S-I stage at Cape Canaveral. The scheduled ten hour countdown began at 2300 EST, October 26, 1961. No technical difficulties requiring holds were experienced during the countdown, but two holds were called because of low clouds over the launch area. Automatic fueling and sequencing processes were satisfactorily conducted. Compatibility of the ground support equipment and the flight vehicle was demonstrated. The general condition of the ground support equipment after launch was better than expected.

The actual flight path of SA-1 was very close to predicted during the period from liftoff to inboard engine cutoff; however, the actual trajectory was slightly higher than predicted due to higher accelerations. Trajectory parameters after inboard engine cutoff were proportionally lower than predicted because of a 1.61 sec early cutoff signal.

With the exception of disturbances in roll due to propellant sloshing, the operation of the control system from the design and hardware standpoint was entirely satisfactory. Indications are that the compliance and bending problems which appeared during static testing were adequately overcome or did not materialize.

One of the few problems encountered on the flight was an instability in sloshing, predominantly in the roll mode. However, even though there was more sloshing than desired, it did not approach the point of endangering the vehicle. Sloshing caused oscillations in all three flight planes during the last portion of powered flight. The maximum

amplitudes of oscillations in the engine deflections due to sloshing were ± 0.4 deg in pitch, ± 0.5 deg in yaw, and ± 0.2 deg in roll.

SA-1 was flown without active path guidance. However, passenger guidance hardware was on-board to establish the operational capabilities of the equipment in the Saturn flight environment. All telemetered information as well as a trajectory comparison indicate satisfactory performance of the equipment.

The over-all performance of the propulsion system was very satisfactory. The total cluster performance was within one percent of predicted. Individual engine performances were satisfactory with a maximum thrust deviation from predicted of about +3.9 percent. The propellant tank pressurization systems functioned properly. All hydraulic systems operated well within the expected limits throughout the powered flight phase.

Vibration instrumentation showed values comparable to or in some cases slightly lower than those expected for the SA-1 flight test. The vibration data was considered from a viewpoint of three main sources of excitation. These were: (1) mechanical source which began with engine ignition, (2) acoustical source which began with the sound field generated by the propulsion system, and (3) aerodynamic source which began as the vehicle approached Mach 1.

Instrumentation for detecting vehicle body bending consisted of 10 bending accelerometers at three stations along the vehicle. The observed bending oscillations cannot be positively identified; however, the oscillations do not meet the requirements for natural bending oscillations and are apparently the results of modified (or forced) structural bending.

The thermal environment of SA-1 was not detrimental to vehicle performance. Total heat flux to both the flame and heat shields was less than predicted; however, thermal radiation to the heat shield was close to that predicted. No fires or other abnormal heat sources occurred in the engine compartment.

Base pressure of the vehicle as telemetered from four measurements was as expected, showing close agreement with wind tunnel results.

A total of 505 inflight measurements were flown on SA-1. Of this total only 8 measurements failed and 11 measurements partially failed. Inflight calibrator on link 3 failed during flight. All other measuring systems performed as expected.

1.2 MISSIONS

The missions assigned to Saturn SA-1 were as follows:

1. Flight test of the 8 clustered 165,000 lb thrust H-1 engines-achieved.

2. Flight test of the S-I stage clustered propellant tanks structure-achieved.

3. Flight test of the S-I stage control system - achieved.

4. Flight test with 4 support arms and 4 holddown arms on launch pad - achieved.

5. System flight test
   a. Bending and flutter - achieved
   b. Sloshing - achieved
   c. Base heating - achieved
   d. Aerodynamic engine torques - achieved
   e. Airframe aerodynamic heating - achieved

1.3 TIMES OF FLIGHT EVENTS

Event	Actual Range Time (sec)	Predicted (sec)	Actual-Predicted (sec)
Ignition Command	-3.03	-2.88	-0.15
Thrust Commit	.23	.43	-0.20
Launch Commit	.59	.79	-0.20
First Motion	.75	--	--
Liftoff Signal (Start Program Device)	.89	.89	0
Begin Tilt	17.89	17.89	0
Mach One Reached	49.00	49.50	-0.50
Maximum Dynamic Pressure	61.00	61.89	-0.89
End Tilt	100.19	100.19	0
Inboard Engine Cutoff	110.10	111.71	-1.61
Outboard Engine Cutoff	116.08	117.71	-1.63
End of Second Thrust Decay	119.00	--	--
Apex	249.24	255.23	-5.99
Loss of Telemeter Signal	409.35	--	--

2.0 (U) INTRODUCTION

The Saturn space vehicle SA-1 was launched at 1006 EST on October 27, 1961, from Saturn Launch Complex 34, Atlantic Missile Range, Cape Canaveral, Florida. SA-1 was the first vehicle to be flight tested in the Saturn C-1 R&D program. The major objective of this test was to evaluate the designs of the propulsion system, control system, and structure of the 1.3 million pound thrust first stage.

This report presents the results from the Early Engineering Evaluation of the SA-1 test flight. The performance of each major vehicle system is discussed with special emphasis on malfunctions and deviations. The report is organized in ten major sections covering all vehicle systems and ground support equipment. Malfunctions and deviations are briefly summarized in the last section. Important supporting data such as mass characteristics are assembled in several appendices.

This report is published by the Saturn Flight Evaluation Working Group whose members are representatives from all Marshall Space Flight Center Divisions. Therefore the report represents the official MSFC position at this time. This report will not be followed by a similarly integrated report unless continued analysis and/or new evidence should prove the conclusions presented here partly or wholly wrong. Final evaluation reports will, however, be published by the MSFC Divisions covering the major systems and/or special subjects.

Special acknowledgement is made to the many individuals of the various MSFC Divisions who contributed to and helped establish this report.

3.0 (C) PRELAUNCH OPERATIONS

3.1 SUMMARY

Saturn vehicle SA-1 was launched approximately 10 weeks after arrival of the S-I stage at Cape Canaveral. The scheduled ten hour countdown began at 2300 EST, October 26, 1961. No technical difficulties requiring holds were experienced during the countdown, but two holds were called because of low clouds over the launch area. Automatic fueling and sequencing processes were satisfactorily conducted. Compatibility of the ground support equipment and the flight vehicle was demonstrated. The general condition of the ground support equipment after launch was better than expected.

3.2 PRELAUNCH EVENTS

3.2.1 PREPARATIONS

Emplacement, Assembly, and Checkout

SA-1 dummy third stage (S-V) arrived by the barge "Palaemon" at Cape Canaveral on May 1, 1961 and was transferred to Hangar D. SA-1 booster (S-I), dummy second stage (S-IV), and dummy payload body arrived by the barge "Compromise" on August 15, 1961. The S-I booster was transferred to Complex 34, and the second and third stages were transferred to the Hangar D checkout area the same day. On August 20, 1961, the booster was erected on the launch pedestal.

The following is a chronological account and description of major workloads accomplished and milestones passed during the vehicle checkout:

August 21, 1961 thru August 25, 1961 - Cables and cable masts installed. Measuring calibrations, continuity tests, umbilical connections and propulsion leakage tests underway. Retract arms positioned and vehicle power applied. Milestone - S-IV, S-V, and nose cone assembled to S-I stage.

August 26, 1961 thru August 30, 1961 - Network power, radio frequency, Azusa transponder, UDOP, and antenna checks underway. Accelerometers installed. Propulsion system and LOX simulation tests performed.

August 31, 1961 thru September 4, 1961 - Measuring calibrations, Ground Support Equipment tests, and engineering changes underway. LOX system and thrust chamber leak checks made.

September 5, 1961 thru September 10, 1961 - Heat exchanger and hydraulic actuator laboratory tests conducted. Hydraulic pressure switches installed and navigation checkout underway. Milestone - Full tank pressurization test completed.

September 11, 1961 thru September 15, 1961 - Canister 15 cable replaced and hydraulic package installed. C-Band radar and Azusa range check made. Engine curtain installation underway. Network sequence malfunction test conducted. ST-90 platform installed and tested. Facilities checkout underway. Canister cooling and RF Range checks completed. Gas generator installations underway. Milestone - Service structure removed for RF checks. While vehicle ties were disconnected, a squall subjected the vehicle to 28.3 m/s gusts with no adverse effects.

September 16, 1961 thru September 20, 1961 - RF Range checks, with service structure removed, performed. Service structure replaced around vehicle; ST-90 alignment checks performed, and navigation system tests underway. Umbilical and cable masts ejection tests performed. Installation of heat shields for engine compartment underway. Overall test Nr. 1 conducted.

September 21, 1961 thru September 25, 1961 - Overall test Nr. 2 conducted. Canister 16 cable replaced. Command receiver tests conducted. Flight control computer checkout underway.

September 26, 1961 thru September 30, 1961 - Bend and twist measurements underway. Heat exchanger and hula-hoop installation underway. Rate gyro aligned. Pressurization test and sphere recovery run conducted. Milestone - Fuel test conducted.

October 1, 1961 thru October 5, 1961 - S-IV and S-V dummy stages loaded with water. Patch panel realignment completed. Launch day set for October 18, 1961. LOX pressurization test and boattail conditioning test completed. Milestone - LOX loading test completed.

October 6, 1961 thru October 10, 1961 - Navigation and platform tests completed. Flight command receivers installed and checked. Telemeter commutation boards installed and checked. Decision made to replace LOX pump seal engine Nr. 2. This required rescheduling the launch for October 21, 1961. Milestone - Overall test Nr. 4 completed.

October 11, 1961 thru October 15, 1961 - Destruct circuitry modified as requested by Range. LOX pump seal engine Nr. 2

replaced. Plug drop test completed. Command receiver Nr. 1 exchanged. Primacord, destruct block, and turbine spinners fitted and checked. Marotta valves vibration tested. Retract arm valve reworked. Milestone - Engine swivel checks completed.

October 16, 1961 thru October 20, 1961 - Retract arm solenoid checks completed. Telemetry link Nr. 3 replaced. In compliance with MSFC directive, the vehicle launch was rescheduled for October 27, 1961. Milestone - Simulated Flight Test performed with the Range.

October 21, 1961 thru October 26, 1961 - Canister leak test completed. Primacord installation underway. GSE components tests completed. Fueling preparations begun. Milestone - Simulated Flight Test repeated. Prepared for LAUNCH.

October 27, 1961 - LAUNCH.

Propellant Loading

The Saturn propellant loading system is designed to tank propellants to a given total propellant weight at a ratio to give simultaneous depletion of propellants at cutoff. By design, it is easier to drain fuel and tank LOX for final adjustments just prior to launch; therefore the fuel is over filled (103% based on fuel density at tanking), and LOX is under filled. Just prior to launch a final fuel density check is made. Based on this density, fuel is drained and LOX tanked in the proportions necessary to give the designed total propellant load. This system is designed to load propellants to an accuracy of 0.25% total weight load.

Fuel

The RP-1 fuel was loaded on L-1 Day. To allow a leak check of the fuel system, the fuel was initially filled to a 10 percent full level in a manual, slow fill sequence at a rate of approximately 200 gallons per minute. The fuel mast vacuum breaker leaked during this check. Evidently the breaker did not reseat after a line drain sequence.

Upon completion of the leak check the fuel was loaded by the automatic fill sequence to 97%. At this point loading was continued by manually selecting a slow fill sequence. This procedure was used due to the uneven filling of the fuel tanks which causes cycling between fast and slow fill. A coarse adjust level drain was made by adding 1.0 percent to the fuel density digital readout and dialing into the computer a correction factor corresponding to that density. A small amount of fuel overflowed from the air removal valve in the fuel

replenish and drain line during the adjust level drain. The fuel level manometer transformer burned out, and the manometer was inoperative on launch day.

A final fuel level adjustment was made at T-90 minutes after the fuel density had stabilized.

LOX

The vehicle liquid oxygen tanks were initially filled to 10 percent full to check the vehicle and transfer systems for leaks. This was accomplished in the precool sequence by using pressure from the main storage tank. The level was maintained by the replenish system after the 75 percent and 98 percent signals were jumpered in, and the electrical connector was removed from the throttling valve. The replenish flow was controlled by manually opening and closing the replenish-by-pass-valve. The system was in this replenish condition for approximately four hours.

Prior to fast filling the vehicle to 100 percent, the 75 percent and 98 percent jumpers were removed and the throttling valve reconnected. The LOX loading was completed in the automatic sequence to 100 percent. After the fuel adjust level drain was made, a correction of +0.105 psi was dialed into the computer, and the replenish system topped the tank level to 100 percent. This level was maintained by periodical replenishing.

The following malfunctions were noted in the LOX propellant system.

1. The liquid oxygen vaporizer blower, for the main tank pressurizing system, cut off. This was apparently caused by overloading the circuit breakers due to icing of the heat exchanger. Since the main tank pressure exceeded the minimum tank pressure, the count was not delayed.

2. Shortly after the main tank blower cut off, the replenish vaporizer blower cut off for the same reason. The replenish tank was fully pressurized and the count was not delayed.

3. The main tank vaporizer heat exchanger developed three liquid oxygen leaks where the fin tubes are welded to the top header. This condition was discovered after the launch.

Density Sensing System

The flight test data indicate a deviation of approximately 0.4% in the fuel density sensing of the tanking system. This conclusion is drawn from the fact that blockhouse measurements of fuel temperature indicate 21.9°C while the density sensed by the propellant tanking system corresponds to a fuel temperature of 26.8°C (Fig. 3-1). This magnitude of deviation would cause 888 pounds of LOX to be overtanked and 913 pounds of fuel to be undertanked and would result in an early engine cutoff of 0.6 seconds in flight.

3.2.2 COUNTDOWN

Weather

General weather conditions at time of launch were considered good. There was no precipitation, and visibility was better than 16 km. Eight-tenths of the sky was obscured by cumulus clouds based 1200 m above the ground, and towering cumulus clouds could be seen in all quadrants. Surface winds at 13.4 m above the launch pad were 6.4 m/sec from 110 degrees just prior to launch. For detailed atmospheric data, refer to Appendix E.

Holds

The launch countdown began at T-600 minutes at 2300 EST on October 26, 1961.

The first hold was called at T-120 minutes (0700 EST) for 34 minutes to await more favorable cloud conditions necessary for photo coverage. Count was resumed at 0734 EST.

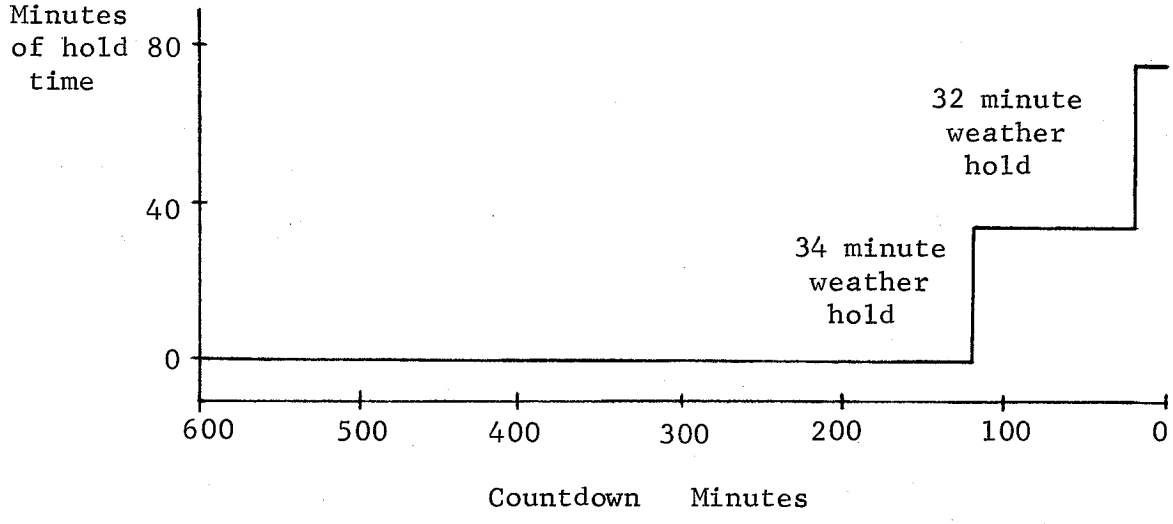

The second and final countdown hold was called at T-20 minutes (0914 EST), again to await improved weather conditions. The hold continued for 32 minutes; count was resumed at 0946 EST and continued to launch.

Automatic Countdown

It was determined during the LOX loading test that LOX pressurization took less time than anticipated; therefore, automatic countdown operation began at T-364 seconds prior to ignition command instead of T-374 seconds.

The automatic countdown operation was normal except for the loss of the following indications:

1. LOX relief Nr. 1 closed (pen 63) - switch failed.
2. LOX vent closed (pen 66) - switch failed.

Ground sequence events are listed in Appendix C.

3.2.3 HOLDDOWN

Vehicle

Engine start and transition were smooth with all engines receiving a positive ignition from a LOX lead in the gas generator ignition sequence. All critical blockhouse measurements were within the established redline values at ignition command. Maximum and minimum values observed during the countdown are shown in Appendix B.

The combustion stability monitor measurements (XE57-1 thru XE57-8) showed no rough combustion. Rough combustion is defined as unstable combustion within an engine combustion chamber resulting in a vibration level at the combustion chamber dome in excess of ± 100G. When the instantaneous acceleration on this measurement exceeds ± 100G for a cumulative total of 20 milliseconds, the engine would be cut off automatically. The highest instantaneous acceleration recorded at any time on these measurements was ± 70G. Close-up photographs of the launcher arms and vehicle revealed severe undulations of the outboard engine shroud during the holddown period and at liftoff; however, neither the vehicle nor the launcher arm performance was adversely affected. An attempt will be made to determine the amplitude of the undulations.

On three of the four hydraulic systems, cycling of the pressure "OK" switches was observed during engine transition and prior to thrust commit. These are the switches which were originally in the cutoff

circuit and would have been monitored at thrust commit to determine if the hydraulic system was satisfactory. However, several weeks prior to launch, this requirement of checking the hydraulic system was removed to improve the reliability of the system by simplifying the electrical circuitry. The cycling of the switch is normal and is caused by pump surges during build-up. (Switch response time is within 2 milliseconds.) Cycling of the switch did stop prior to thrust commit and would not have given a cutoff signal had the switches been in the cutoff circuit.

The flame shield, heat shield, and firewall appeared to provide adequate protection, since no fires were detected during ignition, holddown, and liftoff.

Ground Support Equipment

General condition of the ground support equipment is better than expected. Only the minor damage normally sustained for a flight of this nature was experienced.

The operation of the service structure during the countdown was satisfactory. During vehicle liftoff, the service structure sustained only superficial damage, mainly the pushing in and blowing out of several "blow out" panels in the service structure base buildings.

Short cable masts Nr. 2 and Nr. 4 and tail cable masts Nr. 2 and Nr. 4 performed satisfactorily. Short cable masts Nr. 2 and Nr. 4 disconnected cleanly at thrust commit plus 107 milliseconds. The tail cable masts separated satisfactorily with vehicle motion. These four items suffered approximately 10 percent damage with the exception of the electrical cables which are not reusable items.

The fuel and LOX filling mast assemblies suffered approximately 10 percent damage (see Fig. A-6).

The retractable supports performed satisfactorily as indicated by the available records. They operated the 3/4 inch switches at times varying from 330 milliseconds to 347 milliseconds after thrust commit. They are apparently reusable, but time has not permitted the evaluation necessary to determine the rework required.

The holddown arms performed satisfactorily as indicated by the available records. The damage sustained was apparently superficial.

The fire detection and water quench systems were not required, since no fires developed.

The general condition of the flame deflector is good. Only minor damage was found which consisted of a slight amount of metal flow and erosion, and some structural warping which appears to be of little consequence.

TABLE 3-I

PRE-LAUNCH MILESTONES

May 1, 1961	S-V Dummy Stage arrived by barge "Palaemon"
August 15, 1961	S-I Booster, SIV Dummy Stage, and Dummy Payload arrived by barge "Compromise"
August 20, 1961	S-I Booster erected on launch pedestal
August 23, 1961	SIVD, SVD & Dummy Payload assembled to S-I Booster
September 15, 1961	Service Structure removed for RF checks
September 27, 1961	Fuel test completed
October 4, 1961	LOX loading test completed
October 10, 1961	Overall test No. 4 completed
October 13, 1961	Engine swivel checks completed
October 16, 1961	Simulated Flight test performed
October 23, 1961	Simulated Flight test repeated
October 26, 1961	RP-1 fuel loaded
October 27, 1961	Launch

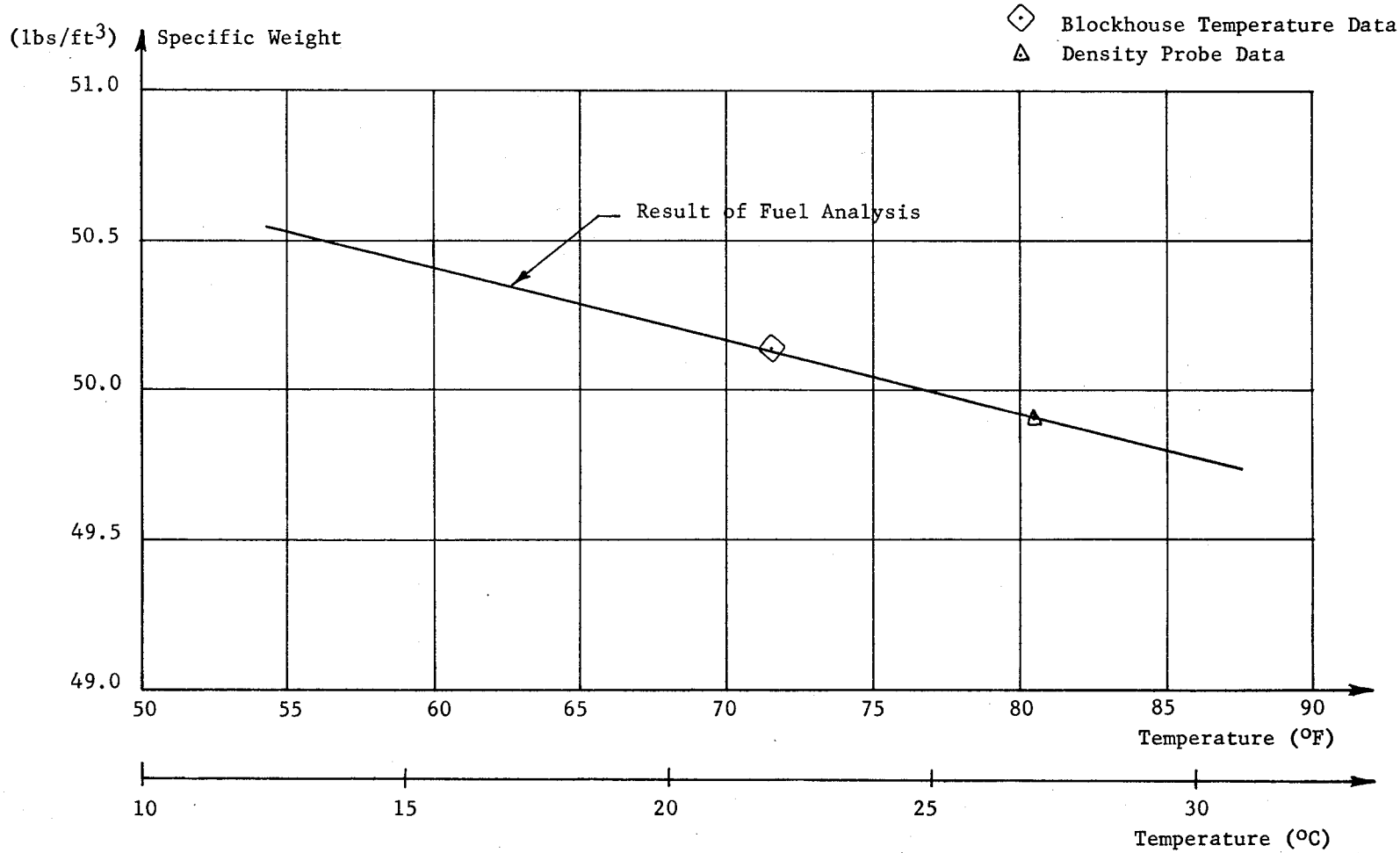

Fig. 3-1	
SA-1	RP-1 SPECIFIC WEIGHT VERSUS TEMPERATURE

4.0 (C) TRAJECTORY

4.1 SUMMARY

The actual flight path of SA-1 was very close to predicted during the period from liftoff to inboard engine cutoff; however, the actual trajectory was slightly higher than predicted due to higher accelerations. The trajectory parameters after inboard engine cutoff were proportionally lower than predicted because of a 1.61 sec early cutoff signal.

The preliminary postflight trajectory was established from external tracking data. Measured winds and atmospheric parameters were used in the trajectory calculations from 0 to 33 km altitude and the 1959 ARDC atmosphere above this altitude.

The postflight trajectory is an essential tool in analyzing the over-all performance of the guidance and propulsion systems (Sections 5.0 and 7.0).

4.2 TRACKING ANALYSIS

Comprehensive tracking coverage was obtained on SA-1. The quality of most of the data was excellent.

4.2.1 DATA SOURCES

External

All tracking data, with the exception of UDOP, was received within four days after the firing. There was continuous redundant coverage from liftoff until loss of telemetry signal at 409.35 sec. All available tracking data is shown in Table 4-I.

Onboard

A malfunction occurred in the in-flight calibration on telemetry link #3, and some difficulties were experienced in the reduction of the measurements on this link.

The onboard measurements which were used in establishing or confirming the trajectory are shown in Table 4-I.

4.2.2 DATA UTILIZATION

External

Tracking data used to establish the trajectory is given below:

Data Source	Interval	*Estimated Accuracy
Fixed Camera (light)	0.0 - 4.9 sec	.01 m
Fixed Camera (nose)	4.9 - 14.0 sec	.08 m
Theodolite	14.0 - 54.0 sec	1 m
Mark II Azusa	54.0 - 120.0 sec	3 m
Mark II Azusa	120.0 - 380.0 sec	37 m
Calculated Trajectory	380.0 - 409.35 sec	100 m

* Estimated accuracies quoted are the worst which occurred during the specified time interval.

The initial acceleration determined from the Fixed Camera tracking the light source was approximately 3-17 times more accurate than from the Fixed Camera tracking the nose of the vehicle. The standard deviations of the acceleration components were as follows:

Light	Nose
$\ddot{X} = \pm .0496$	$\ddot{X} = \pm .1606$
$\ddot{Y} = \pm .0137$	$\ddot{Y} = \pm .2424$
$\ddot{Z} = \pm .0308$	$\ddot{Z} = \pm .2517$

Virtually all acceleration during the first 17 sec of flight was in the vertical direction. The acceleration from the Fixed Camera tracking the light source is about 17 times better determined in this direction than from the Fixed Camera tracking the nose.

Both Radar and Azusa were degraded in quality for the first 30-40 seconds because of multipath effects.

Tracking data was available after 380 sec, but the quality of the data had begun to deteriorate. As a consequence a trajectory using Azusa positions and velocities at 380 sec as initial conditions was calculated to the time of loss of telemetry signal.

Onboard

Telemetered longitudinal accelerations and chamber pressures were used to establish the shape of the acceleration curve from 105.0 - 122.5 sec, the time period of cutoff transients.

4.2.3 ERROR ANALYSIS OF ACTUAL TRAJECTORY

Comparisons of the tracking data with the preliminary post-flight trajectory are given below (also see Figure 4-1):

Time	UDOP - Post Flight			Radar - Post Flight		
	ΔX (m)	ΔY (m)	ΔZ (m)	ΔX (m)	ΔY (m)	ΔZ (m)
Outboard Cutoff	2	-3	5	-7	-27	4
380 sec	-4	+60	27	-60	-49	9

Theodolite was lost before cutoff, but the deviations from the post-flight trajectory at 100 sec were:

ΔX = -20 m; ΔY = -16 m; ΔZ = 8 m

4.3 ACTUAL AND PREDICTED TRAJECTORY COMPARISON

Mach number and dynamic pressure are based on measured Cape Canaveral meteorological data to 33.0 km altitude in the ascent and adjusted to the 1959 ARDC atmosphere at 47.0 km. The 1959 ARDC atmosphere was used above 47.0 km in both ascent and descent. Below 47.0 km in the descent, the annual average Grand Bahama Island atmosphere was used to the loss of telemetry signal.

4.3.1 POWERED FLIGHT

Actual and predicted altitude, range, and lateral displacement, are shown in Figure 4-2.

Earth-fixed velocity is shown in Figure 4-3.

The azimuth of the velocity vector and its correlation with the wind velocity are shown in Figure 4-4. The predicted azimuth is shown both with and without the effects of winds; also shown is the Rawinsonde wind direction as a function of time.

Vehicle displacement versus time and altitude during early flight are shown in Figure 4-5 (see paragraph 6.2.1). The vehicle's lateral

displacement was less than 1 meter at the time the vehicle's altitude exceeded the height of the umbilical tower proposed for use on Block II vehicles.

Mach number and dynamic pressure for the powered flight are shown in Figure 4-6 and for the terminal phase of flight in Figure 4-7.

Longitudinal acceleration is shown in Figure 4-8. The left portion shows the acceleration throughout the powered phase; the right portion shows the acceleration from 104 seconds to the end of outboard engine thrust decay.

The longitudinal acceleration sweeper, measurement F5-13, had a range of 0.5 g's per leg from 0 to 3 g's and 0.2 g's per leg from 3 to 5 g's. This measurement contains an oscillation of 10 to 20 cps during the entire powered flight. The response of the accelerometer was such that the amplitude was attenuated at frequencies higher than 10 cps. From 80 sec to IECO, a 1.5 cps oscillation with an amplitude of about 0.2 m/sec^2 was superimposed over the higher frequency oscillations. The absolute magnitude of the acceleration may be slightly incorrect since the measurement was on telemeter link 3 which experienced an in-flight calibrator malfunction. The accelerometer located in canister 13 is 105.5 inches from the center line of the vehicle and 251.6 inches above the center of gravity of the vehicle at liftoff. Since the accelerometer is located some distance from the C.G., the angular motion of the vehicle affects its output. The output was corrected to the C.G. of the vehicle, but this did not remove the 1.5 cps oscillations (same as sloshing frequency) from the accelerometer output.

A number of significant events, such as liftoff, Mach 1, apex, and loss of telemetry signal, are given in Table 4-II. Maximum values for dynamic pressure, longitudinal acceleration, and earth-fixed velocity are also given. Both actual and predicted values and their differences are given for all these parameters.

This table shows that at the time of telemetry signal loss the altitude of the vehicle was 19.6 km, range was 332.2 km, elevation angle from the Cape was 1.9 deg and from Carter Cay was 9 deg. The height of the vehicle above the optical horizon from the Cape was 10.9 km.

Loss of telemetry and all tracking between 409.3 and 409.5 seconds strongly indicate that structural integrity of the vehicle was no longer maintained. Loss of structural integrity of the SI/SIV adapter section where the telemetry and tracking antennas are located would cause this loss of signal. The following signal losses were noted:

Source	Time of Signal Loss (sec)	Remarks
Telemetry, Hangar D	409.4 sec	
Telemetry, Cape Tel. #2	409.4 sec	
Telemetry, Cape Tel. #3	409.5 sec	
Telemetry, GBI	409.4 sec	
Udop, Site C	409 sec	Approximate, record hard to read
Azusa Mk II	409 sec	Approximate, timing bad
C-Band Radar 1.16 (Cape)	409.3 sec	
C-Band Radar 3.16 (GBI)	409 sec	Approximate, sharp drop in signal
	411 sec	Lost beacon (radar log)
S-Band Radar 1.4 (Mod II)	409.4 sec	Drop in AGC trace

4.3.2 CUTOFF

A comparison of the actual parameters with the nominal at both inboard and outboard cutoff is shown in Table 4-III. All of the significant differences are attributable to the early cutoff time.

Thrust Decay

The velocity gain during thrust decay of both inboard and outboard engines is compared with the nominal below:

	Inboard	Outboard
Actual (m/s)	8.22	7.01
Nominal (m/s)	8.20	8.63
Act - Nom (m/s)	.02	-1.62

TABLE 4-I

Data Sources

Data Source	Interval
External	
Fixed Camera (light)	0.92 - 4.92 sec
Fixed Camera (nose)	0.92 - 20.48 sec
Theodolite	3.75 - 107.50 sec
UDOP	0.00 - 409.25 sec
Mark II Azusa	12.60 - 398.50 sec
FPS-16 Radar 1.16 (Cape)	0.00 - 409.60 sec
FPS-16 Radar 1P.16 (PAFB)	25.00 - 268.00 sec
FPS-16 Radar 3.16 (GBI)	90.00 - 409.00 sec
FPS-16 Radar 3A.16 (Carter Cay)	100.00 - 409.60 sec
Supporting Flight Data	
Tilt Program	Powered Flight
Guidance Outputs (Meas: I1-15, I2-15 and I3-15)	0.0 - 409.35 sec
Longitudinal Acceleration	
Meas: F5-13 Sweeper	0.0 - 110.1 sec
F6-13 Coarse	0.0 - 409.35 sec
F7-13 $\pm$ 1 g	Decay - 409.35 sec
Cutoff Signals	
Observed Meteorological	0.0 - 95.0 sec
Chamber Pressure	
Meas: D1-1, D1-2, D1-3, D1-4, D1-5, D1-6, D1-7, D1-8	0.0 - End Outboard Decay
$\Delta\varphi_p$, Meas: H1-15	0.0 - 409.35 sec
φ_y, Meas: H2-15	0.0 - 409.35 sec

TABLE 4-II

(C) Significant Events

Event	Parameter	Actual	Predicted	Act-Pre
Liftoff	Range Time (sec)	0.89	0.89	0.0
	Longitudinal Acceleration (m/s^2)	13.77	13.60	+0.17
Mach 1	Range Time (sec)	49.0	49.5	-0.5
	Altitude (km)	6.560	6.602	-0.042
Maximum Dynamic Pressure	Range Time (sec)	61.00	61.89	-0.89
	Dynamic Pressure (psi)	5.28	5.26	+0.02
	Altitude (km)	11.018	11.266	-0.248
Maximum Acceleration	Range Time (sec)	110.25	111.81	-1.56
	Longitudinal Acceleration (m/s^2)	41.73	42.93	-1.20
Maximum Earth-fixed Velocity	Range Time (sec)	116.3	117.9	-1.6
	Earth-fixed Velocity	1614.5	1673.3	-58.8
Apex	Range Time (sec)	249.24	255.23	-5.99
	Altitude (km)	136.455	143.031	-6.576
	Range (km)	166.423	178.813	-12.390
Loss of Telemetry	Range Time (sec)	409.35	409.35*	0.0
	Altitude (km)	19.592	35.166	-16.633
	Range (km)	332.200	344.833	-12.633
	Longitudinal Acceleration (m/s^2)	-11.83	-12.25	+0.42
	Dynamic Pressure (psi)	22.48	1.83	+20.65
	Elevation from Pad (degs)	1.87	4.27	-2.40
	Elevation from Carter Cay (deg)	9.2	15.5	-6.3

* Vehicle assumed to be tumbling after OECO for predicted trajectory.

TABLE 4-III

Cutoff Conditions

Parameter	Inboard			Outboard		
	Actual	Predicted	Act-Pred	Actual	Predicted	Act-Pred
Range Time (sec)	110.10	111.71	-1.61	116.08	117.71	-1.63
Range (km)	23.10	24.69	-1.59	29.12	31.02	-1.90
Altitude (km)	48.48	49.82	-1.34	55.63	57.19	-1.56
Cross Range (km)	.17	.16	+.01	.21	.21	0.0
Earth-fixed Velocity (m/s)	1522.8	1574.7	-51.9	1611.7	1669.5	-57.8
Longitudinal Acceleration (m/s^2)	41.70	42.87	-1.17	21.65	22.01	-0.36
Elevation Velocity Vector (deg)	50.36	49.86	+.50	48.89	48.49	+.40
Azimuth Velocity Vector (deg)	100.20	100.33	-.13	100.27	100.39	-.12

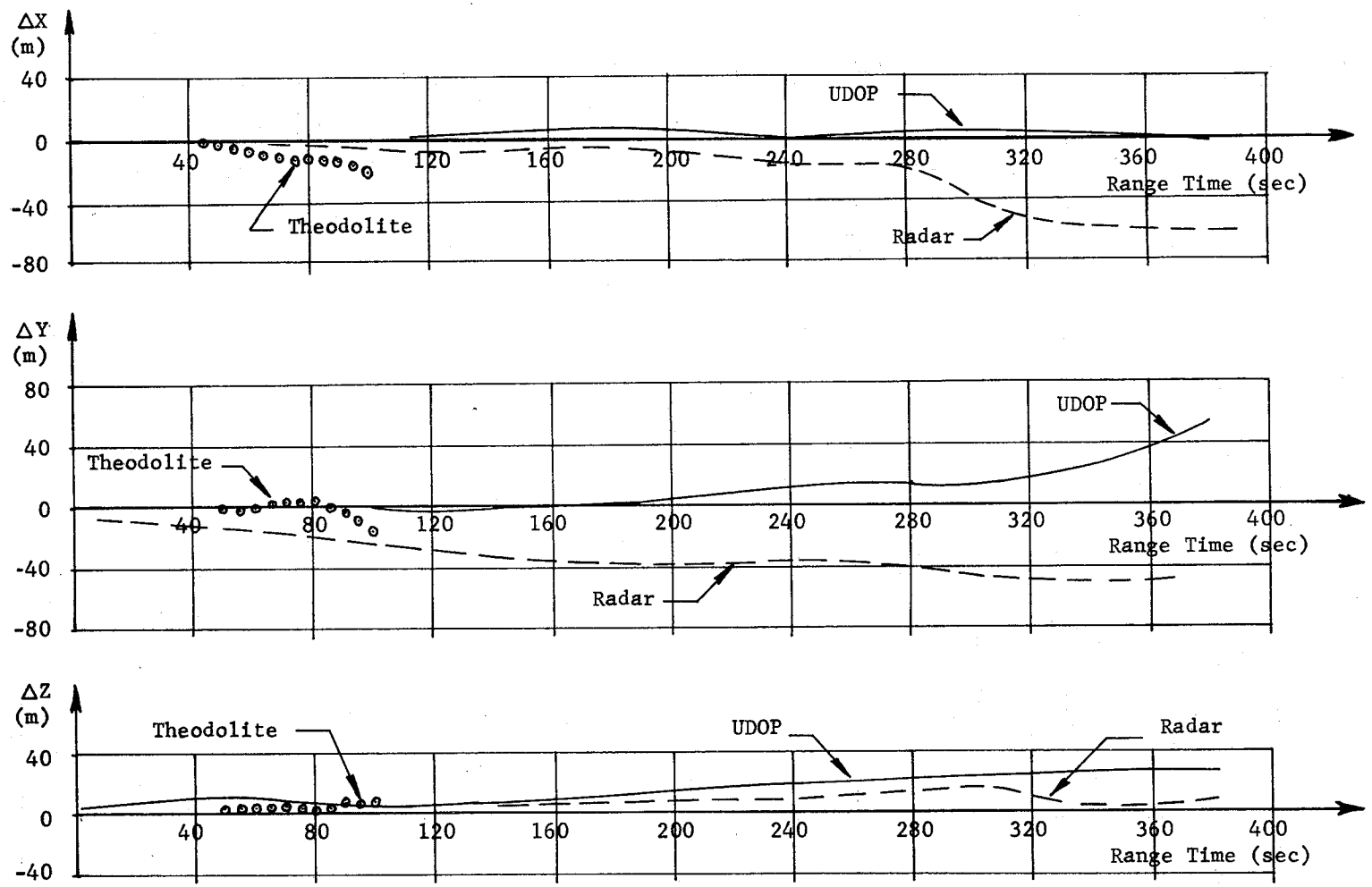

Fig 4-1	TRACKING COMPARISONS (TRACKING - REFERENCE)
SA-1	

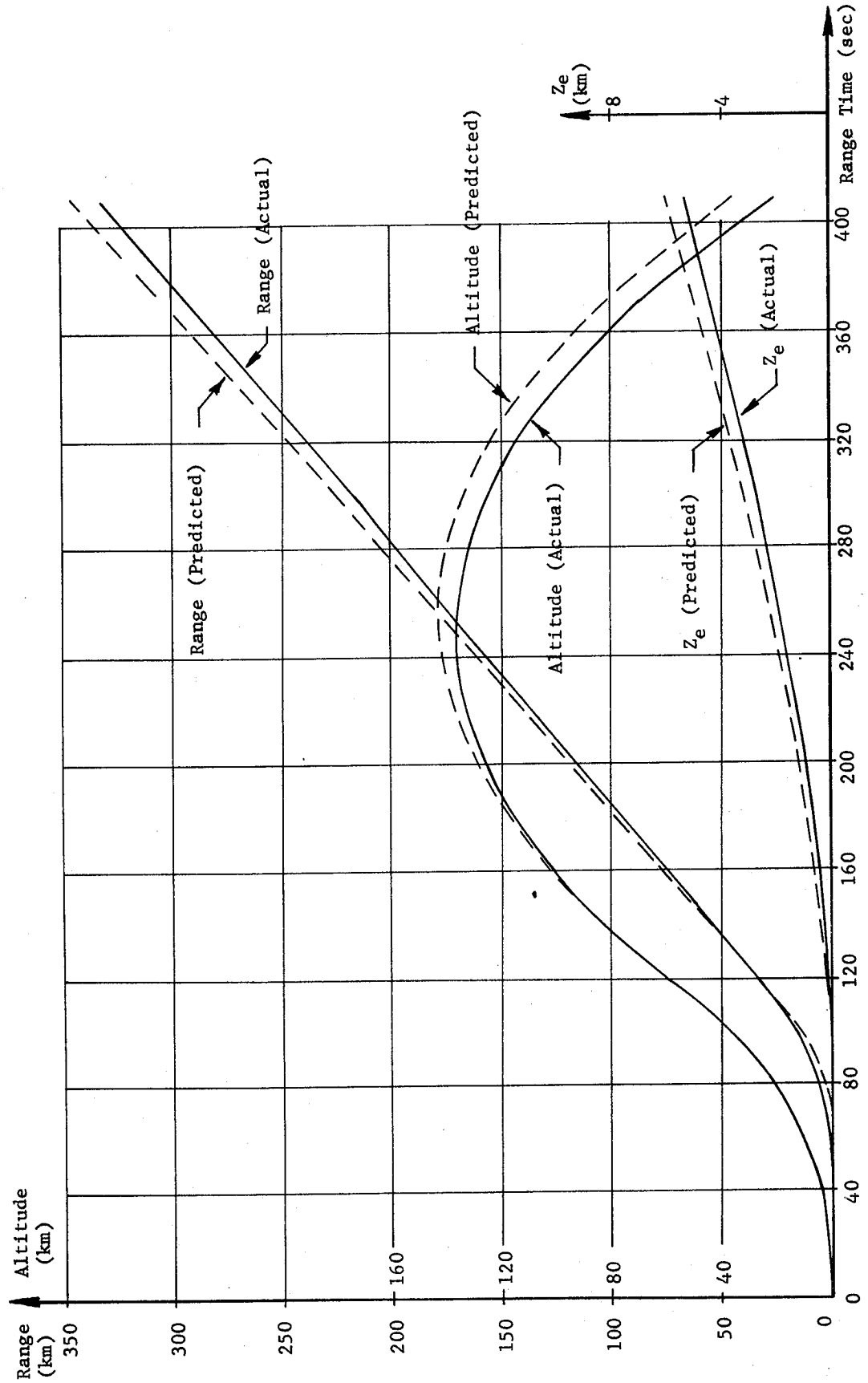

Fig. 4-2 SA-1 TRAJECTORY

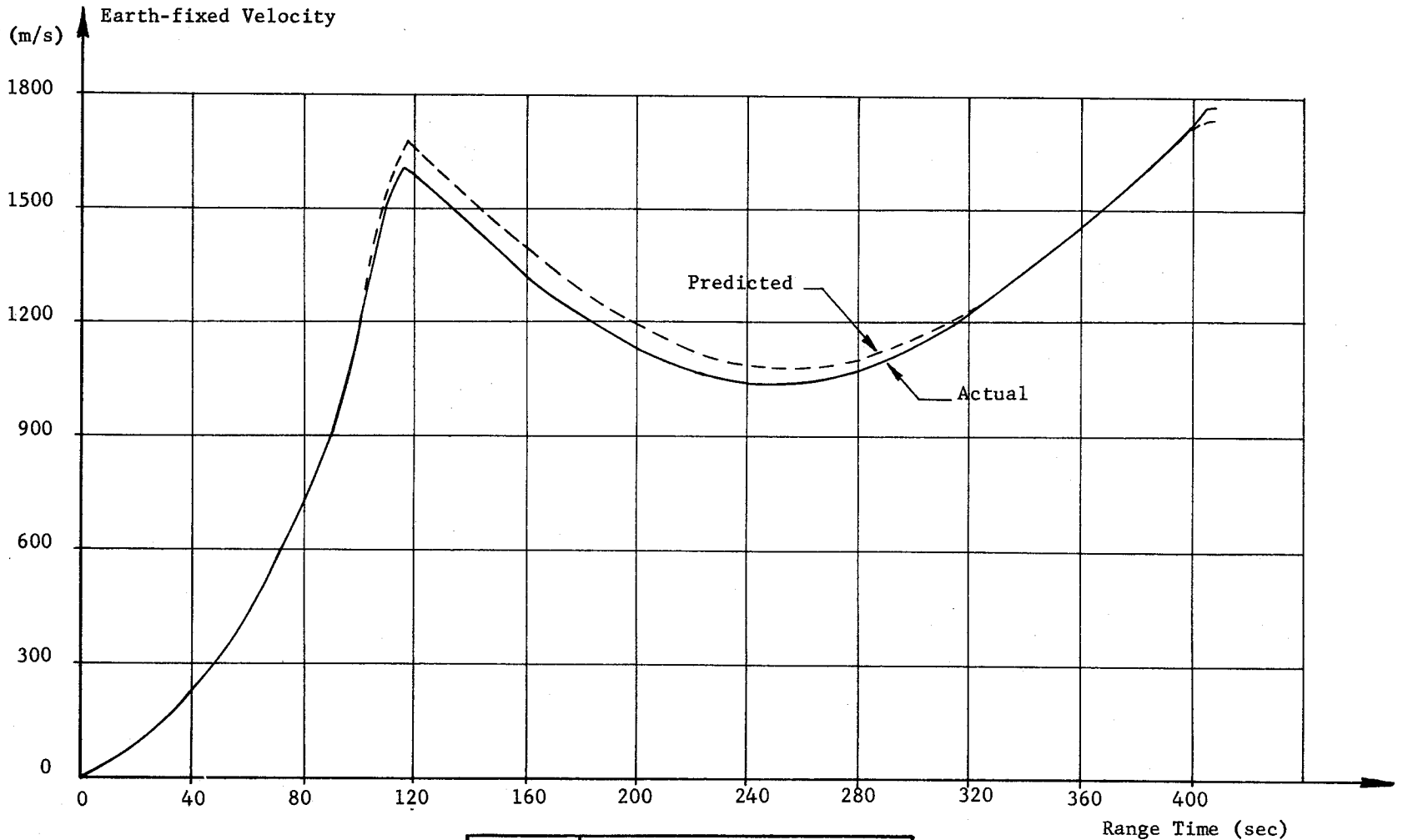

Fig. 4-3	
SA-1	EARTH-FIXED VELOCITY

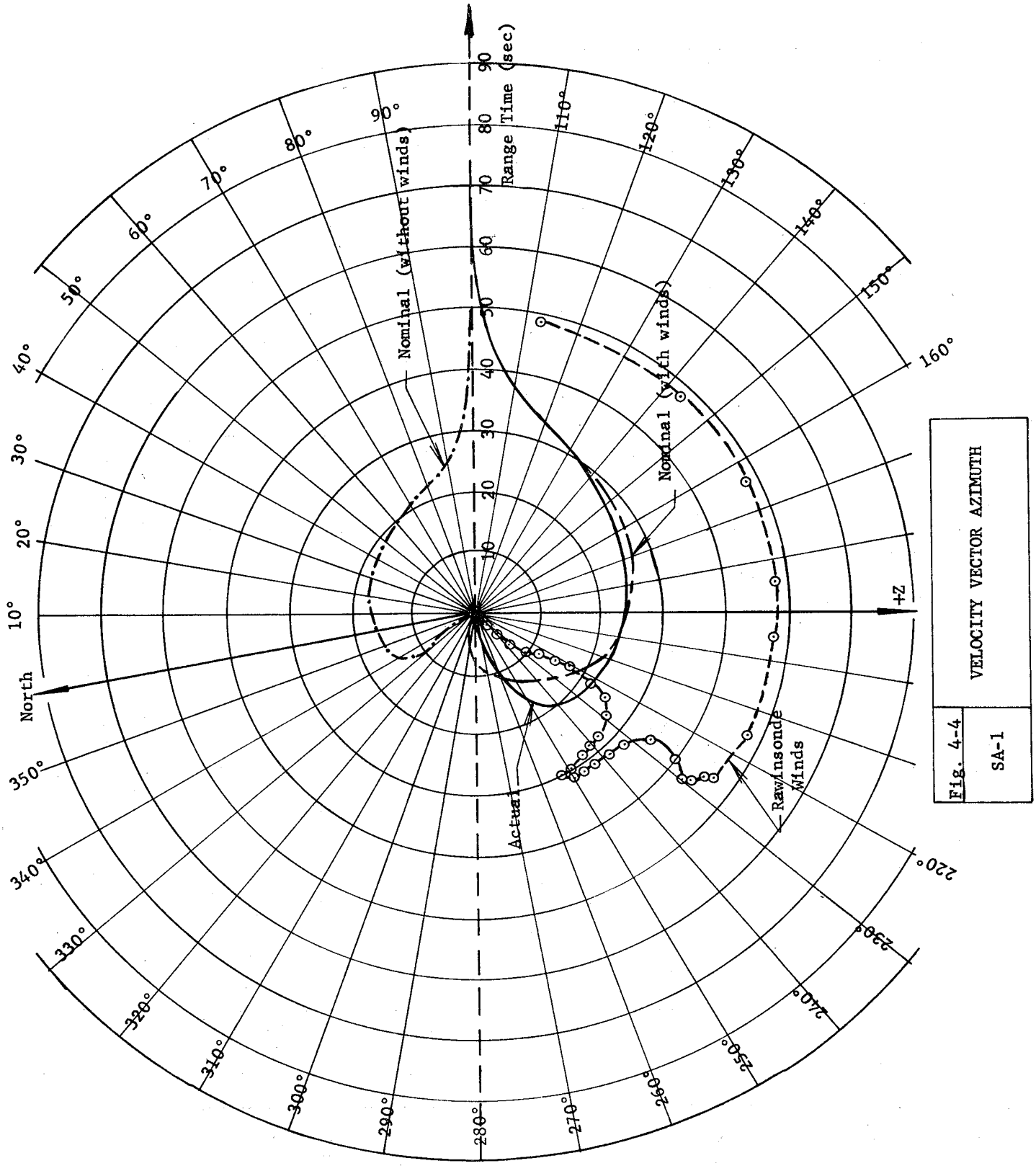

Fig. 4-4 SA-1 VELOCITY VECTOR AZIMUTH

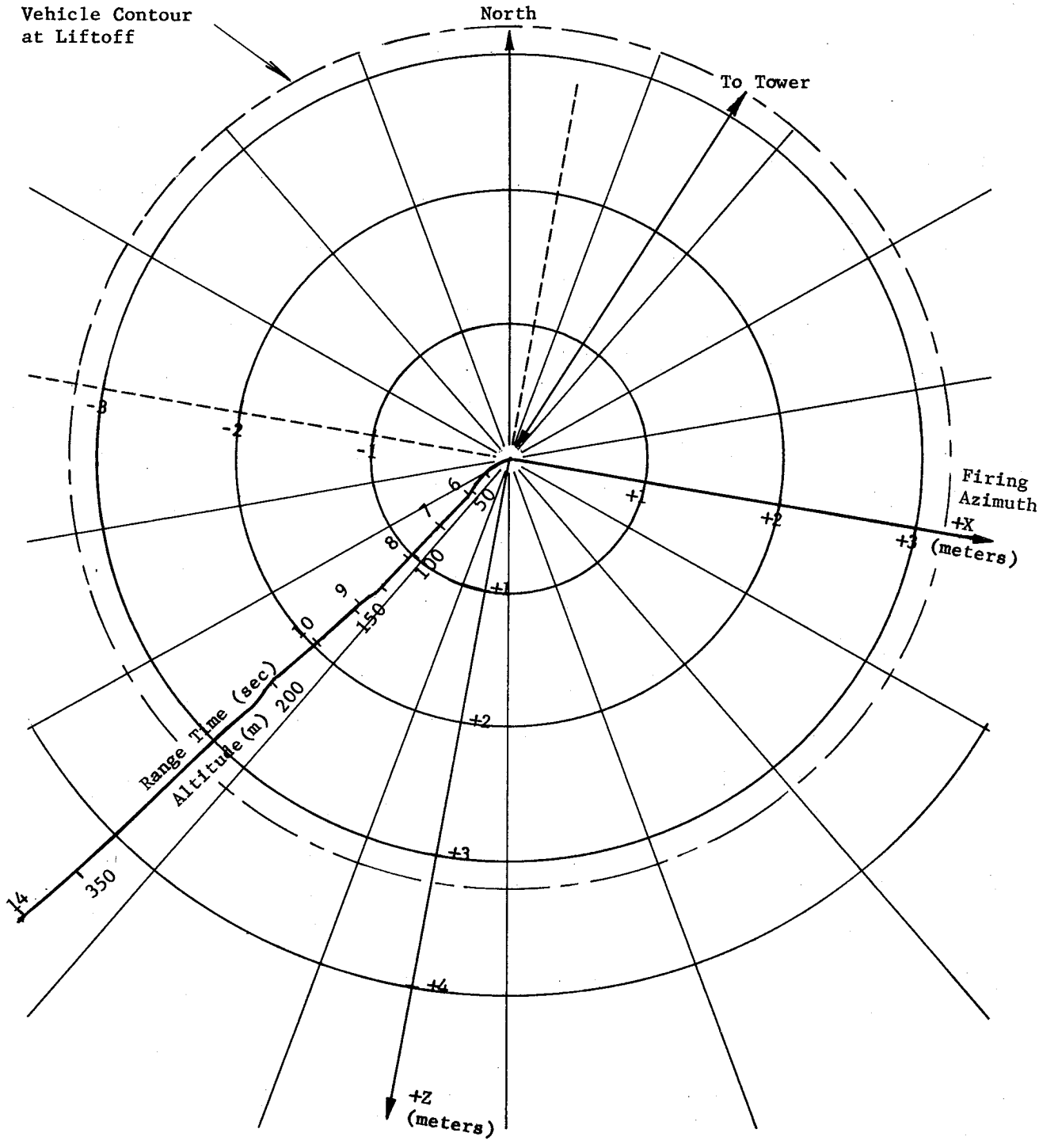

Fig.4-5	DISPLACEMENT AND ALTITUDE IMMEDIATELY AFTER LIFTOFF
SA-1	

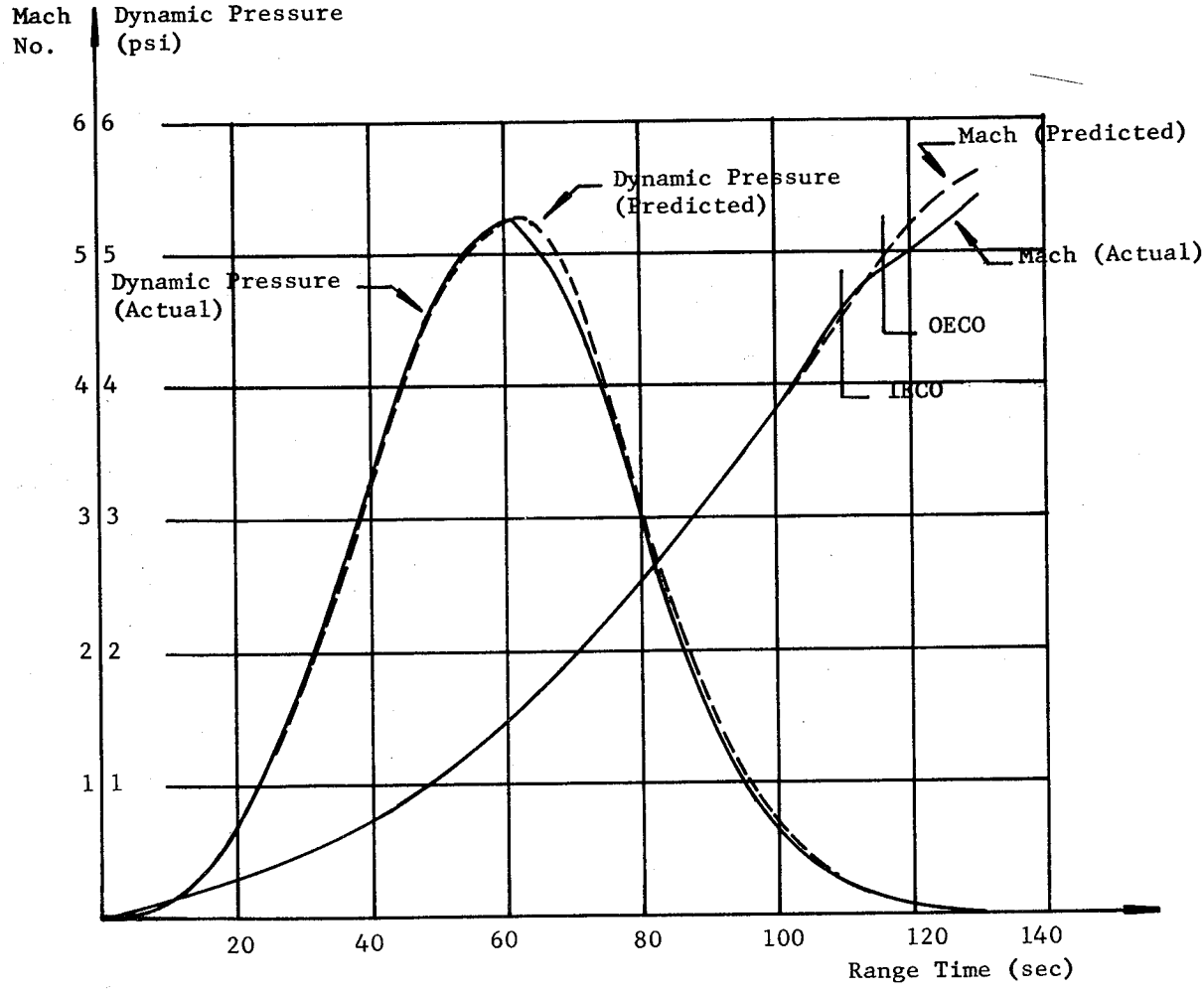

Fig.4-6	DYNAMIC PRESSURE AND MACH NUMBER
SA-1	

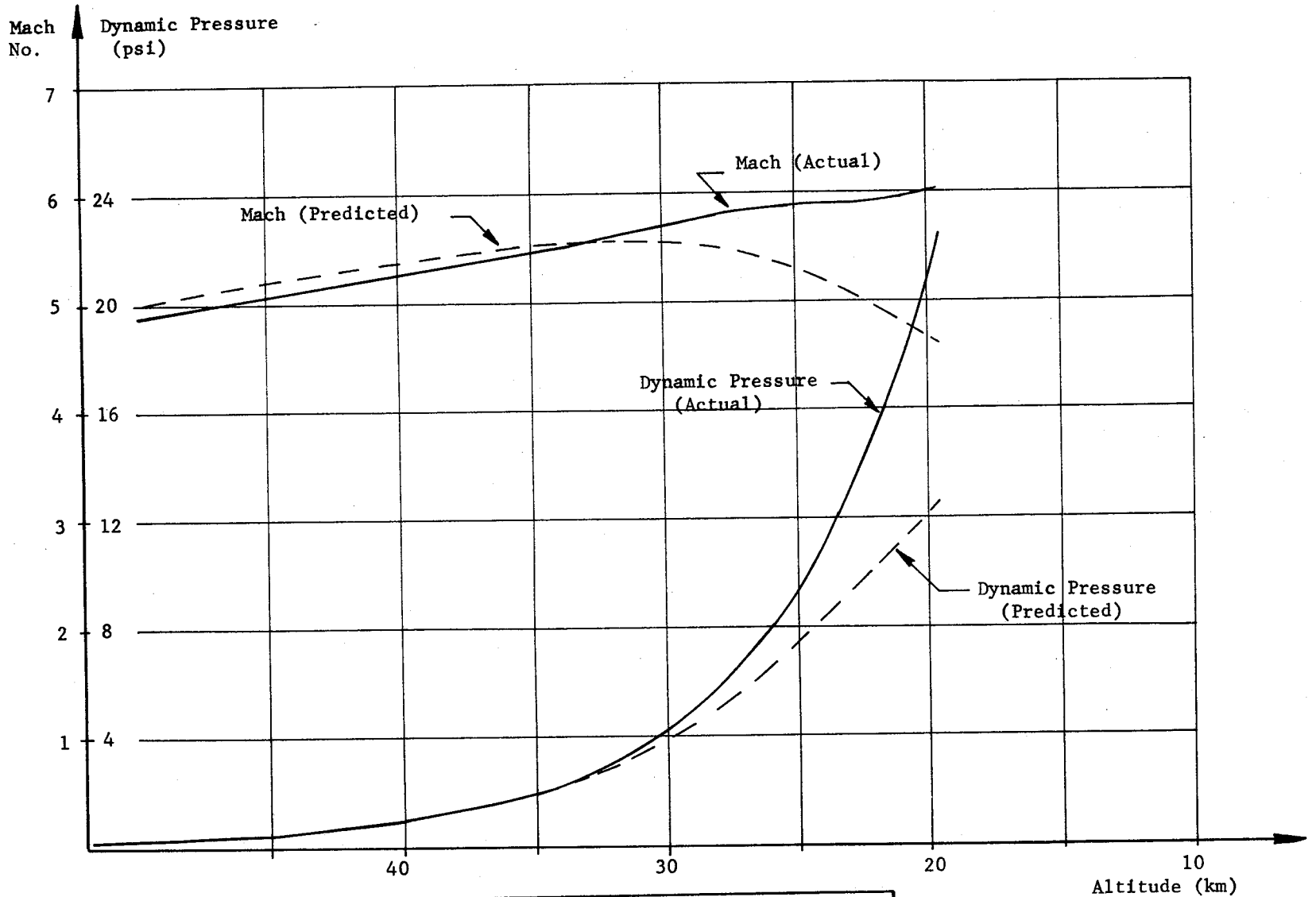

Fig.4-7	MACH NUMBER AND DYNAMIC PRESSURE DURING DIVE PHASE
SA-1	

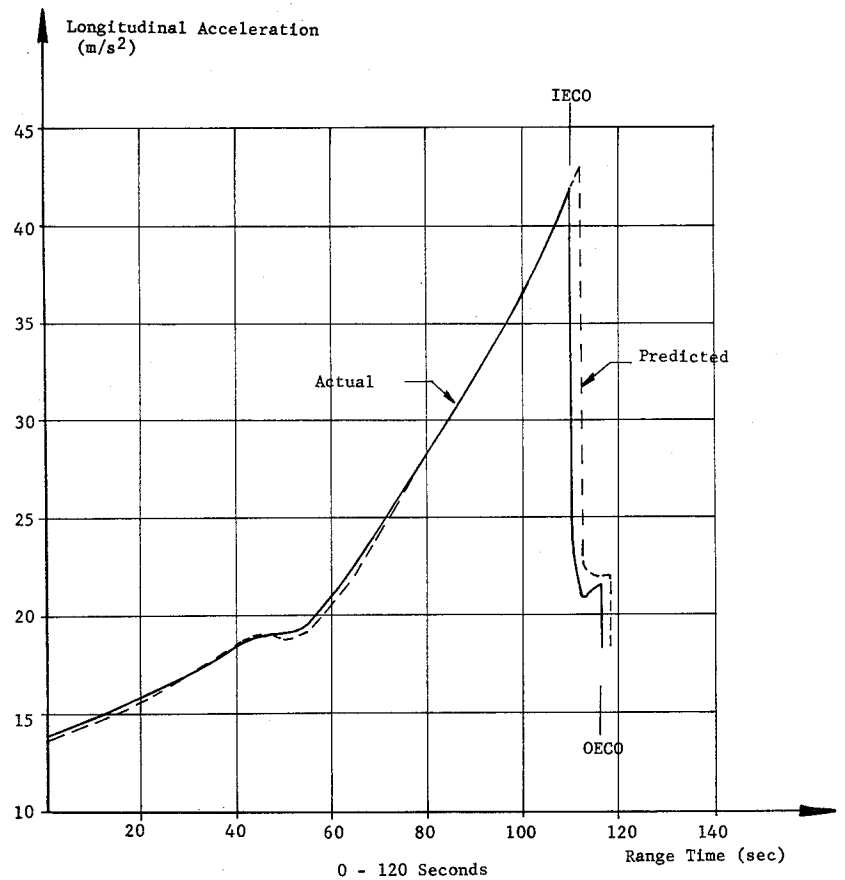

0 - 120 Seconds

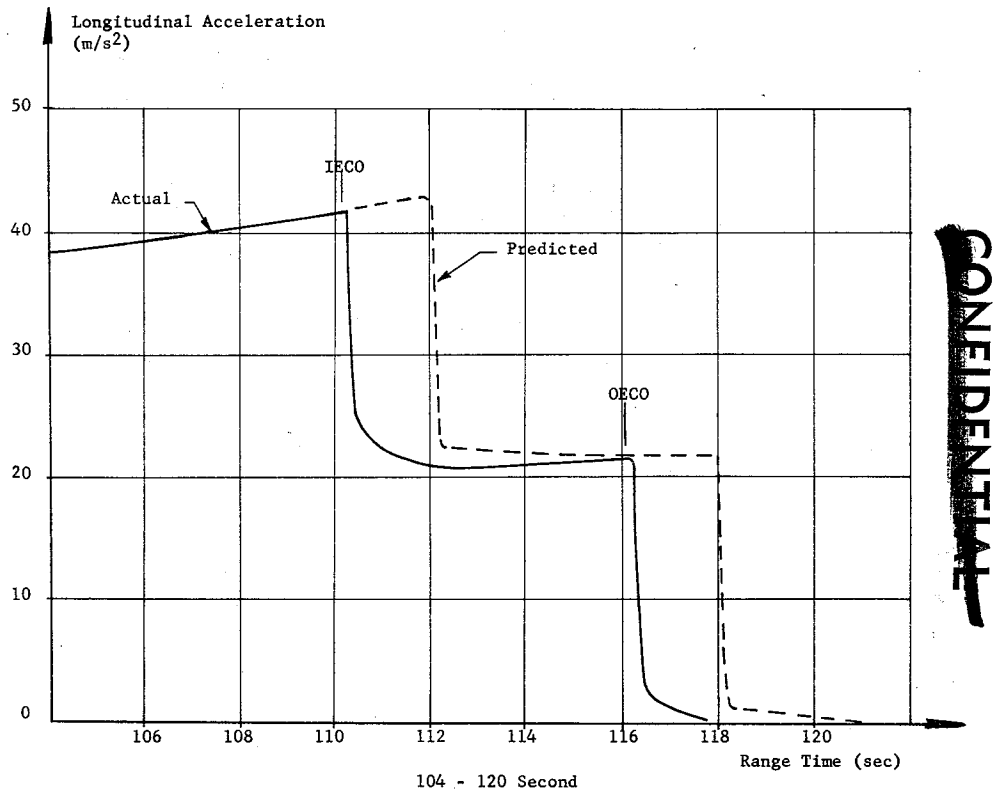

104 - 120 Second

Fig. 4-8	
SA-1	LONGITUDINAL ACCELERATION

5.0 (C) PROPULSION

5.1 SUMMARY

The functional performance of the propulsion system and its major constituents was determined from the 267 telemetered propulsion and associated systems measurements. Over-all propulsion system operation during the flight test was very satisfactory. The total cluster performance averaged within approximately one percent of predicted. Individual engine performances were satisfactory with a maximum deviation in thrust from predicted of about +3.9 percent. The propellant tank pressurization systems functioned properly, resulting in satisfactory tank pressures during flight. All hydraulic systems operated well within the expected limits throughout the powered flight phase.

Cluster performance was derived by using some of the telemetered and tracking measurements in a simulation of the actual trajectory. Individual engine performance was derived by a reconstruction of the flight by using the Saturn Mark IV Computation Program. These two methods showed results which were in agreement within 1 percent.

5.2 INDIVIDUAL ENGINE PERFORMANCE

Total thrust and specific impulse curves for each engine are shown in Figures 5-1 through 5-4. These curves indicate that the performance of each engine was satisfactory based on the performance predictions. The flight curves shown are based on a reconstruction of the flight by using the Saturn Mark IV Computation Program. In this program certain significant items of flight data are put into the original flight prediction program to achieve an analytical reconstruction of propulsion system performance during flight. Engine thrusts based on telemetered chamber pressures agree very closely with the thrusts determined from the flight reconstruction.

The maximum deviation in engine thrust of approximately +3.9 percent occurred on engine position #5. Six engines operated with less than ± 1.7 percent deviation from the predicted thrust. Engine specific impulse based on the flight reconstruction was higher than predicted for all engines. Maximum deviation was only 2.5 percent, however, indicating satisfactory over-all performance for each individual engine.

Start and transition were smooth for all engines. Figure 5-5 shows the thrust buildup of all engines. The starting pairs by position numbers were 5,7; 6,8; 2,4; and 1,3 with a programmed 100 ms delay between pairs. The largest deviation was between 1 and 3, where 3 started approximately 60 ms early. This difference was also noted during the static testing of SA-1 and was not detrimental to the propulsion system starting

sequence. Engine main propellant valve opening times are shown in Table 5-I. Shutdown was satisfactory for all engines. Main propellant valve closing times are shown in Table 5-I and cutoff impulse in Table 5-II.

All engine subsystems and components operated satisfactorily with the exception of a possible deviation in performance of the hydraulic system on the engine in position #2. Telemetered data indicated that the hydraulic pressure source (D29-2) on position 2 was 500 psig below the normal value of 3000 psig. This data is subject to question because:

(a) The hydraulic "OK" pressure switch picked up and was okay at thrust commit. (The pick-up pressure of the switch is 2775 psig).

(b) No level change occurred in the hydraulic reservoir (a 7% increase would have occurred if the pressure had dropped 500 psig).

(c) The pressure transducer (D29-2) that measured this low pressure also measured the pressure output of the auxiliary pump prior to firing command in the form of a lamp (on-off signal). The lamp was off prior to liftoff indicating a low auxiliary pump pressure. If the D29-2 measuring system gave an accurate reading, both the auxiliary pump and the main pump partially malfunctioned which is improbable.

Based on the above, it is concluded that the high pressure source on position 2 was at the proper level of approximately 3000 psig.

TABLE 5-I

Valve Operation Times

Engine No.	Ign. Signal Time After Ign. Command (ms)	GG LOX Lead (ms)	MLV Opening Time (ms)	MFV Opening Time (ms)	MLV Closing Time (ms)	MFV Closing Time (ms)
1	330	5	230	760	200	1200
2	240	15	210	710	230	1200
3	340	7	220	660	170	1250
4	240	*	200	640	230	1270
5	30	11	190	580	200	1300
6	140	8	200	720	160	1300
7	30	11	210	630	200	1200
8	140	18	210	630	170	1400

NOTE: Engines started in pairs with a predicted 100 ms difference in starting time as follows:

No. 5 and No. 7
No. 6 and No. 8
No. 2 and No. 4
No. 1 and No. 3

LEGEND: GG - Gas Generator
MLV - Main LOX Valve
MFV - Main Fuel Valve

* Unreliable data

TABLE 5-II

(C) Cutoff Impulse

Engine No.	Engine Cutoff Impulse (lb sec)	Comparison With Nominal (lb sec)
1	71,551	+ 151
2	64,840	- 6,560
3	63,926	- 7,474
4	73,441	+ 2,041
5	88,516*	+ 17,116
6	76,439	+ 5,039
7	74,158	+ 2,758
8	70,508	- 892

NOTES:
1. The nominal cutoff impulse is 71,400 ± 5200 for a 1σ confidence level.
2. All values in Table 5-II are based on chamber pressure decay data.
3. Complete thrust decay had occurred by $2.4^{+0.3}_{-0.2}$ sec after cutoff signal. This was the average time for all positions.
4. For vehicle cutoff impulse see paragraph 5.3.3.

* Questionable data

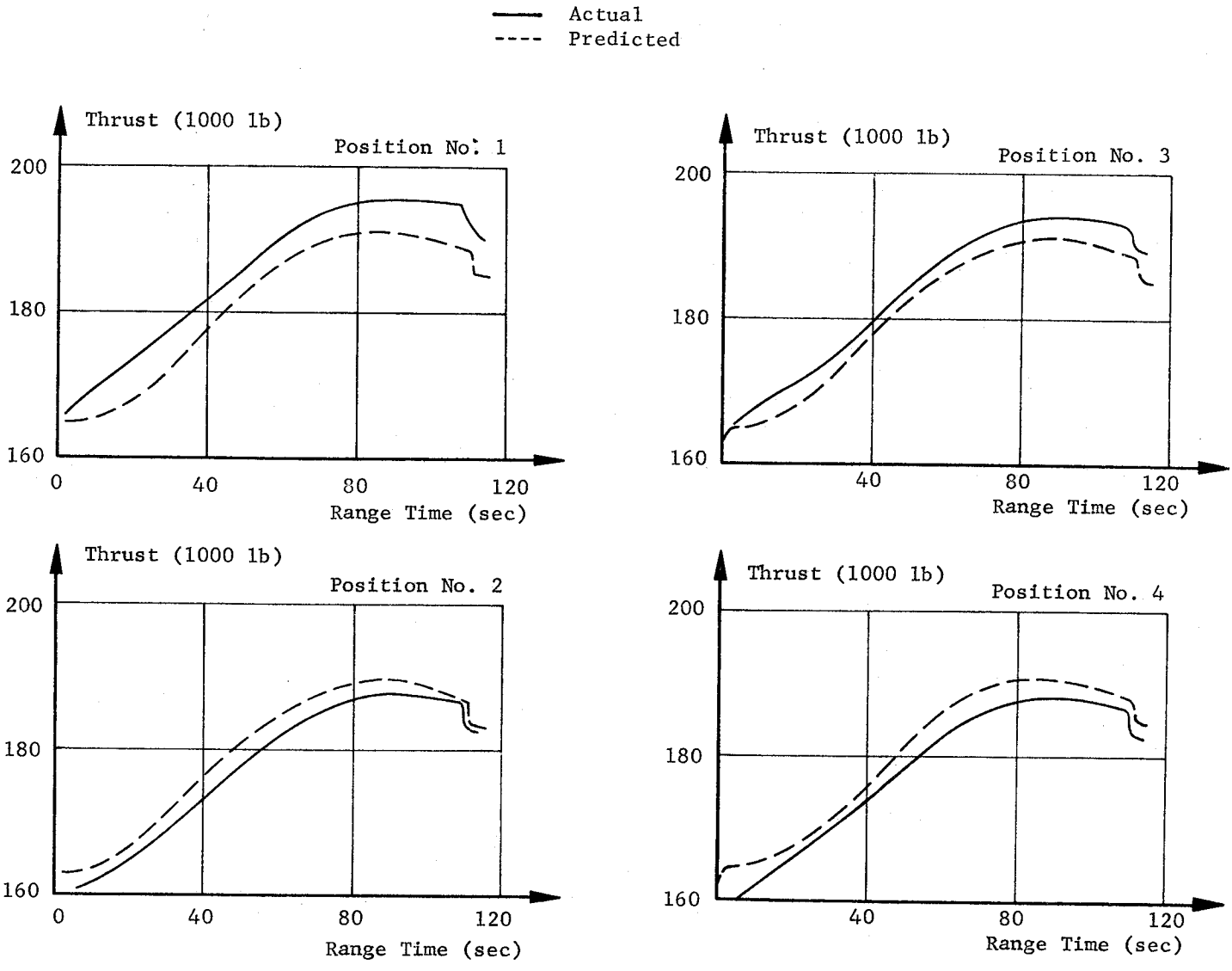

Fig. 5-1	OUTBOARD
SA-1	ENGINE THRUST

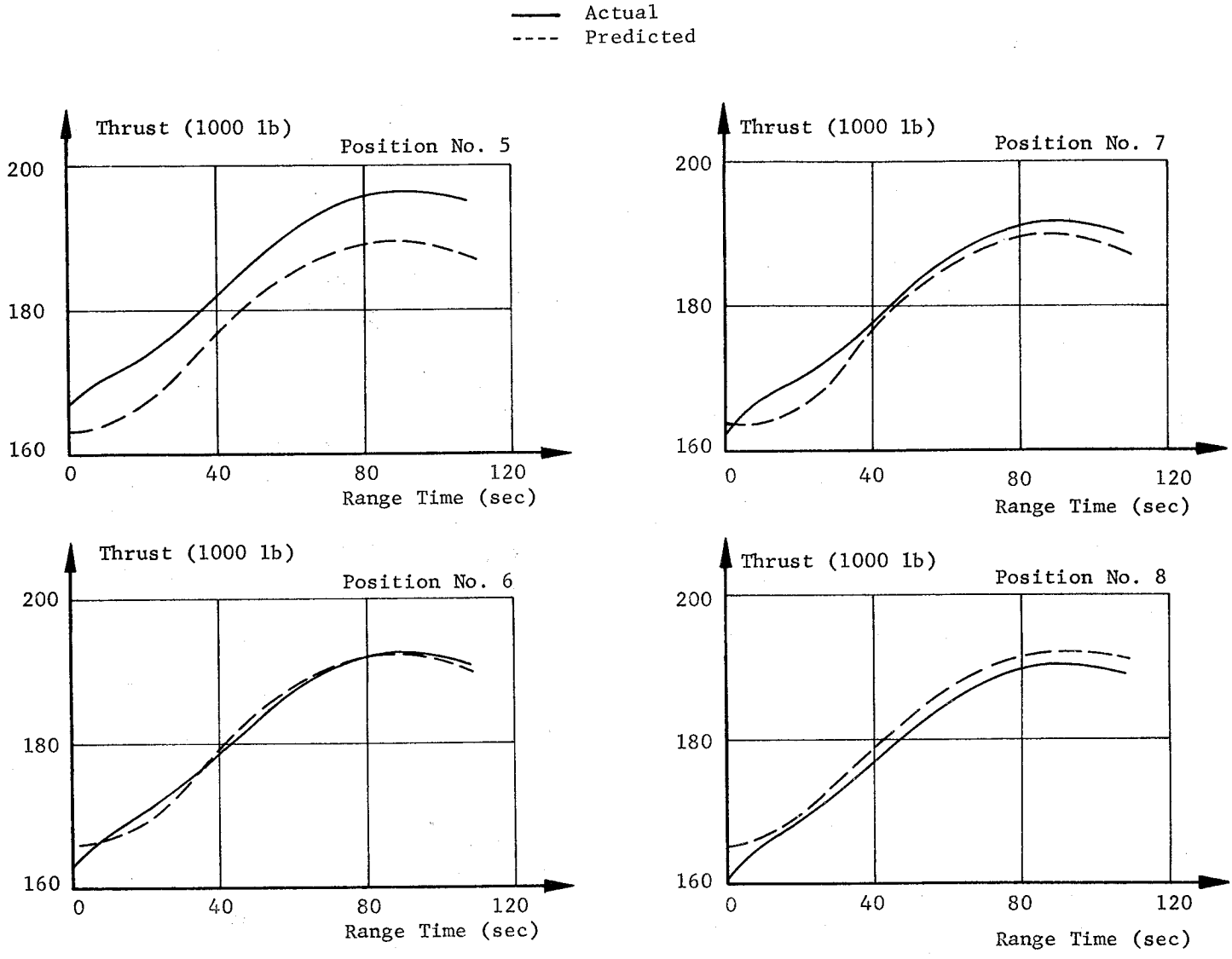

Fig. 5-2	INBOARD ENGINE THRUST
SA-1	

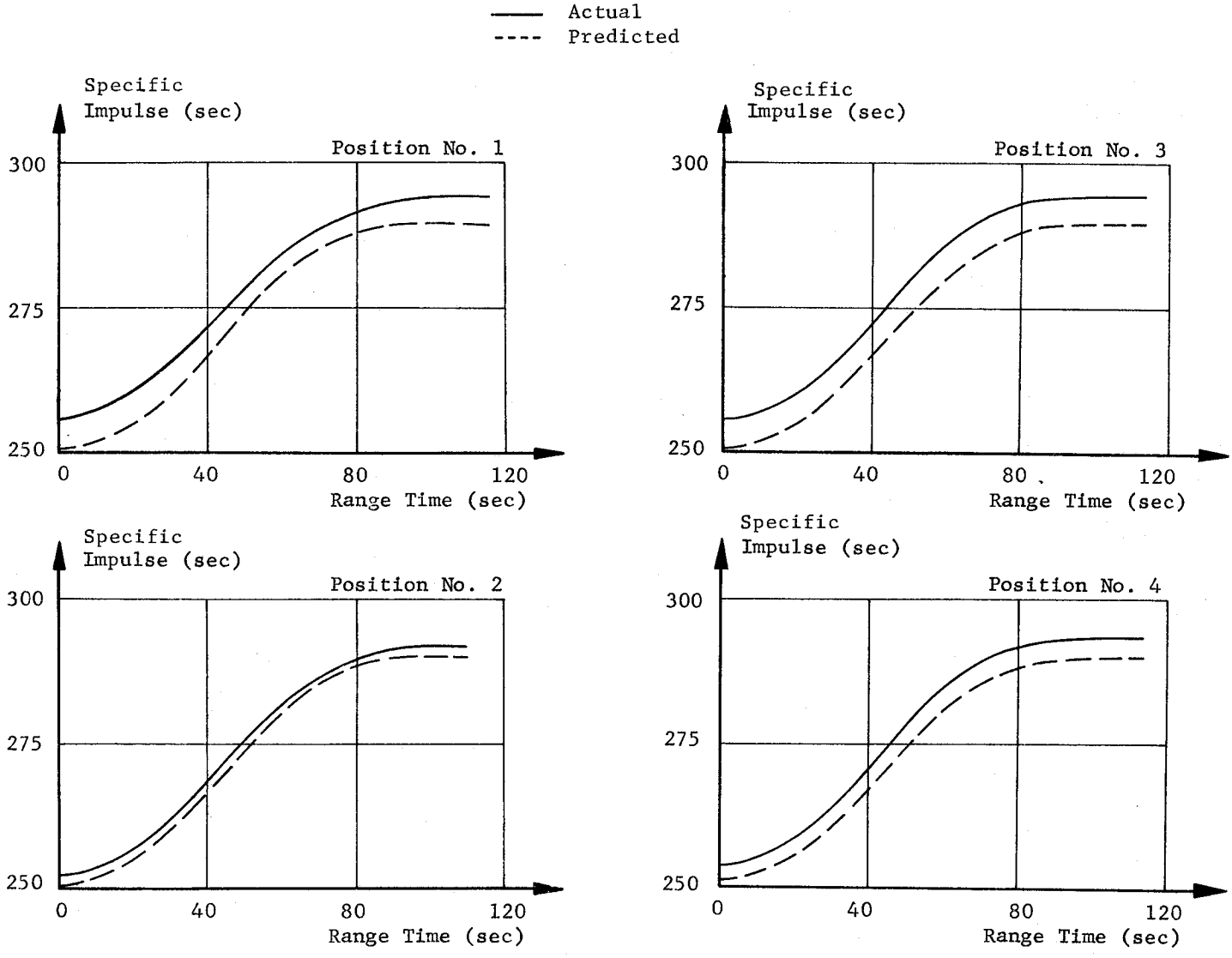

Fig. 5-3	OUTBOARD ENGINE SPECIFIC IMPULSE
SA-1	

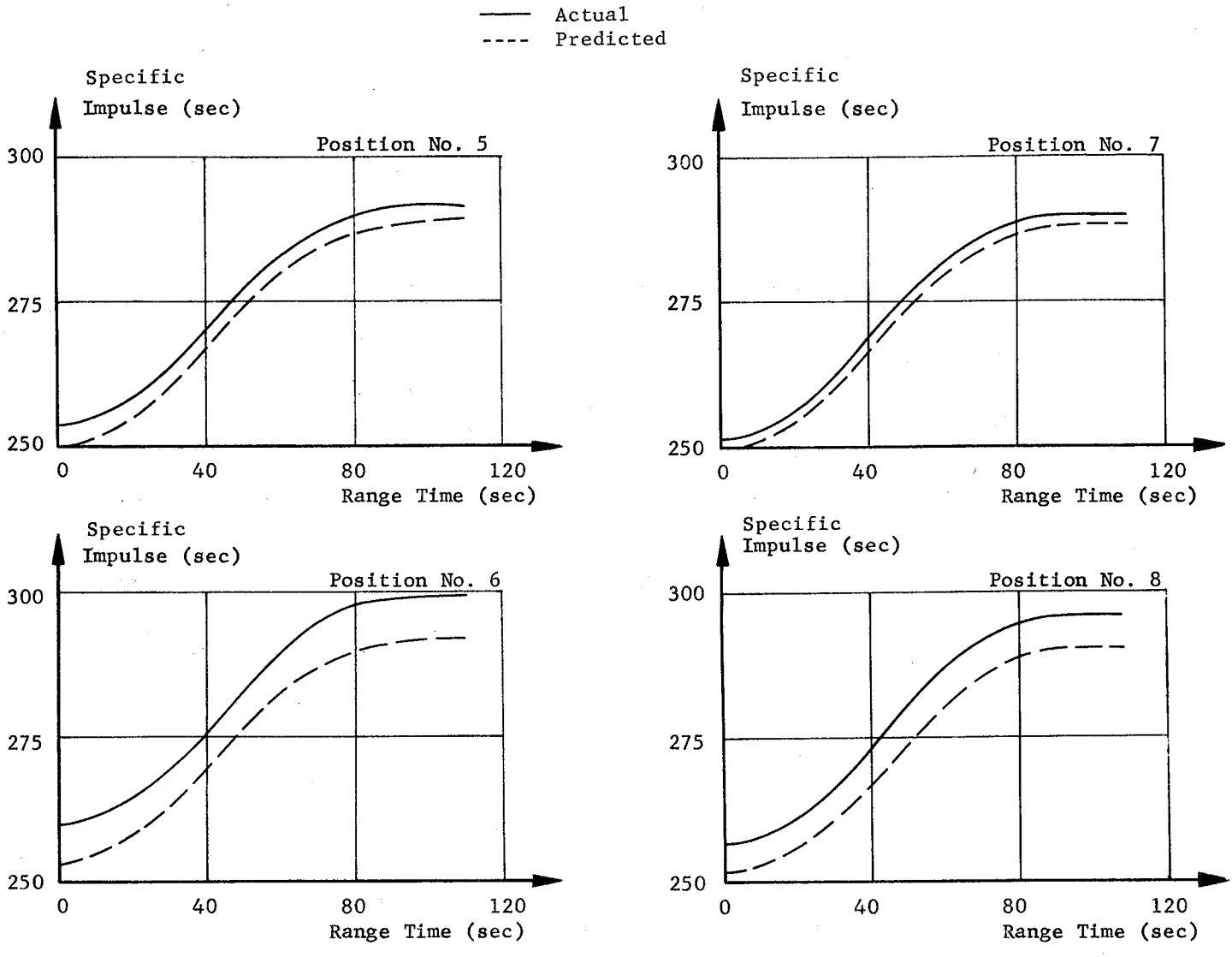

Fig. 5-4	INBOARD ENGINE SPECIFIC IMPULSE
SA-1	

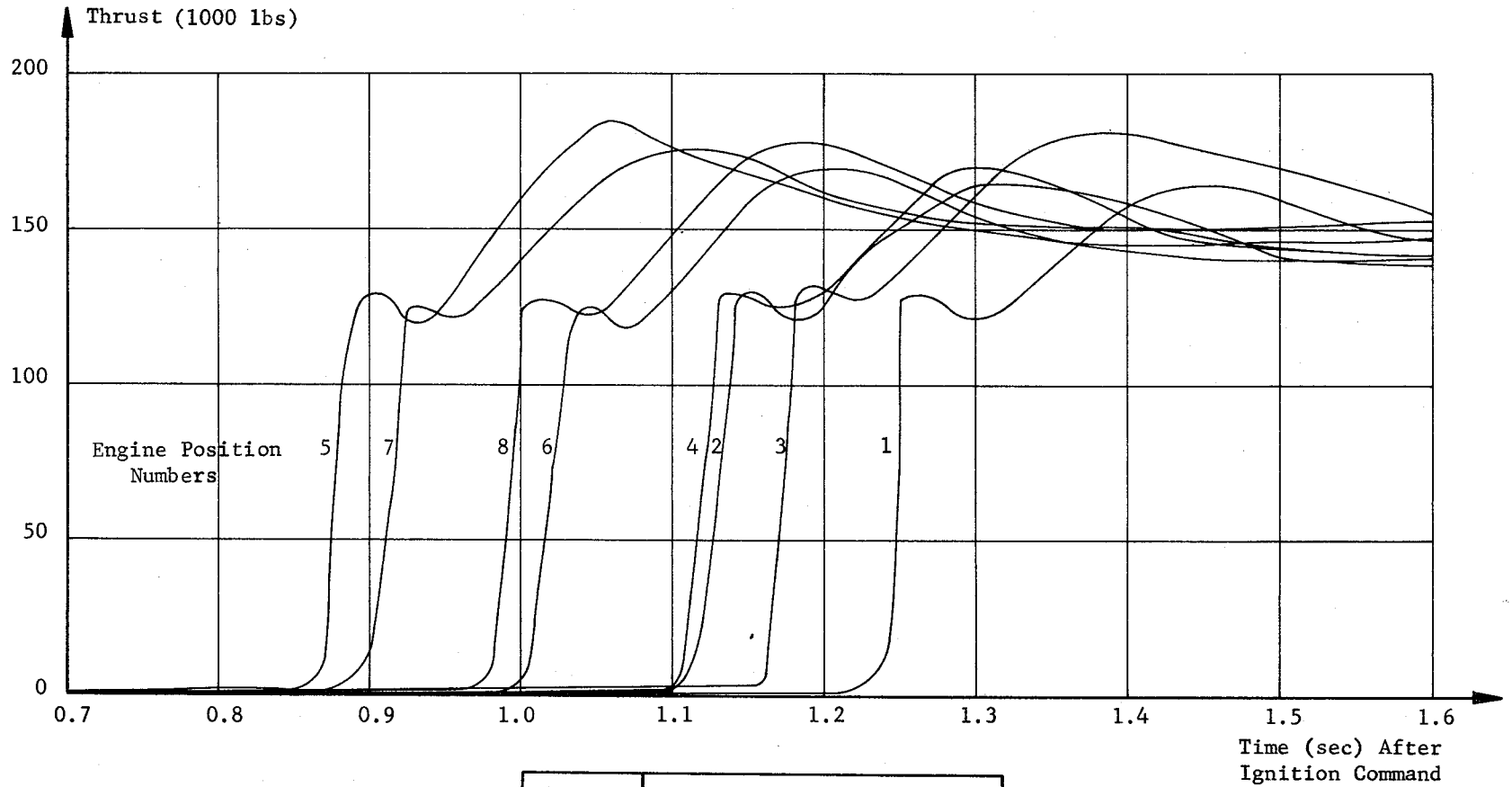

Fig. 5-5	
SA-1	THRUST BUILDUP

5.3 VEHICLE PROPULSION SYSTEM PERFORMANCE

5.3.1 CLUSTER PERFORMANCE

Over-all propulsion system performance as reflected in vehicle performance was very satisfactory. Inboard engine cutoff occurred 109.21 seconds after vehicle liftoff signal, and outboard engine cutoff approximately 6 seconds later. Both the inboard and the outboard engines shut down smoothly within the expected time. Cutoff impulse for each group of engines is given in paragraph 5.3.3.

Vehicle thrust as determined by a reconstruction of the flight utilizing the Saturn Mark IV Computation Program averaged within one percent of predicted (Figure 5-6). Vehicle specific impulse (Figure 5-7) deviated from predicted by less than one percent indicating satisfactory over-all propulsion system performance. Vehicle mixture ratio is also shown in Figure 5-7.

5.3.2 FLIGHT SIMULATION OF CLUSTER PERFORMANCE

Introduction

Propulsion system performance was derived from a simulation of the actual trajectory using telemetered propulsion measurements. The flight simulation is the result of integrating the differential equations which represent the vehicle's powered flight motion in all six degrees of freedom. Measured values or best estimates of mass, navigation, forces, moments, environments, and vehicle characteristics are required in addition to the propulsion system measurements as inputs for these equations. The trends and transients indicated by the various measurements are generally maintained in the flight simulation with only the absolute level of the measurements corrected.

A least squares solution was obtained for corrections to vehicle thrust and rate of mass loss producing the best fit to the tracking results. These corrections were applied to the individual engines by utilizing the engine reconstruction program.

A number of the propulsion system measurements, especially flow rates and chamber pressures, were correlated with the flight reconstructed data obtained from the Saturn Mark IV Computation Procedure which makes use of gain table values established by the engine manufacturer and other propulsion system measurements, such as RPM of the turbine, pump inlet pressures, and tank pressures. The data used as inputs for the flight simulation of the actual trajectory are the results from this correlation.

Performance from Flight Simulation

The vehicle specific impulse, thrust, and total weight loss rate are derived from the telemetered propulsion system measurements, which have been correlated with the values derived from post flight reconstruction in a simulation of the tracked trajectory. Measured values or best estimates for the liftoff weight and propellant tanking weights are part of the inputs required in addition to the propulsion system measurements for the differential equations which represent the vehicle's powered flight motion.

Many combinations of specific impulse, thrust, and flow rates, which will satisfy the tracked trajectory within its accuracy limitations, can be derived if the liftoff weight and propellant tanking weights are allowed to vary.

Mean sea level vehicle specific impulse is shown versus liftoff weight in the upper portion of Figure 5-8. All the values of specific impulse and liftoff weight which fall on the solid line will satisfy the tracked trajectory very closely. Any values which lie within the dashed lines will satisfy the tracked trajectory within its accuracy limitations.

Mean sea level vehicle thrust is shown versus mean vehicle total weight loss rate in the lower portion of Figure 5-8. Variations of $\pm$ ½% in liftoff weight are also shown in this figure.

Liftoff weight was determined to be about 929,725 lbs.* Thrust and weight loss rate were then derived which satisfied the tracked trajectory.

Mean sea level vehicle thrust is 1,339,800 lbs; mean total vehicle weight loss rate is 5244 lb/sec, and mean specific impulse is 255.5 sec.

The differences between the earth-fixed velocity and slant distance from the computed and tracked trajectories are shown versus range time in Figure 5-9. The maximum difference between the velocity for the actual and simulated trajectories was less than 0.5 m/s.

5.3.3 VEHICLE CUTOFF IMPULSE

The vehicle cutoff impulse as derived from the chamber pressure decay was 309,621 lb sec for the inboard engines and 273,758 lb sec

* This weight included an assumption of 1000 lbs of ice (located between the propellant tanks on the inside) which was carried through most of the powered flight.

for the outboard engines. The values obtained from guidance measurements were 296,065 lb sec for inboard engines and 240,639 lb sec for the outboard engines. These values are 2.5% (inboard) and 11.6% (outboard) lower than those derived from chamber pressure decay. Since there are still several uncertainties in computing the impulse from cutoff mass and guidance velocities, the values derived from launch pressure decay data are considered the best estimate of the actual SA-1 cutoff impulse values.

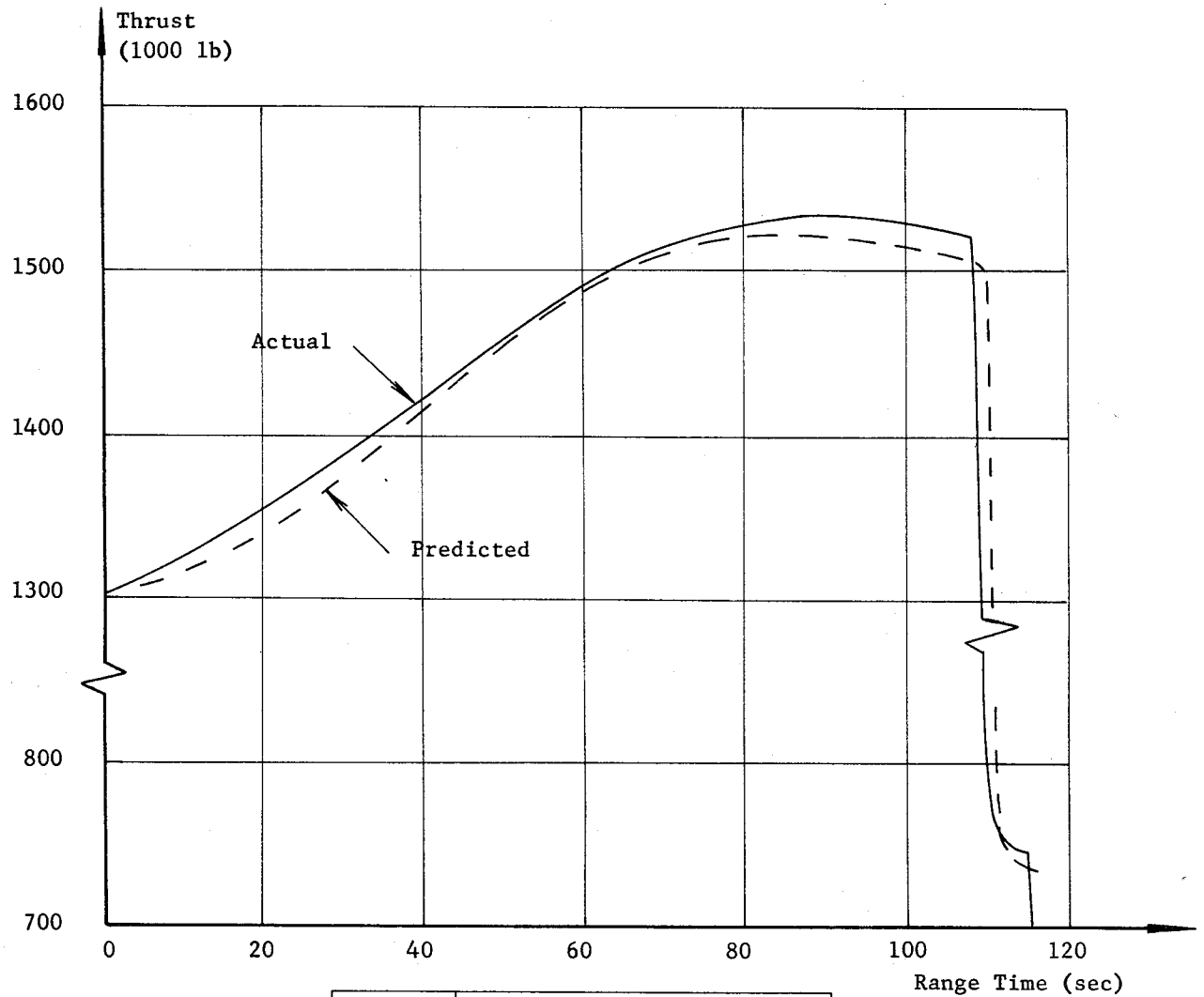

Fig. 5-6	
SA-1	VEHICLE LONGITUDINAL THRUST

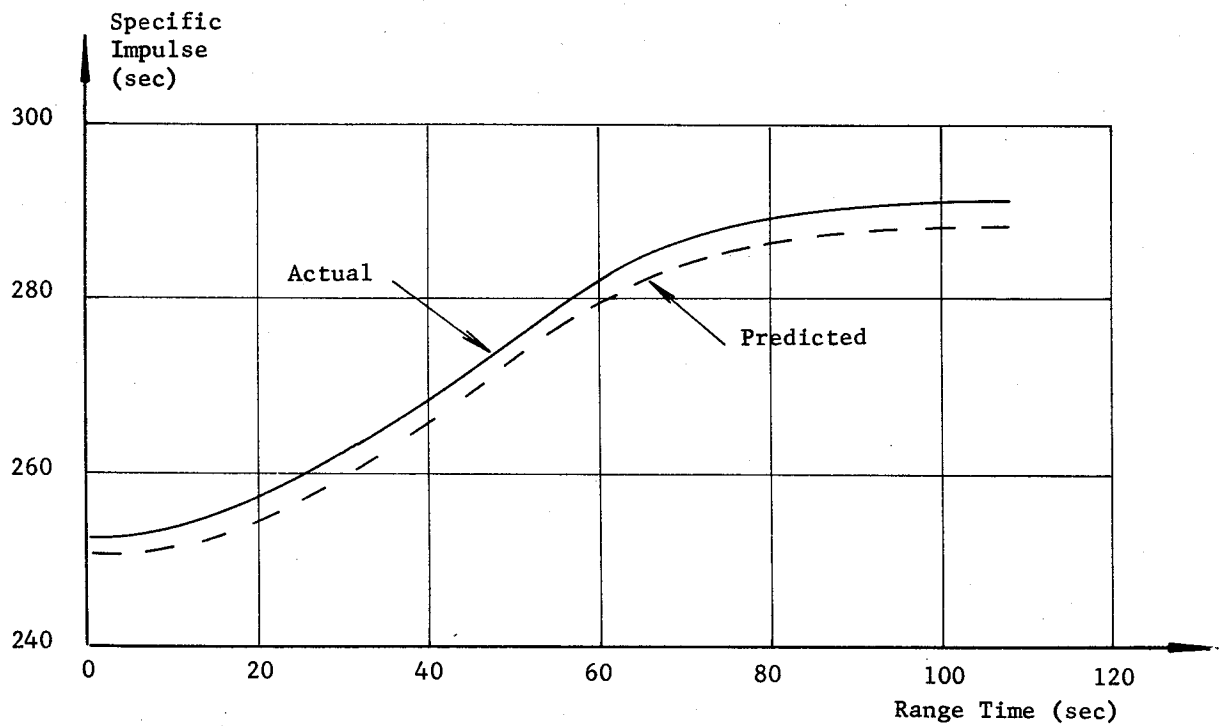

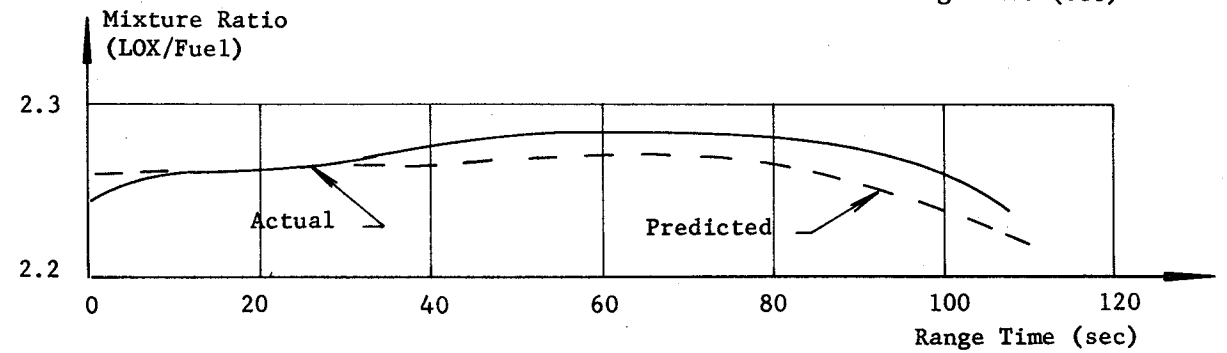

Fig. 5-7	VEHICLE SPECIFIC IMPULSE AND MIXTURE RATIO
SA-1	

CONFIDENTIAL

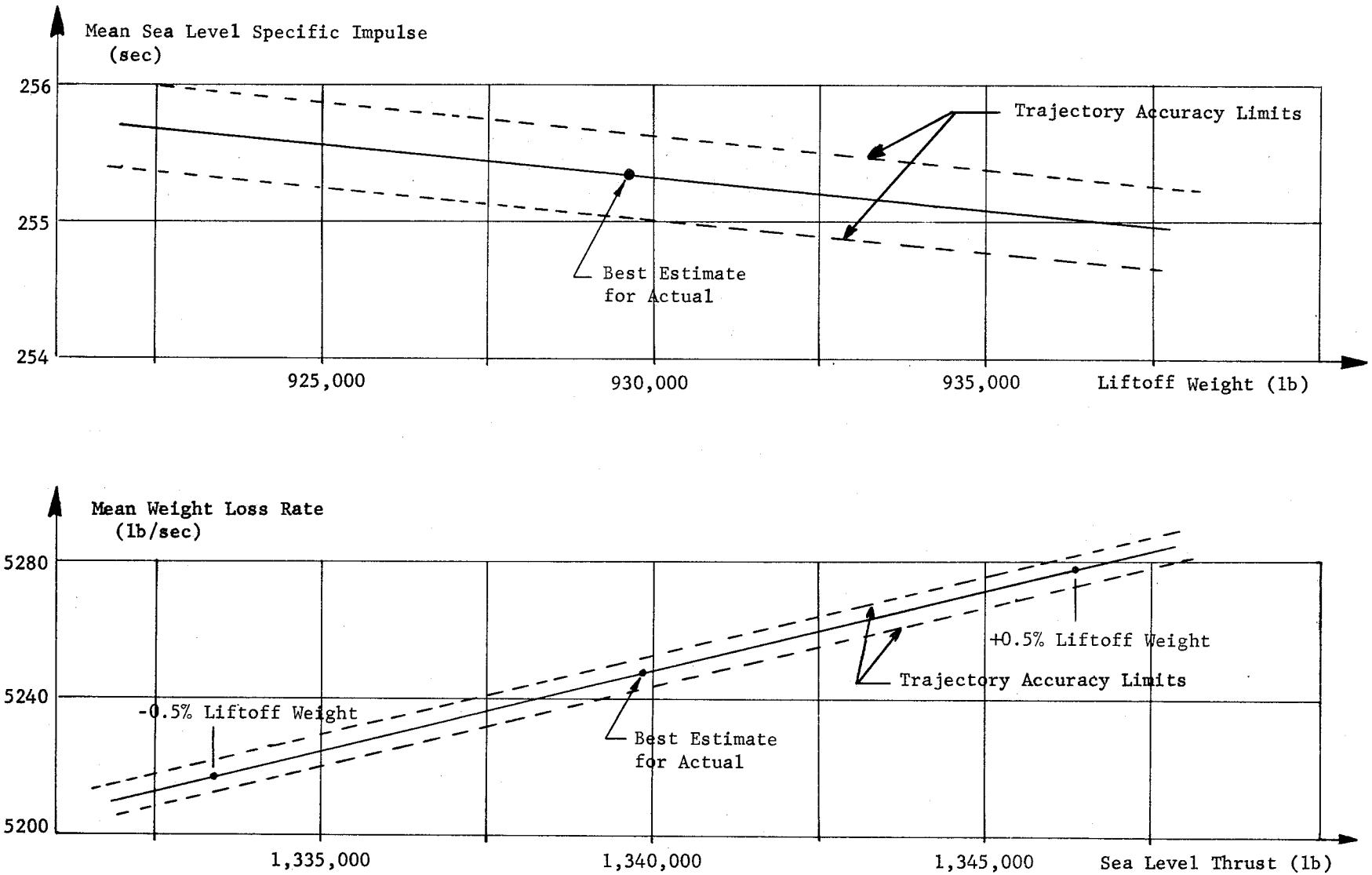

Fig. 5-8	VEHICLE SEA LEVEL SPECIFIC IMPULSE VERSUS LIFTOFF WEIGHT AND MEAN WEIGHT LOSS RATE VERSUS SEA LEVEL THRUST
SA-1	

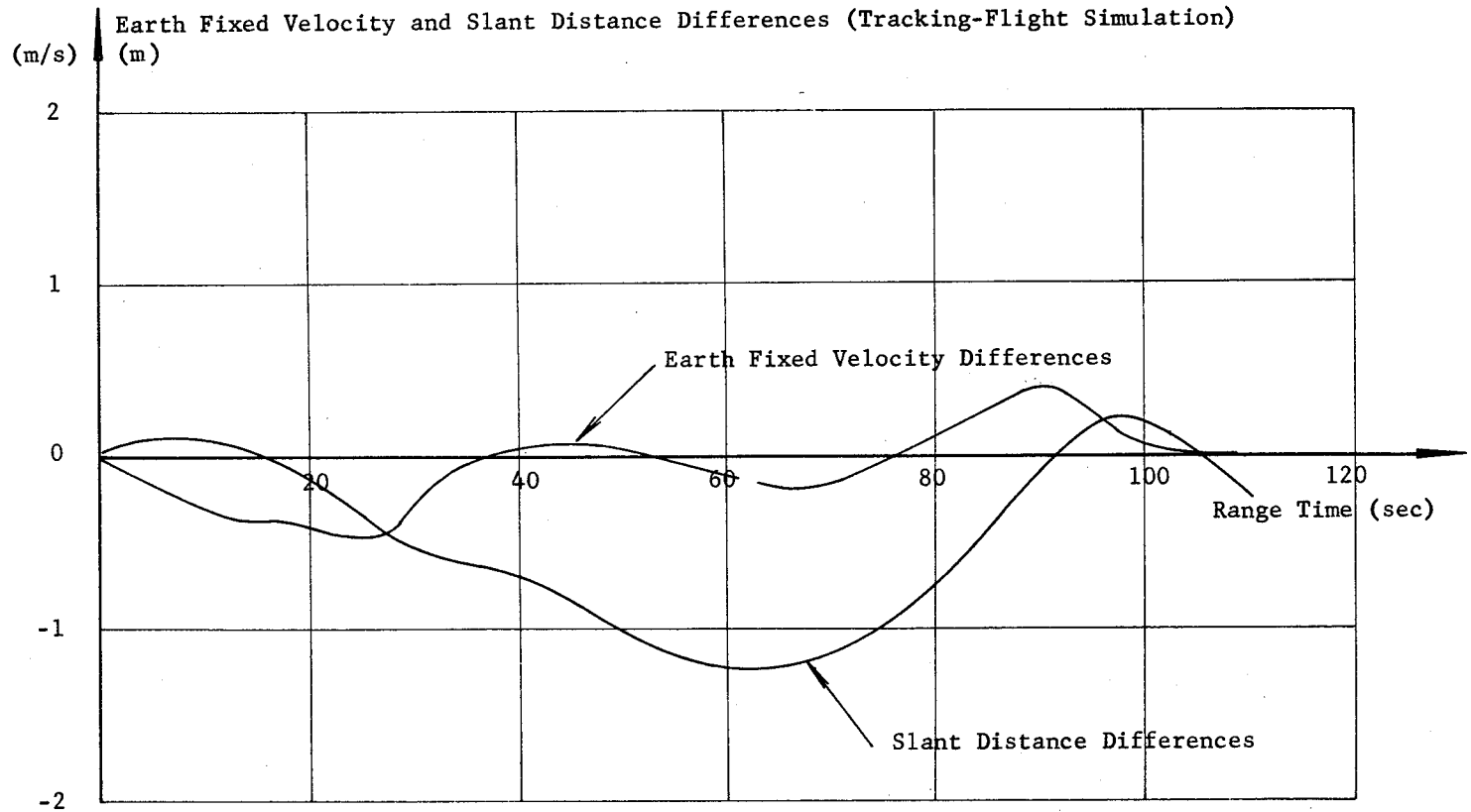

Fig. 5-9	EARTH FIXED VELOCITY AND SLANT DISTANCE DIFFERENCES (TRACKING-FLIGHT SIMULATION)
SA-1	

CONFIDENTIAL

5.4 PRESSURIZATION SYSTEMS

5.4.1 FUEL TANK PRESSURIZATION

The system operated satisfactorily throughout flight. Nitrogen pressure, supplied by 48 spheres, was 3010 psig at liftoff and gradually decayed during flight reaching a value of 1780 psig at cutoff.

Fuel tanks are initially pressurized in the automatic sequence, which starts with firing command. The time required to pressurize the tanks was 20 seconds, 5 seconds longer than required for SA-1 static test. The difference is due to the overfilling of fuel for the static firings which is required to assure LOX depletion. During initial pressurization, the spheres are replenished. Pressure in the fuel tanks is then maintained throughout powered flight by action of the pressure switch located in fuel tank F-1. This switch controls the operation of four pressurizing valves which were all operative at liftoff. (Figure 5-10 shows a schematic of the fuel pressurization system used on SA-1.) Pressure in the tanks gradually decreased from 16.7 psig after initial pressurization to 15.3 psig at liftoff. A maximum pressure of 17 psig was reached in the fuel tanks approximately 30 seconds of flight time and a minimum of 15 psig at 86 seconds (Fig. 5-11).

Due to pressure decay in the high pressure spheres (see Fig. 5-11) and the change in ambient pressure, varying nitrogen flow rates are required throughout flight. This is done by controlling the four pressurizing valves which are sequenced during powered flight by programmed tape. The pressurizing valves, which are normally closed, can be opened only when they are in the electrical circuit which is sequenced by the tape during flight. The following table gives the times at which the pressurizing valves have the capability of being controlled by the fuel tank pressure switch.

Time (sec)	Purpose
L.O. + 22	Fuel pressurizing valve #4 off, three valves still operative
L.O. + 31	Fuel pressurizing valve #2 off, two valves still operative
L.O. + 39	Fuel pressurizing valve #3 off, one valve still operative
L.O. + 76	Fuel pressurizing valve #3 on, two valves now operative
L.O. + 86	Fuel pressurizing valve #2 on, three valves now operative
L.O. + 104	Fuel pressurizing valve #4 on, four valves now operative

Based on telemetered data, the fuel container pressurization system performed as expected.

5.4.2 LOX TANK PRESSURIZATION

Prepressurization of the containers was achieved by the use of helium supplied through a ground source. It started at L.O. -115 seconds, and 78 seconds was required for the pressure to reach 44.2 psig. After engine ignition, LOX was bled to the heat exchanger where it was converted to the GOX used for tank pressurization. The GOX entered a diffuser which directed it to the center tank. From the center tank GOX was distributed to the four outer tanks through orificed lines to reduce the outboard tank pressure slightly. The LOX center tank pressure was higher to assure emptying of the center tank before the outboard tanks emptied. The LOX relief pressure switch located in top of the center tank attempts to maintain a pressure of 60 psia by operation of one 4 inch relief valve. Figure 5-12 shows a schematic of the LOX pressurization system.

During flight, the center LOX tank pressure was slightly higher (3 to 4 psia) than the expected 60 psia (Fig. 5-13). This is reflected in the outboard tank pressures' also being higher than expected. This higher tank pressure is not considered a significant problem and is attributed to higher performance of the heat exchangers. Pressure in the center tank rose to approximately 64 psia at 40 seconds flight time. The 4 inch relief valve was observed from camera coverage to open shortly after liftoff and is assumed to have remained open for the duration of flight since the center tank pressure was above the relief switch setting of 59.5 ± 1.0 psia. If the pressure rises above 65.5 ± 1 psia, an emergency switch, also located in the center tank, opens the 7 inch vent valve and the other 4 inch relief valve; however,

the emergency valves did not vent during powered flight. The gas temperature in the tanks (Fig. 5-13) also reflects the slightly higher than predicted tank pressure.

The supply of GOX was more than sufficient to pressurize the LOX containers. The LOX relief valve did not vent at a sufficient rate to maintain pressure in the center LOX tank at the switch setting. Instead, the pressure rose above the switch setting of 59.5 ± 1.0 psia.

5.4.3 CONTROL PRESSURE SYSTEM

The control pressure system operated satisfactorily during flight. This system consists of a high pressure supply (GN_2), a 750 psig regulator, and a regulated pressure manifold from which is taken control pressure for the control valves, vent valves, relief valves, prevalves pressure for gearbox pressurization, and pressure for calorimeter and LOX seal purges. At liftoff the high pressure supply sphere pressure was 2920 psig. The pressure dropped during flight to 2300 psig. This small drain on the supply indicates an overdesign in this system which should be re-evaluated. A reduction in the supply sphere volume for this system would result in a weight savings for future vehicles.

5.4.4 AIR BEARING SUPPLY

Blockhouse records show that the air bearing high pressure supply (XD39-11) was maintained at approximately 3100 psig which is within the redline limits of 3200 psig maximum and 2600 psig minimum. This pressure was also measured during flight (D39-11). Telemetered data showed that the pressure decayed during flight as expected. The low pressure GN_2 to the air bearing (D33-15) was constant throughout flight at approximately 31 psid which is 1 psi below the tolerance (Ref. para. 7.3.2).

Specifications for the air bearing inlet air temperature (XC56-15) state that the temperature must be maintained at 25 ± 1°C. Blockhouse records showed that the temperature was maintained within specified limits. They also show a cycling in the temperature of approximately 10.5 cycle/minute - probably the effect of a cycling of the thermostatically controlled inlet air heater used in the system.

Ambient air temperature in the ST-90 (XC57-15) was maintained within the specified range of 25° ± 2°C. Blockhouse records show a cycling in this temperature of approximately 1.7 cycle/minute which was the result of the ST-90 blower's cycling.

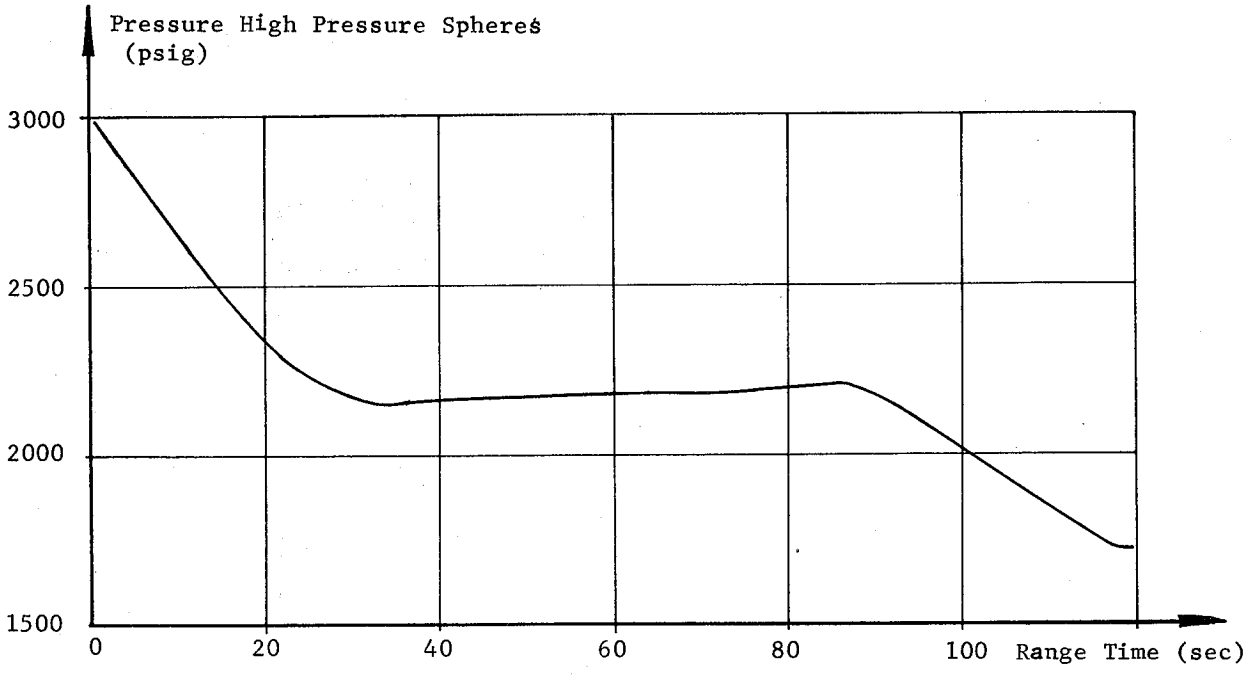

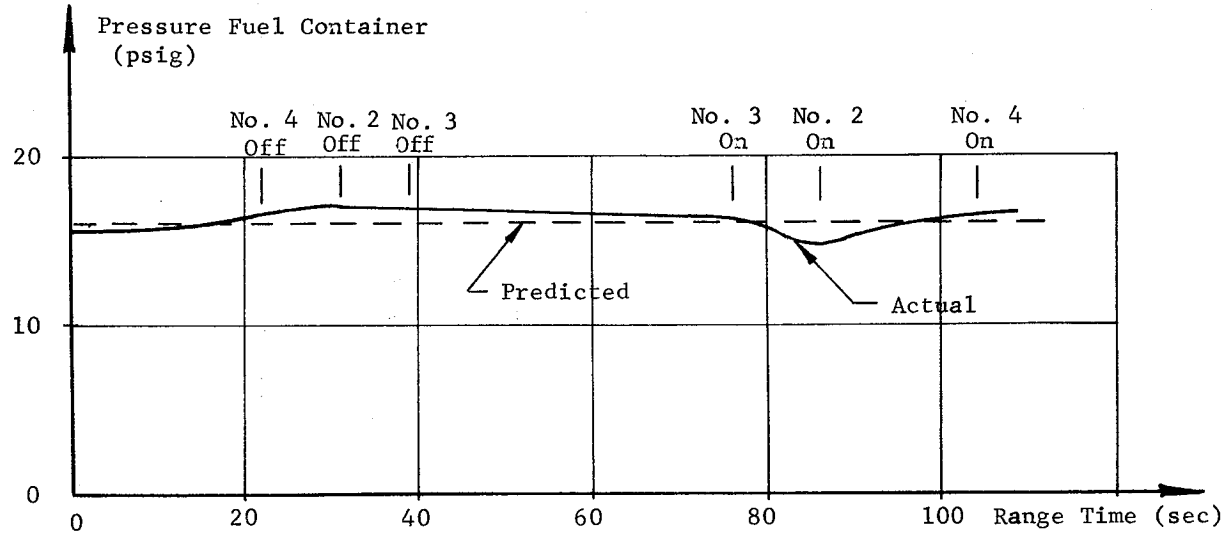

Fig. 5-11	PRESSURE HIGH PRESSURE SPHERES AND PRESSURE FUEL CONTAINER
SA-1	

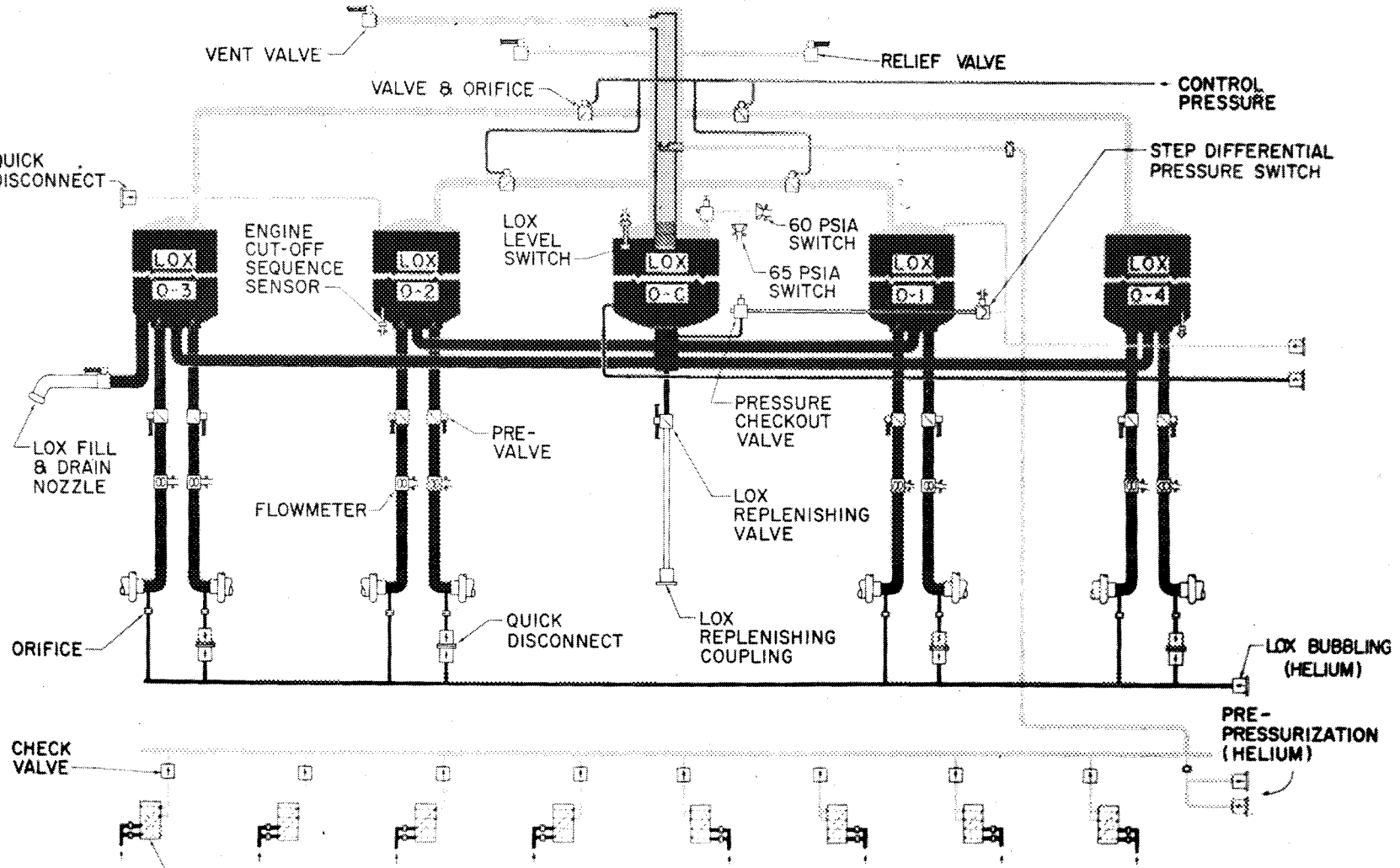

Fig. 5-12	SATURN S-1 STAGE LOX
SA-1	SUPPLY SYSTEM

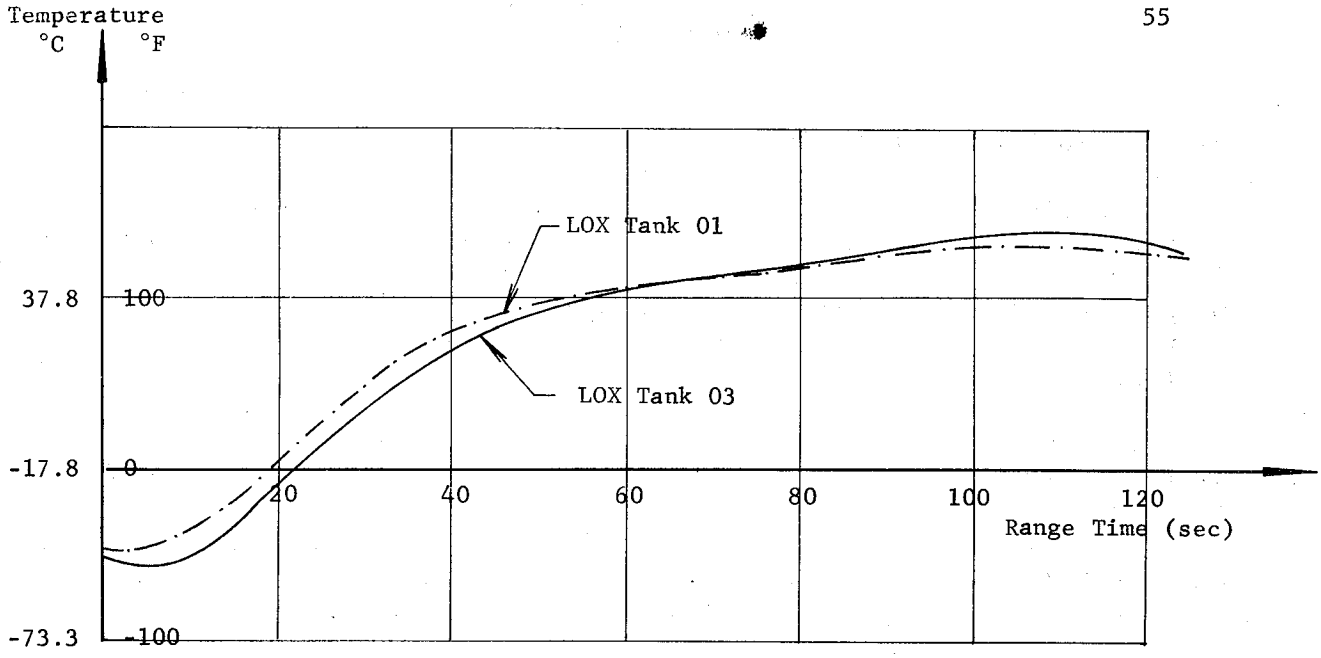

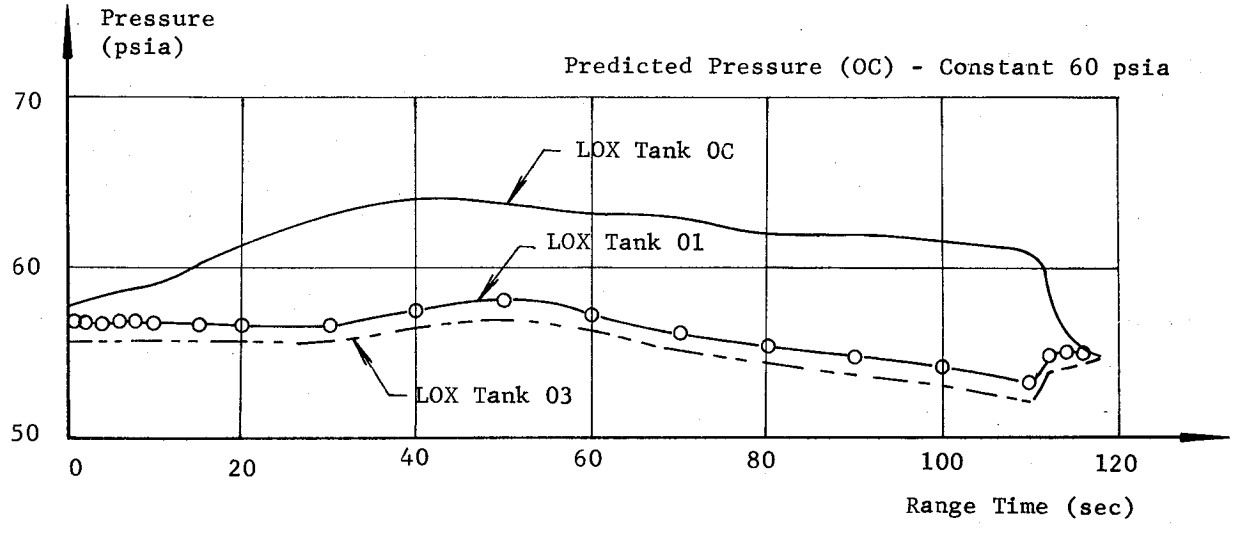

Fig. 5-13	TEMPERATURE AND PRESSURE IN LOX TANKS
SA-1	

5.5 VEHICLE PROPELLANT UTILIZATION

Vehicle propellant utilization was within 2 percent of predicted with a fuel level cutoff occurring 1.61 seconds earlier than predicted. The early cutoff was due primarily to performance dispersion and propellant sloshing. Performance dispersions, which may cause deviations in consumption rates, are variables in engine calibration, container pressures, propellant densities and propellant loading.

Fuel and LOX container levels for the last 26 seconds of propulsion system operation are shown in Figures 5-14, 5-15, and 5-16. The fuel container level (Fig. 5-14) was close to predicted, indicating a satisfactory fuel consumption rate. At outboard cutoff, the LOX level was approximately 28 inches while the predicted level was 15 inches. Gas breakthrough indicates that the center LOX container emptied close to the predicted time (110 seconds flight time).

Figure 5-17 depicts the total vehicle consumption which is close to predicted except from approximately 110 seconds to cutoff. The deviation during this time is attributed primarily to the early cutoff.

A tabulation of vehicle weights at various times is shown in Appendix D. Since propellants are loaded according to the fuel density at tanking, it is not necessary for the tanked LOX and fuel to agree with predicted; however, the total propellants loaded should and did correlate. The actual total weight deviations from predicted at inboard engine cutoff, outboard cutoff, and end of thrust decay (ETD) are due primarily to the early cutoff. The total propellant weight deviation at ETD was 14,200 lbs, of which approximately 8,600 lbs may be attributed to the early cutoff.

It is noted that an insignificant error in propellant tanking weights would create a large error in propellant weights at ETD. If LOX is overloaded 1 percent at ignition and the engines run as predicted, a deviation of 77 percent would be expected at ETD.

5.5.1 PROPELLANT UTILIZATION SYSTEM

General Description

The propellant utilization (PU) system was carried on the SA-1 flight test to determine the system reliability and performance but was not a control feature of the Saturn first stage. The system reliability and performance was satisfactory and in agreement with predicted data and propellant consumption data.

Each fuel and LOX container had two discrete level probes near the container bottom. The levels indicated by these probes were in fair agreement with the PU system; however, the discrete probe performance was poor and several probes failed.

The propellant utilization system (Fig. 5-18) contains four primary components:

1. Fuel Container ΔP Transducer
2. LOX Container ΔP Transducer
3. Propellant ΔP Ratio Computer
4. Helium Purge System

The fuel ΔP transducer measures the differential between the top container gas pressure and a pressure at a probe located near the container bottom. The function of the LOX ΔP transducer is similar.

Pressure from the upper and lower pressure taps of LOX container #4 and fuel container #2 are sensed by the propellant ΔP ratio computer. This instrument computes the ratio of LOX container ΔP to fuel container ΔP.

The purpose of the helium purge system is to prevent liquid from entering the submerged probes (LOX and fuel). The helium storage sphere is filled to 2100 psig and replenished through the long cable mast. The high pressure OK switch monitors the sphere pressure and actuates at an increasing pressure of 2100 psig ± 50 psig and drops out at 1940 psig minimum. From five seconds flight time to cutoff, helium flows from the high pressure sphere through a regulator (450 psig outlet), a by-pass control valve, a constant flow regulator and into the container. The function of the by-pass control valve is to increase the purge from a predetermined time to 5 seconds flight time by directing the helium flow through the by-pass orifice.

PU System Performance

LOX container #4 ΔP transducer (Fig. 5-19) indicates a slightly higher than predicted differential pressure, and fuel container #2 ΔP transducer (Fig. 5-19) indicates a slightly lower than predicted differential pressure. A ΔP ratio was computed from the LOX and fuel container ΔP data. This ratio was in agreement with the output of the propellant ΔP ratio computer (Fig. 5-19); however, the computer ΔP ratio was higher than predicted and the computer reached its upper limit (1.8) at approximately 93 seconds range time. The range for this measurement will be changed to 2.5 for future flight tests.

Figures 5-14 and 5-15 depict the liquid level in LOX container #4 and fuel container #2 during the latter part of powered flight. These levels were calculated using the container differential pressures, the vehicle longitudinal acceleration, and the propellant densities. Calculated LOX level was higher than predicted, and calculated fuel level was slightly lower than predicted (which is in agreement with the original ΔP data and propellant consumption data). Figure 5-15 also shows the time and level of several other measurements (cutoff probes, level discrete probes, and slosh probes). It is noted that the PU system was not designed to give an exact level; however, the accuracy of the calculated levels are considered to be good.

Liquid Level Discrete Probe Performance

Two discrete level probes were located at the bottom of each propellant container to obtain propellant level information toward the end of powered flight. Several probes did not give a signal even though the level was considered to have passed the probe. An exact time (corresponding to a liquid level) could not be established, since propellant sloshing caused the probes to give several signals. Even though the over-all probe performance was poor, a fair agreement between the information from several level probes and the propellant utilization system was obtained. (Ref. para. 12.2)

Conclusions

The propellant utilization system performance was satisfactory and in agreement with propellant consumption data. The liquid level discrete probe performance was not satisfactory due to either a measurement failure or propellant sloshing.

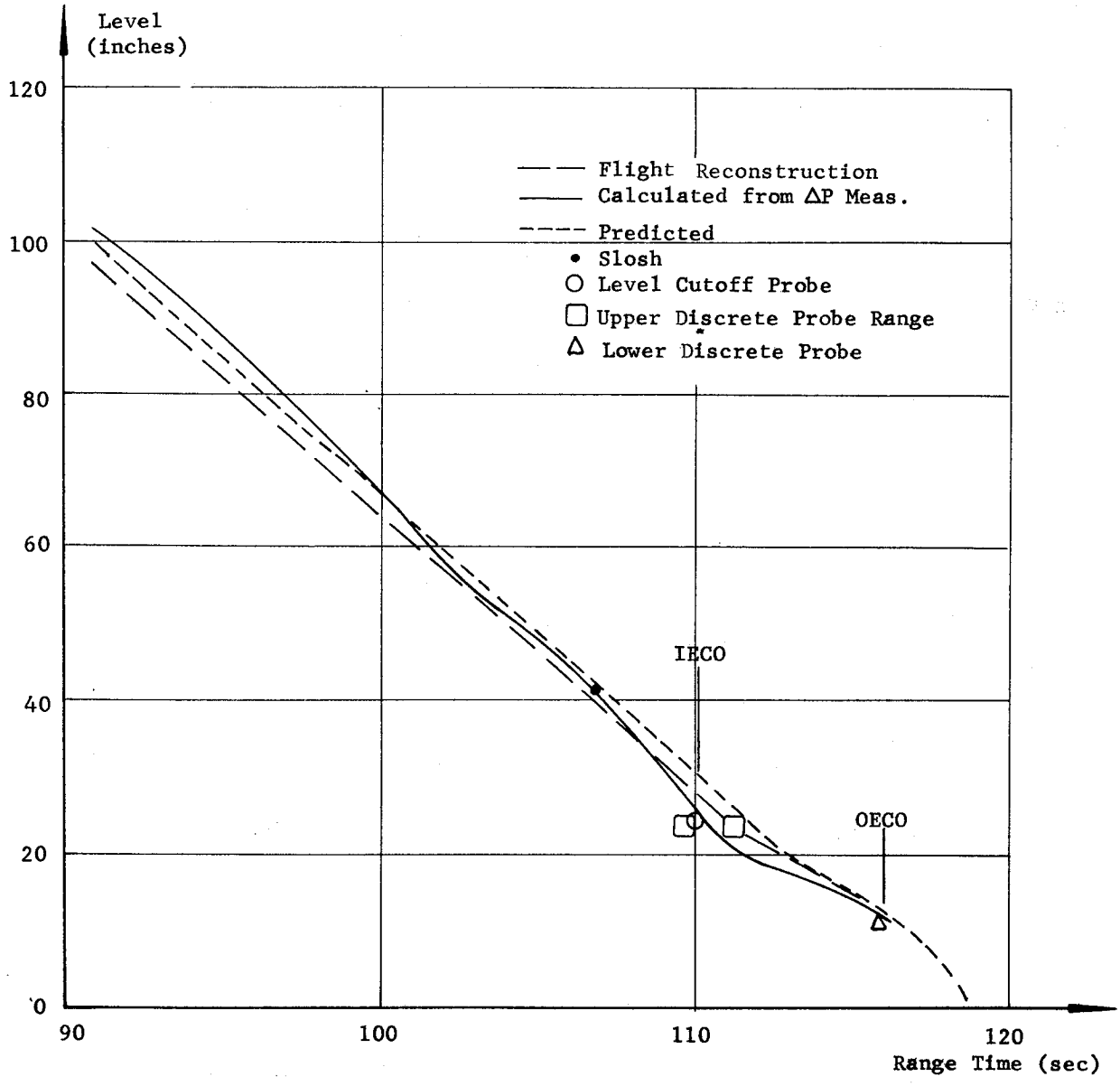

Fig. 5-14	PROPELLANT LEVEL FUEL CONTAINER No. 2
SA-1	

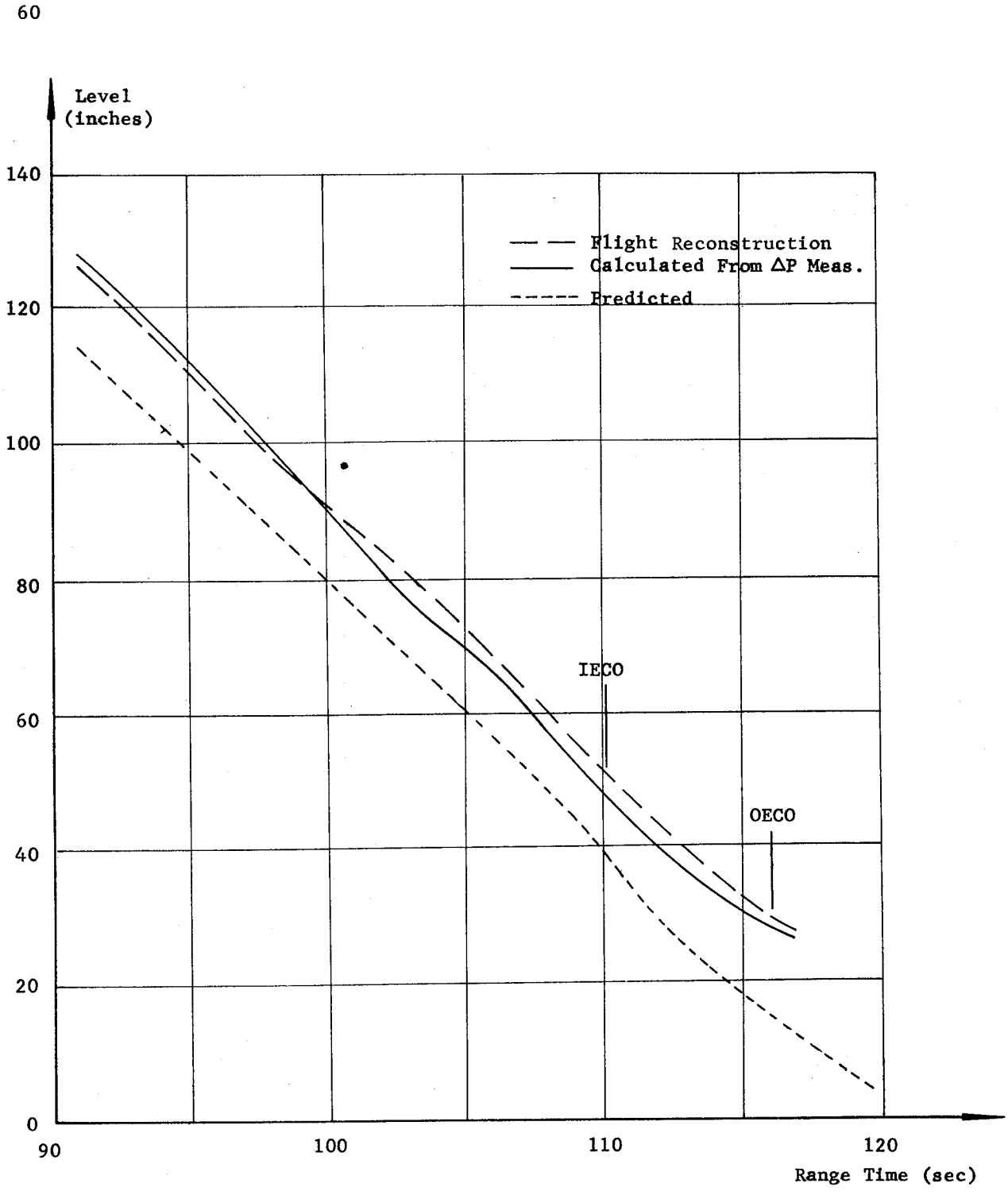

Fig. 5-15	PROPELLANT LEVEL LOX CONTAINER NO. 4
SA-1	

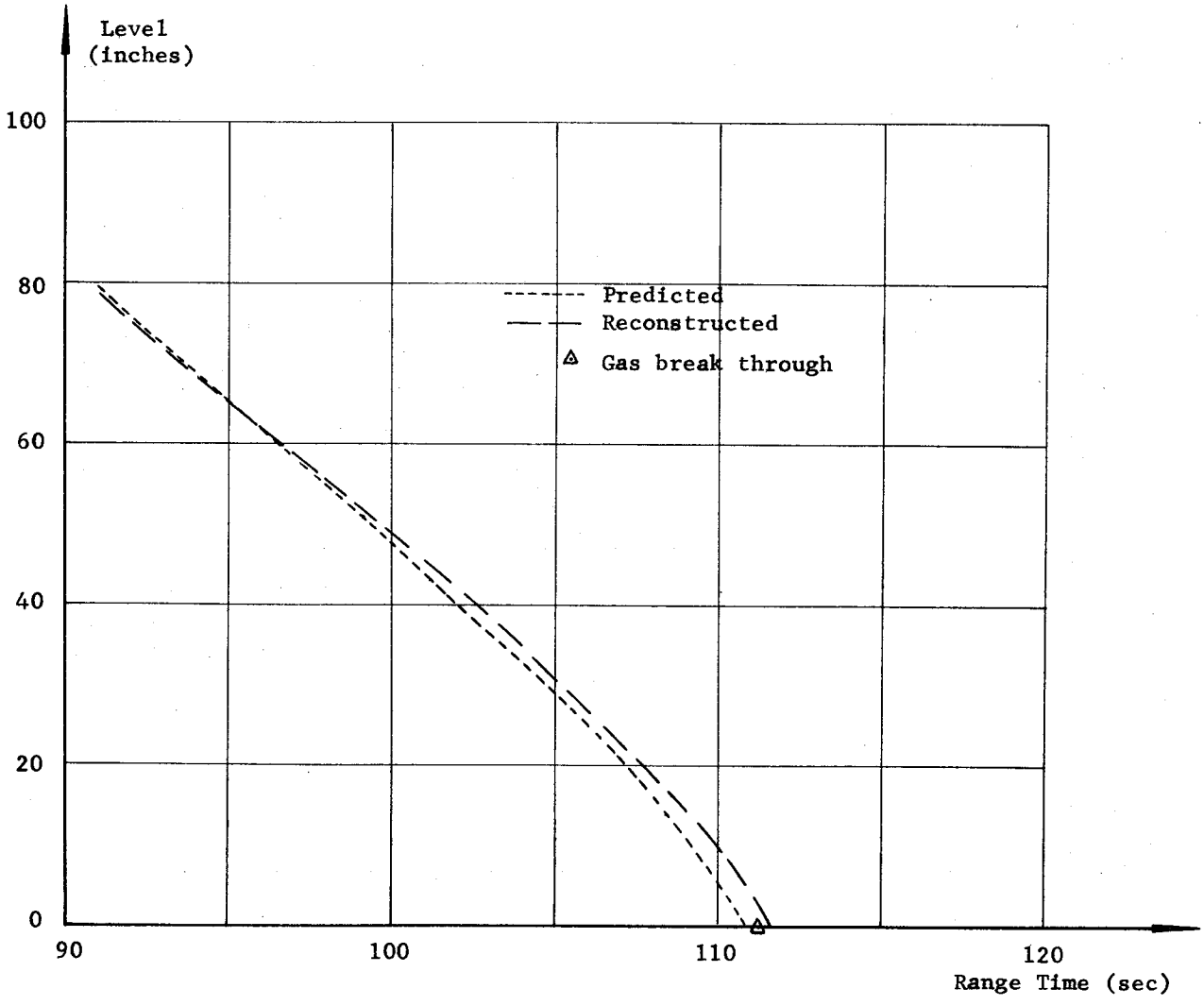

Fig. 5-16	PROPELLANT LEVEL LOX CENTER CONTAINER
SA-1	

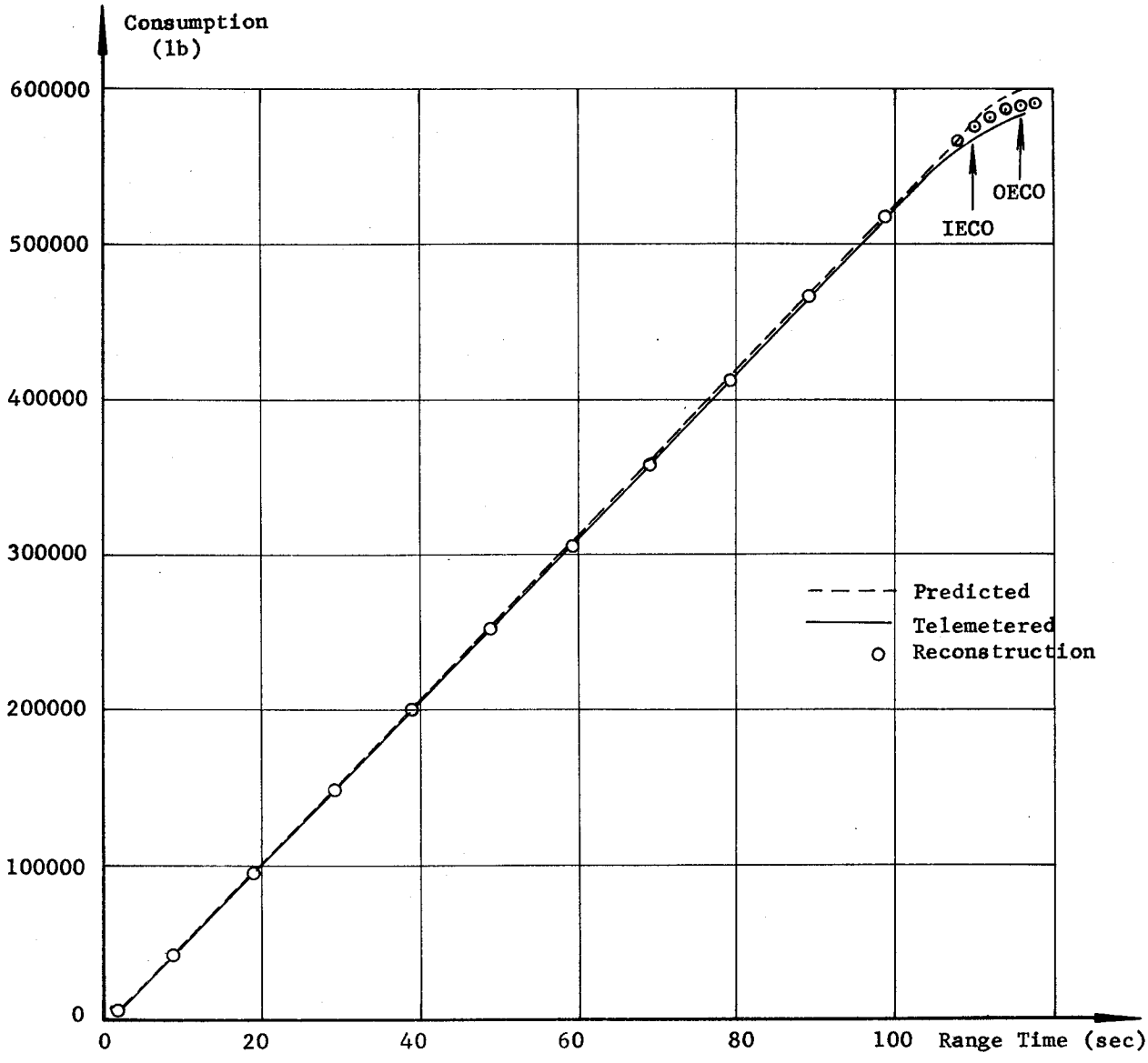

Fig. 5-17	VEHICLE TOTAL PROPELLANT CONSUMPTION
SA-1	

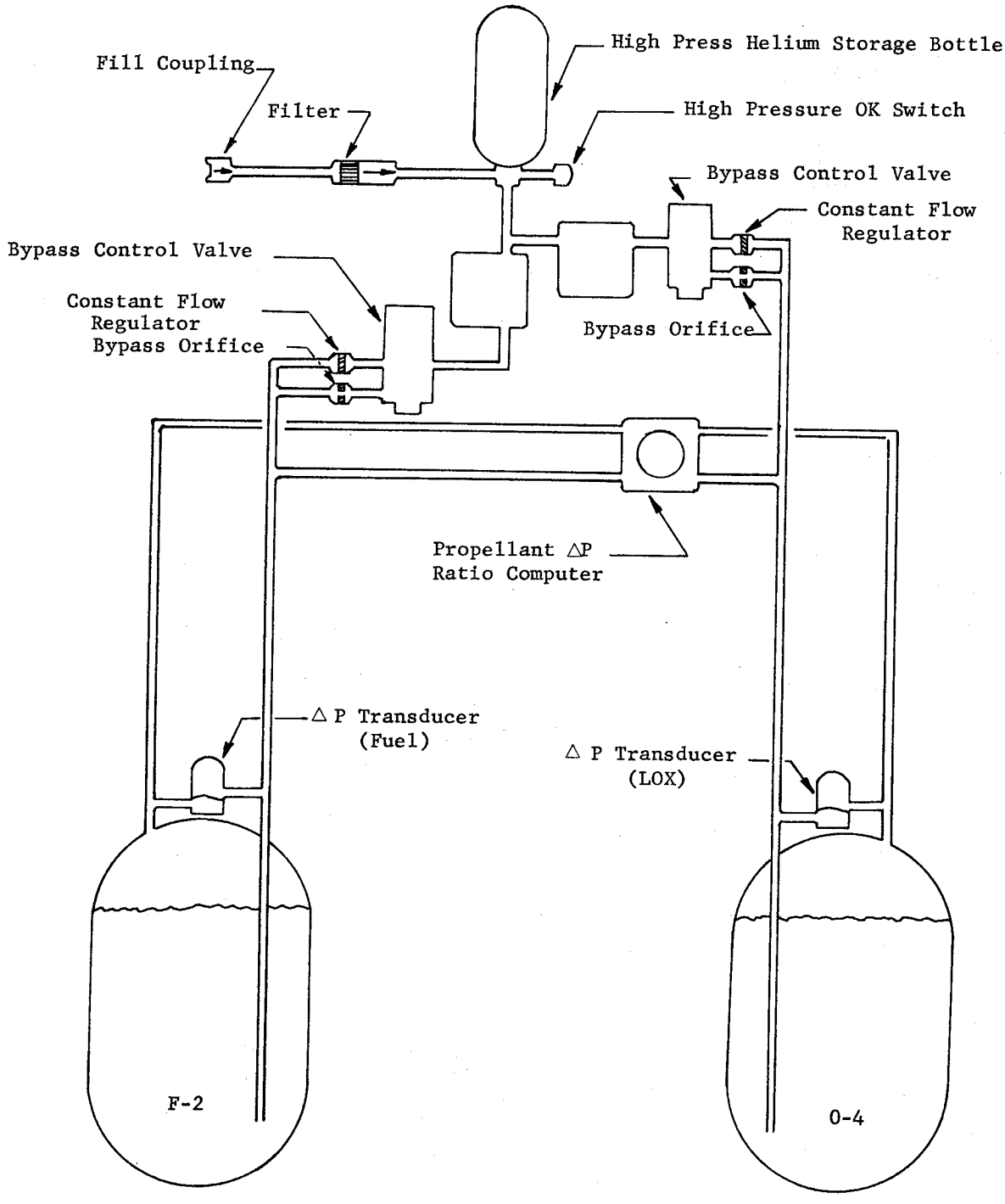

Fig. 5-18	PROPELLANT UTILIZATION SYSTEM
SA-1	

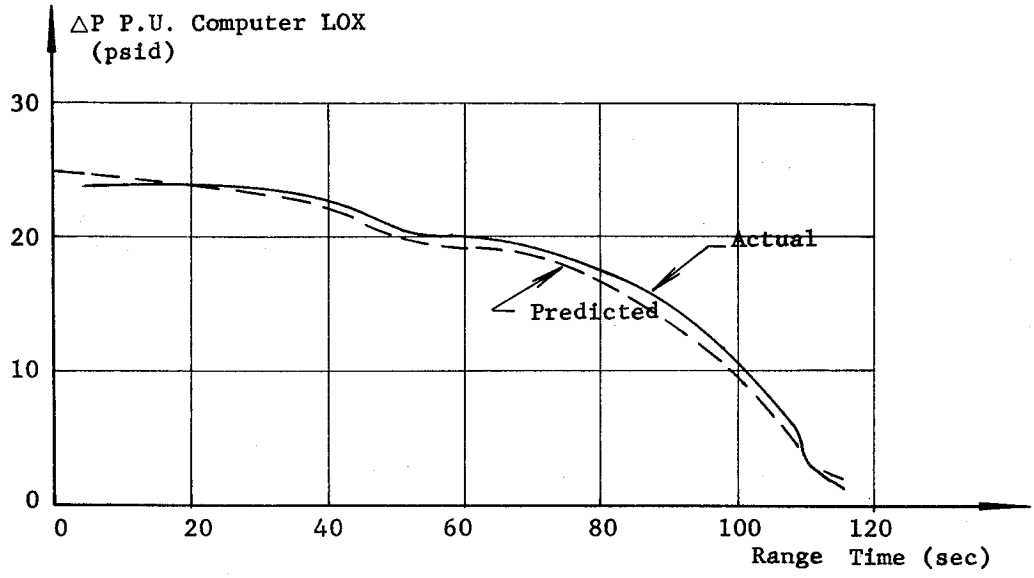

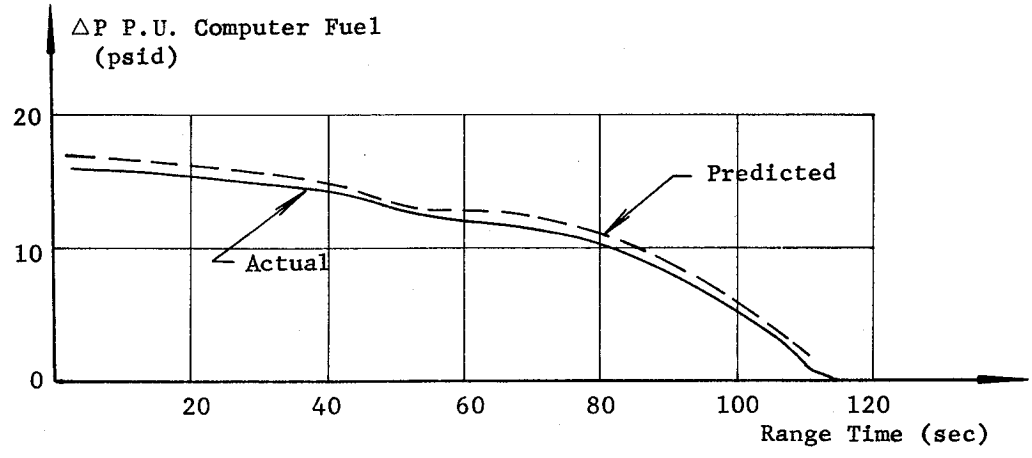

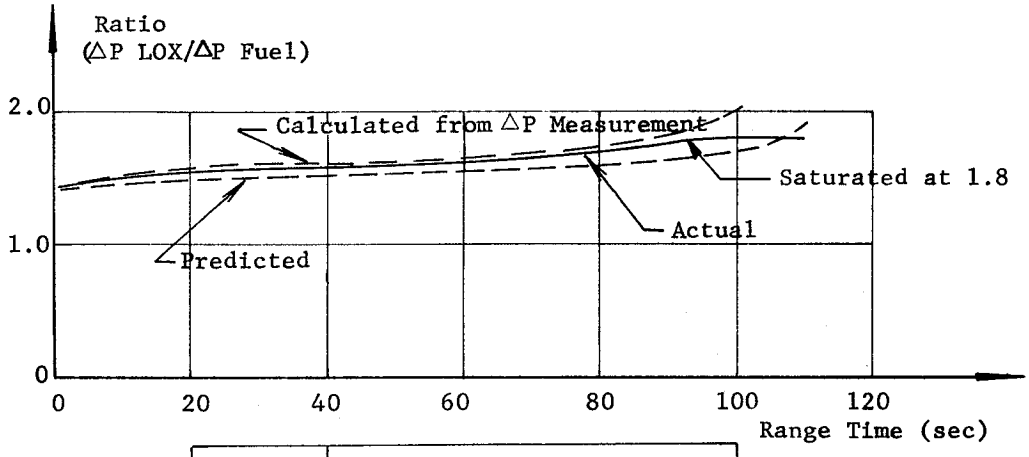

Fig. 5-19	COMPARISON OF MEASURED AND PREDICTED VALUES FROM P.U. SYSTEM
SA-1	

5.6 MASS CHARACTERISTICS

Mass characteristics of SA-1, including predicted and actual values, are presented in Appendix D. The mass characteristics of all dry assemblies and water ballast are the same as predicted values because no measurements were made for these items by LOD. Since these items were not weighed, a possible deviation of $\pm$ 2500 pounds should be considered in addition to the deviation shown in Appendix D.

To obtain agreement between propulsion system performance as established by flight reconstruction and flight trajectory simulation, it was necessary to adjust the original vehicle dry weight and water ballast by + 2000 pounds and the original LOX tanking weight by + 2500 pounds (.5% of liftoff weight). The additional 2500 pounds of LOX does not agree, however, with the LOX weight determined by the propellant loading system. This discrepancy is being investigated further. The flight trajectory simulation also considered 1000 lbs of ice on the LOX tanks at liftoff and carried this ice throughout most of the powered flight.

6.0 (C) CONTROL

6.1 SUMMARY

With the exceptions of the noted disturbances in roll due to propellant sloshing, the operation of the control system from the design and hardware standpoint was entirely satisfactory. Indications are that the compliance and bending problems which appeared during static testing were adequately overcome or did not materialize.

One of the few problems encountered on the SA-1 flight was an instability in sloshing, predominantly in the roll mode. However, even though there was more sloshing than desired, it did not approach the point of endangering the vehicle. Sloshing caused oscillations in all three flight planes during the last portion of powered flight. The maximum amplitudes of oscillations in the engine deflections due to sloshing were $\pm$ 0.4 deg in pitch, $\pm$ 0.5 deg in yaw, and $\pm$ 0.2 deg in roll.

The most distinct vehicle reactions occurred in roll and became apparent after 90 seconds of flight. A peak amplitude of 2.5 deg/sec occurred in the roll angular velocity at 107 seconds due to the sloshing. Maximum amplitude of sloshing measured in a 70 inch LOX tank was 3 inches at 107 seconds. This sloshing instability was due to a combination of two factors; first, the phase lead of the roll control filter became insufficient at the sloshing frequency. Secondly, the propellant damping was low because of lack of baffles in the lower portion of the outer tanks. The sloshing damping after IECO was due to a decrease in sloshing frequency, and the amplitudes were quickly damped out after OECO.

The step tilt program used on SA-1 did not appear to cause any problems. Actuator deflections of 2 deg resulted from the program pulses as expected.

A fairly high wind environment was encountered. The maximum wind speed during high dynamic pressure of 46.6 m/sec occurred at 12.3 km corresponding to about 63.5 seconds flight time. The maximum wind shear encountered was 0.04 m/sec/m over a 250 m interval. These winds were adequately handled by the vehicle.

There were only relatively minor attitude deviations occurring during the outboard thrust decay period. Analysis of the flight measurements indicated an average thrust vector angularity of the engines during thrust decay to be 0.98 deg in pitch and -0.52 deg in yaw. The angles, angular rates, and angles of attack were well within the design limits being used in separation studies for Block II.

The maximum load on the control actuators was 4300 lbs during the high q period of flight, well below the design limits.

6.2 S-I CONTROL ANALYSIS

6.2.1 PITCH PLANE

Attitude control during the S-I powered flight phase was obtained by swiveling (± 7 deg capability) the four outboard engines. No attitude control was provided on SA-1 after outboard engine cutoff (OECO).

Liftoff signal was given by SA-1 at 0.89 seconds range time, 3.92 seconds after ignition command. Immediately after liftoff the vehicle started a slight pitching motion downrange (Figure 6-1). A maximum angle of 0.3 deg was reached 2 seconds after liftoff. The maximum engine deflection during this transient was 0.3 deg. While the vehicle was pitched over slightly downrange, the flight path actually went in the reverse direction (see para. 4.3.1).

Attempts to duplicate the liftoff motion with calculated six-degree-of-freedom trajectories have not been successful for both the flight path motion and vehicle attitude. Using wind measurements gives essential agreement with the tracking results but not with the attitude measurements. It appears that there are probably some additional forces and moments acting on the vehicle which are not accounted for (the variation of the wind along the vehicle length has been considered). Possibly the flame deflector in the launch pedestal may be causing some significant circulation effects resulting in the observed vehicle attitude deviations.

Vertical flight was maintained until 17.89 seconds range time when the tilt program was first initiated (Figure 6-2). The tilting program, which was based on the case of only seven engines operating, was stored on magnetic tape. The SA-1 tilt program used a constant tilting rate of 0.667 deg/sec. To properly shape the trajectory using a constant tilting rate, it was necessary to arrest the tilt program periodically. The actual times (range time) the tilt program was started and stopped are listed below.

Started (sec)	Stopped (sec)	Tilt Increment (deg)
17.89	20.89	2
32.39	42.89	7
46.79	85.79	26
86.99	95.99	6
97.19	100.19	2

Final tilt arrest was made at 100.19 seconds with a tilt angle of 43 deg from the launch vertical.

The tilt program used for SA-1 employed step functions for the angular rate. The effect of these steps on the engine actuator response can be seen in Figure 6-1. A maximum engine deflection of 2.1 deg with a rate of 9 deg/sec resulted from the first tilt pulse at 17.89 seconds. This is in good agreement with the Astronics Division's analog simulation. The tilt program effect can also be clearly seen in the pitch angular velocity shown in Figure 6-1.

When the tilt program was arrested at 100.19 seconds the pitch local angle of attack was near maximum, 9.6 degrees. This angle of attack was almost entirely due to the tilt program and trajectory shaping. The angle of attack was reduced after this time (see Figure 6-3).

Around 28 seconds the angle of attack control gain (b_o) was phased into the control loop. At this time the average pitch local angle of attack was only 0.2 deg with a wind component velocity (W_x) of 6 m/sec from the rear.

The maximum wind component in the pitch plane as measured by Rawinsonde during the high dynamic pressure region of flight was 37 m/sec occurring at 65 seconds at an altitude of 12.8 km. The local pitch angle of attack at this time was -8.6 deg. Approximately 65% of this angle of attack can be attributed to the winds and the fact that the control gains used did not correspond exactly with the drift minimum concept. (If drift minimum control gains had been used, the local angle of attack would have been -7.4 deg.) The remaining portion is attributed to the tilt program's being optimized for the seven engine case.

Figure 6-3 shows a comparison of the pitch component winds from three sources of information - rawinsonde, rocketsonde and angle of attack winds. The angle of attack winds (solid line) are based on measurements made on-board the vehicle of attitude and angle of attack which are combined with trajectory angles and velocity components obtained from tracking. Local angles of attack as measured by the Topp indicators were used in this calculation.

The solid circles from 109 to 117 seconds are rocketsonde measured wind velocity components. These are considered more reliable than the angle of attack winds determined from the vehicle measurement because of the low vehicle dynamic pressure at this time. Rocketsonde measurements showed a maximum total wind velocity of 86 m/sec at 52 km altitude corresponding to the vehicle range time of 113 seconds.

All four outboard engines are deflected for control. The average of these four telemetered deflections in the pitch direction is shown in Figure 6-1. Also shown for comparison are the results from a six degree of freedom trajectory calculation (circled points). This calculated trajectory was based on the best estimate of the actual weights and engine cluster performance. In addition, an idealized control equation was used which is actually not very representative of the actual control system action during transients and oscillations. Even with these limitations, the agreement between the calculated and telemetered engine deflections is good.

The telemetered pitch normal acceleration from the control accelerometer is shown in Figure 6-4. This accelerometer was not in the control loop but was flown as a passenger for environmental information. Telemetered acceleration is shown in the upper portion of Figure 6-4, and the calculated is shown below. The calculated is based on telemetered angles of attack and engine positions and assumes a rigid body. A maximum normal acceleration of 2.3 m/sec^2 (0.23 g's) was experienced in pitch at 62.5 seconds. Except for the higher frequency oscillations, telemetered acceleration was in good agreement with the calculated acceleration.* This accelerometer was located at station 879 on the web of the spider beam 44.5 inches from the longitudinal axis towards fin position III.

Very noticeable oscillations showed up in most of the pitch attitude measurements after 100 seconds. These were the result of a propellant sloshing instability during this time. The predominant effects were experienced in roll and will be discussed later in paragraphs 6.2.3 and 6.3.

* Maximum difference was 0.2 m/sec^2.

TABLE 6-I

FLIGHT MECHANICAL TELEMETER BIASES
(TELEMETERED MINUS TRUE)

Telemetered Variable	Measurement Number	Bias Used to Adjust Telemetry	Bias Calculated from 25-90 sec	Standard Deviation of Calculations
Local Angle of Attack I	F-16-30	0.35 (deg)	0.339 (deg)	0.025 (deg)
Local Angle of Attack III	F-18-30	0 (deg)	(1.)	
Local Angle of Attack II	F-17-30	0 (deg)	-0.027 (deg)	0.025 (deg)
Local Angle of Attack IV	F-19-30	0 (deg)	(2.)	
Program Minus Platform Pitch Angle	H-1-15	-0.26 (deg)	-0.294 (deg)	0.014 (deg)
Platform Yaw Attitude Angle	H-2-15	-0.28 (deg)	-0.171 (deg)	0.014 (deg)
Normal Acceleration Pitch	F-10-11	0 (m/sec^2)	-0.018 (m/sec^2)	0.059 (m/sec^2)
Normal Acceleration Yaw	F-11-11	-0.52 (m/sec^2)	-0.606 (m/sec^2)	0.059 (m/sec^2)
Actuator Pos. 1 Pitch	G-1-1	0.20 (deg)	0.158 (deg)	
Actuator Pos. 2 Pitch	G-1-2	0.10 (deg)	(3.)	0.010 (deg)
Actuator Pos. 3 Pitch	G-1-3	0.10 (deg)		
Actuator Pos. 4 Pitch	G-1-4	0.35 (deg)		
Actuator Pos. 1 Yaw	G-2-1	0 (deg)	-0.146 (deg)	
Actuator Pos. 2 Yaw	G-2-2	-0.28 (deg)	(4.)	0.010 (deg)
Actuator Pos. 3 Yaw	G-2-3	0 (deg)		
Actuator Pos. 4 Yaw	G-2-4	-0.27 (deg)		

(1.) Total bias in local angles of attack I and III
(2.) Total bias in local angles of attack II and IV
(3.) Average bias in actuator positions 1, 2, 3, 4, pitch
(4.) Average bias in actuator positions 1, 2, 3, 4, yaw

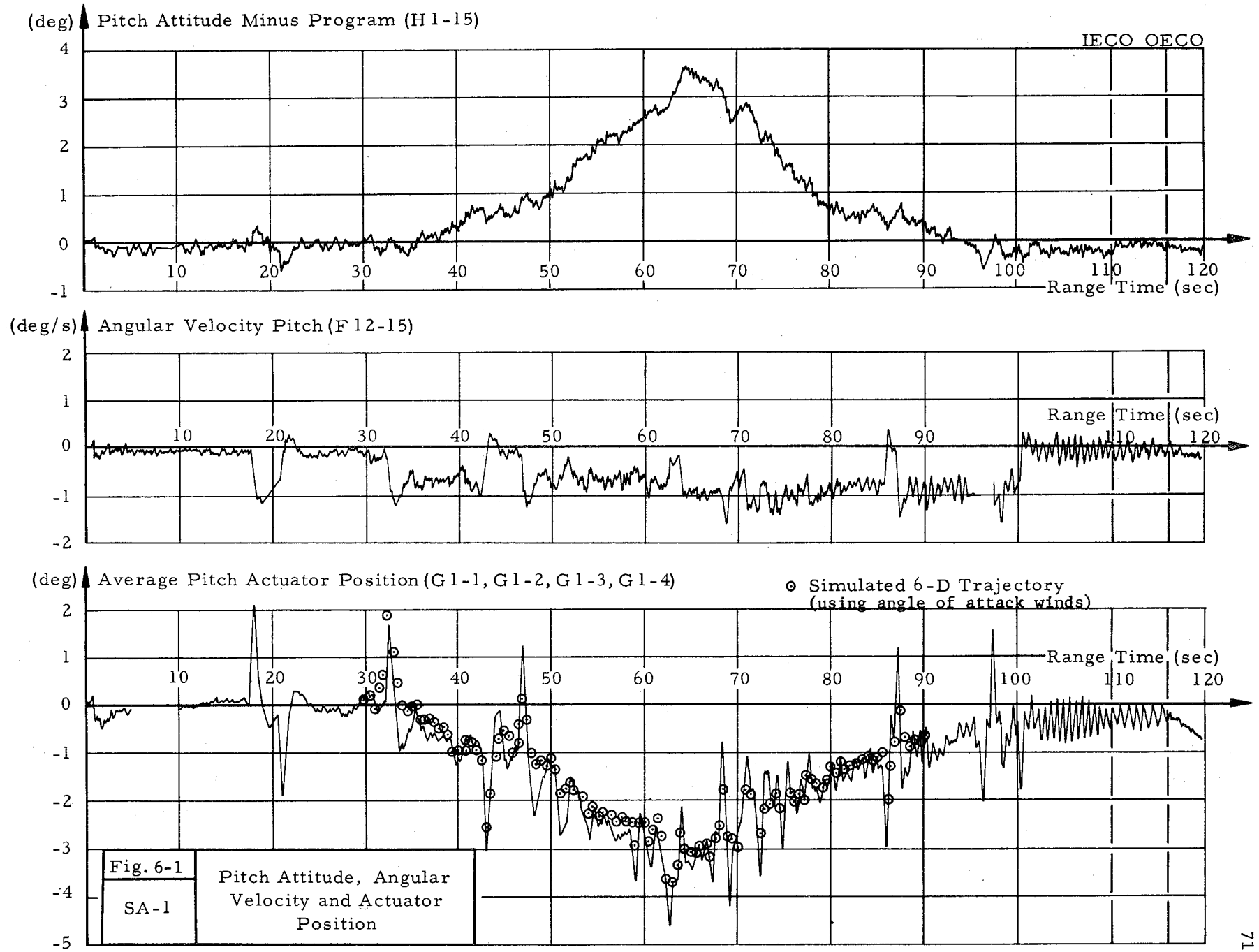

Fig. 6-1
SA-1

Pitch Attitude, Angular Velocity and Actuator Position

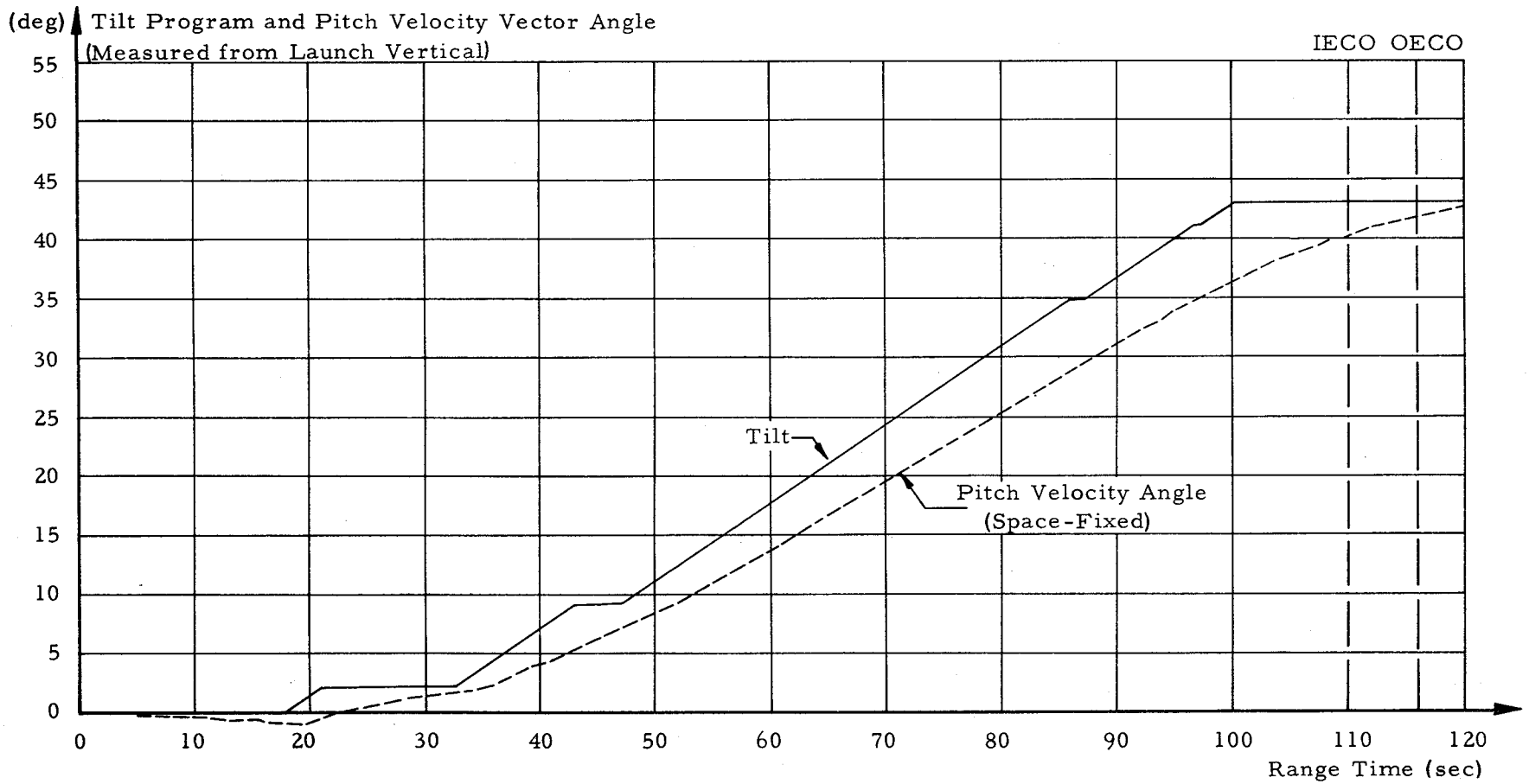

Fig.6-2	Tilt Program and Pitch Velocity Vector Angle
SA-1	

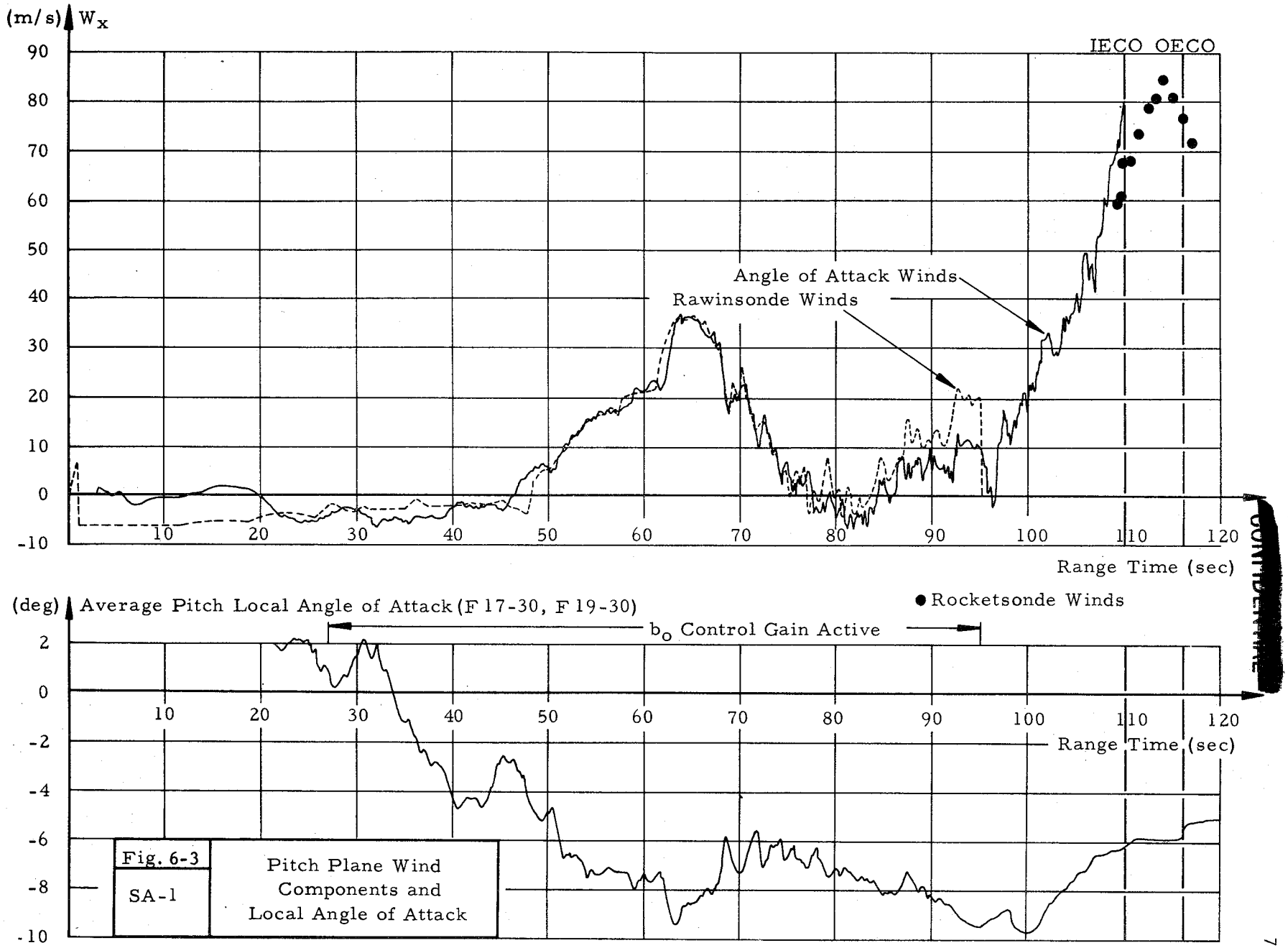

Fig. 6-3
SA-1
Pitch Plane Wind Components and Local Angle of Attack

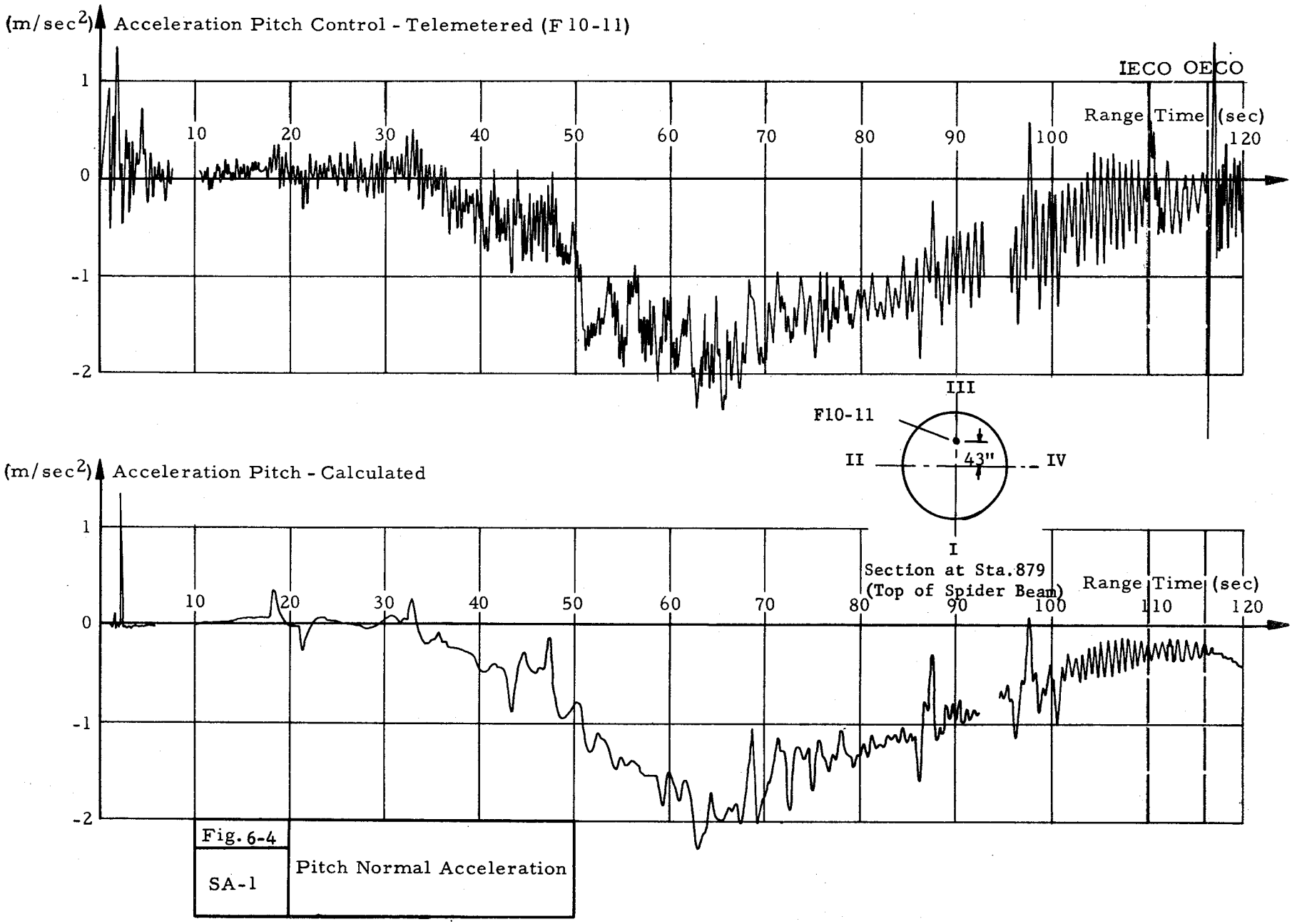

Fig. 6-4

SA-1

Pitch Normal Acceleration

6.2.2 YAW PLANE

Immediately after liftoff the vehicle yawed slightly to the right an average of 0.2 degree with accompanying engine deflections (Figure 6-5). This angle was maintained essentially until 32.5 seconds and was probably caused mostly by winds.

Yaw plane wind components shown in Figure 6-6 were very light until the region around maximum dynamic pressure (60-70 seconds) They also reached a comparable magnitude around vehicle cutoff. The circles shown in the upper portion of Figure 6-6 were the wind components determined by Rocketsonde measurements. Angle of attack winds in yaw as determined from the Topp local angle of attack indicators onboard the vehicle are considered unreliable after 106.5 seconds. Rocketsonde winds do appear to be reliable. Dynamic pressure at this time was 0.33 psia.

The maximum yaw wind component was -30 m/sec, occurring once at 63.5 seconds and again at 114 seconds. When the angle of attack control gain was phased into the control loop at 28 seconds the yaw wind component was essentially zero. The corresponding local angle of attack at this time was 0.5 degree.

Averages of the local measured angles of attack in yaw are shown in the lower portion of Figure 6-6. Yaw attitude angle, angular velocity, and average actuator deflections in yaw are shown for the entire powered flight phase in Figure 6-5.

Except for the period after 90 seconds, oscillations in the engine yaw actuator positions (see Figure 6-5) were essentially the result of wind gusts. The gusts possibly have more effect on the vehicle in yaw than in pitch because the tilt of the vehicle in pitch results in reducing the wind component normal to the vehicle. This is under the assumption that vertical wind shears in the atmosphere are small compared to the horizontal shears.

The greatest gust effects were experienced around 70 seconds. A blown up portion of the yaw angles and winds is shown for the period from 60 to 80 seconds in Figure 6-7. Yaw angle of attack winds (solid line) are compared with the Rawinsonde measured values (dashed line) in the lower portion of this figure. The free-stream angle of attack obtained by correcting the local measured angles for the upwash is shown at the top of Figure 6-7. One effect to notice is the attenuation of the wind gust as measured by rawinsonde between 71.5 and 73 seconds. The gust as shown by the rawinsonde had a velocity increment

of 4 m/sec whereas that shown by the angle of attack winds had an increment of 10 m/sec. Inspection of the engine actuator deflections in Figure 6-7 shows that this gust resulted in a fairly large telemetered actuator response (solid line). An oscillation in the engine deflections occurred with a peak amplitude of ± 1.0 degrees.

The maximum wind gradient during this gust as indicated by vehicle measurements was 0.03 /sec, compared to 0.02 /sec as obtained from rawinsonde data for a 250 m altitude interval. This resulted in 0.38 degrees of actuator deflection per m/sec increment in wind velocity at 72 seconds. The effect was probably as pronounced as it was because of the particular phasing of the successive gusts. Figure E-5 compares the actual wind shears encountered on this flight in yaw with the design specifications. The gusts under consideration at this time were those occurring just above 15 km altitude.

Results from the six degree-of-freedom trajectory calculated using the idealized control equation and the angle of attack winds as input data are shown in Figure 6-7. The resulting yaw angle of attack and engine deflections are shown as the dashed lines. Agreement is good except for a reduced amplitude in the 6D actuator response to the gusts. Control gains used were based on steady-state conditions. The actual control system response is fairly nonlinear* even in the low frequency range. As a result this is difficult to simulate with digital computations of the time response.

Actuator positions from the six degree-of-freedom trajectory are shown for a more extended period compared with telemetered in Figure 6-5 (circled points).

Telemetered normal acceleration as measured by the yaw control accelerometer (not in the control loop) is shown in the upper portion of Figure 6-8. The corresponding calculated acceleration is shown in the lower portion. This accelerometer was located at station 879 on the web of the spider beam, 44.5 inches from the longitudinal axis toward fin position IV. Excluding the periods at liftoff and after IECO, maximum telemetered yaw normal acceleration was -0.8 m/sec^2 (-0.081 g's). This agrees within 0.3 m/sec^2 (.03 g's) with the corresponding calculated acceleration from the telemetered angle of attack and engine deflections. Higher frequency oscillations showed up in the measured acceleration, as in pitch, but with a lower amplitude.

Both pitch and yaw oscillations showed up late in the flight, again attributed to propellant sloshing. In yaw the oscillations were apparent about 5 seconds earlier than in pitch and were somewhat greater in magnitude. (See also paragraphs 6.2.3 and 6.3.)

*The digital simulation does not consider the variation of amplitude and phase with frequency.

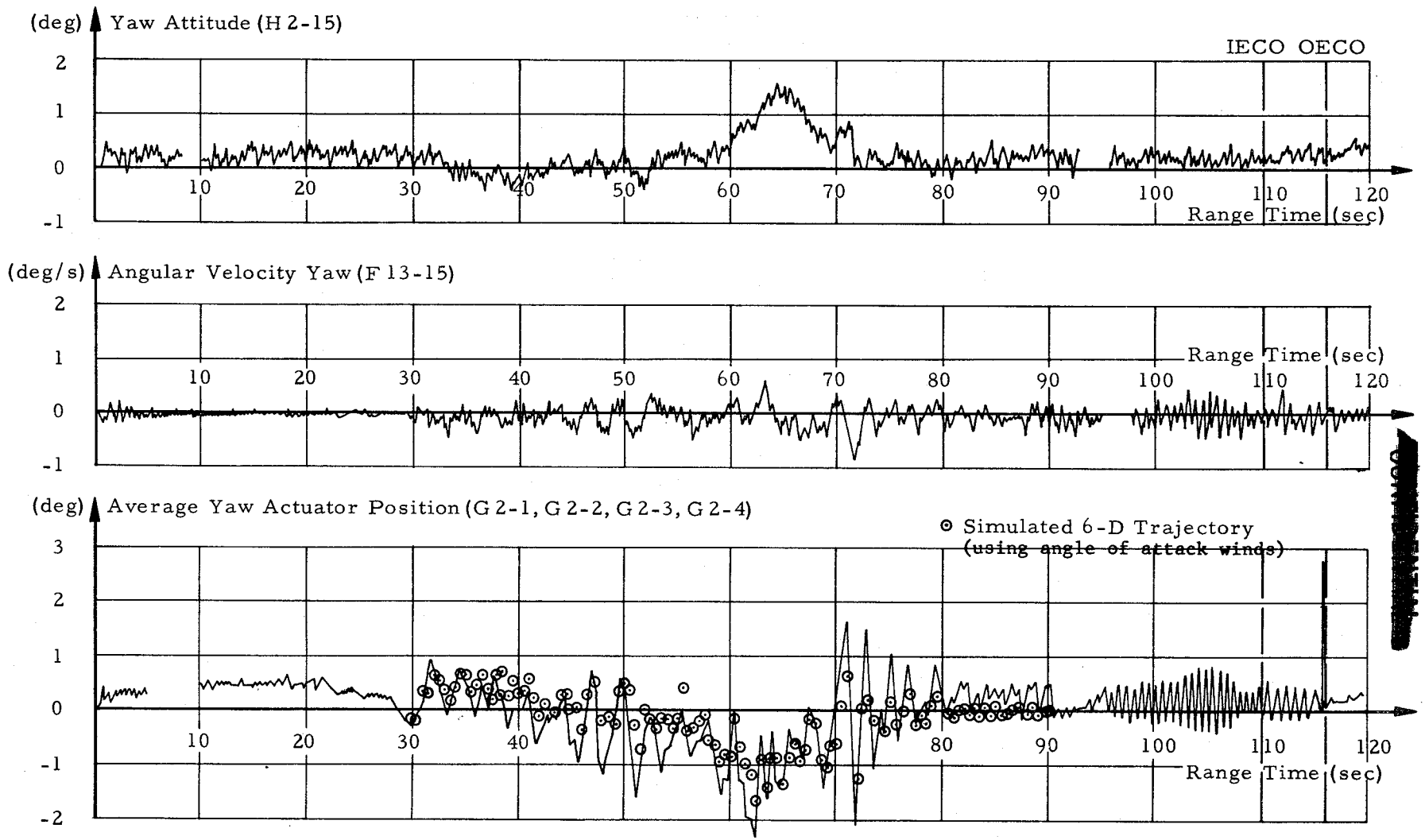

Fig. 6-5	Yaw Attitude, Angular Velocity and Actuator Position
SA-1	

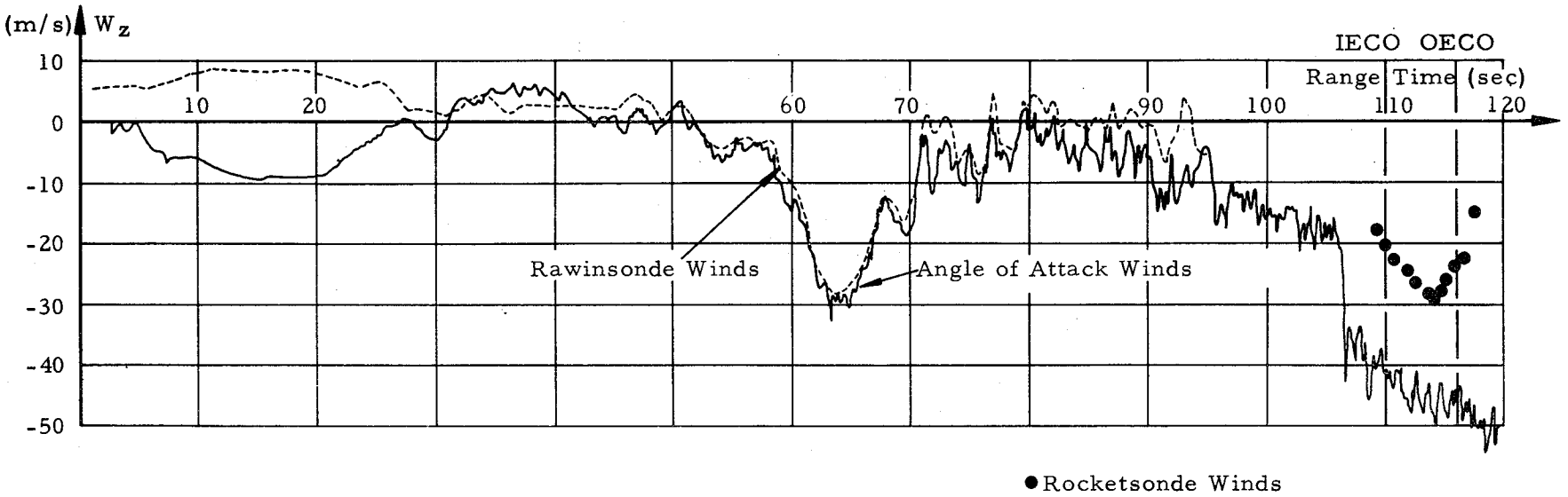

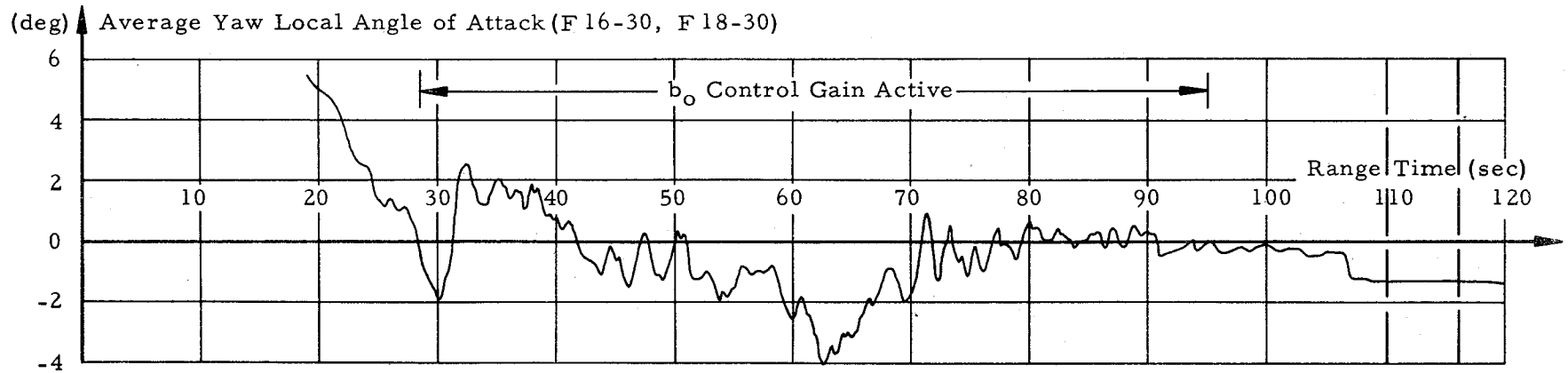

Fig. 6-6	Yaw Plane Wind Components and Local Angle of Attack
SA-1	

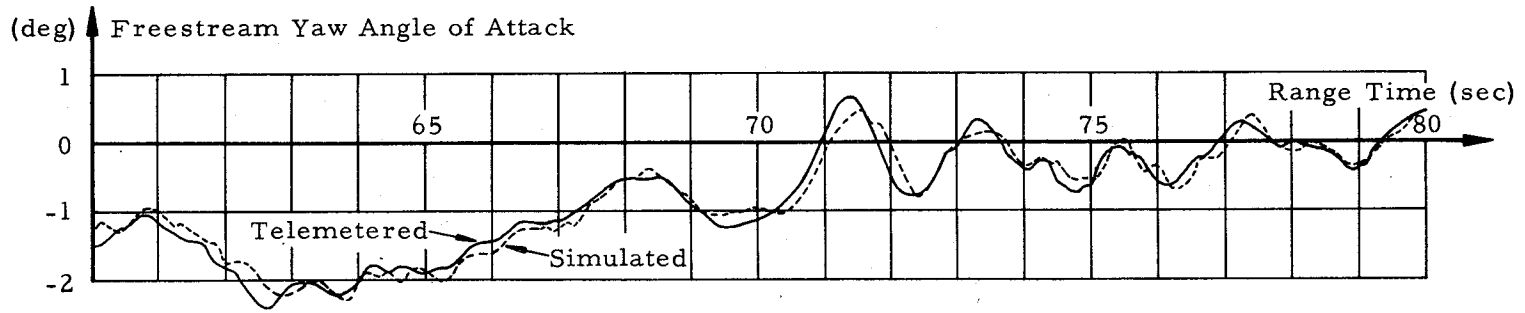

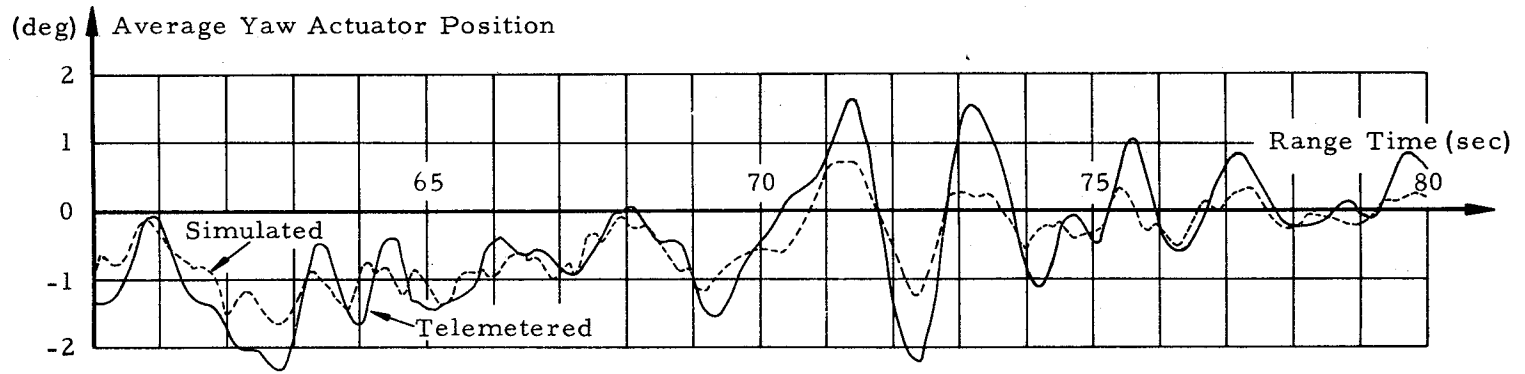

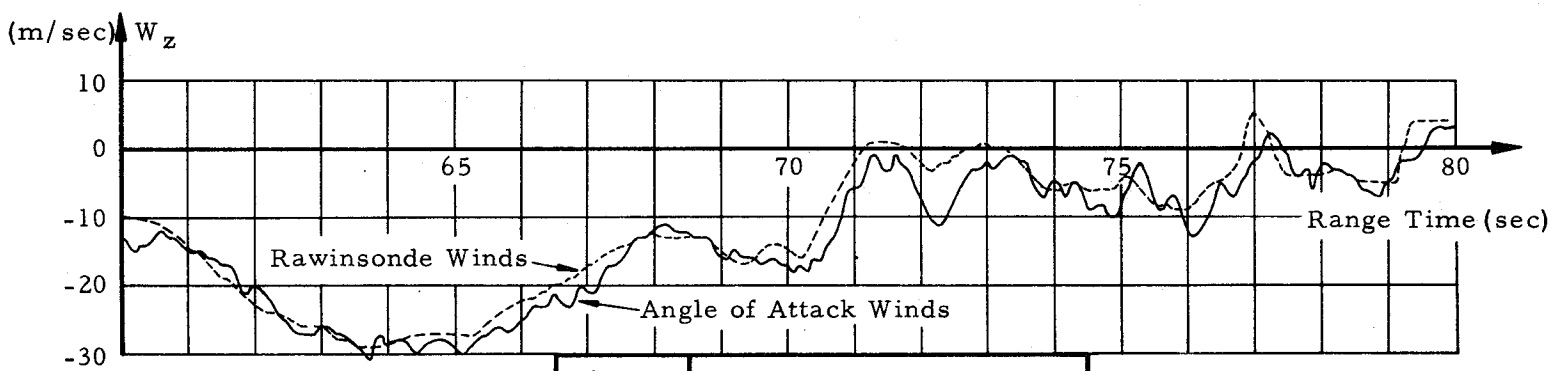

Fig. 6-7	Yaw Angles and Wind Component (60 - 80 sec)
SA-1	

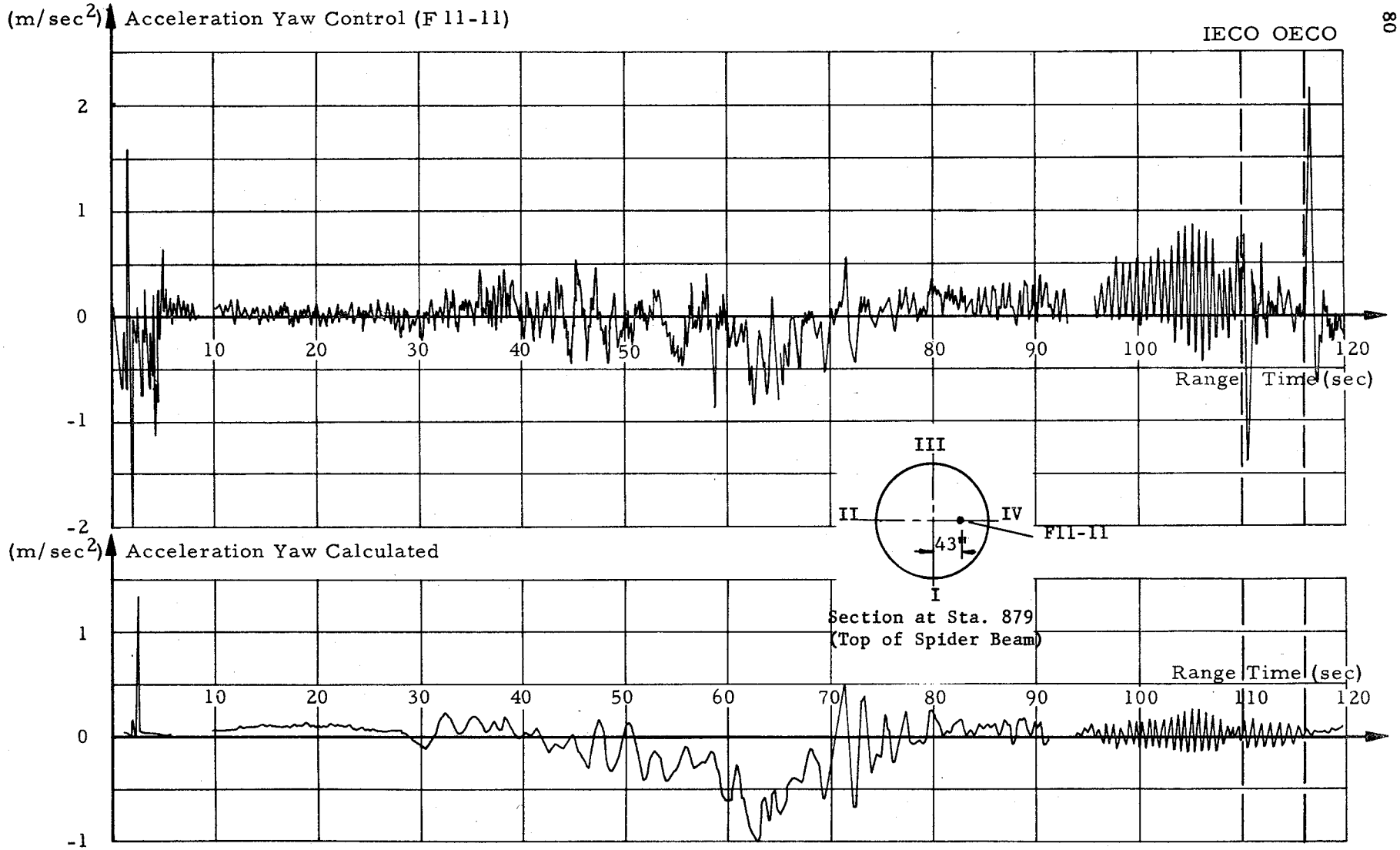

Fig. 6-8	Yaw Normal Acceleration
SA-1	

6.2.3 ROLL PLANE

The roll attitude of the vehicle was controlled by differentially deflecting the outboard control engines in both pitch and yaw. This was accomplished by electrically mixing pitch and roll and yaw and roll error signals in the control computer.

The roll attitude, angular velocity, and averaged engine deflections in roll are shown in Figure 6-9. A roll oscillation with a peak amplitude of 0.4 deg occurred shortly after liftoff. This was completely damped out by 5 seconds. The only other significant roll attitude reached was 0.3 deg occurring around 107 seconds. This was due to a propellant sloshing instability.

Beginning around 90 seconds a divergent roll oscillation with an average frequency of 1.5 cps was excited by the propellant sloshing in roll and had a pronounced effect on the roll angular velocity (Figure 6-9). This instability was essentially the result of a phase lag of the filter network in the roll control loop with the first sloshing mode, beginning around a frequency of 1.2 cps.

The original design of the roll control filter was thoroughly investigated in sloshing stability studies and found to be stable. Later, however, uncertainties in the torsional model arose from the test results from SA-D dynamic tests. As a result, the roll control filter design was recently changed to cover these uncertainties in the torsional modes. This filter stabilized all torsional modes by attenuation stabilization. To accomplish this attenuation at 4 cps and above, there is an inherent phase lag in the loop. This phase lag comes in at about 1.2 cps and coupled with the low propellant damping at this time leads to the sloshing instability.

The new filter network was designed shortly prior to the SA-1 flight. During this period a great deal of concern existed over the body bending modes, and the sloshing stability using the new filter was not thoroughly studied.

The peak roll angular velocity of 2.5 deg/sec occurred at 107 seconds. If it is assumed that all of the outer tanks had sloshing exactly in roll then about 70% of the vehicle reaction in roll at this time could be attributed to the forces of the sloshing propellants. The damping after 107 sec may have resulted from some decrease in the propellant sloshing amplitudes and/or changing phasing between the sloshing in the various outer tanks and to some decrease in the sloshing mass. After IECO the oscillations continued with a slight damping because the sloshing again approached stability with a decreasing

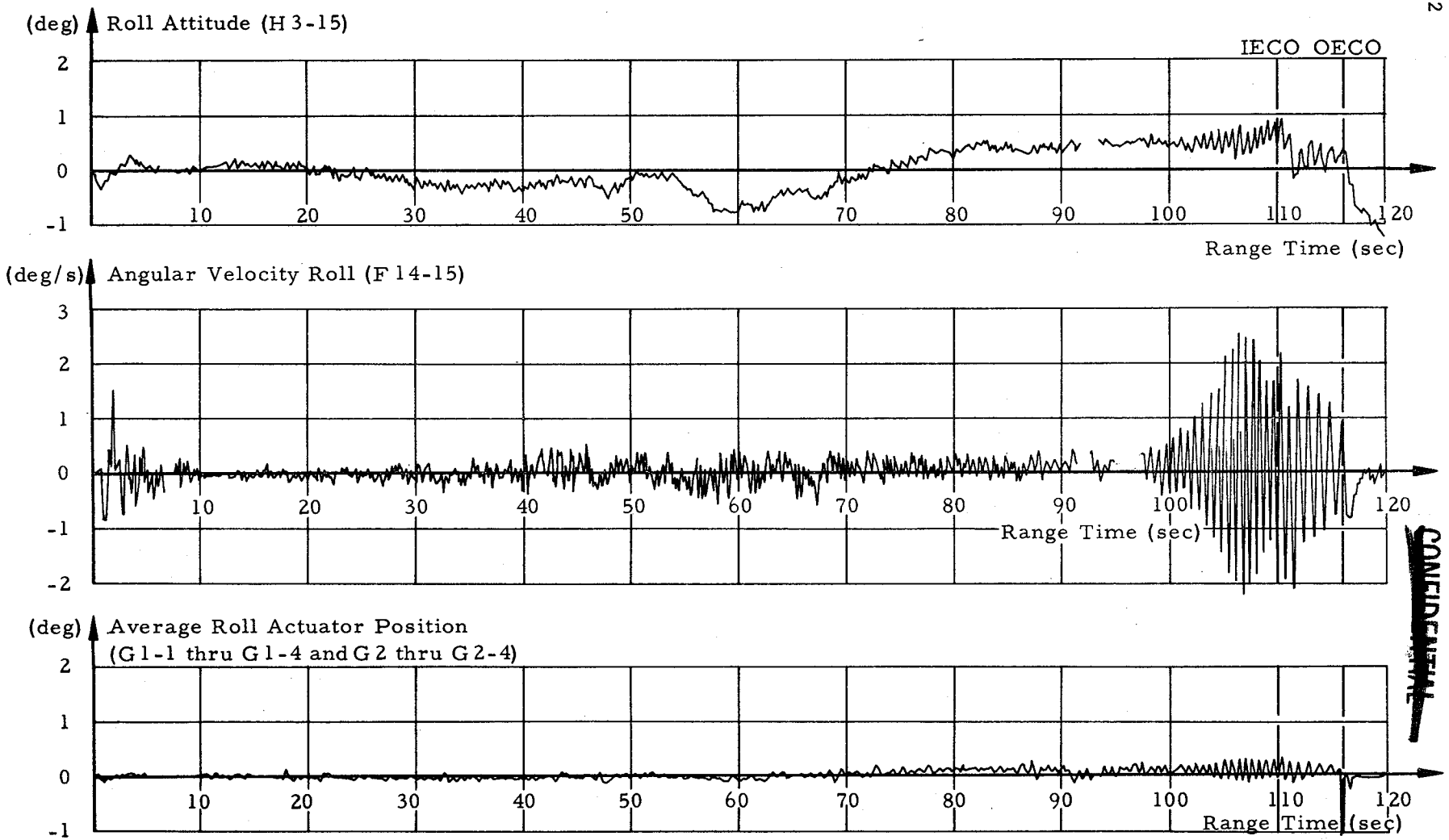

Fig. 6-9	Roll Attitude, Angular Velocity and Actuator Position
SA-1	

sloshing frequency due to the drop in longitudinal acceleration. At OECO the roll oscillations stopped rapidly.

Further discussion on the sloshing is given in paragraph 6.3.

6.2.4 ATTITUDE AFTER CUTOFF

The missions assigned to SA-1 concerned only the powered flight phase. However, there are several pieces of information to be obtained from the free-flight phase. One concerns the effect of the engine thrust decays on the attitude which is of interest for Block II vehicles. The other is the loading on the vehicle at the loss of telemetry signals which was probably caused by some components failing structurally.

Figure 6-10 shows the telemetered pitch and yaw angular velocities around OECO. There was an average pitch angular velocity of about -0.05 deg/sec (nose down) at OECO with an angle of attack of about -3 deg (nose down). Figure 6-10 shows an angular acceleration between 116 and 119 seconds. A small portion of this can be attributed to the angle of attack. The remainder is therefore attributed to an average angularity of the thrust vectors in the engine nozzles. Using the telemetered thrust decay this net thrust angularity was calculated. These results were 1.0 deg for pitch and -0.5 deg for yaw which are in good agreement with Jupiter flight test results.

A comparison of the SA-1 angular deviations with design values at the time contemplated for S-IV separation on Block II is given in the following table.

Conditions 1.7 Seconds After OECO

Parameter	Design Consideration	SA-1		
		Pitch	Yaw	Vector Sum
Angle of Attack (deg)	8	-2.5	-0.8	2.6
Angular Velocity (deg/sec)	1	0.11	0.05	0.12
Attitude Error (deg)	1	-0.4	0	0.4
Dynamic Pressure (psia)	0.07	0.09		

As indicated by the table above the attitude deviations around cutoff (OECO) were very small.

The attitude deviations (angles and rates) around cutoff caused a slow drift of the attitude angles in pitch and yaw during the coast flight. These are shown up to 195 seconds in Figure 6-11. The pitch

attitude error curve shows a continual change in slope during this time (15 deg is telemetry limit), indicating the presence of some moment other than aerodynamic. An average moment of 5,121 inch-pounds was calculated from this motion. The center of gravity of the dry vehicle was located at station 1210. The circled points in Figure 6-11 are a reconstruction of the pitch motion assumming this constant moment.

The yaw plane motion also indicates the presence of a moment of approximately 4,254 inch-pounds until approximately 155 seconds. After this there is no apparent effect. The source of these moments is not known at this time. Telemetered gas pressures in the propellant tanks were below the level set for the vent valves so there is no evidence that there are any gases coming out from the propellant tanks.

The vehicle re-entered the atmosphere with about 40 degrees angle of attack. Because of the relatively large amount of propellants remaining after cutoff, deceleration during re-entry would cause the propellants to move to the top of the tanks. This yielded a stable configuration with a static margin of approximately 0.1 calibers and, therefore, the pitch and yaw angles of attack and normal accelerations are shown for the period preceeding L.O.S.* in Figures 6-12 and 6-13. The telemetered angles of attack have been correlated with other information and are considered to be valid. Circled points on the normal acceleration plots were calculated from the telemetered angles of attack. Even though the SA-1 configuration was aerodynamically stable during re-entry, this does not indicate that the S-I booster alone would be stable.

6.2.5 ANGLE OF ATTACK MEASUREMENT ANALYSIS

Topp local angle of attack indicators as used in the Jupiter program were employed for control purposes on SA-1. Four of these were mounted 90 deg apart radially on the payload body surface (a Jupiter nose cone) at station 1841. Two indicators measured in the pitch plane and two in the yaw plane. These results as telemetered are shown in Figures 6-3 and 6-6. Since these indicators are located on the body they are influenced by the body upwash. The telemetered values may be converted to free-stream angles of attack by means of a wind tunnel determined upwash factor which was verified by Jupiter flight tests. The resulting free-stream angles of attack are shown as dashed lines in Figure 6-14.

Other angle of attack measurements were flown as passengers on SA-1. These were nose cap differential pressure measurements. They were made from a set of six pressure orifices drilled in the spherical nose cap of radius 12.17 inches; four were used for differential pressure measurements and two others were used to sense a dynamic

* L.O.S. - Loss of signals

pressure correction factor. These measurements are forerunners of the more sophisticated Q-ball to be flown later in the program. Free-stream angles of attack determined from the nose cap differential pressures are compared with those from the local indicators and shown as the solid line in Figure 6-14.

Also shown in Figure 6-14 are calculated angles of attack based on the rawinsonde winds (squares) and those from the rocketsonde winds (circles). During the period between 30.7 and 48 seconds the calculated angles of attack are unreliable due to unreliable rawinsonde winds (interpolated values were substituted).

The angles of attack as measured by the local indicators are the most reliable between 27 and 95 seconds. After 95 seconds the local angles of attack (pitch) increased in error. At 106.5 seconds locals 1 and 3 showed a sharp drop and then an essentially constant value. This is considered to be erroneous.

The nose cap angles of attack are expected to have an accuracy only on the order of 1 degree. These measurements, although not extremely accurate, do appear to be reasonable during the entire flight and agree well with the calculated values through cutoff. After 90 seconds the nose cap measurements showed a greater degree of oscillations than the local measurements. However, these oscillations showed up in the ΔQ correction measurement (D60-30) rather than the differential pressure measurements and therefore cannot be considered as valid angle of attack information.

6.2.6 BIAS ADJUSTMENT OF FLIGHT MECHANICAL DATA

Flight data contains certain errors due to the telemetering and data reduction processes. Since the flight mechanical measurements are fundamental to a large number of investigations, an attempt has been made to take out at least the major portion of the systematic errors. This was done by a statistical process using a least squares estimate of the errors in a system of linear equations. The equations used were the linearized moment, normal force, control, and wind equations. Only the pitch and yaw planes were considered and the following functions were included; angles of attack, attitude angles, normal accelerations (control accelerometers), and the average of the engine deflections in each plane.

During the early portion of the flight the aerodynamic parameters of the vehicle may not be sufficiently well defined; hence the inherent error in the equations leads to improbable solutions. Also, for SA-1 the measured rawinsonde winds were questionable between 2 and 7 km altitude due to some balloon tracking problems. Rawinsonde winds were not available after 95 seconds flight time.

Several 15 second time span runs were made on the bias determination program over the period from 55 to 95 seconds. These results were plotted, and a set of average biases for the entire flight time was determined graphically, leaving out segments which appeared to be erratic. These results were used to adjust the telemetered data and are listed in the third column of Table 6-I.

The present program can determine only the bias in the average engine deflections and the average local angles of attack in the pitch and yaw planes. These shifts were applied to the individual measurements in such a way as to obtain the best consistency of the data in all respects.

At a later time in the analysis the biases were re-run for a 65 second time span from 25-90 seconds. These results were in good agreement with the first results and are shown in the last two columns of Table 6-I. Also shown for this case are the 1σ standard deviations of these results based on the assumptions used for the random error components.

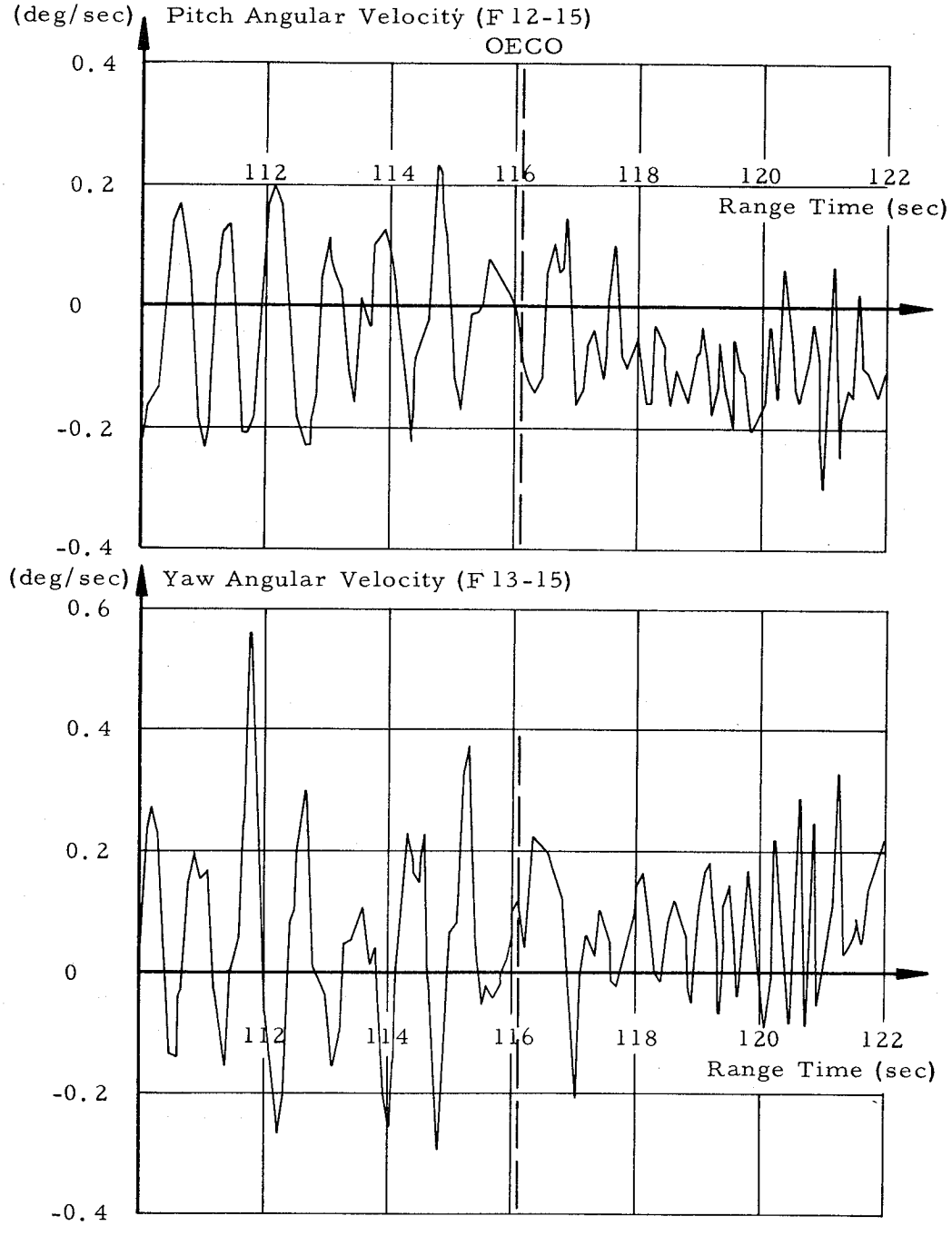

Fig. 6-10	Angular Velocities During Cutoff
SA-1	

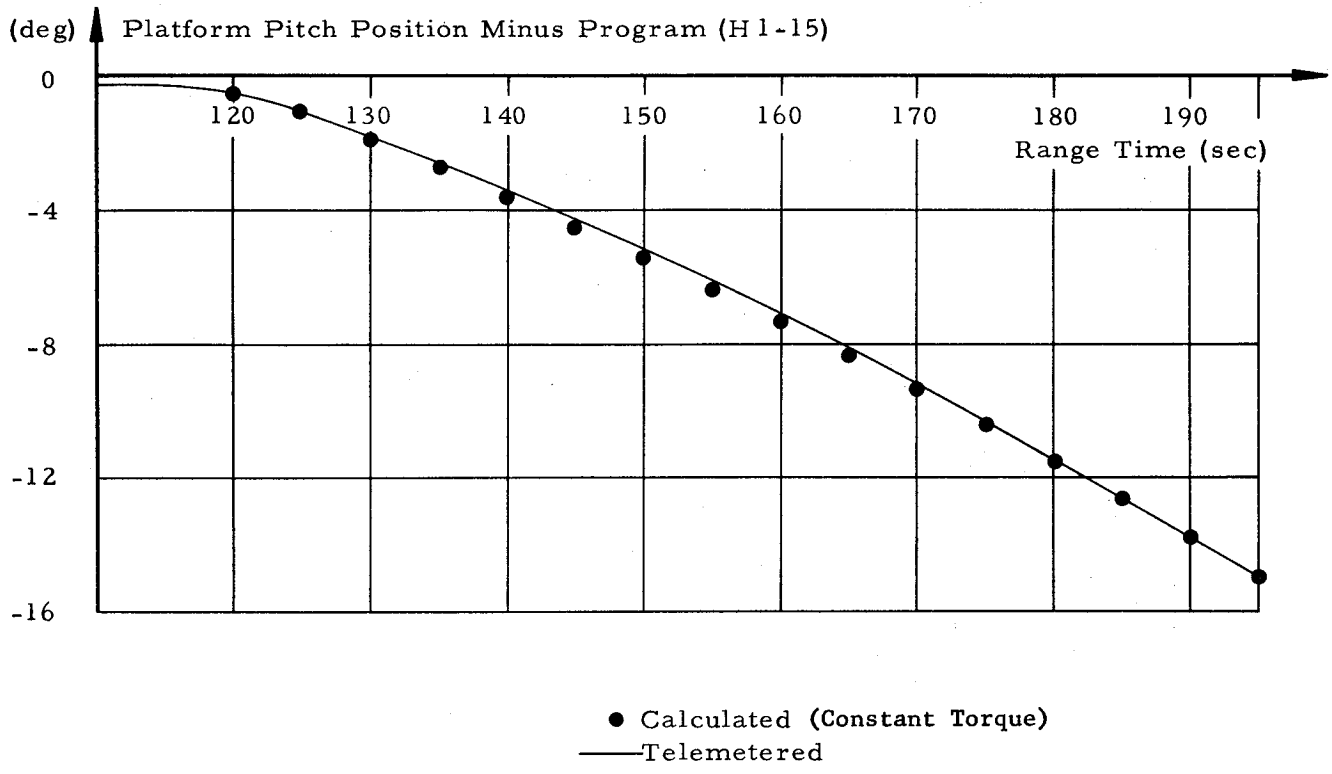

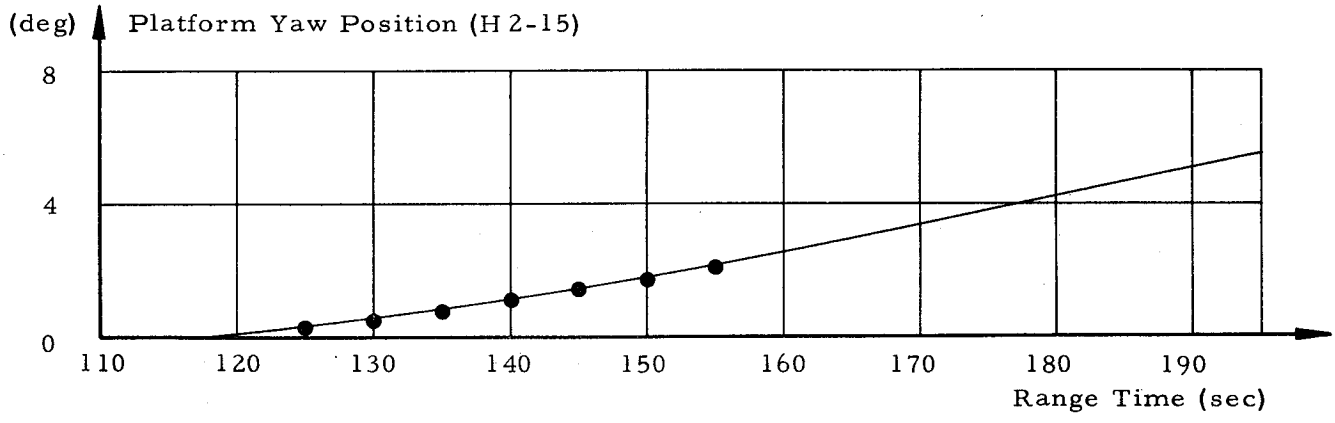

Fig. 6-11	Attitude Angles After Cutoff
SA-1	

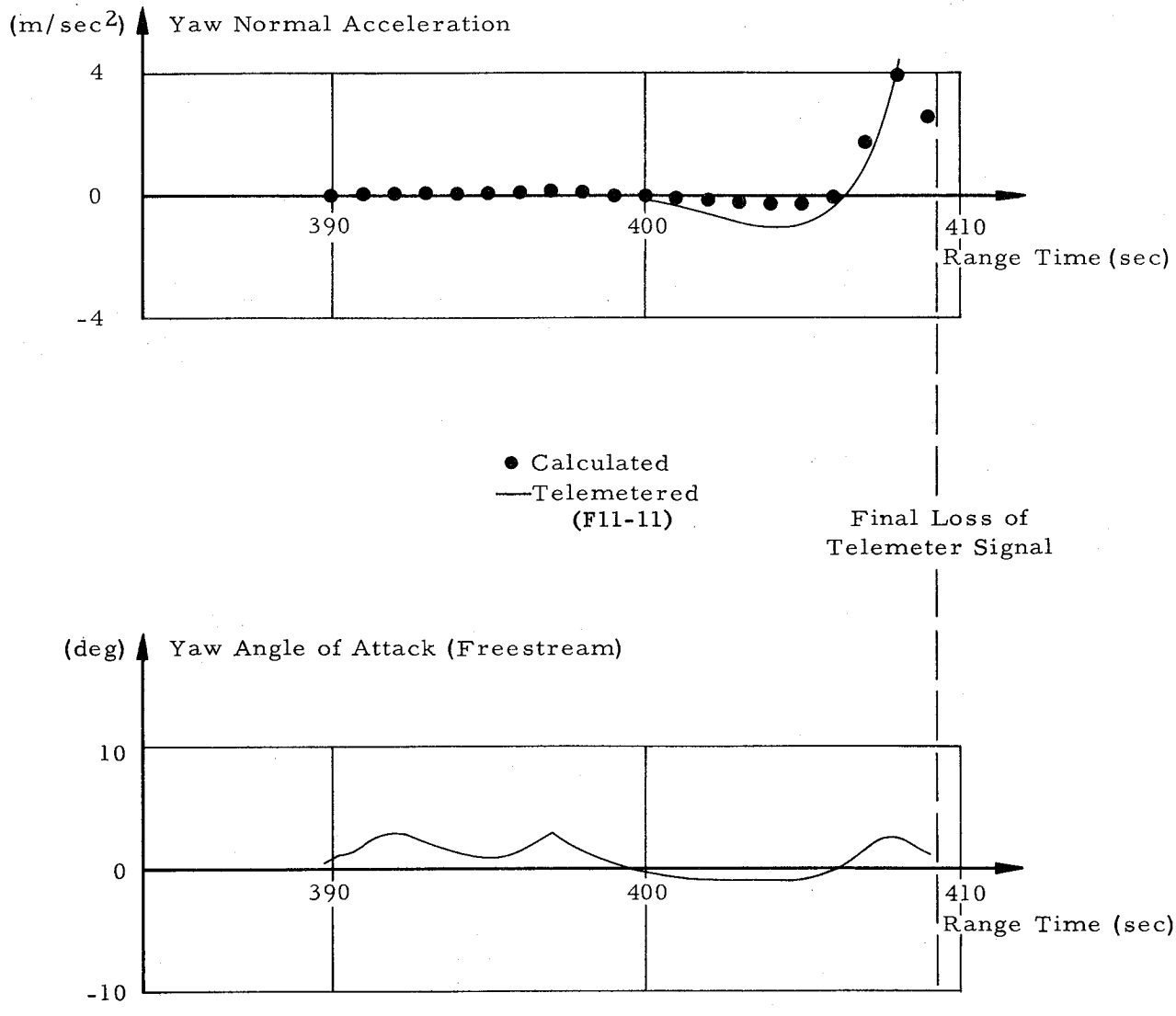

Fig. 6-12	Yaw Angle of Attack and Normal Acceleration (RE-ENTRY)
SA-1	

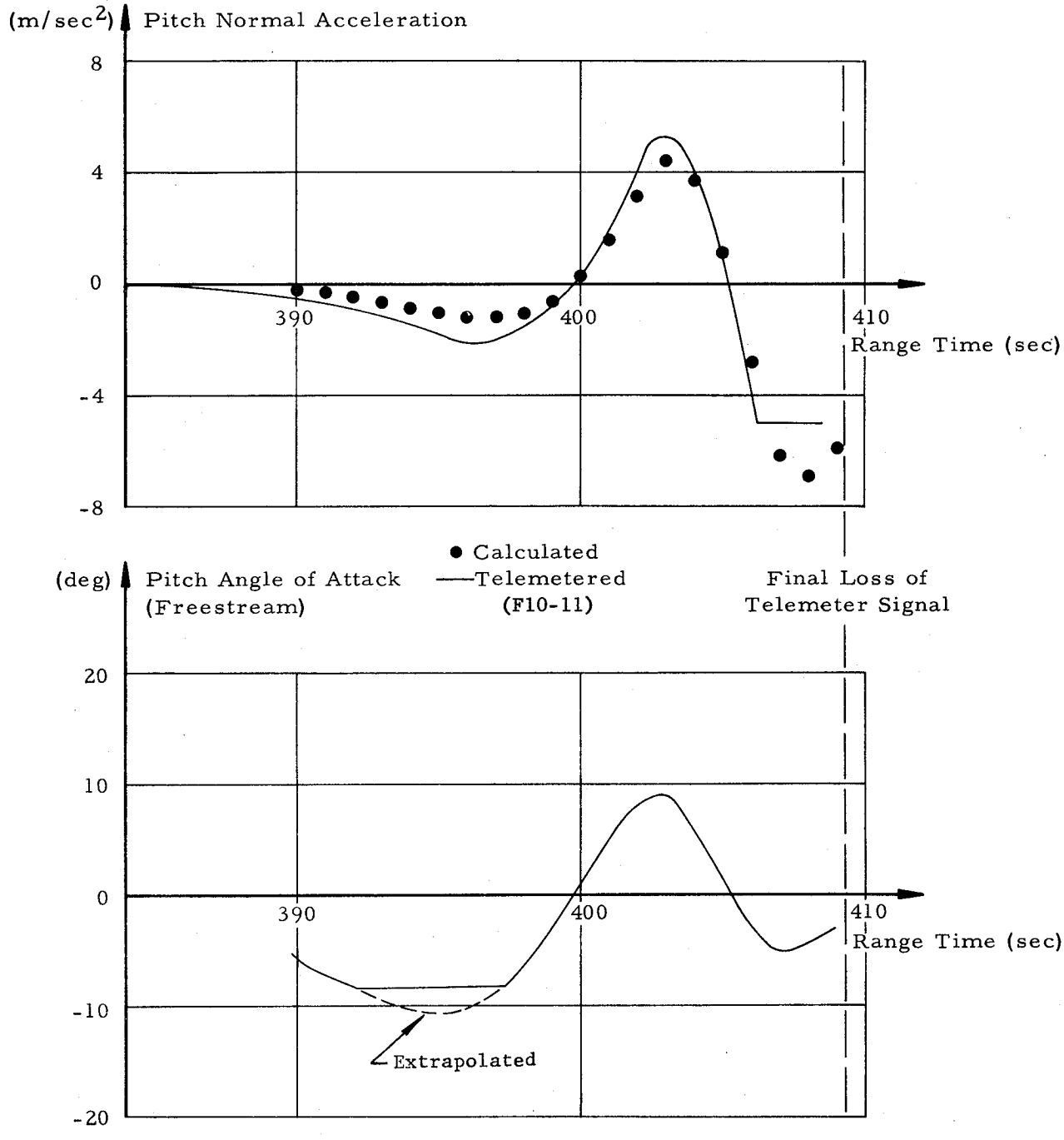

Fig. 6-13	Pitch Angle of Attack and Normal Acceleration (RE-ENTRY)
SA-1	

CONFIDENTIAL

Fig. 6-14	Freestream Angles of Attack
SA-1	

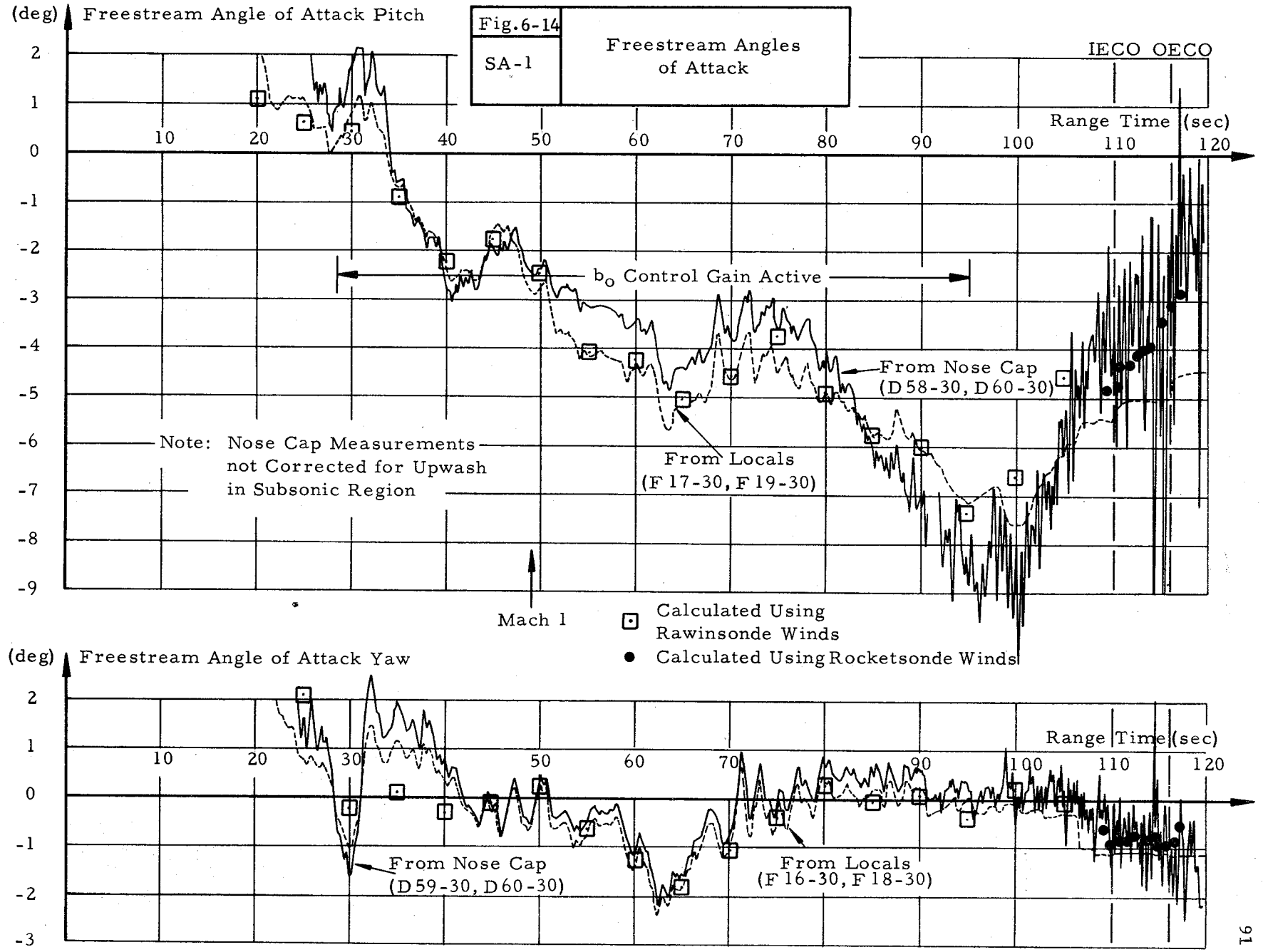

6.3 FUEL AND LOX SLOSHING

One of the few problems encountered on the SA-1 flight was an instability in sloshing, predominantly in the roll mode. However, even though there was more sloshing than desired, it did not approach the point of endangering the vehicle. One consequence of the sloshing on SA-1 may have been some contribution to an earlier cutoff than predicted.

Sloshing was measured on SA-1 by means of differential pressure measurements in three of the nine propellant tanks. Slosh measurements were made in the center 105 inch LOX tank and in LOX tank 04 and fuel tank F2. The locations of these tanks are shown below.

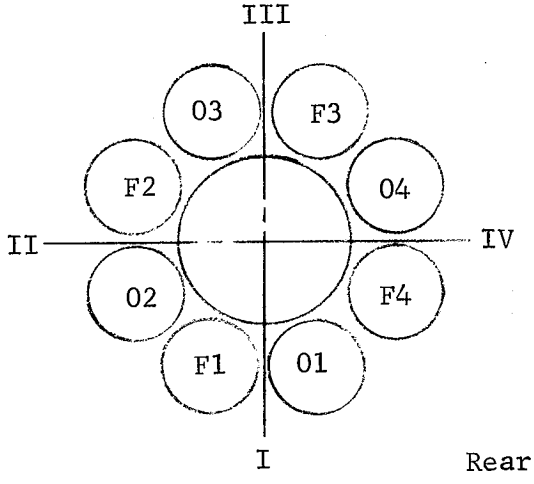

Rear View

Sloshing measurements did not begin to function until a considerable time after liftoff (see paragraph 12.2). Steps are being taken to improve the situation for SA-2.

The telemetered sloshing differential pressure measurements must be multiplied by a conversion factor to obtain the sloshing height in inches. This factor is a function of the liquid level in the tank, longitudinal acceleration and frequency of the oscillations. The converted heights are shown after 68 seconds in Figures 6-15 through 6-18. The results are extremely sensitive with respect to the fluid heights and frequencies used. The results shown here are believed to be the best results which can be obtained from the measurements without an extremely exhaustive evaluation. There is an uncertain degree of confidence in them which will be discussed later.

Figure 6-19 shows the sloshing frequencies observed in the three tanks measured. The dashed lines represent the calculated natural frequencies of the first sloshing mode in the respective tanks. These calculated frequencies were based on the actual longitudinal acceleration and propellant heights. The observed frequencies, represented by the individual data points, were higher than the calculated natural frequency since they were actually the result of a coupling between the sloshing and vehicle motion. The decreased frequency of sloshing after IECO is a consequence of the decreased vehicle longitudinal acceleration. The sloshing frequency is proportional to the square root of the acceleration.

After the SA-1 flight the sloshing stability was critically examined by Aeroballistics Division. The damping roots for the sloshing in pitch and yaw are shown in the lowest portion of Figure 6-20. The parameter shown is the percent of critical damping of the propellants in the tanks. These studies indicated that the sloshing in the pitch and yaw planes should be stable for any of the propellant damping values existing until 90 seconds. After this time some small instability would exist when the propellant surface was between the Z-rings or off the baffles on the smooth wall. The baffle locations and configurations in the three types of tanks are shown in Figure 6-21. Figures 5-14, 5-15, and 5-16 show the propellant surface heights in these tanks as a function of time as best as can be determined from available engine performance information.

Although some small surface amplitudes may exist in the pitch or yaw mode when the propellant surface is between the Z-rings, they should not build up to any degree. The percent of critical damping of the sloshing is approximately 6% for the baffles, 3% when the propellant surface is about 3 inches above the Z-rings, and from ½ to 1% when the propellant surface is on the smooth tank wall.

Figure 6-18, which presents the actual amplitudes in the center LOX tank, shows the effect of the pitch - yaw sloshing instability. A regular, increasing amplitude oscillation started in the center tank around 94 seconds after the LOX level had passed below the last baffle. After 101.5 seconds the measurement is no longer valid; apparently the propellant surface had passed below the sloshing probe. A note of caution needs to be expressed concerning the propellant heights as deduced from the engine performance analysis shown in Figures 5-14, 5-15, and 5-16. In some cases the propellant heights are not consistent with those indicated by the sloshing measurements.

While the sloshing instability in pitch and yaw is not serious, that in roll is considerably different. A control feedback stability investigation, considering the flight control filters, was made using the equivalent spring-mass-damper model below.

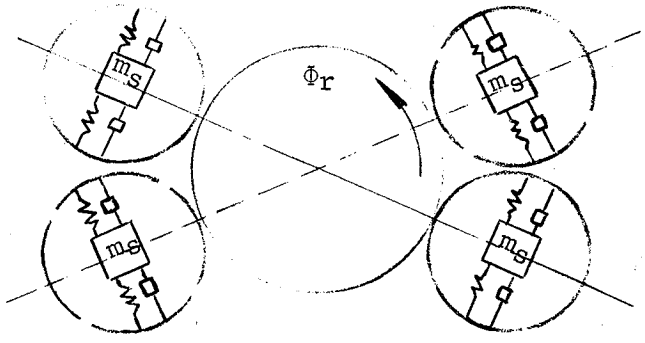

The rate of damping (σ) determined from the model above is shown for two situations in Figure 6-20; either all outer tanks were out of phase, or all outer tanks in phase. Again the parameter in these curves is the percent of critical damping of the propellant in the tanks. The in phase case shows a high degree of instability for even the highest propellant damping beginning around 60 seconds. The out of phase case has a much higher damping until later in flight. However, when the propellant surface is away from the Z-rings this mode is unstable between 80 and 107 seconds.

The analysis shows the slosh instability in roll at 100 seconds produces a buildup rate of $e^{0.3t}$ if all tanks are in phase and $e^{0.15t}$ if they are out of phase. For any other phase condition between, the oscillating propellants in the tanks will be between the two cases above.

Sloshing amplitudes measured in the two outer tanks are shown in Figures 6-15 and 6-16. Also shown are the locations of the ring frames (or Z-rings). Figure 6-17 shows some polar plots of the propellant motion in these tanks for several periods. The exact validity of this information is not known quantitatively. Some of the behavior indicated is open to several possible interpretations. Contributing to the uncertainty are measurements being available in only two of the eight outer tanks, the accuracy of the questionable differential pressure

measurement technique, and the exact height of the propellants in the tanks. The locations of the sloshing ΔP measuring probes are shown in Figure 6-21.

Oscillations in the center LOX tank took place primarily in the pitch plane. Sloshing measured in the two outer tanks was irregular until around 93 seconds (see Figure 6-19). Then, the sloshing in tank 04 was essentially in roll (normal to the radius vector from the longitudinal axis of the vehicle until around 97 seconds). The sloshing in the fuel tank remained somewhat erratic, essentially in pitch. For a short period the sloshing in both of the small tanks was erratic. After 97 seconds the sloshing in both tanks changed from essentially linear to a circular motion which continued until the loss of the measurements. This circular motion at low liquid levels was probably a vortex type of motion induced by the draining of the propellants from the tanks.

Maximum sloshing amplitudes probably occurred around 107 seconds. This is indicated by the peak amplitudes in vehicle reaction in roll at this time (see Figure 6-9). The maximum amplitude in the roll angular velocity, which is attributed to sloshing, was ± 2.5 deg/sec. Maximum amplitudes of the engine deflection oscillations due to the sloshing were ± 0.4 deg in pitch, ± 0.5 deg in yaw, and about ± 0.2 deg in roll. The larger magnitudes in pitch and yaw compared to those in roll are attributed to the much larger rate gain in the control loop and are of concern because of the possibility of approaching the actuator limits sooner than in roll.

The maximum amplitude of sloshing indicated in LOX tank 04 was 3 inches at 107 seconds. Fuel tank F2 indicated a maximum of 2.5 inches in yaw at 104.5 seconds, with a rapidly damped amplitude after this time. The rate of damping shown appears to be too high to be a realistic decrease in actual slosh amplitude. At this time the propellant surface was approximately at station 290, only about 3 inches above the slosh probe. It is therefore theorized that the oscillating surface passed back and forth over the slosh probe giving erroneous information. Actually, the conversion factor applied to the telemetered differential pressures to obtain sloshing heights is no longer valid when the probe is within the equivalent sloshing mass. Therefore, it appears that the sloshing measurements made in fuel tank F2 are of questionable accuracy after approximately 102 seconds.

A check was made of the required sloshing amplitudes to explain the observed roll oscillations using the equivalent mass-spring-damper model if all eight outer tanks were in phase. This showed a maximum amplitude of 3.8 inches at 107 seconds, decreasing to 2.0 inches at IECO. However, this model may not really be very representative of

the actual situation occurring in flight at this time (see Figure 6-20). Therefore, the sloshing heights in some of the tanks may actually have been higher, especially in the last portion of powered flight.

Actual IECO on SA-1 occurred 1.61 seconds earlier than predicted cutoff and was given by the cutoff sensor in fuel tank F2. If there were any significant sloshing at this time, this could cause an early cutoff. The cutoff probe was located 19.5 inches from the center of the tank. A sloshing amplitude of about 6.5 inches near the tank wall would give a 1 second early cutoff.

Engine performance evaluation has indicated that actual cutoff came 0.8 seconds earlier than was explained by engine and weight parameters. If this analysis were assumed exact it would require a sloshing amplitude of 5 inches at the wall in tank F2 to make the earlier cutoff. However, the engine performance analysis, with the limited telemetered information available, could probably have been modified enough to give the actual cutoff. Therefore, it is almost impossible to deduce sloshing heights at cutoff from the engine performance analysis.

6.4 FUNCTIONAL ANALYSIS

With the exceptions of the noted disturbances in roll due to propellant sloshing, the operation of the control system from the design and hardware standpoint was entirely satisfactory. Indications are that the compliance and bending problems which appeared during static testing, were adequately overcome or did not materialize (see Section 9.0).

The program device supplied the ST-90 with the desired tilt program during flight and provided discrete commands for vehicle inflight sequencing.

The vehicle response to the disturbance introduced by the slope changes in the tilt program appear to agree favorably with the expected response, i.e., there was rigid body motion to obtain the desired attitude and the first bending mode was excited and damped out. The excitation and highly damped bending response was expected since the control system design is based on providing, for the first mode frequencies, the proper phasing to supply energy to damp the first mode oscillations.

Excitation of the higher modes apparently did not occur on SA-1. Simulation studies indicated that the second mode would not be appreciably excited by the engine deflections resulting from the tilt program.

Generally, rigid body and elastic body response and stability appear to be satisfactory.

6.4.1 ACTUATOR AND HYDRAULIC SYSTEM

All loads on the control actuators and hydraulic system were well below design limits. Maximum actuator loads occurred during the high Q period of flight with a peak of 4300 lbs (50% of design limits). A 3200 lb peak was reached during inboard engine cutoff. The general operating levels were in the order of 2000 lbs or less.

Telemetry data indicates a possibility that the hydraulic pressure for the actuator on engine #2 could have been 500 psi low. The pump inlet pressure should show a corresponding value, but the measurement scale factor does not allow verification. In any case this condition would only limit maximum load capability of the system and was not of consequence to the operation of the SA-1 control system. The remaining three hydraulic systems indicate proper operating pressure ($\approx$ 3000 psi) (Ref. para. 5.2).

6.4.2 CONTROL COMPUTER

The control computer functioned properly in all respects throughout the flight. Control gains were as programmed and were switched at the proper flight times. Input signals to the control computer were generally within the expected range of values. Telemetered outputs of the computer compare satisfactorily with calculated outputs determined from the telemetered input signals.

Maximum control parameters of the SA-1 powered flight were as follows.

Function	Magnitude	Range Time (sec)
Pitch Attitude Error	3.6 deg	64.5
Pitch Angle of Attack (Free-stream)	-7.6 deg	99.7
Pitch Angular Velocity	-1.6 deg/sec	69.0
Pitch Normal Acceleration	-2.3 m/sec^2	65.5
Pitch Actuator Positions	-4.6 deg	62.9
Yaw Attitude Error	1.5 deg	64.3
Yaw Angle of Attack (Free-stream)	-2.3 deg	62.6
Yaw Angular Velocity	-0.9 deg/sec	71.6
Yaw Normal Acceleration	-0.9 m/sec^2	58.7
Yaw Actuator Positions	-2.3 deg	62.5
Roll Attitude Error	0.9 deg	110.5
Roll Angular Velocity	2.5 deg/sec	106.5
Effective Engine Deflections in Roll	0.3 deg	110.6

The pitch angle was larger than expected but was adequately handled by the system. The pitch actuator angles were large but are considered safe compared to the actuator limits of ± 7 deg.

6.4.3 CONTROL SENSING DEVICES

Three passenger sensor systems were flown on SA-1 for operational evaluation purposes. Telemetered signals from the pitch and yaw control accelerometers, pitch, yaw, and roll rate gyros, and a simple Q ball type angle of attack system indicated a general level of acceptable performance. The areas of particular interest were saturation of the roll rate gyro during liftoff and control accelerometer response to the vehicle bending ring-out following outboard engine cutoff. Also of interest were the high frequencies observed in the rate gyro and control accelerometer outputs. Further flight tests are necessary to fully qualify the equipment for active use on later flights.

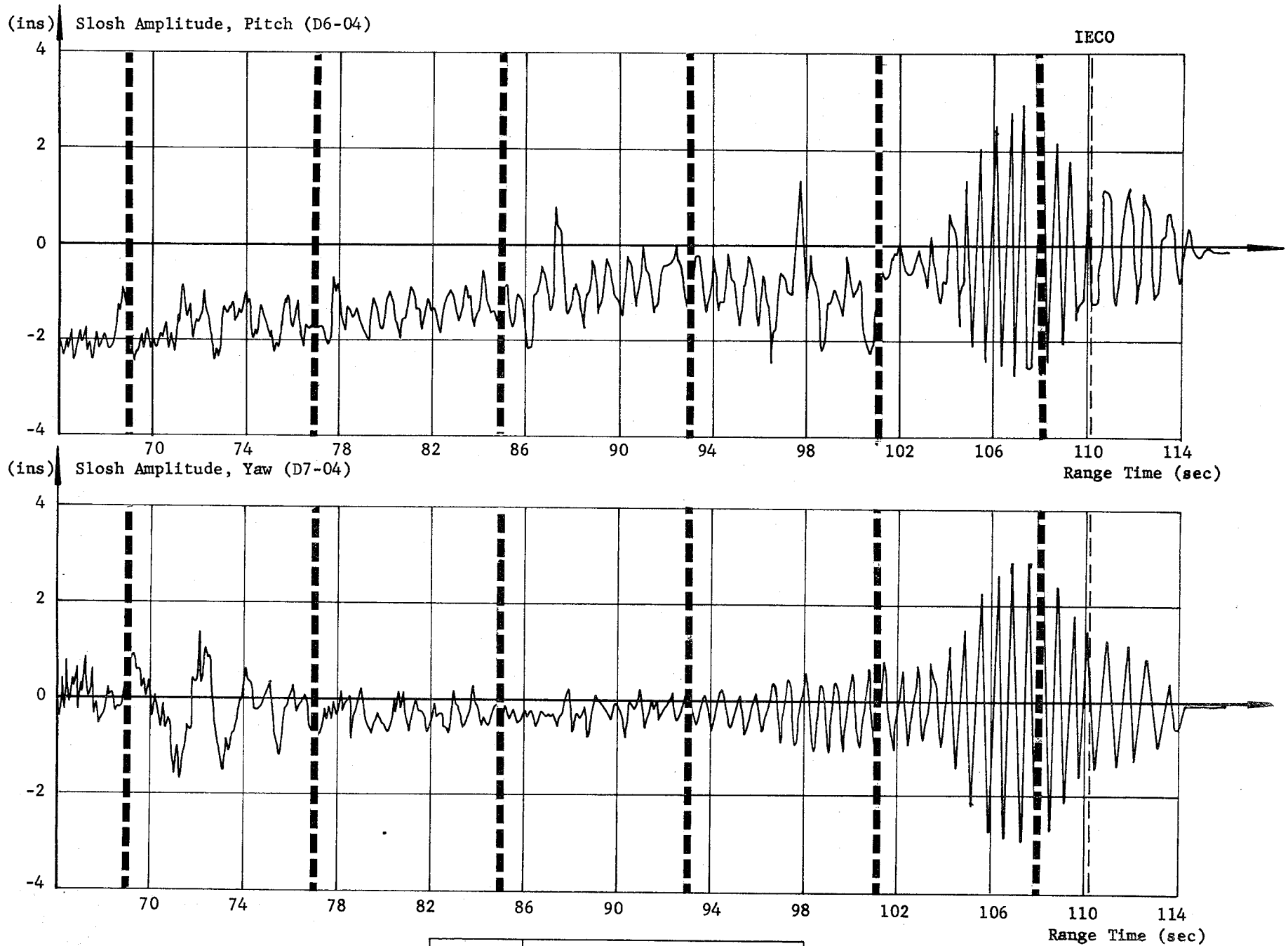

Fig. 6-15	OUTER LOX TANK 04 TELEMETERED SLOSHING AMPLITUDES
SA-1	

Ring Frame Locations

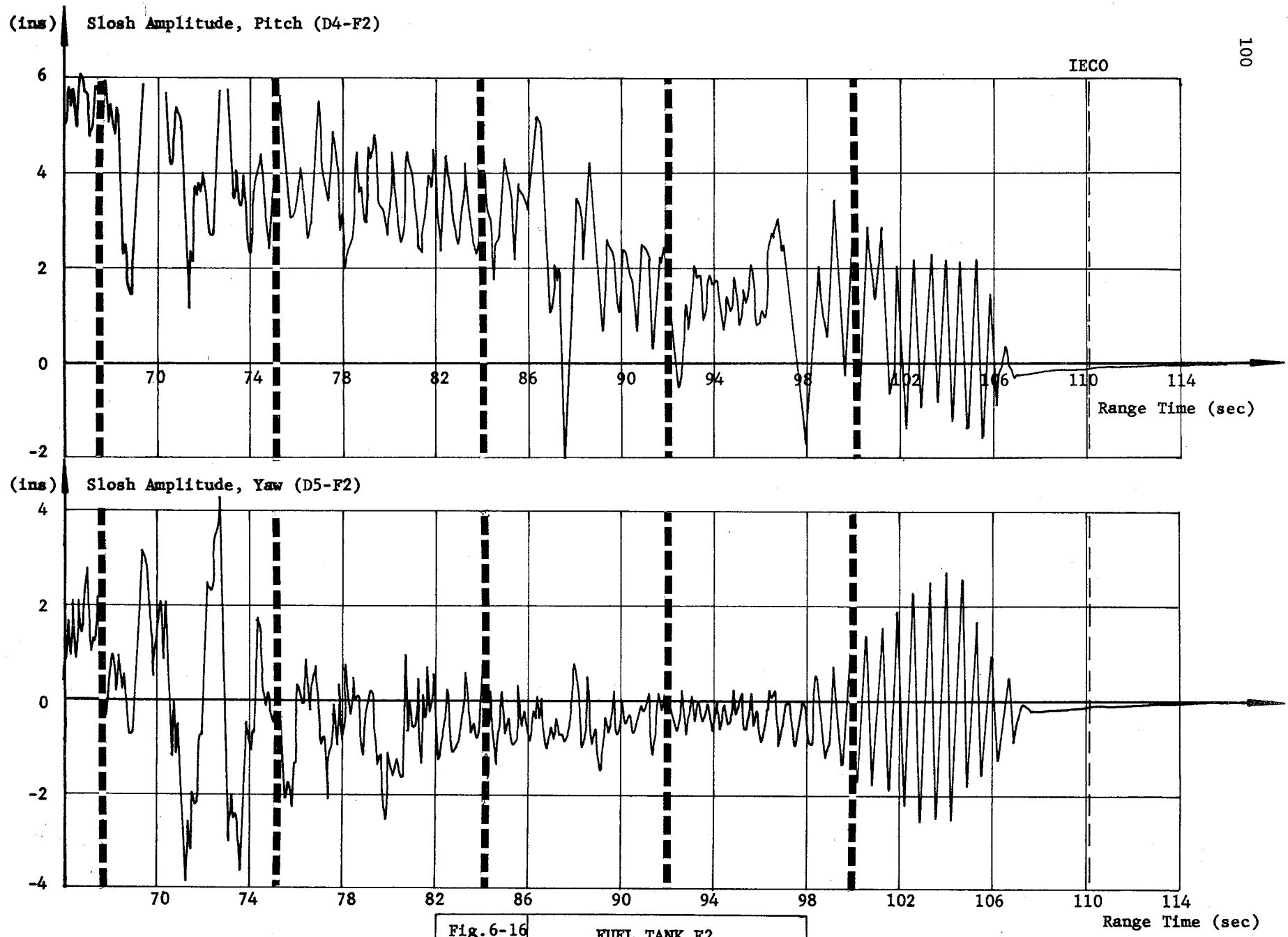

Fig. 6-16	FUEL TANK F2 TELEMETERED SLOSHING AMPLITUDES
SA-1	

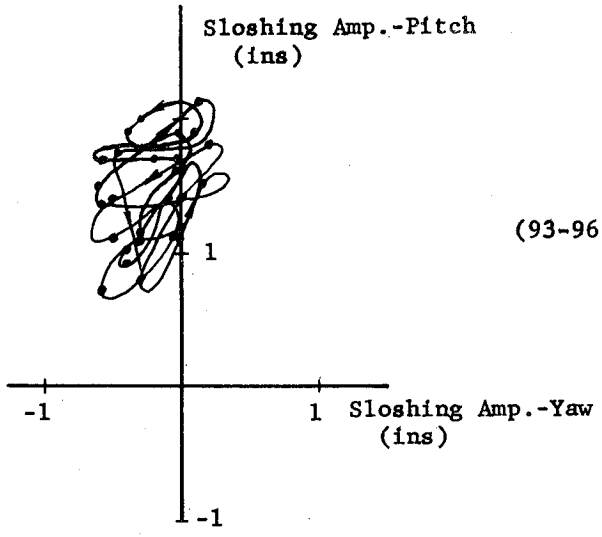

(93-96 sec)

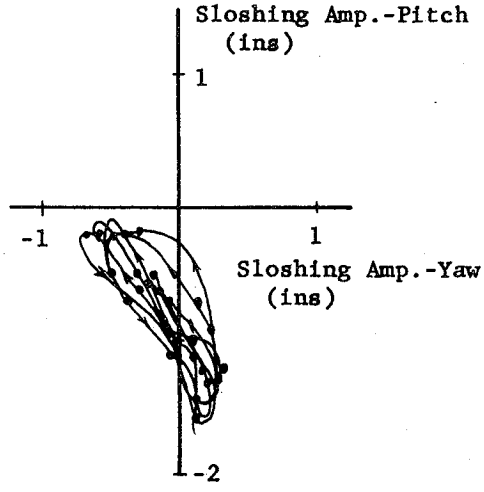

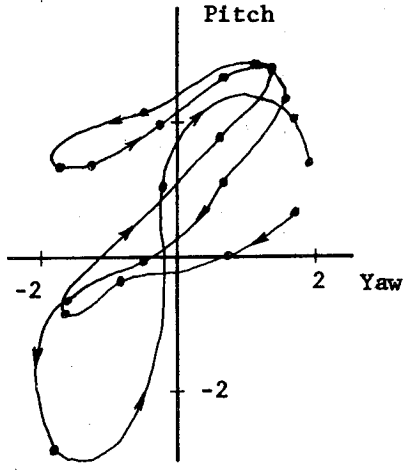

(100-102 sec)

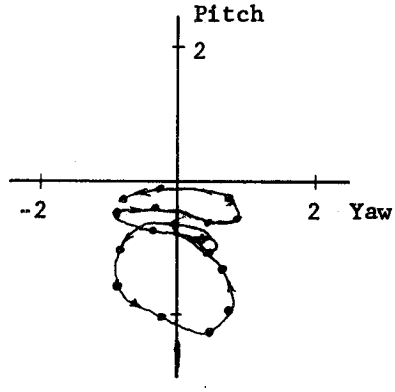

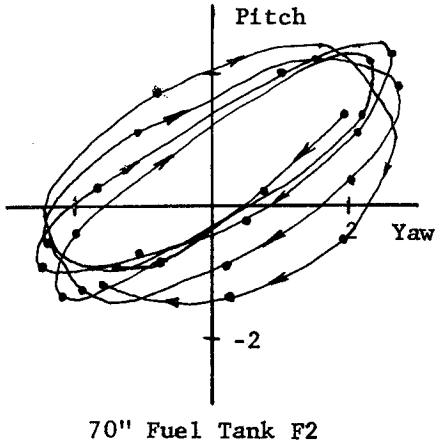

70" Fuel Tank F2

(102-105 sec)

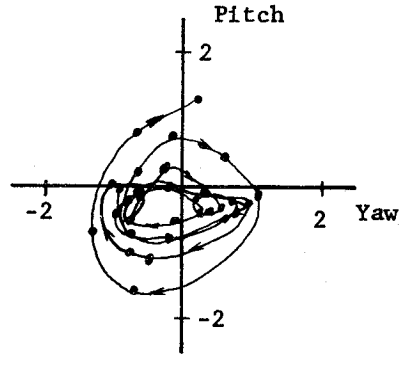

70" LOX Tank 04

0.1 second interval

Fig. 6-17	
SA-1	SPATIAL PLOTS OF SLOSHING MOTION

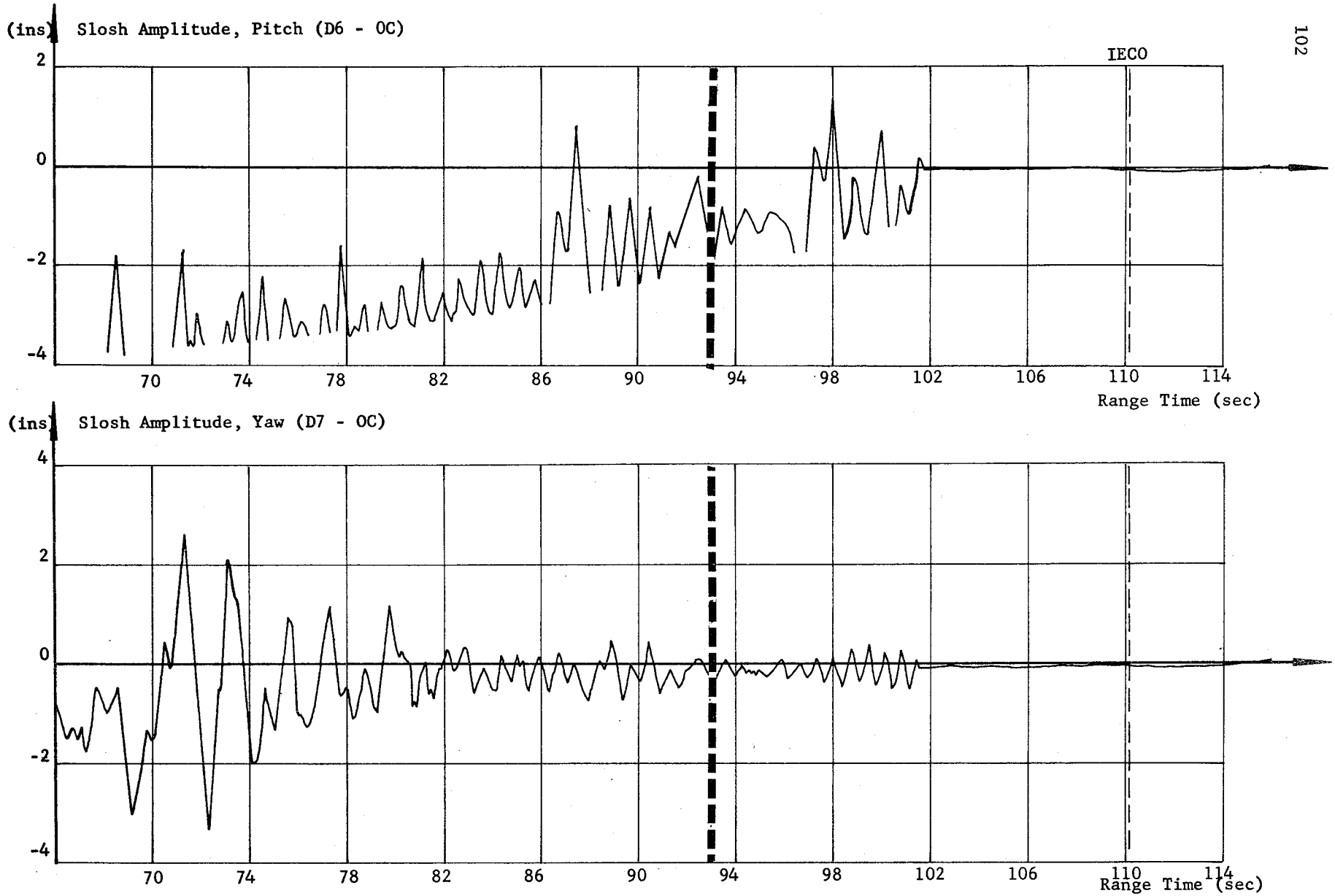

Fig. 6-18	CENTER LOX TANK OC TELEMETERED SLOSHING AMPLITUDES

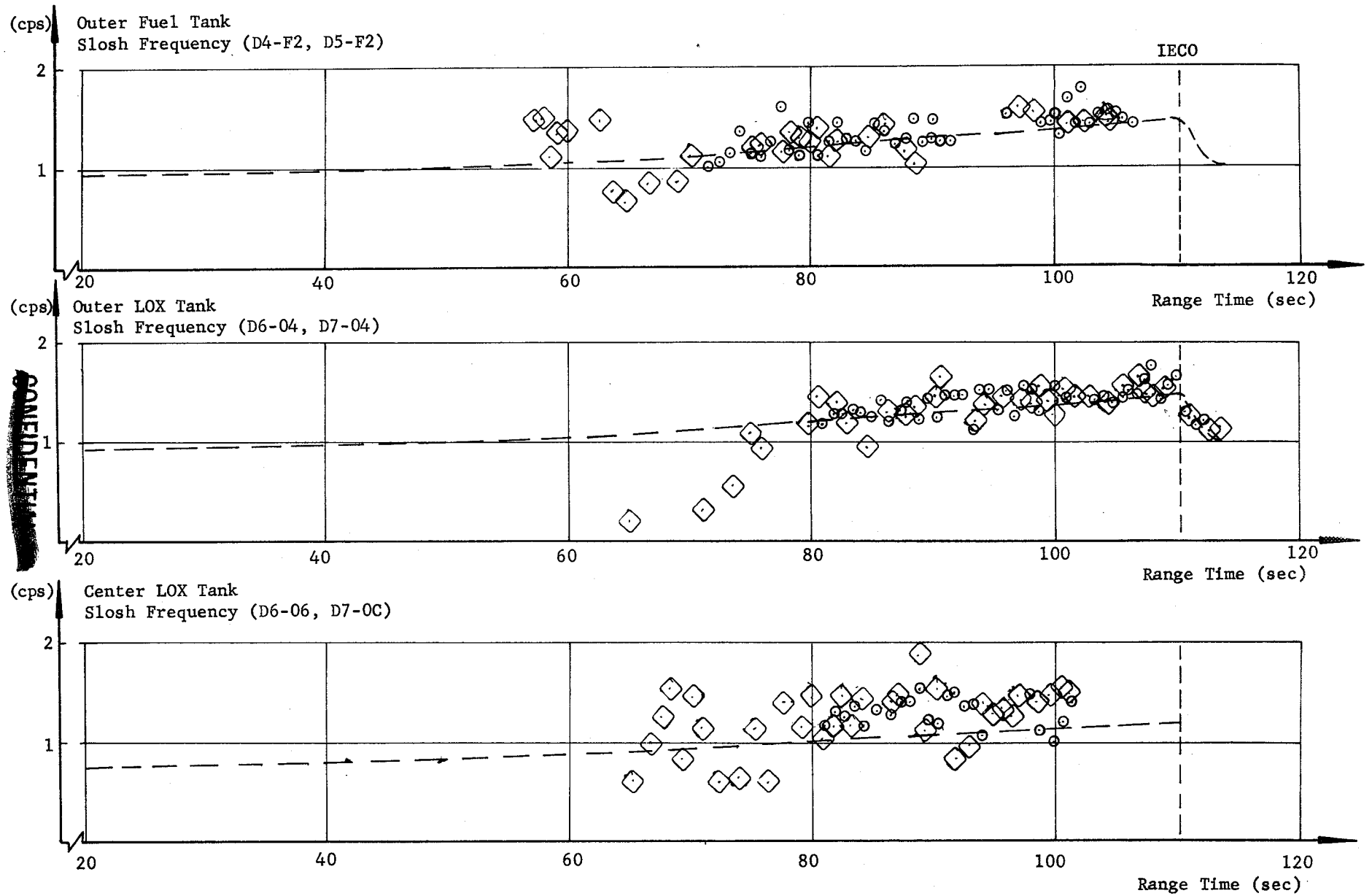

Fig.6-19	SLOSHING FREQUENCIES
SA-1	

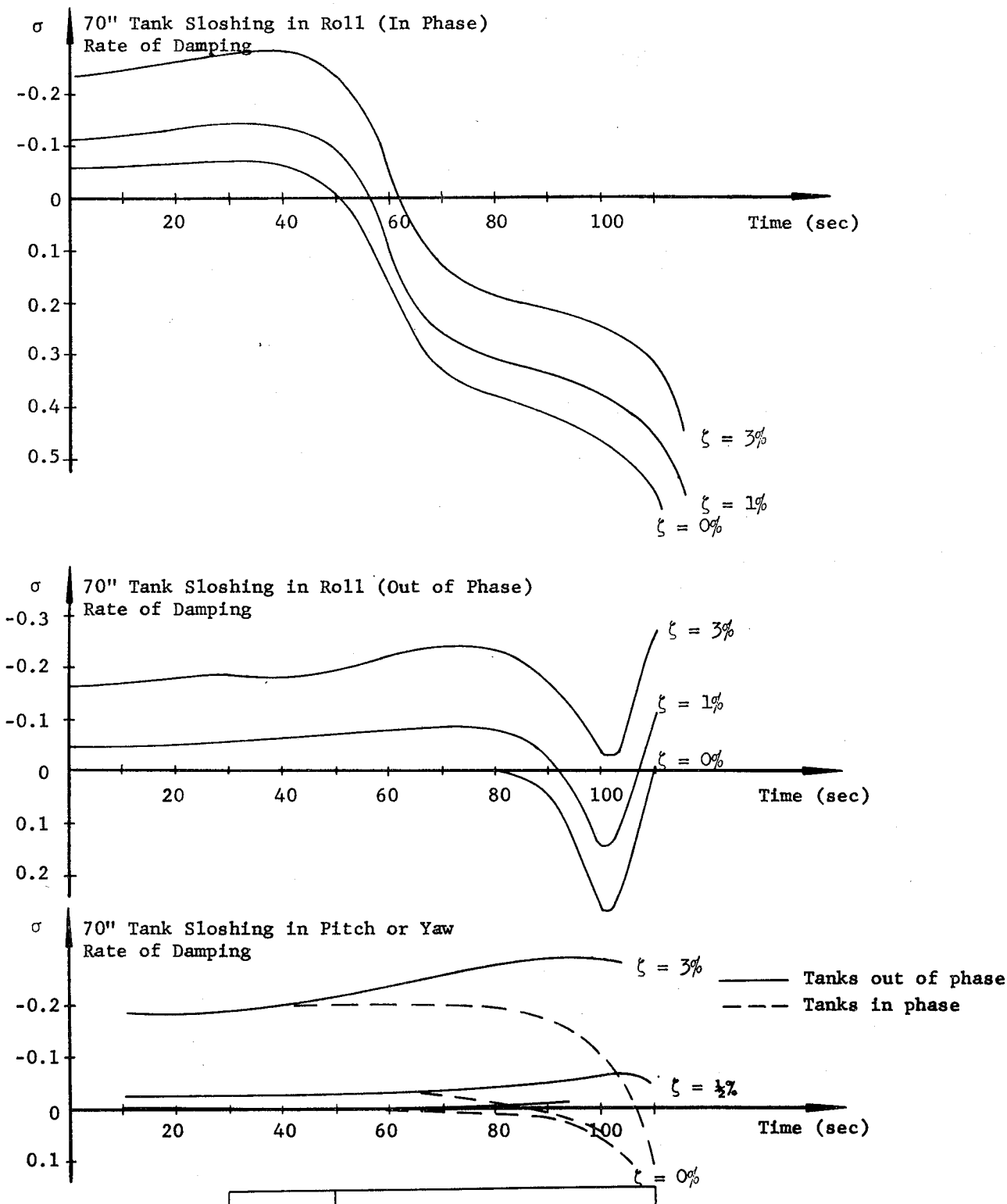

Fig.6-20	SLOSHING DAMPING ROOTS (THEORETICAL ANALYSIS)
SA-1	

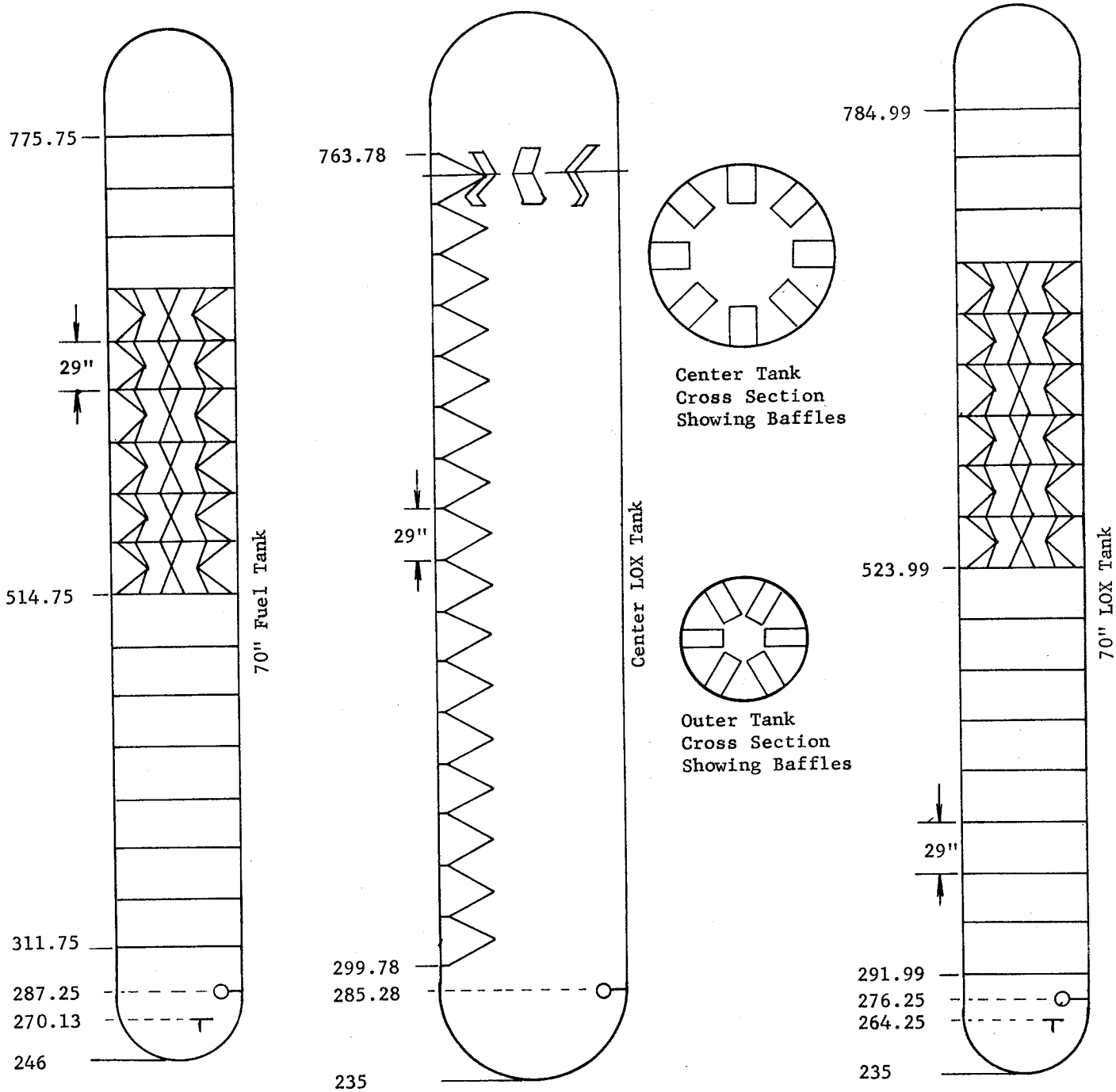

Note: Numbers indicate station locations

Fig. 6-21	
SA-1	BAFFLE CONFIGURATIONS

⊤ Level C.O.

○— ΔP Slosh Probe

7.0 (C) GUIDANCE

7.1 SUMMARY

SA-1 was flown without active path guidance. However, passenger hardware was on-board to establish the operational capabilities of the equipment in the Saturn flight environment. All telemetered information as well as a trajectory comparison indicate satisfactory performance of the equipment.

7.2 DESCRIPTION OF GUIDANCE SYSTEM

The guidance hardware included three pendulous integrating gyroscopic accelerometers (AMAB-4) mounted on an ST-90 stabilized platform. These accelerometers were mounted to sense forces along a set of inertial axes oriented with respect to the stabilized platform X, Y, Z axes. The slant range axis was directed downrange and elevated 41 degrees from the launch site horizontal; the slant altitude axis was directed up and 41 degrees counterclockwise from the local plumbline at launch; the positive cross range axis was in the local horizontal plane at launch and normal to the slant range - slant altitude plane forming a right-handed cartesian coordinate system. The platform axes were maintained in orientation by three AMAB-7 air bearing gyros. No second integrators were carried, and the guidance measurements were in open loop. A three axes analog velocity repeater unit was flown to telemeter the output signals of the accelerometers. This equipment was, with only minor modification, the same as that used on certain Jupiter and Juno II flights. Changes in the ST-90 were the inclusion of integral microsyn pickoffs, some additional shielding in the platform wiring, and new preamplifiers in the alignment pendulum circuits.

7.3 OPERATIONAL ANALYSIS

7.3.1 ACCELEROMETER OUTPUTS

The inertial velocity outputs of the integrating accelerometers furnished reliable data to substantiate the post flight trajectory. These data were reduced and compared with corresponding velocities calculated from external tracking data showing a very favorable agreement. The small, observed errors may be attributed to some combination of errors in the data reduction of telemetry, tracking and guidance hardware errors.

The platform remained in proper reference, with essentially no errors greater than established on sigma deviations. Difference values at cutoff are all less than 1 m/s and within the noise level of the comparison.

Slant Range Velocity

The outputs of the slant range accelerometer were compared with corresponding values calculated from the earth-fixed velocity components. These differences are plotted versus time in Figure 7-1. Differences were less than ± 0.5 m/s for the entire powered flight.

Cross Range Velocity

The telemetered cross range velocity is plotted versus time in Figure 7-2. Due to winds, the cross range velocity had increased to about 2 m/sec (right) when the angle of attack control coefficient, b_o, entered the control loop (27.0 sec after liftoff). A maximum velocity of about 2.4 m/sec was reached at 40 sec. The cross range velocity reached zero at about 62.5 sec and changed directions until a level of about 1.3 m/sec (left) was reached at 75 sec. At outboard engine cutoff the vehicle had a cross range velocity of about 1.5 m/sec to the left of the predicted flight path.

In Figure 7-1 the differences between the telemetered and calculated cross range velocities are plotted versus time. These differences are essentially zero until about 60 sec; after this time the differences increased to a maximum of about 0.7 m/sec at inboard engine cutoff.

Slant Altitude Velocity

SA-1 was flown with open loop guidance; therefore, no slant altitude velocity program was required, and the telemetered velocity was the repeated output of the accelerometer. Figure 7-3 presents the telemetered and precalculated slant altitude velocities plotted versus time. Telemetered velocity was slightly higher than precalculated values until inboard engine cutoff which occurred about 1.61 seconds earlier than precalculated. The telemetered slant altitude velocity was 1042.7 m/sec at outboard engine cutoff or 4.6 m/sec lower than the precalculated velocity due to the early cutoff.

The differences between the telemetered and calculated slant altitude velocities are plotted versus time in Figure 7-1. The differences were within ± 0.5 m/sec for the entire powered flight. At outboard engine cutoff the difference was 0.5 m/sec.

Table 7-I presents a comparison of the guidance velocities at some significant flight events. Telemetered values and those calculated from external tracking data are in close agreement. Most of the differences between the actual and precalculated values result from a burning time of about 1.61 seconds less than the standard time.

7.3.2 FUNCTIONAL ANALYSIS

Composite vibration levels encountered on the platform during flight were lower than expected. Peak composite levels reached were 4.5 g and 5.5 g during short time (10 millisecond) ignition transients. Other levels through liftoff plus 4 seconds showed peaks of 3 g or less. The levels rapidly dropped to about the measurement threshold level then peaked again at 45 seconds (2.4 g - Y axis, 1.8 g - Z axis) returning to the threshold level at 77 seconds for the remainder of powered flight.

Accelerometer servo error signals showed some disturbances during the higher vibration levels, but this was expected and was well below operation interference levels. The air bearing air pressure was 1 psi below tolerance (32 psi), but did not cause any disturbance to the equipment operation. (Ref. para 5.4.4). The analog velocity repeater unit performed satisfactorily in all three channels although some difficulty was experienced in data reduction of the cross range velocity due to noise at the measuring potentiometer cross over points. The noise is presently believed to be due to comparatively high vibration levels in the 22 to 25 cps region. An attempt is being made to better define and analyze the vibration condition in the area of instrument canister number 15.

First motion of the vehicle indicated by the longitudinal accelerometer was 140 milliseconds before liftoff signal (tail plug separation).

7.3.3 GUIDANCE INTELLIGENCE ERRORS

The guidance intelligence errors are defined as deviations in the guidance measurements resulting from hardware errors. Intelligence errors are obtained by comparing the telemetered guidance system values with those calculated from trajectory data. The guidance intelligence errors as presented include errors from tracking and data reduction, as well as actual guidance hardware errors. Therefore, the small differences shown in Figure 7-1 indicate only that no major malfunction occurred in the system. Due to the numerous error sources in the comparison technique, minor deviations of the hardware cannot be determined by this method.

The earth-fixed trajectory established from tracking data is mathematically transformed into inertial, space-fixed guidance indications. These calculated guidance velocities are then compared with the telemetered velocities to establish their agreement.

TABLE 7-I

(C) Guidance Comparisons

Event	Slant Range Velocity (m/sec)			Cross Range Velocity (m/sec)			Slant Altitude Velocity (m/sec)		
	Telem	Calc	Precal	Telem	Calc	Precal	Telem	Calc	Precal
Computer Preset	0.0	0.0	0.0	0.0	0.0	0.0	0.0	0.0	0.0
Inboard Engine Cutoff	2207.6	2207.9	2172.0	-1.5	-2.2	-0.5	1029.6	1029.3	1033.9
Outboard Engine Cutoff	2339.8	2340.1	2409.8	-1.5	-2.2	-0.5	1042.7	1042.2	1047.3
End of Thrust Decay	2346.8	2347.1	2418.4	-1.5	-2.2	-0.5	1043.2	1042.7	1049.2

Fig. 7-1	GUIDANCE VELOCITY COMPARISON (TELEMETERED - CALCULATED)
SA-1	

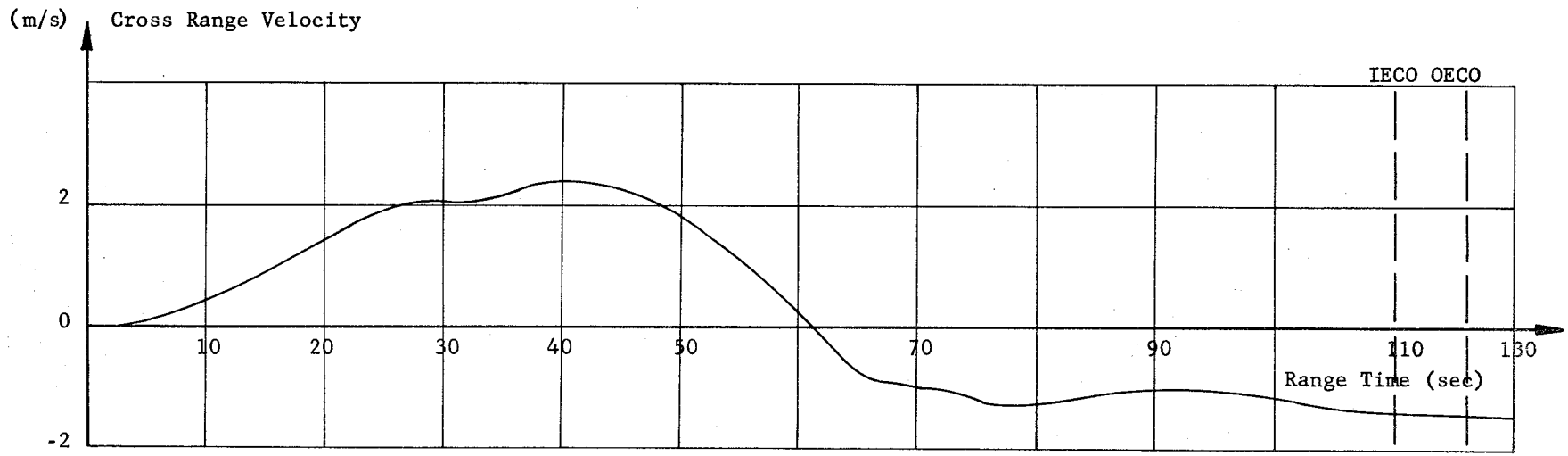

Fig. 7-2	CROSS RANGE VELOCITY (TELEMETERED)
SA-1	

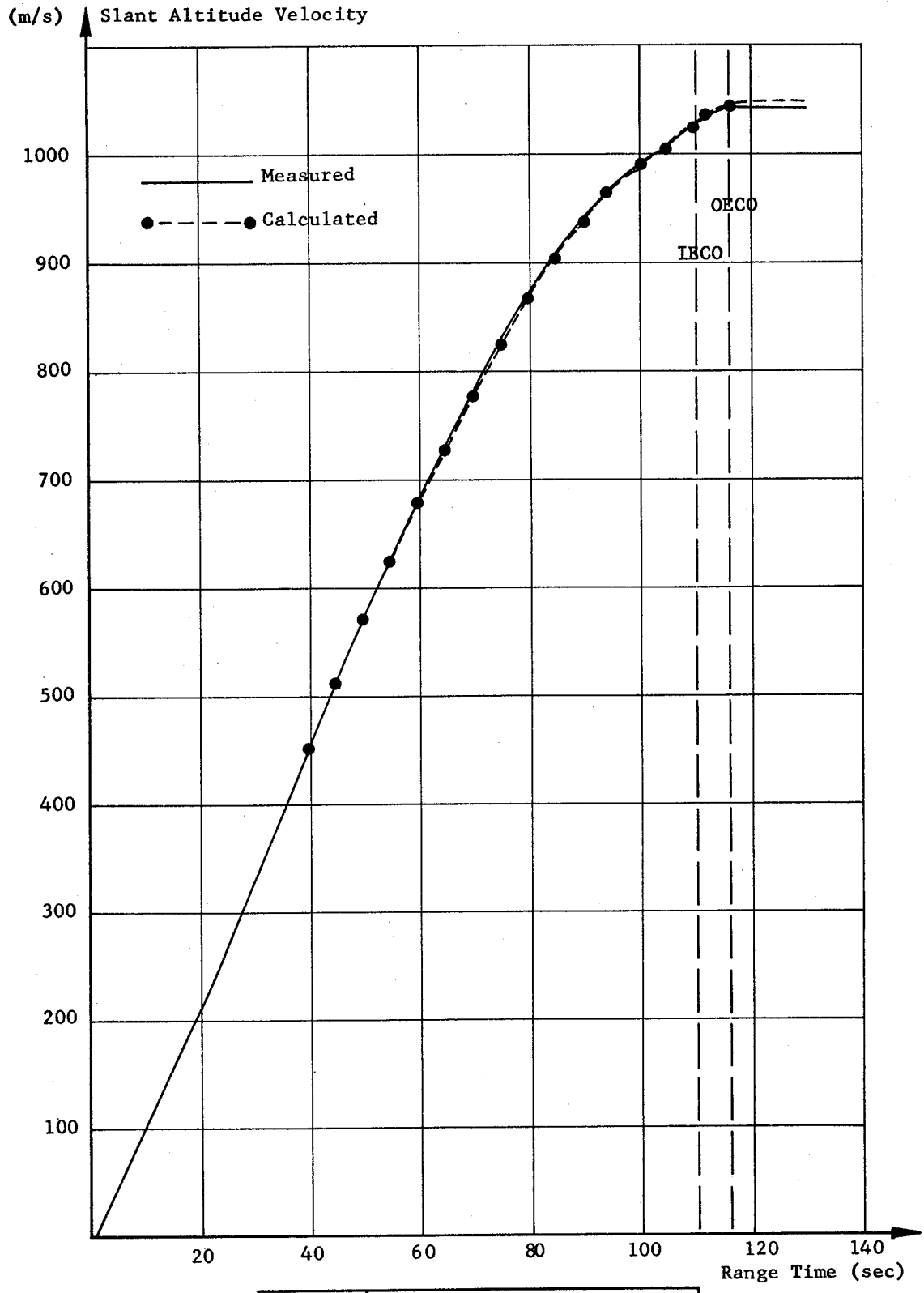

Fig. 7-3	SLANT ALTITUDE GUIDANCE VELOCITY (TELEMETERED)
SA-1	

8.0 (C) VEHICLE ELECTRICAL SYSTEM

8.1 SUMMARY

All vehicle networks performed as desired with only minor deviations.

8.2 POWER SUPPLIES

The vehicle power sources (Fig. 8-1) operated satisfactorily; however, the voltage measured on D11 bus showed some minor fluctuations when the air bearing regulator heater turned on and off. This voltage was 27 volts at power transfer and increased to 28 volts when the angle of attack heaters went off at T-21 seconds. All eight measuring voltages stayed at a constant 5 volts. The beta reference voltage and command voltage were also constant at 5 and 60 volts respectively.

The frequency of the precision guidance inverter (1800VA Rotary Inverter) was 400.009 cps during flight with the exception of the usual small liftoff transient. Short term frequency deviations after liftoff were less than 0.009 cps. The average frequency and all excursions were within the allowed operating limit of $\pm$ 0.025 cps.

8.3 FLIGHT SEQUENCER

All flight sequence steps occurred at the desired times.

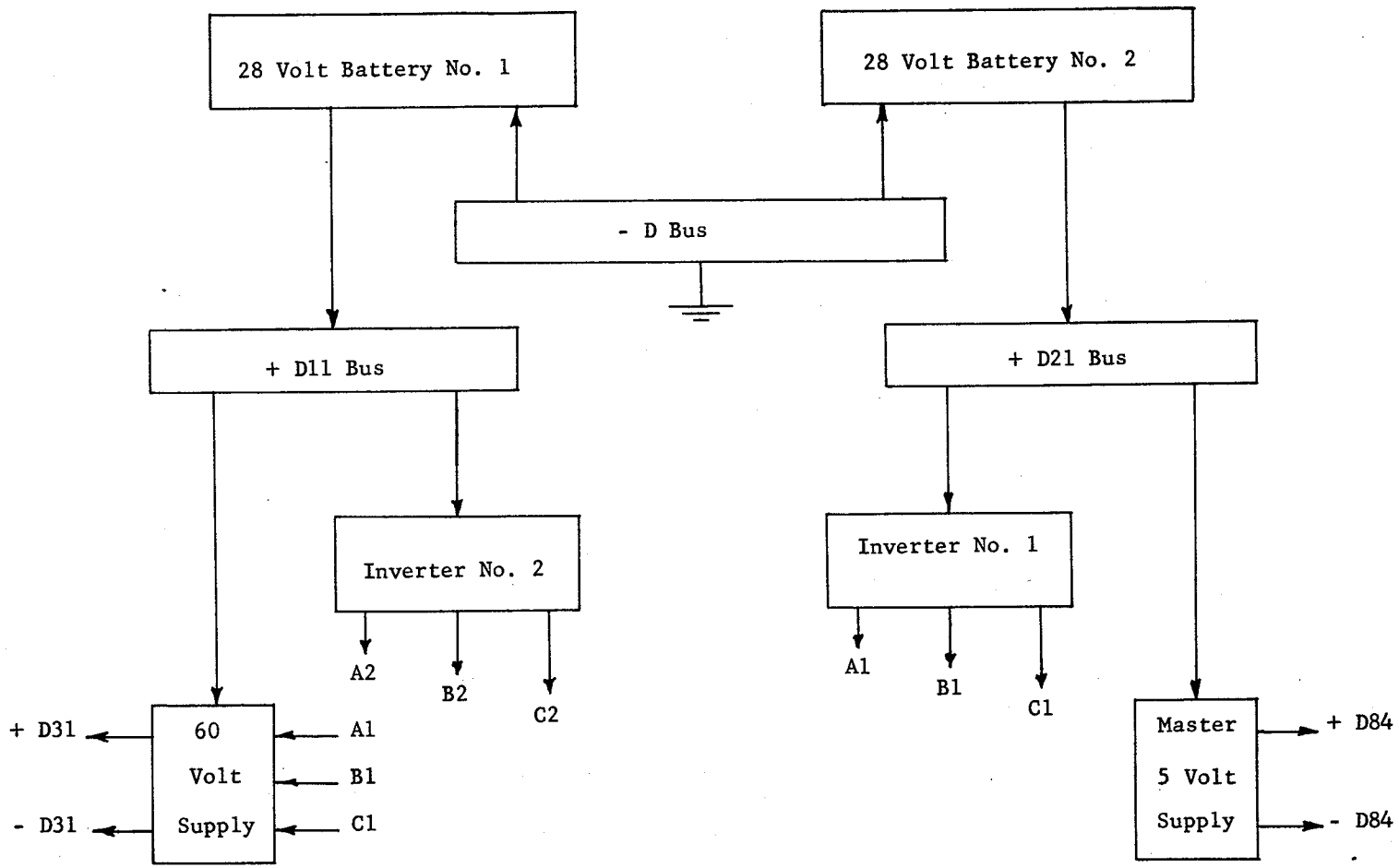

Fig. 8-1	SIMPLIFIED VEHICLE POWER SCHEMATIC
SA-1	

9.0 (C) STRUCTURES AND VIBRATIONS

9.1 SUMMARY

The original instrumentation for SA-1 included 8 strain measurements on the truss members and 8 strain measurements on LOX pins (mounting stud). From the truss measurements' resultant moment, longitudinal force and the angular position of the neutral axis were computed at various flight times. The results of these compared well with predicted values. Of the original 8 strain measurements on the LOX pins, only 2 were operative during the flight. The other 6 gages were found damaged and unfit for use during the prelaunch operations. Calculation of bending moments and longitudinal forces on the booster was not possible with strains from only two gage locations.

Instrumentation for detecting vehicle body bending consisted of 10 bending accelerometers at three stations along the vehicle. The observed bending oscillations cannot be positively identified; however, the oscillations do not meet the requirements for natural bending oscillations and are apparently the results of modified (or forced) structural bending.

Vibration instrumentation showed values comparable to or in some cases slightly lower than those expected for the SA-1 flight test. The vibration data was considered from a viewpoint of three main sources of excitation. These were: (1) mechanical source which began with engine ignition, (2) acoustical source which began with the sound field generated by the propulsion system, and (3) aerodynamic source which began as the vehicle approached Mach 1.

9.2 BENDING MOMENTS AND NORMAL LOAD FACTORS

9.2.1 INSTRUMENTATION

Instrumentation for SA-1 included 8 strain measurements on the truss members at Station 929 (see Figure 9-1). Bending moment and normal load factor distributions were also available from the 10 bending accelerometers located along the vehicle. (Ref. para 9.4)

Strain gages were also installed on the steel pins attaching the outer LOX tanks to the Spider Beam Assembly. Of the 8 original measurements, six were found damaged during vehicle checkout at the launch site and therefore were not active during the flight. The remaining 2 gages were apparently satisfactory.

Actual trajectory data (established from tracking sources) was used to derive bending moment and normal load factors during the dive phase.

9.2.2 RESULTS

Considerable variation existed in strain measurements recorded just prior to engine ignition. Since the bending moment history at Station 979* was not known during this time interval, none of these measurements could be considered a "base" value. The actual strains used for analysis purposes were calculated as follows:

(a) The average of 110 strain readings recorded prior to ignition was computed for each truss member. This average constituted a "base" value for each strain gage.

(b) The "base" values were subtracted from their respective strain measurements recorded during flight, (Fig. 9-2). These differential strains were used to calculate bending moments, neglecting any moment present prior to ignition. (Note: Low wind velocity at liftoff generates extremely small bending moments.) These measurements were also used to compute the change in longitudinal load at Station 979. To this value, the static weight of the upper structure and ballast (223,000 lbs.) was added to obtain total longitudinal load.

Calculation of Moments and Longitudinal Load

The following equations were used to relate the strain readings to the moment and longitudinal load:

$$M_{I\text{-}III} = 5.108 \quad \epsilon_{15} - \epsilon_{19} + .707\,(\epsilon_{14} + \epsilon_{16} - \epsilon_{18} - \epsilon_{20})$$

$$M_{II\text{-}IV} = 5.108 \quad \epsilon_{17} - \epsilon_{13} + .707\,(\epsilon_{16} + \epsilon_{18} - \epsilon_{14} - \epsilon_{20})$$

$$M_R = M^2_{I\text{-}III} + M^2_{II\text{-}IV}$$

$$L = .06245 \quad \Sigma\epsilon_N + P$$

* Although strain measurements were taken at Sta. 929, equations for bending moments and longitudinal force calculate values at Sta. 979.

where:

ϵ_N = Differential strain measurements E13-11 through E20-11 respectively, in μ inches per inch.

M_{I-III} = Moment about an axis through Fins I and III, inch-kips

M_{II-IV} = Moment about an axis through Fins II and IV, inch-kips

M_R = Resultant moment, inch-kips

P = Weight of upper structure and ballast, kips

L = Total longitudinal load, kips

A program was written to standardize the strain measurements and solve the equations above using the RPC 4000 computer. The equations were solved in 1/10-second intervals for the following time slices:

Seconds from Range Zero	Significant Events
0.8 - 4.04	Liftoff
23.04 - 26.0	Arbitrary Intermediate Time
48.0 - 50.07	Mach 1
59.23 - 64.04	Dynamic Pressure Maximum
68.06 - 70.08	Maximum Wind Shear
106.96 - 111.06	Inboard Engine Cutoff
405.94 - 409.03	End of Flight

This data was used to determine the instantaneous bending occurring about axes through Fins I and III (yaw) and Fins II and IV (pitch). Resultant moment, longitudinal force, and the angular position of the neutral axis were computed at various flight times.

Figures 9-3 and 9-4 indicate the trend of the moments during flight. Maximum moments occurred between 62 and 70 seconds range time. The moment data must be considered qualitative since small errors in the strain measurements cause large variations in the moment values.

The maximum moments computed from the differential strain measurements are considerably larger than those determined from other flight

data. While determining moments for this report, strain measurement E14-11 was found to be consistently higher during flight than all other measurements. The moment values presented in Figures 9-3 and 9-4 are therefore considered high, due to the strain indications of measurement E14-11.

The moment, Figures 9-3 and 9-4, can be seen to exhibit low frequency quasi-periodic variations. To check the validity of these variations, the moments were computed for a time period prior to ignition. Since the moments computed prior to ignition exhibit fluctuations similar to those occurring during flight, these variations cannot be considered of any physical significance.

Figure 9-5 shows the bending moment and total normal load factor distributions at the time of maximum dynamic pressure in ascent. The solid line curve results from the angle of attack and gimbal angle taken from actual flight measurements. The moment shown by the dashed line curve is the predicted 8 engine operation moment for the SA-1 vehicle.

Load factor distributions show the normal g's imposed on the vehicle due to the applied external forces.

Readings from the accelerometers, installed to establish bending modes and frequencies, were plotted at their stations to demonstrate the validity of the calculations. The resultant moments from strain measurements (only one station) are shown for comparison.

Figure 9-6 presents the bending moment and normal load factor information for 69.6 seconds, the time at which the vehicle experienced high wind shears.

Dive phase bending moment (408 and 409 seconds) is shown in Figures 9-7 and 9-8. This moment results from flight trajectory data. The load factor curve shows the normal g's imposed on the vehicle due to the applied external forces. While the magnitude of the moments is somewhat in doubt the trend is correct. No accelerometer readings were available since the measuring range of the accelerometers was limited to 0.5 g's and the normal acceleration exceeded that limit. It should be noted that there is a definite decrease in the moment from 408 to 409 seconds.

The strain measurements exhibited sharply defined discontinuities between 409.3 and 409.4 seconds range time. From this time to the end of the data record at approximately 409.4 seconds, the strain readings oscillated wildly. Several of the strain measurements in this time period were obliterated by calibration pulses. Therefore, no analysis

was attempted beyond 409.1 seconds. The maximum measured moment (about Fins II-IV at station 979) was 12×10^6 in-lbs occurring at 407.6 seconds, while the maximum calculated from flight data was 16×10^6 in-lbs occurring at 408 sec.

Since only two of the eight LOX pin strain measurements were active during the flight, it was not possible to use these measurements to calculated bending moments and load factors.

In order to preclude damage to the LOX pin strain gages on SA-2 through SA-4, the studs have been modified to provide better protection to the gages.

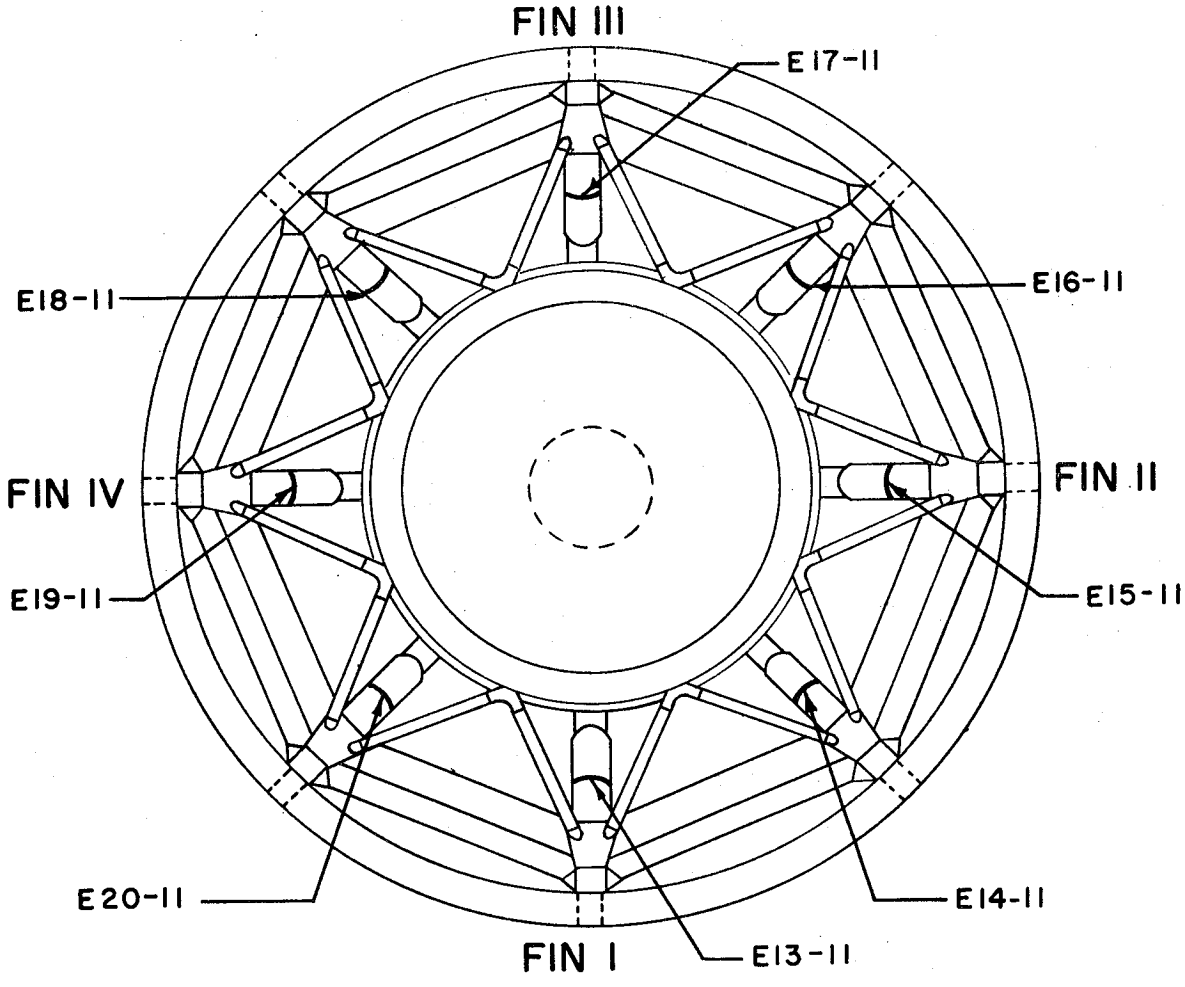

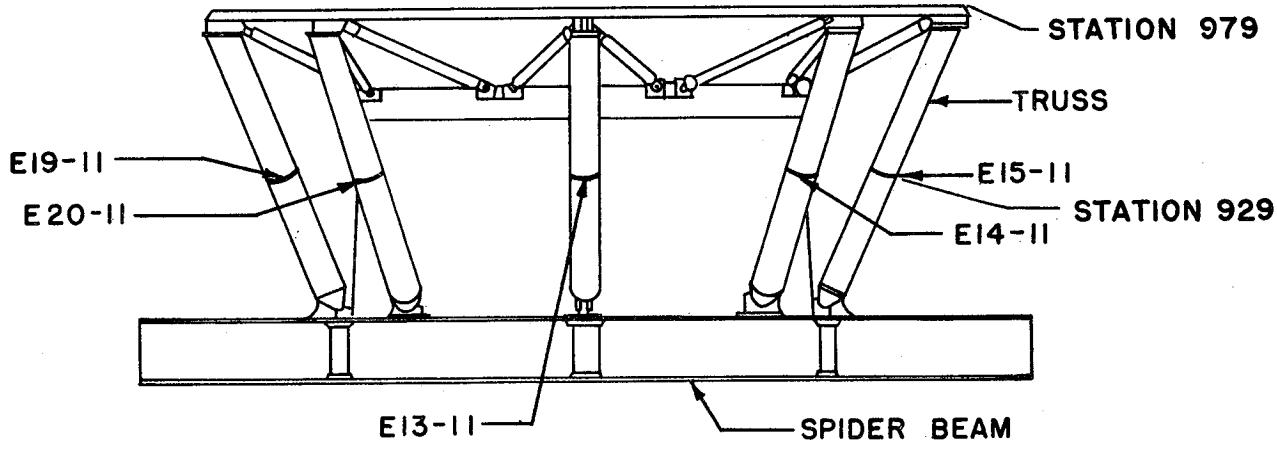

Fig. 9-1 SA-1	STRAIN GAGE LOCATIONS

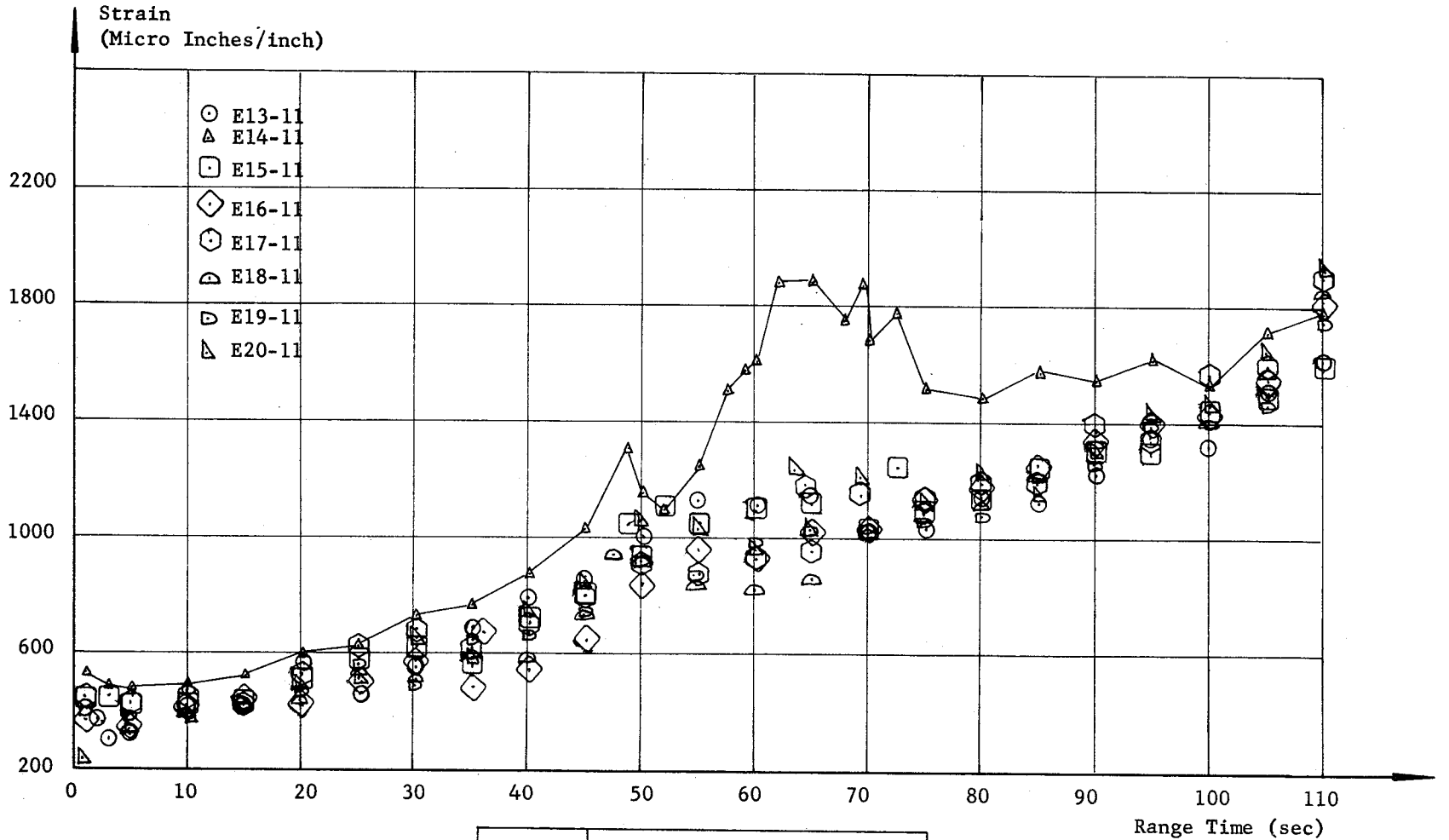

Fig. 9-2	DIFFERENTIAL STRAIN READINGS
SA-1	

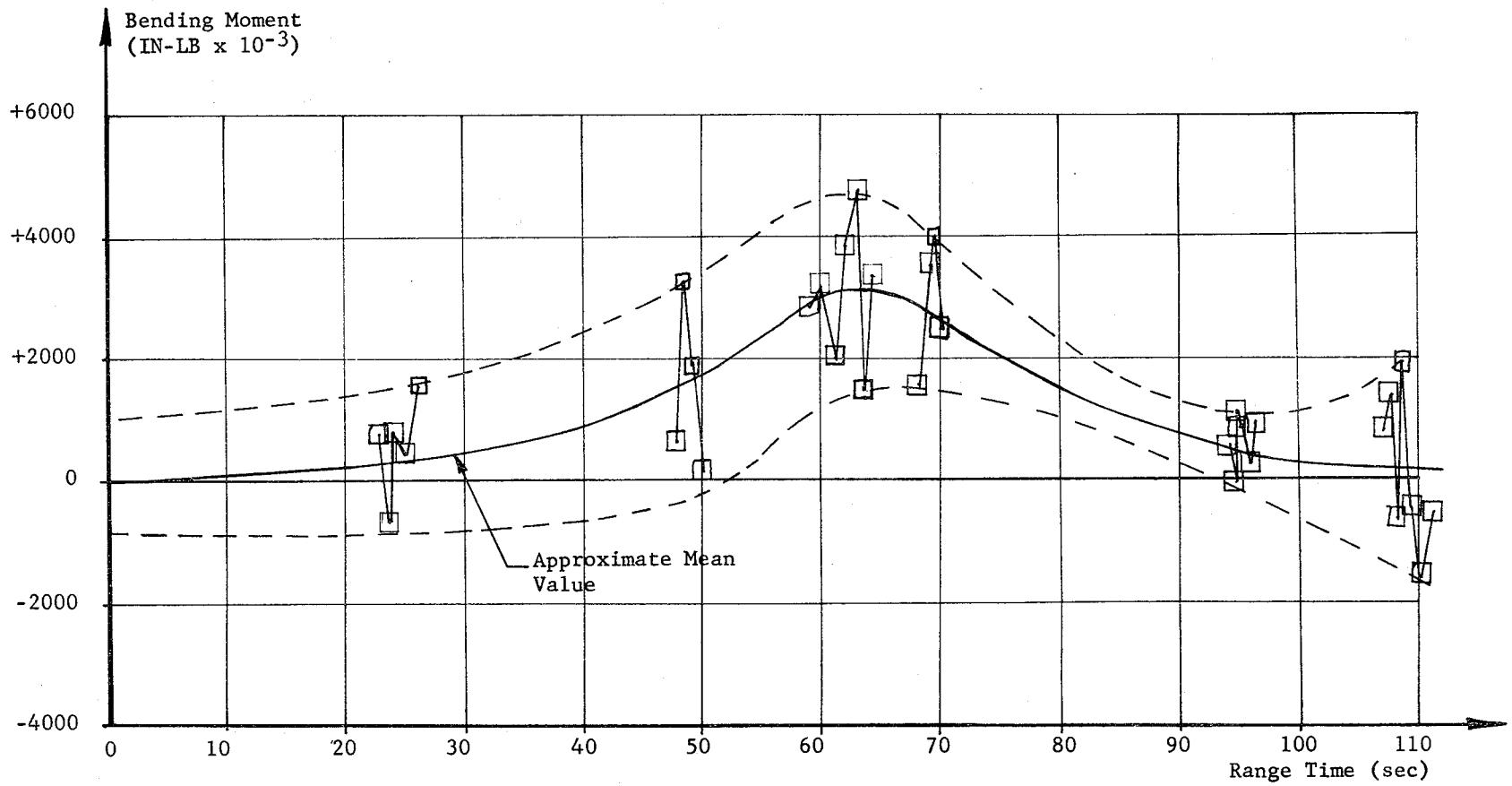

Fig. 9-3	ENVELOPE OF BENDING MOMENT ABOUT FINS I - III (YAW)
SA-1	

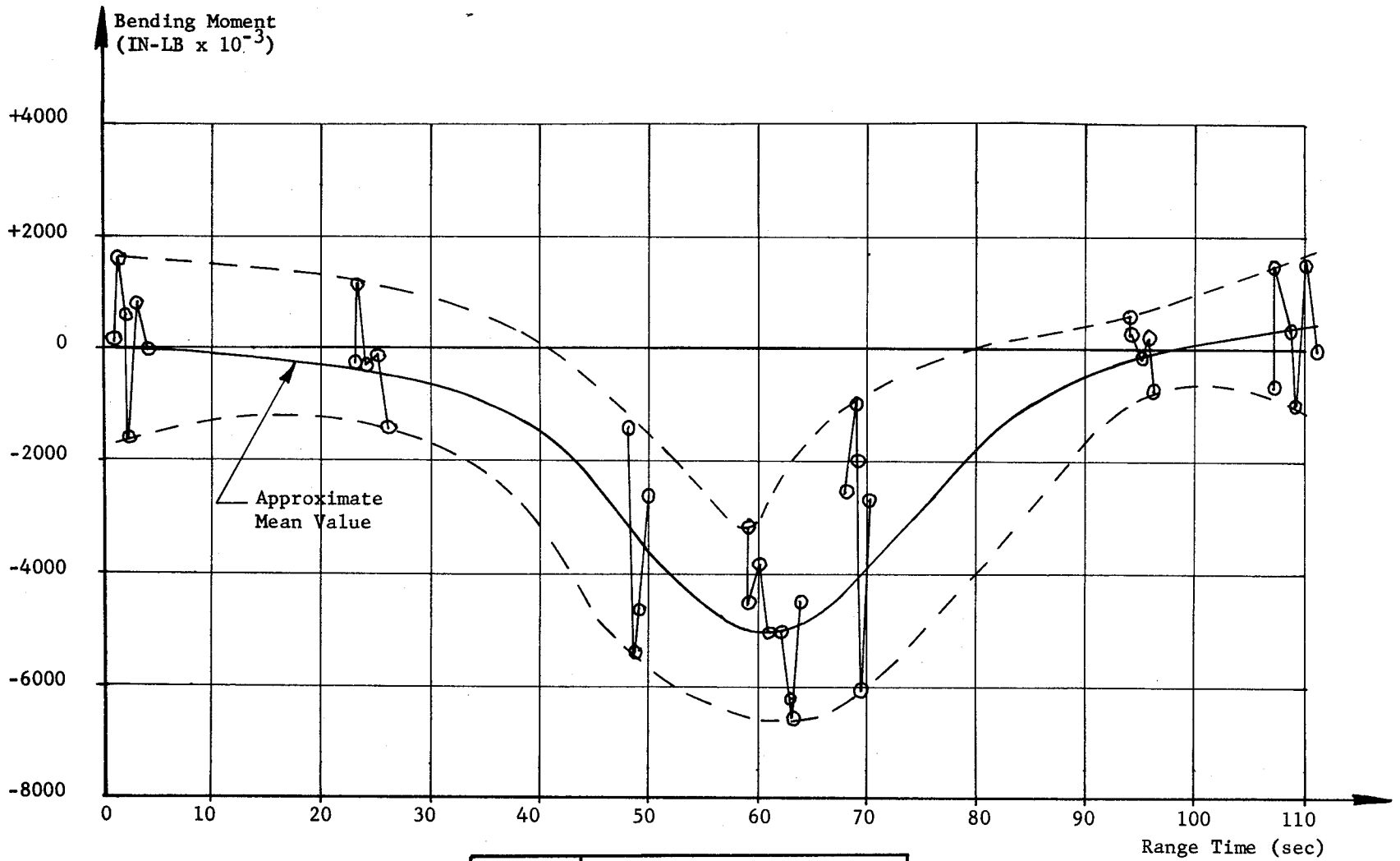

Fig. 9-4	ENVELOPE OF BENDING MOMENT ABOUT FINS II - IV (PITCH)
SA-1	

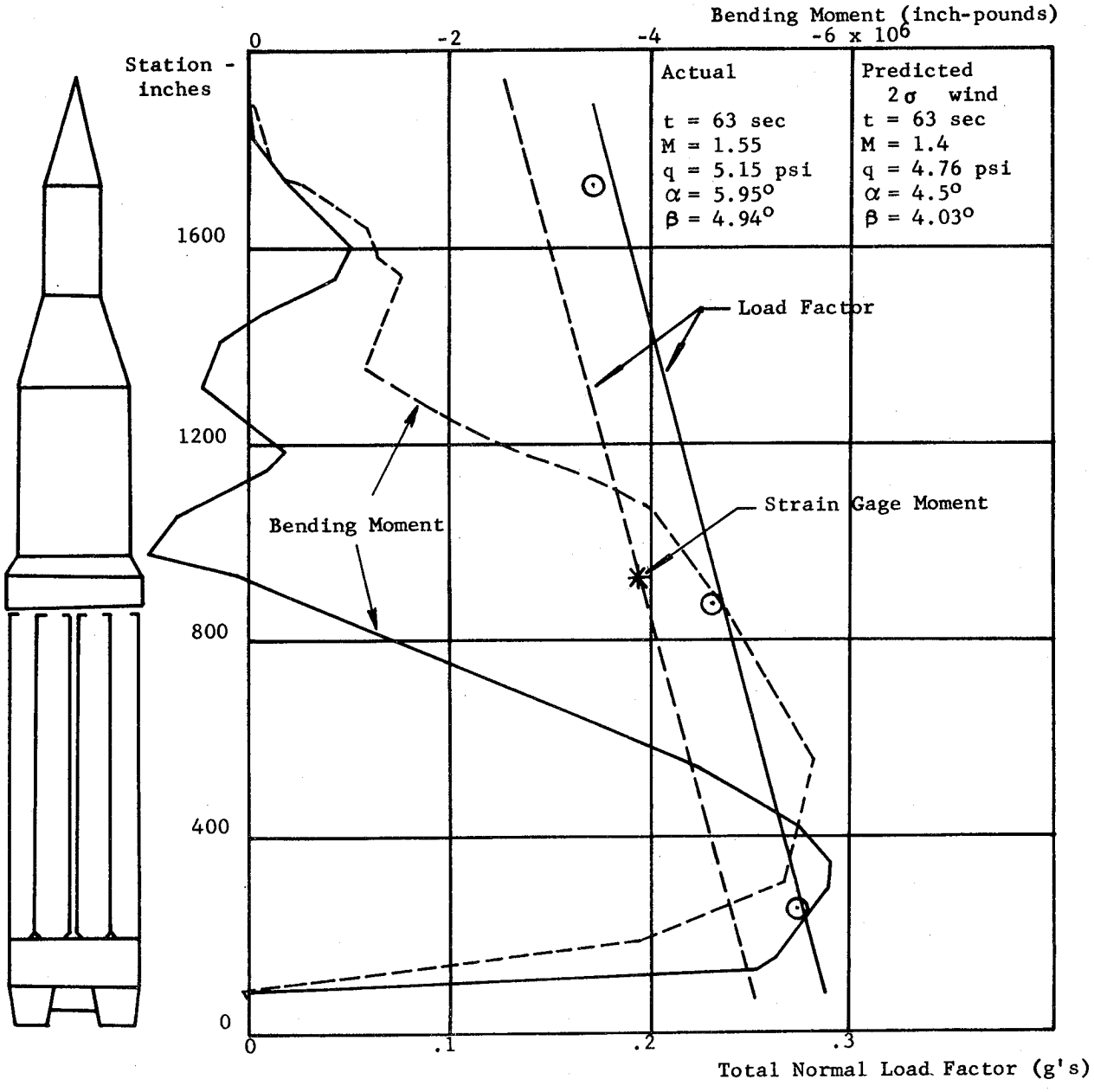

⊙ Accelerometer Readings - g's
—— Actual
– – – Predicted

Fig. 9-5	BENDING MOMENT COMPARISON (63 sec)
SA-1	

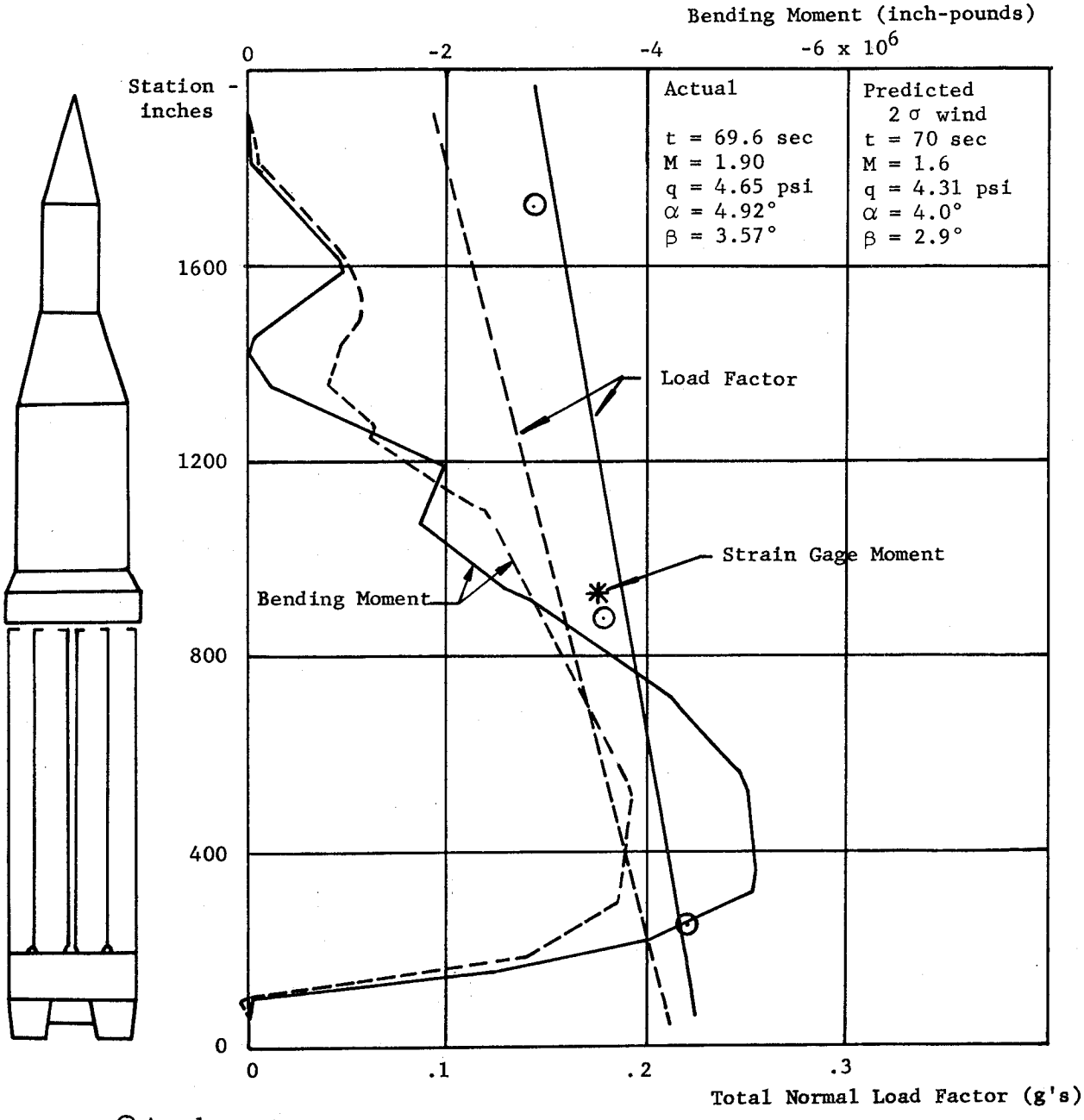

Fig. 9-6	BENDING MOMENT COMPARISON (69.6 sec)
SA-1	

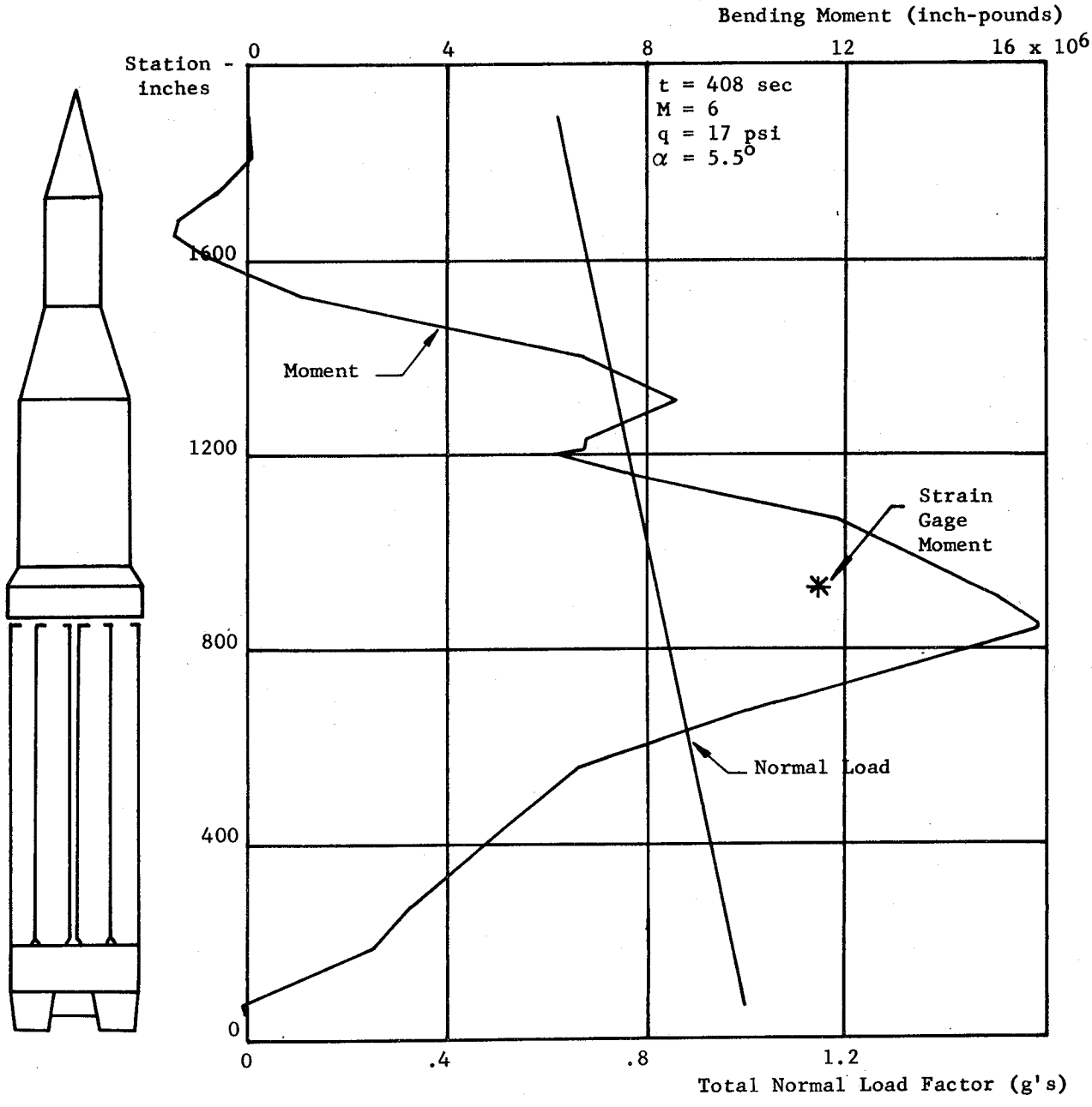

Fig. 9-7	
SA-1	Dive Phase Bending Moment (408 sec)

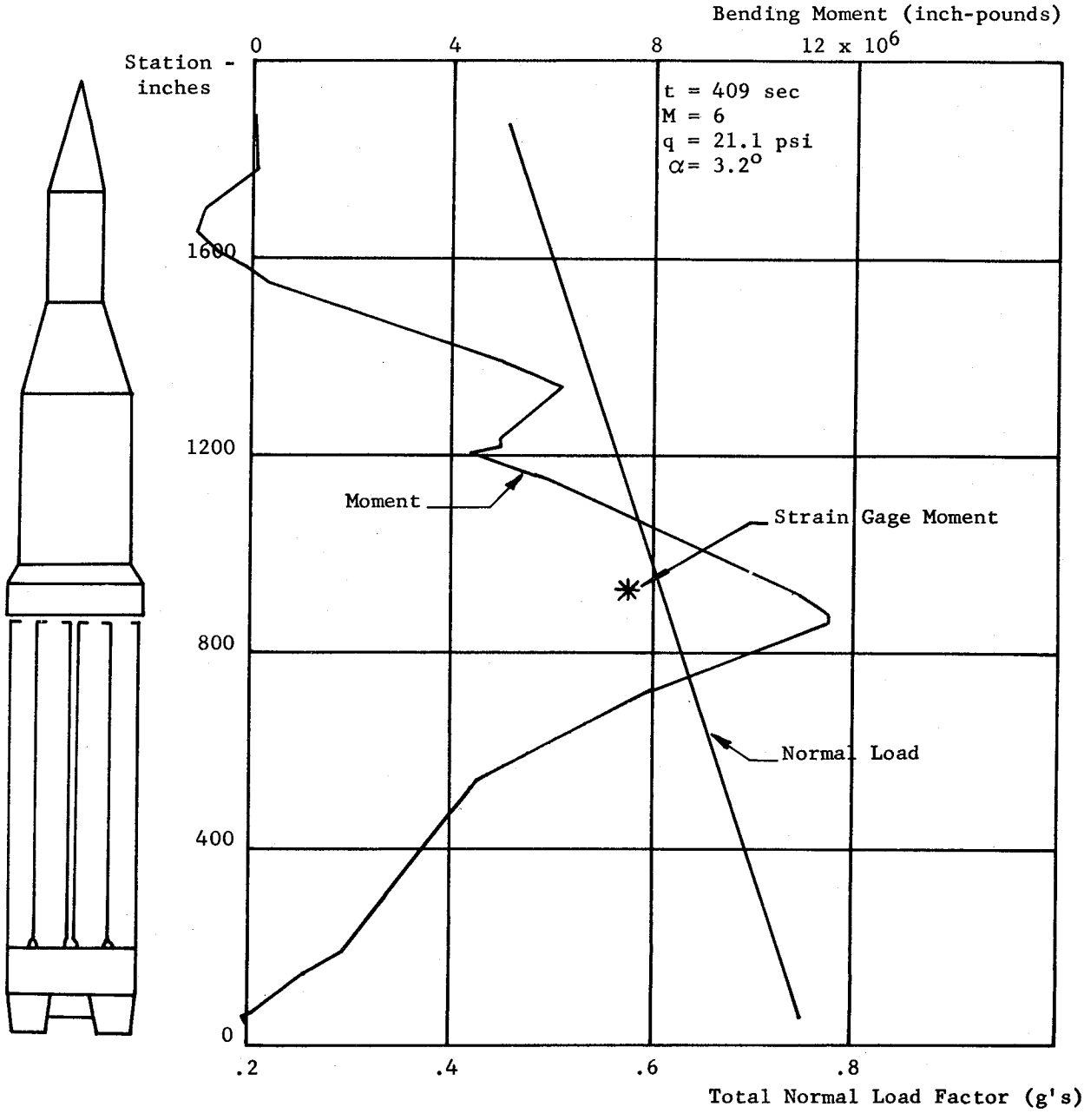

Fig. 9-8	
SA-1	Dive Phase Bending Moment (409 sec)

9.3 LONGITUDINAL LOAD

The longitudinal load at Station 979 is shown on Figure 9-9. The maximum load occurred at 110.06 seconds, just prior to inboard engine cutoff. Low frequency oscillations of the longitudinal loads (shown as circled points on Figure 9-9) were tested for validity in the same manner as the moments (Ref. para 9.2.2). Since the variation of the load prior to ignition was of very low amplitude, the oscillations occurring during flight may be of physical significance. The solid line on Figure 9-9 represents the longitudinal load as calculated using SA-1 flight data. As can be seen, the strain measurements and calculated values are in basic agreement with each other.

During buildup of the engines before launch command, dynamic forces arise in the deflecting masses of the system. These forces can be amplified and cause vehicle vibratory excursions of large amplitude. It was expected that a staggering time of 100 milliseconds between engine pairs would keep the vibrating force lower or equal to twenty percent of the maximum static thrust. Figure 9-10 is the result of an investigation made to determine if staggering the ignition times of the engines still kept the vibrating force below the 20 percent thrust value. Since the exact natural frequency of the system is unknown, it is necessary to assume a frequency interval from 2.1 to 4.8 cps. From this interval of frequencies the possible maximum vibrating force was obtained and plotted as shown by the maximum theoretical response (calculated). These results show that the possible maximum response is sixteen percent of the maximum static thrust.

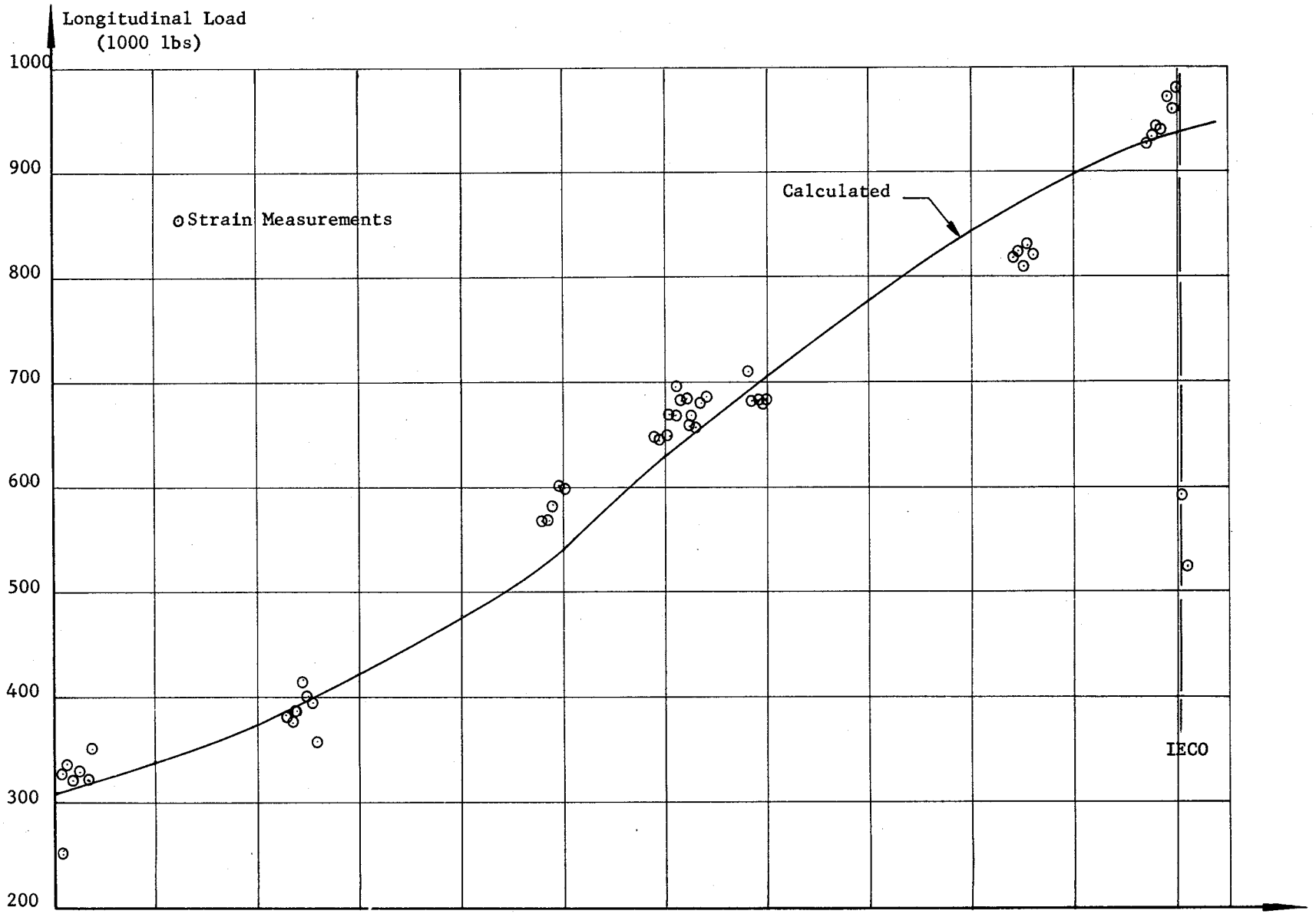

Fig. 9-9	LONGITUDINAL LOAD AT STATION 979
SA-1	

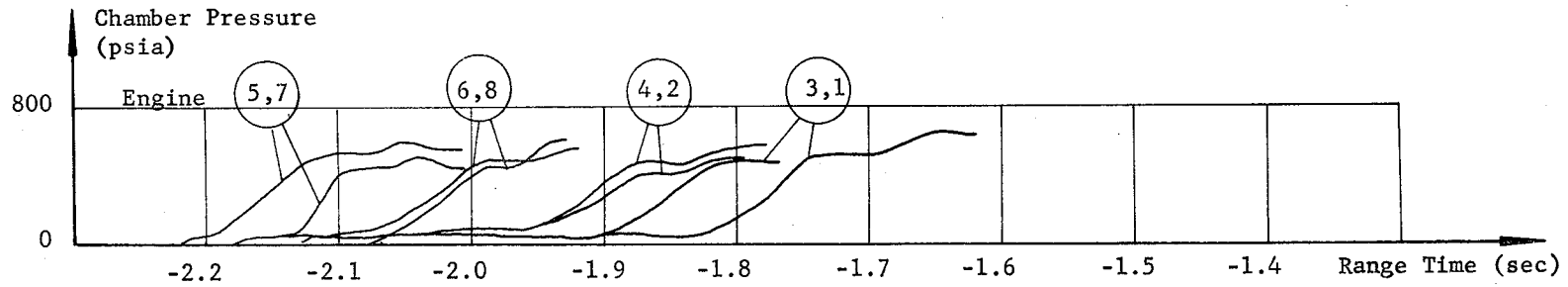

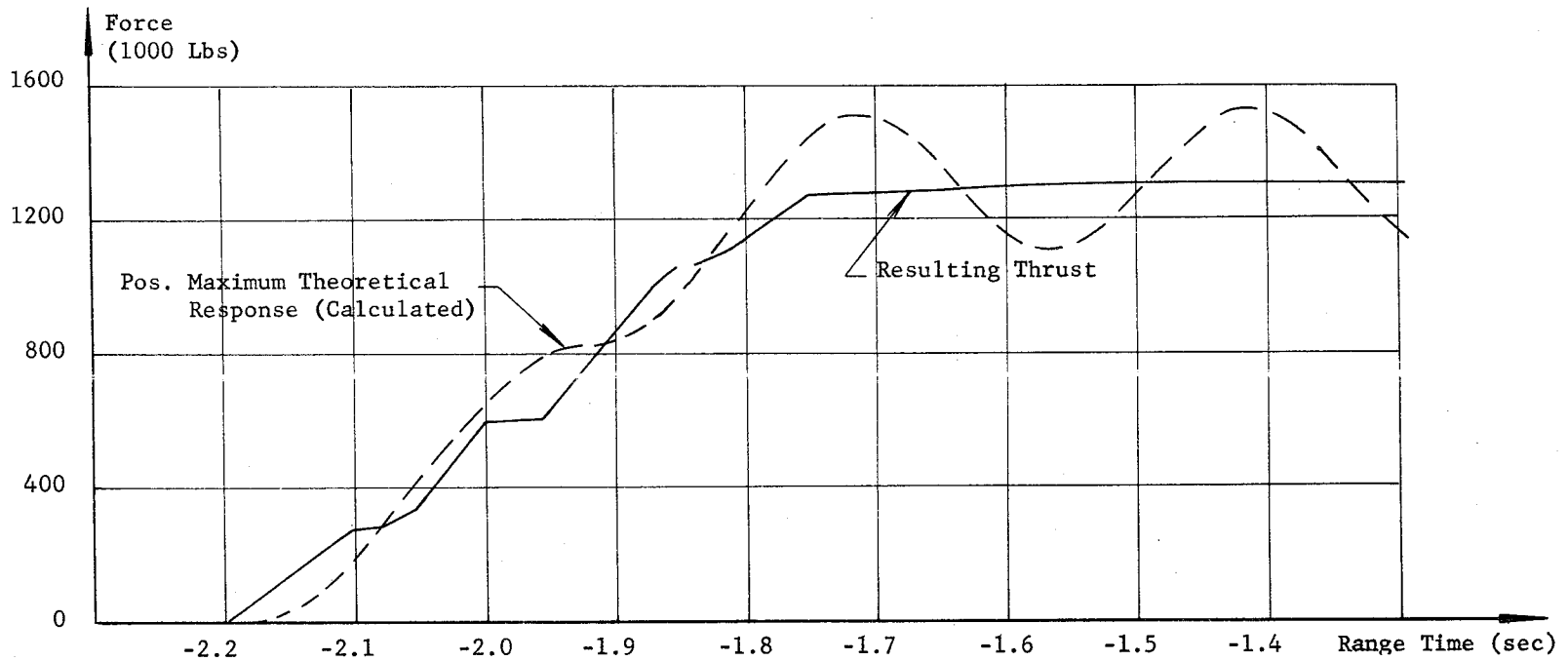

Fig. 9-10	POSSIBLE MAXIMUM DYNAMIC RESPONSE
SA-1	

9.4 BENDING OSCILLATIONS

The instrumentation for detecting vehicle body bending aboard SA-1 consisted of accelerometers near the nose, on the spider beam, and on the lower part of the center tank in both the pitch and yaw plane (see Fig. 9-11). One fuel tank and one LOX tank also had pitch and yaw accelerometers at the lower end, making a total of ten (10) bending accelerometers.

To define a vehicle bending mode with this instrumentation in either the pitch or yaw plane, the following three requirements must be met: (1) an oscillation near an acceptable bending mode frequency, (2) the proper phase relationship between the three vehicle bending mode accelerometers, and (3) an oscillation which endures for a minimum of one cycle. Ideally the oscillation should endure for several cycles, but the absence of sustained sinusoids at all three accelerometers, other than those caused by liquid sloshing, made this ideal unrealistic.

Throughout the flight, oscillations existed which would appear to be attributable to flexural vibrations, but these fail to meet the requirements.

The telemetered results have been analyzed at every point where a frequency, close to a known structural frequency, could be determined. Numerous time points exist where oscillations occurred at or near a structural frequency - but no oscillation occurred which satisfies the criteria. Furthermore, the normal variation in the fundamental bending frequency cannot be realized. In fact, the frequency shifts from the expected low frequency (around 2.2 cps) to slightly higher than expected (around 3.3 cps at 36 seconds flight time) and then drops to approximately 2.6 cps at 117 seconds. This frequency shift indicates that some other unidentified phenomenon is present.

Harmonic analyses of about three seconds duration have been accomplished at numerous time periods when sustained oscillations appeared on one or more accelerometer traces. These harmonic analyses show numerous frequencies present which are near to the fundamental flexure frequency. In some instances, there are three or more predominant frequencies present between 1.5 and 3.5 cps; some have greater amplitudes than the fundamental flexure frequency attributed to vehicle bending. The frequency spectra of the different accelerometers do not necessarily have the same harmonic content at the same time slice. Of course, some particular frequency may exist in all traces but have an insignificant relative amplitude. The engine gimbal frequency appears in all harmonic analyses.

Digital correlation analyses have also been completed at the time periods when a sustained oscillation occurred. This was done in attempting to find a rational, physical relationship between a cause and an effect or between different effects with a common cause. The results of the correlation studies indicate that the accelerometer at the base of the vehicle (Station 250) was not well correlated with the upper accelerometers, but correlated well with the engine gimballing measurements at frequencies ranging from 1/3 to 2/3 cps. The upper accelerometers are closely correlated at the expected fundamental frequency; however, the correlated frequency also exhibited the same shift from low to high then back to low. Accurate phase relations are not realized from correlation analyses; however, proper phase relations can usually be determined at a single point in time. These phase indications are in agreement with the phasing determined from the recordings themselves and contradicted the existence of a realistic bending mode.

The largest acceleration measured at elastic frequencies, although not a bending mode, was approximately .035 g's at 2.7 cps which corresponds to a deflection from equilibrium of about .047 inches (Station 875 - yaw direction). The measuring range of the accelerometers is ± .5 g's, so the maximum reading at an elastic frequency amounts to 7% of the full scale reading. Taking into consideration the instrument drift, noise, and the effect of the vibration environment, the difficulty in reading the resultant recording established an arbitrary confidence factor of ± 20% in amplitude. Phase is questionable to the extent of ± 15°, but in no case could the interpreted phase be off by 180°.

In bending analysis special consideration must be given to the transients induced by outboard engine's cutoff. There was a period where standing waves appear to exist; however, careful attention must be given to the exact time at which the transients are excited. The center tank acceleration leads in time. The spider beam acceleration in turn leads the nose acceleration. The shape of the first excited spike of the center tank indicates that an impulsive type of excitation existed which was propogated along the vehicle. This is substantiated by the peak values being staggered in time. The traveling wave was propogated along the vehicle at different velocities, with the velocity of each wave traveling at a velocity proportional to its own frequency. There is no reflected wave from the free ends of the vehicle so the traveling waves disappear very rapidly. In fact, there was also a negligible amount of damping associated with the traveling waves. This phenomena is still being investigated and will be reported later if the analysis is successful. The period after decay of the traveling waves is being investigated further. However, the peaks on the accelerometers are flat, not clipped, which introduces a few difficulties which have not been resolved to date. The apparent phasing between the three accelero-

meters in each plane was correct and is the most encouraging information determined so far. However, the frequency was lower than predicted and was lower than had been determined at earlier flight times, which shows again the paradoxical variation.

In summary, the observed bending oscillations cannot be positively identified; however, these observed oscillations do not meet the classical requirements previously stated for natural bending oscillations and are apparently the results of modified (or forced) structural bending. Apparently the major modifying factors are control loop response, individual outer tank modes, wind shear and propellant sloshing.

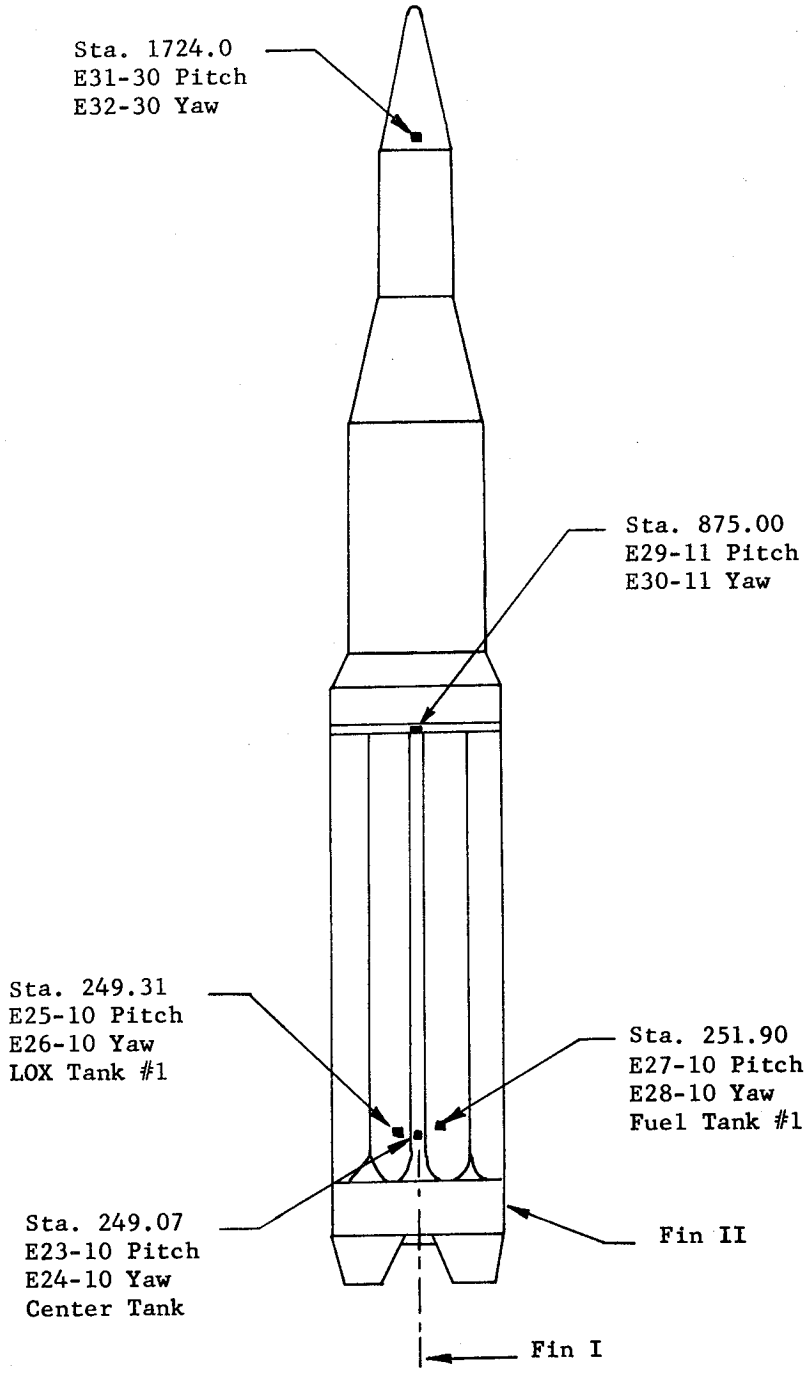

Fig. 9-11	BENDING MODE ACCELEROMETER LOCATIONS
SA-1	

9.5 TORSIONAL OSCILLATIONS

SA-1 was not adequately instrumented for determining torsional oscillations. The roll rate gyros measured rigid roll plus or minus the torsional oscillations. The dominant frequencies measured by the rate gyro were well below the fundamental torsional natural frequency and imply that any torsional compliance was negligible.

9.6 VIBRATION

9.6.1 INTRODUCTION

There are three main sources of excitation which produce the vehicle vibration environment. These are mechanical, acoustical and aerodynamic sources. The mechanical source begins with engine ignition, and, after the ignition transients, does not change significantly until cutoff. The acoustical source begins with the sound field generated by the engines at ignition. This source is a maximum at liftoff and becomes negligible after Mach 1. The aerodynamic source begins as the vehicle's velocity increases and is most influential during transition at Mach 1 and at maximum dynamic pressure.

The term "vibration mainstage" used with reference to SA-1 flight refers to the sustained vibration level occurring after the vehicle has left the acoustically reflective influence of the earth's surface and before the transonic conditions are reached. This term should not be confused with the mainstage term as used in propulsion. When referring to vibration data received from static firings, "vibration mainstage" is the sustained vibration level occurring after ignition and existing until cutoff.

There were a total of 45 vibration measurements monitored during the SA-1 flight, excluding the bending mode measurements. The 45 measurements were located as follows:

Location	Number of Measurements
Upper Structure (Spider Beam Area)	3
Platform (Canister No. 15)	2
Thrust Frame	2
Engines	12
Actuators	24
Actuator Yoke	1
Distributor Mounting Bracket	1

Actuator vibration measurements on SA-1 were telemetered on a time shared basis. The twenty-four vibration measurements were divided among

six telemeter channels allowing one channel for four measurements. Each measurement was connected to the channel transmitter by one segment of a four segment commutator. The commutator had a rotational period of 13.6 seconds which allowed each measurement 3.4 seconds of transmission in each period. This method resulted in the receipt of only one of four measurements for each channel during the actual time of liftoff Mach 1, max. q, and inboard and outboard cutoffs. There was no programmed time of transmission for any measurement; therefore, data was received from any one of the four measurements which might be commutating at that time.

The vibration summary curves (see example in Figure 9-12) present a time history of flight vibration and 10 cps narrow bandwidth analyses at various time slices. The time history curve shows G_{rms} metered values in relation to flight time. The plotted values were read at the time of liftoff, vibration mainstage, Mach 1, max. q, inboard and outboard cutoffs. The points were connected by a faired curve which approximated the composite vibration curve. The 10 cps narrow bandwidth analyses were taken over time periods which covered the indicated times of liftoff, vibration mainstage, Mach 1, max. q and inboard or outboard cutoff except for the time shared measurements which were taken as close as possible to these times. Either the inboard or outboard cutoff time slice was plotted depending on magnitude of response. The limit of linear frequency response for the particular channel is indicated by the asterisk (*) and vertical line intersecting the curve. A 1/3 octave analysis of each vibration measurement was also made. Since this analysis agreed closely with the narrow band analysis, none of the 1/3 octave analyses is shown in the vibration plots.

9.6.2 STRUCTURAL VIBRATION

Thrust Frame (Fig. 9-13)

The narrow band analysis of these measurements (E6-9 and E7-9) revealed the presence of 400 and 810 cps frequencies throughout the powered flight. As shown in Figure 9-13 the predominate frequencies for E6-9 and E7-9 are 810 cps and 400 cps respectively. The 1/3 octave analysis showed the 400 and 810 cps as well as the presence of beating on the 31.5 cps center frequency for measurement E7-9. The composite trace for the thrust frame measurements remained relatively constant throughout the powered flight with the exception of a slight buildup occurring at ignition and liftoff.

Yoke, Yaw Actuator (Fig. 9-13)

The predominate frequencies as shown by narrow band analysis for

liftoff are 8 and 14 cps; vibration mainstage are 5, 7, and 17 cps; Mach 9 are 7 and 8 cps; Max q 7 cps; and cutoff 10.5 cps. The composite vibration levels appear to be normal; however, clipping occurred at ignition, liftoff, and cutoff, thus indicating the need to change the calibration range from $\pm$ 0.5 g to at least $\pm$ 1.0 g. Increases in the magnitude of the composite level were noted during both pitch and yaw gimballing. A frequency of 5 cps was noted in the composite trace at 46 seconds, 4 cps was noted at 51 seconds, and 10 cps was noted at cutoff.

Mounting Bracket Distributor (Fig. 9-14)

The composite trace displayed a buildup at ignition and liftoff then decayed into vibration mainstage at 6 seconds, peaked at 65 seconds, and decreased to the vibration mainstage level at 90 seconds. A frequency of 3 1/2 cps appeared on the composite trace at 41 seconds and 10 cps at cutoff. The 1/3 octave and narrow band analysis (Fig. 9-14) reveal that maximum energy at ignition, liftoff, and during the period between 35 and 90 seconds appears to be contained within the 400 and 500 cps center frequencies. The 31.5 cps center frequency filter indicates the presence of beating.

Upper Structure (Fig. 9-15)

The three upper structure measurements showed smooth and rapid transition at ignition. Vibration levels decreased smoothly from liftoff to vibration mainstage values in approximately 6 seconds. Maximum energy levels during ignition transition and liftoff are in the frequency range from 250 to 500 cps. A 3 to 5 cps vibration was present in varying degrees of prominence throughout the composite trace of E1-11 and E2-11. This low frequency vibration is not present in E3-11. Measurements E1-11 and E3-11 show a slight vibration level buildup at Mach 1; E2-11 shows a very pronounced level increase at this time. None of these measurements show response at the time of max. q. Response to engine cutoff is slight at both inboard and outboard cutoff.

9.6.3 PROPULSION SYSTEM VIBRATION

Thrust Chamber Dome and Gear Box (Fig. 9-16 through 9-19)

The four gear box measurements (Fig. 9-16 and 9-19) and the eight thrust chamber measurements in general showed relatively high vibration levels during the ignition period as compared to the vibration mainstage levels. These ignition transients lasted approximately 0.2 to 1.0 second, after which the vibration levels rapidly adjusted to the vibration mainstage levels. The vibration levels remained relatively unchanged from range zero minus 1.0 seconds until immediately before cutoff of the

engines. The cutoff of the inboard engines did not appear to influence the outboard engine vibration levels an appreciable amount, but in some cases did raise the vibration levels on the inboard engines for a short period of time. At some times outboard engines' cutoff also raised the vibration levels on the outboard engines. Cutoff vibration levels were generally lower than the ignition transition levels. There also appeared to be very little interaction between the engines (i.e., one engine does not appear to be exciting the other engines an appreciable amount). In general the engine measurements are very smooth except for what appears to be trouble with telemetry in some of the traces. (Ref. Section 12.0)

9.6.4 COMPONENT VIBRATION

Hydraulic Actuators (Fig. 9-20 through 9-27)

The vibration measurements on the hydraulic actuators were time shared; consequently the data from every measurement was not available at all the desired flight times.

Vibration levels during liftoff and during cutoff of the outboard engines were, in general, slightly higher than the levels recorded during vibration mainstage. There appeared to be no change in vibration response at the time of inboard engine cutoff. There also appeared to be no change in the vibration levels at Mach 1 or during the period of maximum dynamic pressure. Vibration mainstage levels appeared relatively uniform with the exception of high amplitude transients which appeared intermittently in the data throughout the powered flight. These transients did not appear to be realistic data, and their indicated magnitudes were therefore considered erroneous.

Twenty-four telemetered measurements were used in obtaining vibration data on the pitch and yaw actuators during the SA-1 flight. All the measurements were time shared.

High level transients were observed in the data throughout the powered flight. An investigation revealed a definite correlation between these transients and the gimballing times which were recorded during the flight. The results of this investigation will be included in a subsequent report comparing flight and static environments.

Data from measurement E39-2 appeared questionable. The composite and filtered traces appeared as a straight line, i.e., no vibrational response was indicated. Narrow band analysis for this measurement is shown in Figure 9-23. Measurements E34-3 and E35-3 (Fig. 9-24 and 9-25) also appeared questionable after narrow band analyses were performed.

ST-90 Gyro Platform (Fig. 9-28)

Measurement E4-15 was located on the ST-90 gyro platform and measured vibration in the longitudinal direction. The composite trace shows a buildup during ignition to a level approximately six times that of vibration mainstage. There is a slight decrease after ignition until liftoff. At liftoff there is a slight buildup again to a level approximately five and one-half times that of vibration mainstage. There is a gradual decrease after liftoff until the vibration mainstage level of 0.24 G's rms is reached (See Fig. 9-28). The narrow bandwidth analysis indicates that there was 27 cps present throughout the powered flight. Also, the 1/3 octave analysis indicates there is 100 cps present throughout the flight. At approximately 32 seconds, the composite trace begins to buildup gradually until a peak is reached at 44.4 seconds. There is a gradual decrease and then another increase until a peak occurs at 61 seconds. The measurement begins to decrease after 61 seconds and continues to decrease until inboard engine cutoff. At inboard engine cutoff, there is a transient followed by what appears to be a low frequency sinusoid (approximately 10 cps). The narrow bandwidth analysis at this time does indicate the presence of 10 cps. There is another slight buildup at outboard engine cutoff, but it is not as pronounced as the inboard engine cutoff.

Measurement E5-15 was located on the ST-90 gyro platform and measured vibration in the yaw direction. The composite trace indicates a small amount of vibration prior to ignition, but the only indication of vibration at this time found in the 1/3 octave data is at 31.5 cps and 25 cps. This would indicate that there is a small amount of excitation at approximately 26 - 28 cps. These frequencies were also detected in the output of the cross range velocity (Ref. para 7.3.2).

At ignition, the accelerometer sensed several high "g" level pulses. The time lag between the thrust buildup of engines five and seven produced the largest transient. Another transient can be observed which corresponds to thrust buildup for engines six and eight. The vibration level remains relatively high for 500 milliseconds and then begins to gradually decrease. The liftoff effect can be detected in the composite trace. A steady-state vibration mainstage level is not reached until approximately ten seconds. There is a gradual buildup in the composite beginning at approximately thirty-four seconds and reaches a maximum at approximately forty-four and four-tenths seconds. The composite trace decreases and then increases until another peak is reached at sixty-one seconds. The trace decreases from sixty-one seconds until inboard engine cutoff at 110.1 seconds. There are slight buildups at each cutoff.

9.6.5 DISCUSSION OF VIBRATION DATA

Liftoff Comparison for Jupiter and Saturn Vehicles

Jupiter missile launchings did not employ any type of mechanical hold down, and liftoff occurred as soon as engine thrust reached a value which exceeded the vehicle weight. This thrust value was reached approximately 0.6 seconds after ignition. Therefore ignition and liftoff transients were considered as occurring simultaneously for the purpose of vibration analysis on Jupiter missiles.

The Saturn vehicle is held down for a period of approximately 3.6 seconds, and the liftoff period is now defined as the time from range zero to +5 seconds. Since the liftoff period on Saturn is separate from engine ignition, it does not include the high vibration ignition transient period. In general, it can be said that acoustical and mechanical excitation from the engines has a high level transition period within two seconds after ignition. This ignition transient period can no longer be included in the liftoff period but still must be evaluated as part of the environment of the vehicle. The evaluation of this ignition transition period can not be accomplished with a narrow band analysis because the period usually lasts less than one second; therefore, a one-third octave time history oscillograph is usually employed.

A summary of all the vibration measurements showing peak levels reached at liftoff, vibration mainstage, max q, IECO, and OECO is given in Table 9-I. Vibration envelope of engine and structure measurements is shown in Figure 9-29.

TABLE 9-I

SA-1 FLIGHT VIBRATIONS

Measurement			Peak G Levels					
No	Description	Dir.	L.O.	M.S.	Mach 1	q Max	IECO	OECO
E1-11	Vib. Upper Stru.	Long't	2.97	0.64	1:06	0.68	0.76	1.02
E2-11	Vib. Upper Stru.	Pitch	2.38	0.76	1.02	0.93	0.93	1.19
E3-11	Vib. Upper Stru.	Yaw	4.75	1.95	2.29	2.12	1.87	1.02
E4-15	St-90 (Y-Axis)	Long't	1.88	0.31	1.09	0.66	0.66	0.41
E5-15	St-90 (Z-Axis)	Lat	1.48	0.30	1.06	0.81	0.47	0.64
E6-9	Vib. Thrust Frame	Long't	4.24	3.39	3.39	3.39		
E7-9	Vib. Thrust Frame	Pitch	5.09	3.39	3.22	3.39	4.24	
E11-2	Vib. Thrust Cham Dome	Lat	7.64	5.94	6.36	6.36	6.36	
E11-4	Vib. Thrust Cham Dome	Lat	6.79	5.94	6.36	5.94	7.21	
E11-6	Vib Thrust Cham Dome	Lat	10.18	7.21	6.36	5.94		
E11-8	Vib. Thrust Cham Dome	Lat	7.21	5.09	5.09	5.09	6.36	
E12-1	Vib. Turbo Gear Box	Long't	10.18	13.57	12.30	11.45	11.88	16.54
E12-2	Vib. Turbo Gear Box	Long't	7.89	8.06	8.48	10.86	11.03	12.30
E12-3	Vib. Turbo Gear Box	Long't	11.03	8.48	7.64	7.64		
E12-4	Vib. Turbo Gear Box	Long't	8.06	8.48	8.48	8.06	8.48	
E33-1	Vib. Thrust Cham Dome	Long't	8.48	8.06	8.48	7.21	25.45	
E33-3	Vib. Thrust Cham Dome	Long't		8.48	7.64	6.79	7.64	
E33-5	Vib. Thrust Cham Dome	Long't	12.73	13.57	13.57	13.57	12.73	
E33-7	Vib. Thrust Cham Dome	Long't	6.79	6.79	6.36	5.94	6.36	2.12
E141-4	Vib. Yoke Yaw Act		0.61	0.09	0.09	0.14	0.36	
E202-9	Vib. Mt. Brkt. Dist.	Long't	8.91	1.12	3.39	3.82	2.54	2.97
E34-1	Vib. Pitch Act	Pitch	4.24	3.39				
E34-2	Vib. Pitch Act	Pitch	4.67	3.82			4.67	
E34-3	Vib. Pitch Act	Pitch	3.39	1.70				
E34-4	Vib. Pitch Act	Pitch	5.09	2.97				
E35-1	Vib. Pitch Act	Yaw		3.39			7.64	
E35-2	Vib. Pitch Act	Yaw		16.12				
E35-3	Vib. Pitch Act	Yaw		1.70			1.27	
E35-4	Vib. Pitch Act	Yaw		2.55			2.97	
E36-1	Vib. Yaw Act	Pitch		2.97	14.0	16.9		7.64
E36-2	Vib. Yaw Act	Pitch		2.97	6.36	5.94		4.24

SA-1 FLIGHT VIBRATIONS (Cont.)

E36-3	Vib. Yaw Act	Pitch		1.70	5.09	5.09		4.66
E36-4	Vib. Yaw Act	Pitch		4.24	8.06	18.66		3.39
E37-1	Vib. Yaw Act	Yaw		3.39				
E37-2	Vib. Yaw Act	Yaw		3.39				
E37-3	Vib. Yaw Act	Yaw		2.97				
E37-4	Vib. Yaw Act	Yaw		2.97				
E38-1	Vib. Pitch Act	Long't	6.79	5.09				
E38-2	Vib. Pitch Act	Long't		4.07			3.05	
E38-3	Vib. Pitch Act	Long't	5.51	4.24				
E38-4	Vib. Pitch Act	Long't		3.39			3.05	
E39-1	Vib. Yaw Act	Long't		4.07	3.90	3.90		11.54
E39-2	Vib. Yaw Act	Long't		0.85				
E39-3	Vib. Yaw Act	Long't		3.39	3.39	4.24		8.5
E39-4	Vib. Yaw Act	Long't		5.09				

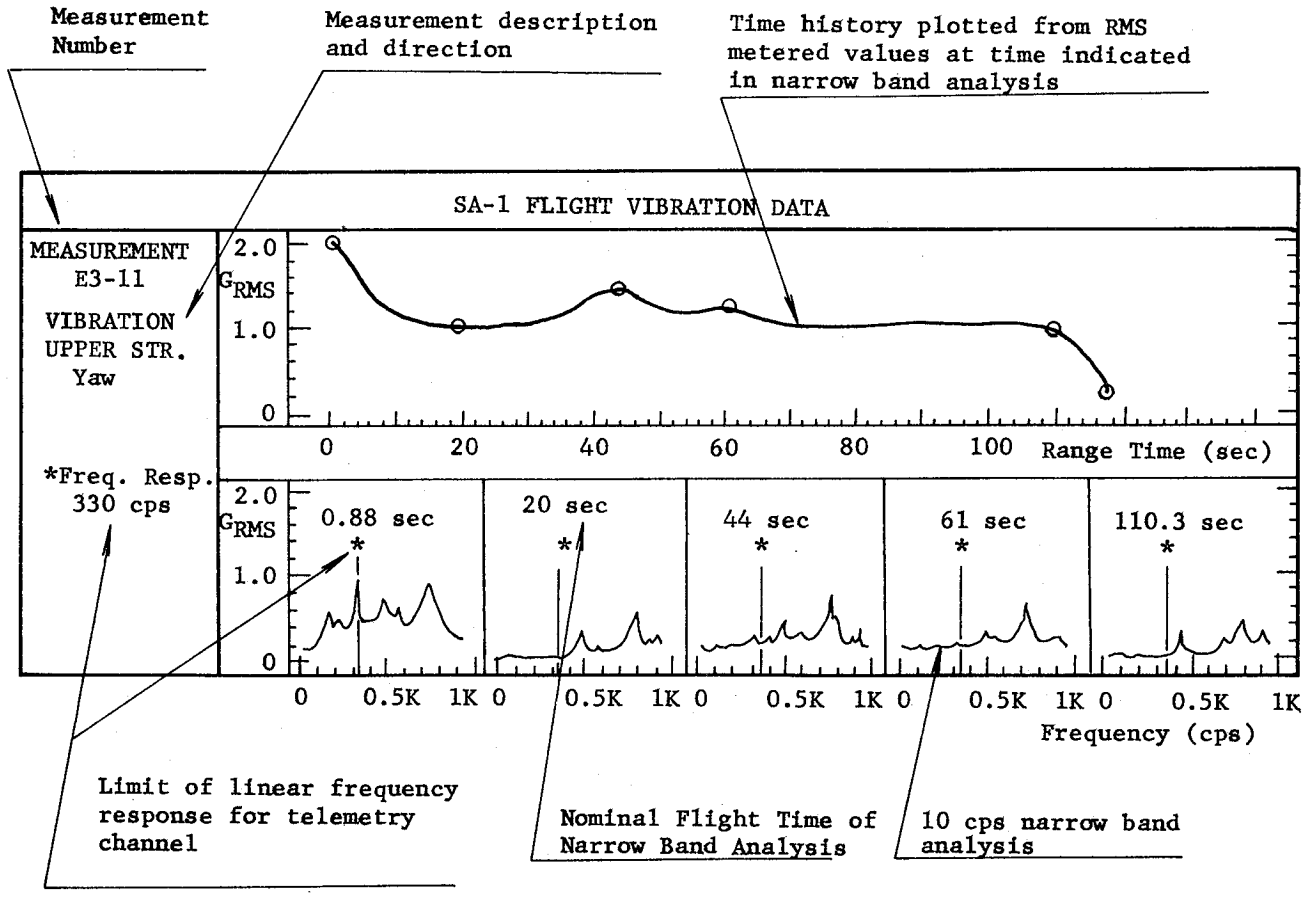

Fig.9-12	EXPLANATION OF DATA PRESENTED IN VIBRATION SUMMARY CURVES
SA-1	

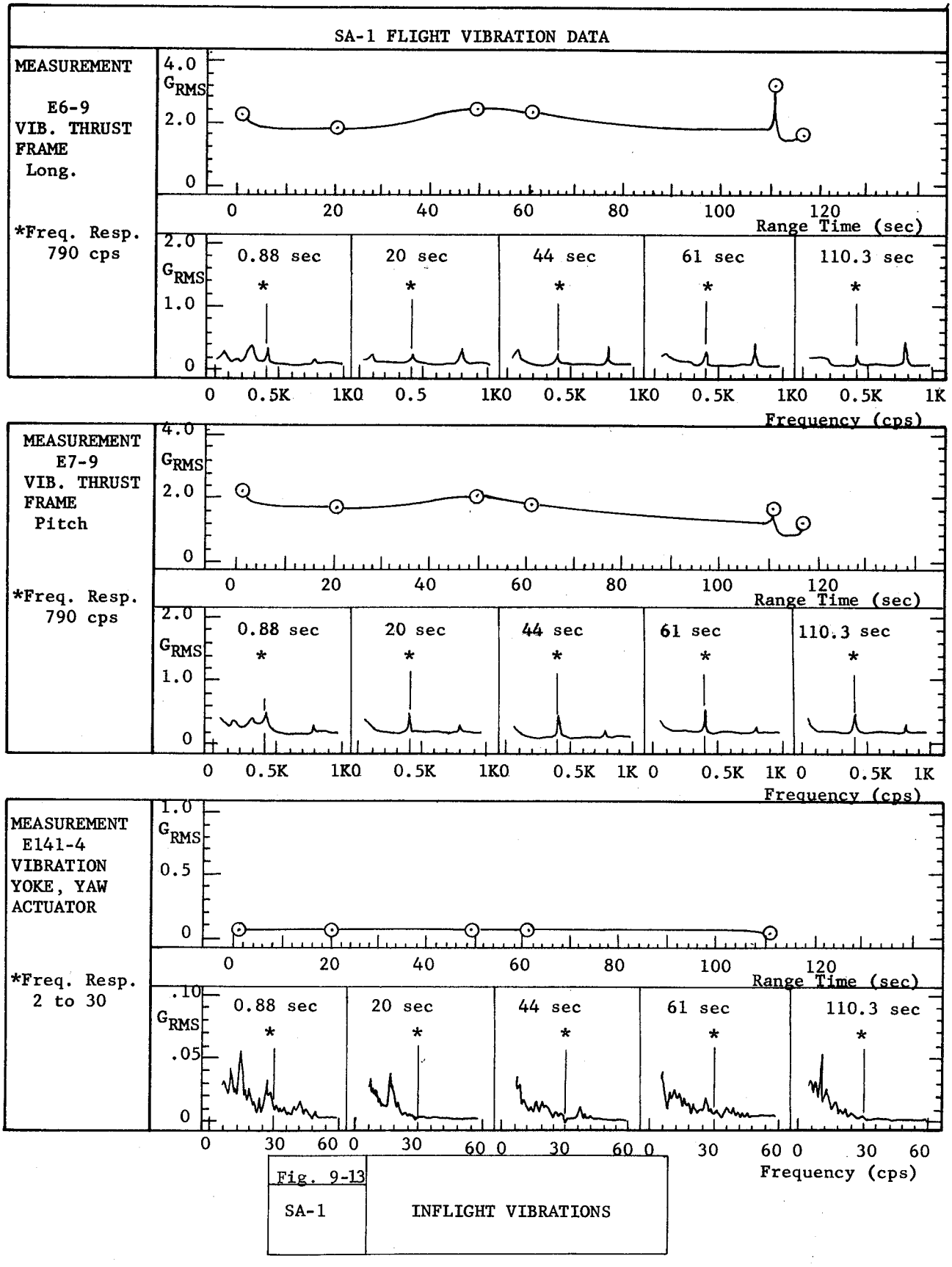

Fig. 9-13

SA-1 INFLIGHT VIBRATIONS

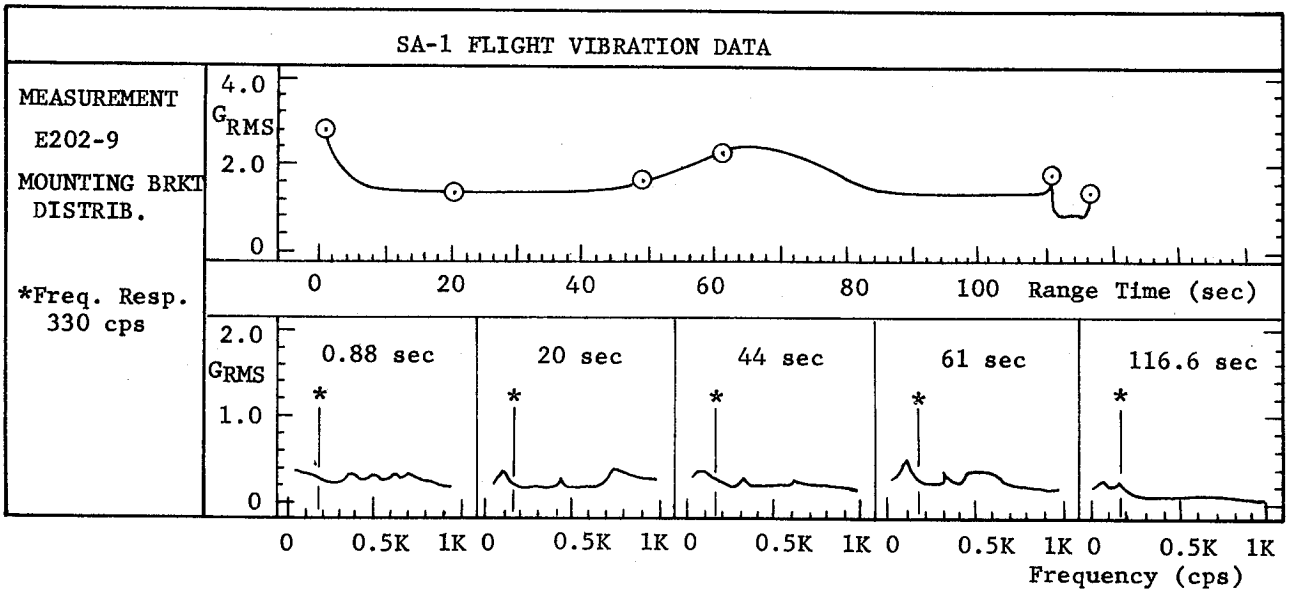

Fig.9-14	INFLIGHT VIBRATIONS
SA-1	

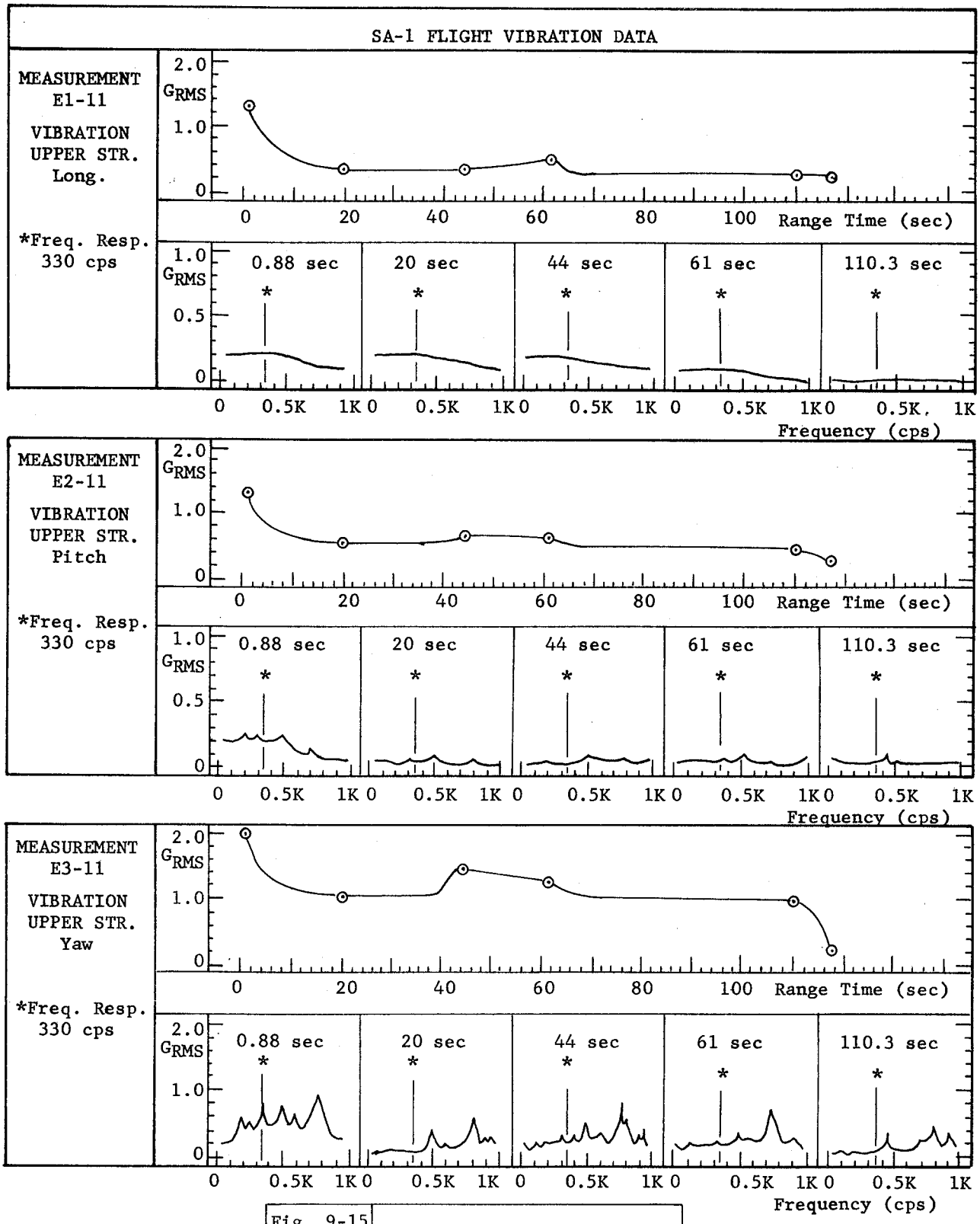

Fig. 9-15	INFLIGHT VIBRATIONS
SA-1	

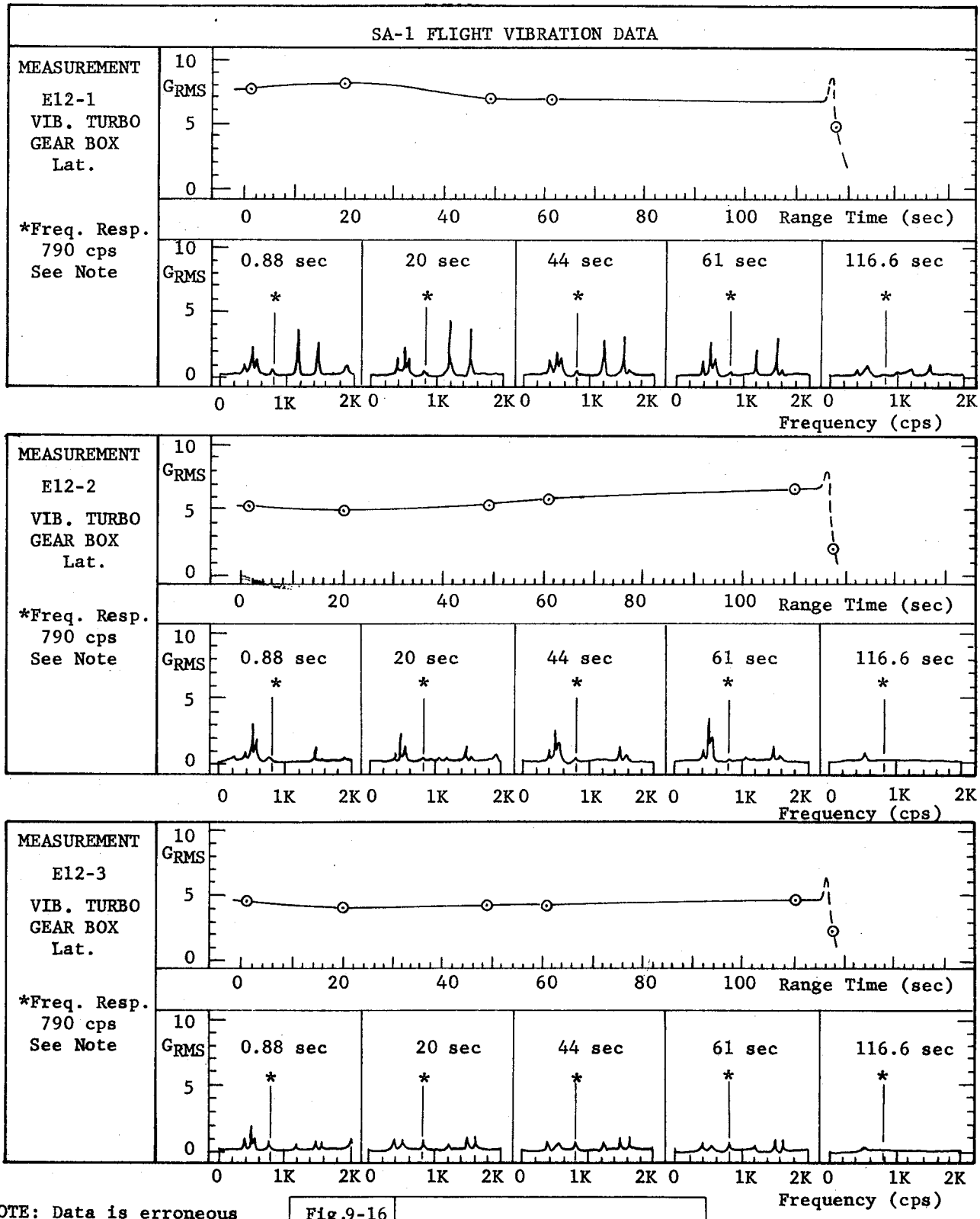

NOTE: Data is erroneous due to accelerometer mounting

Fig.9-16	INFLIGHT VIBRATIONS
SA-1	

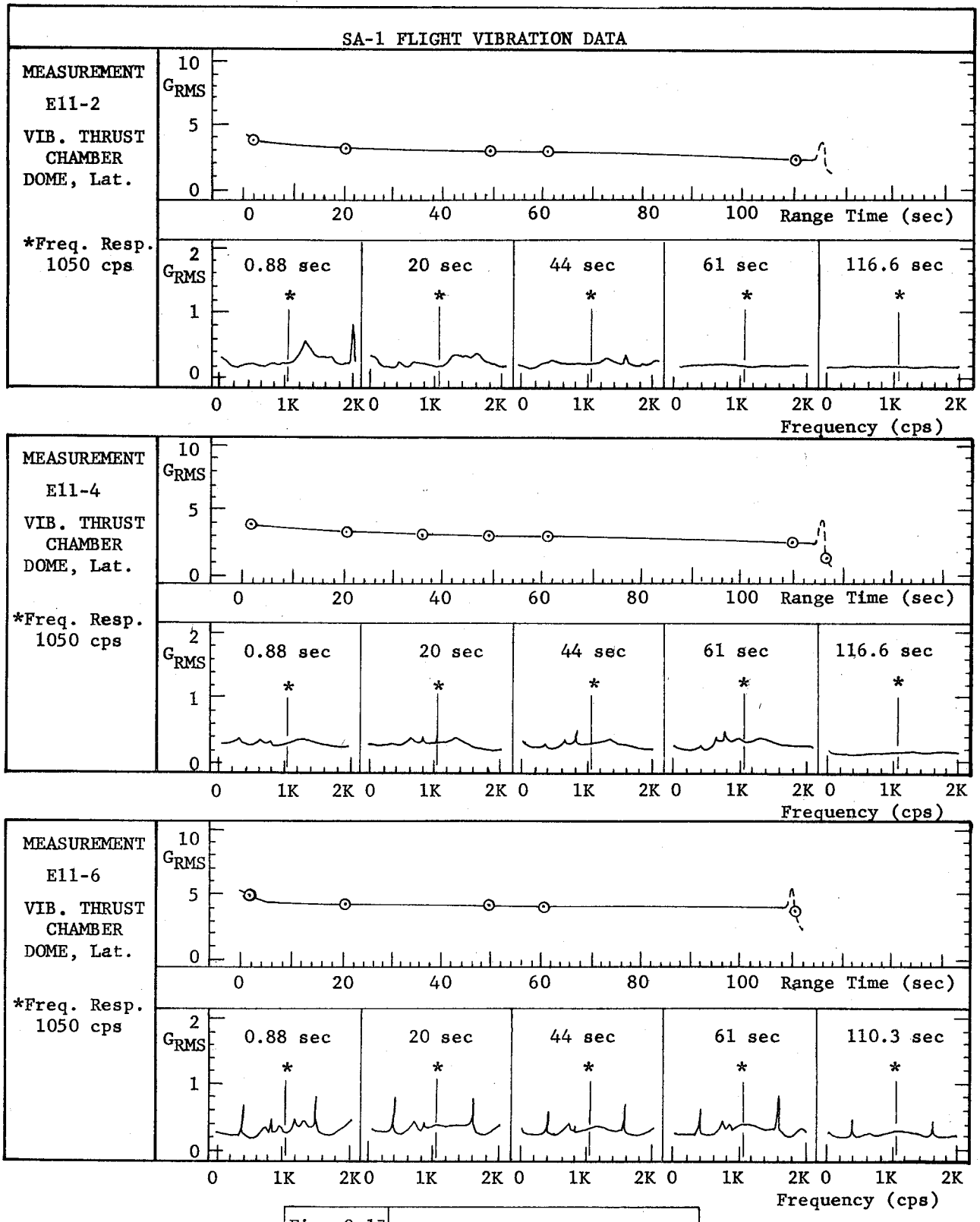

Fig. 9-17	INFLIGHT VIBRATIONS
SA-1	

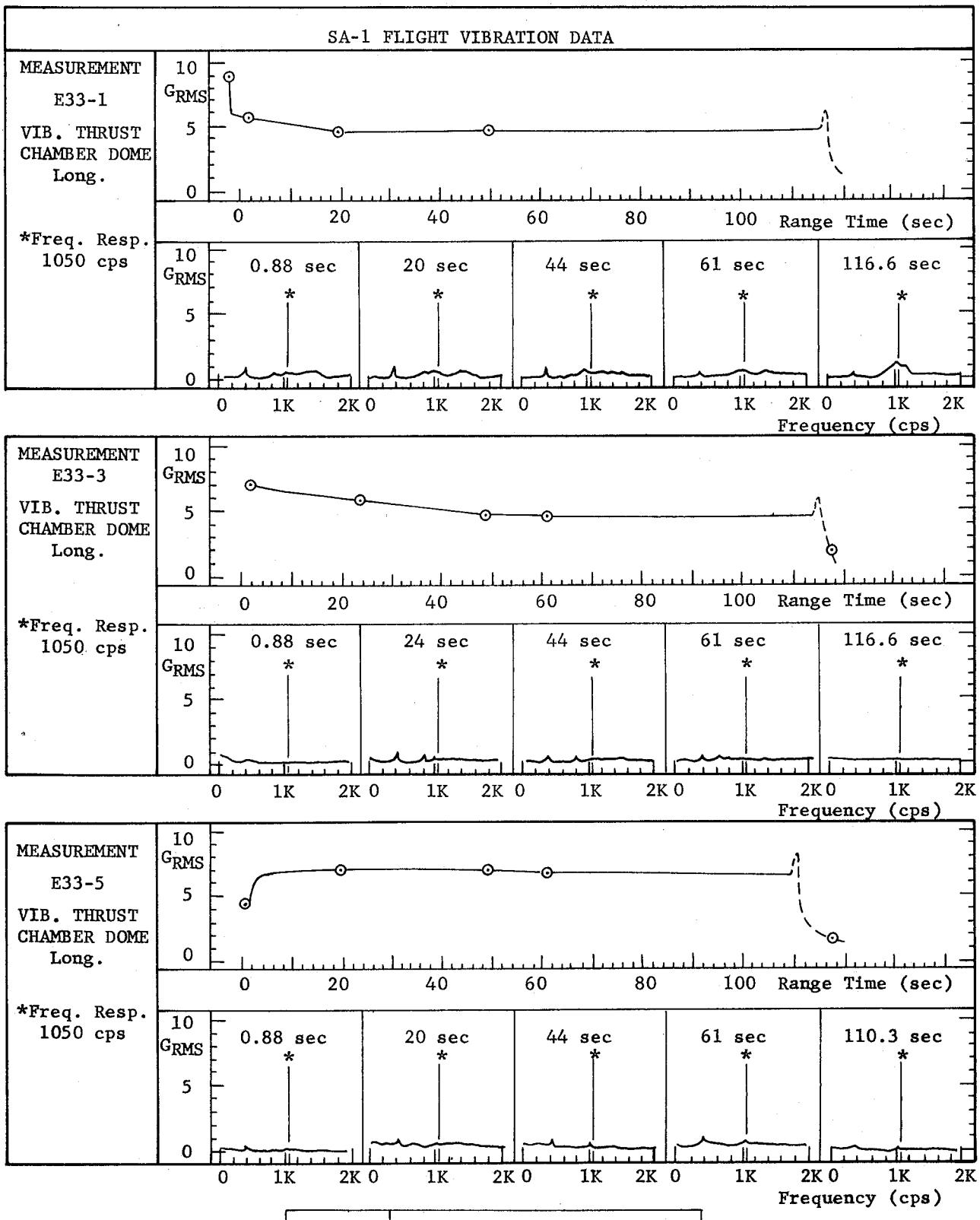

Fig. 9-18	INFLIGHT VIBRATIONS
SA-1	

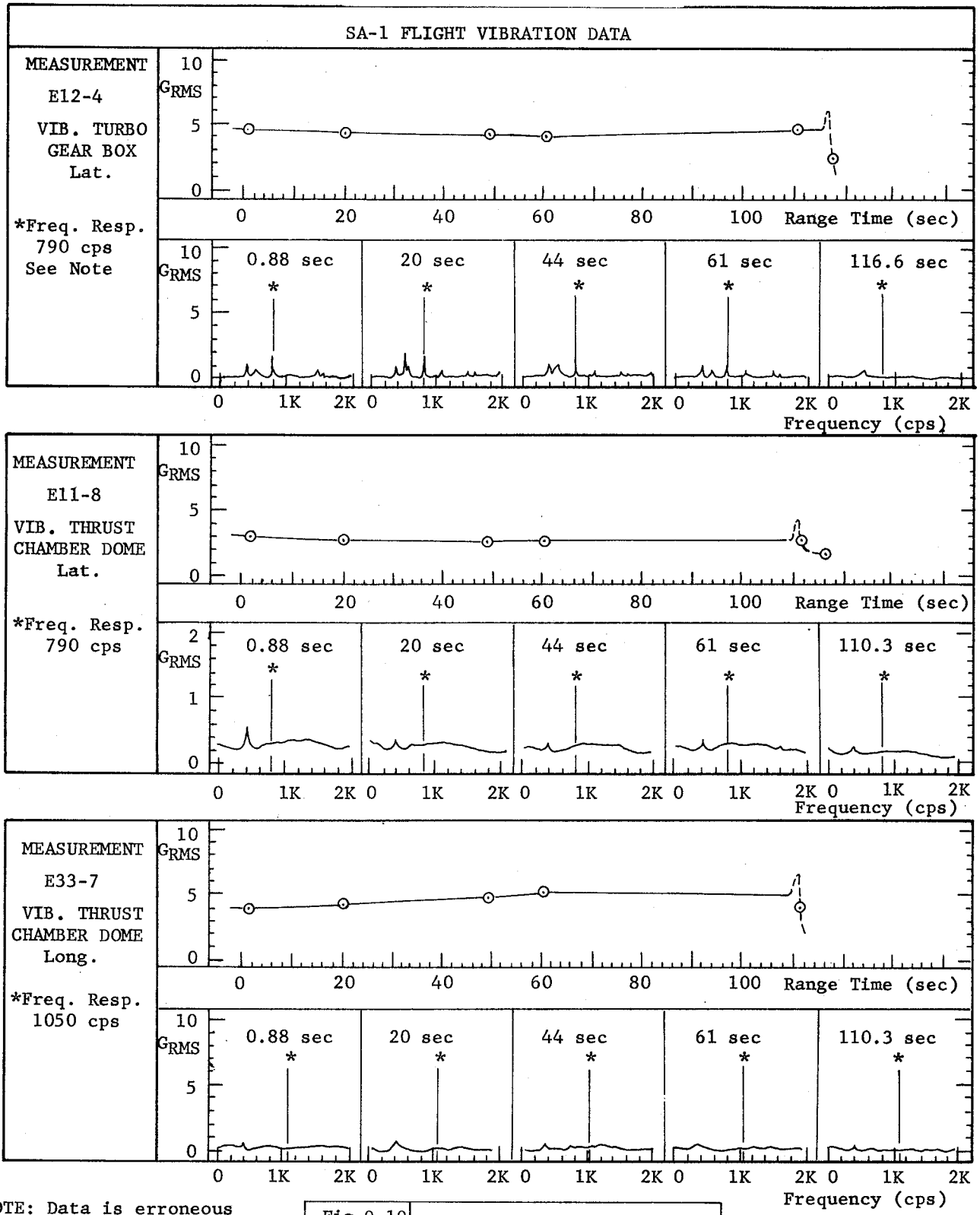

NOTE: Data is erroneous due to accelerometer mounting.

Fig.9-19	
SA-1	INFLIGHT VIBRATIONS

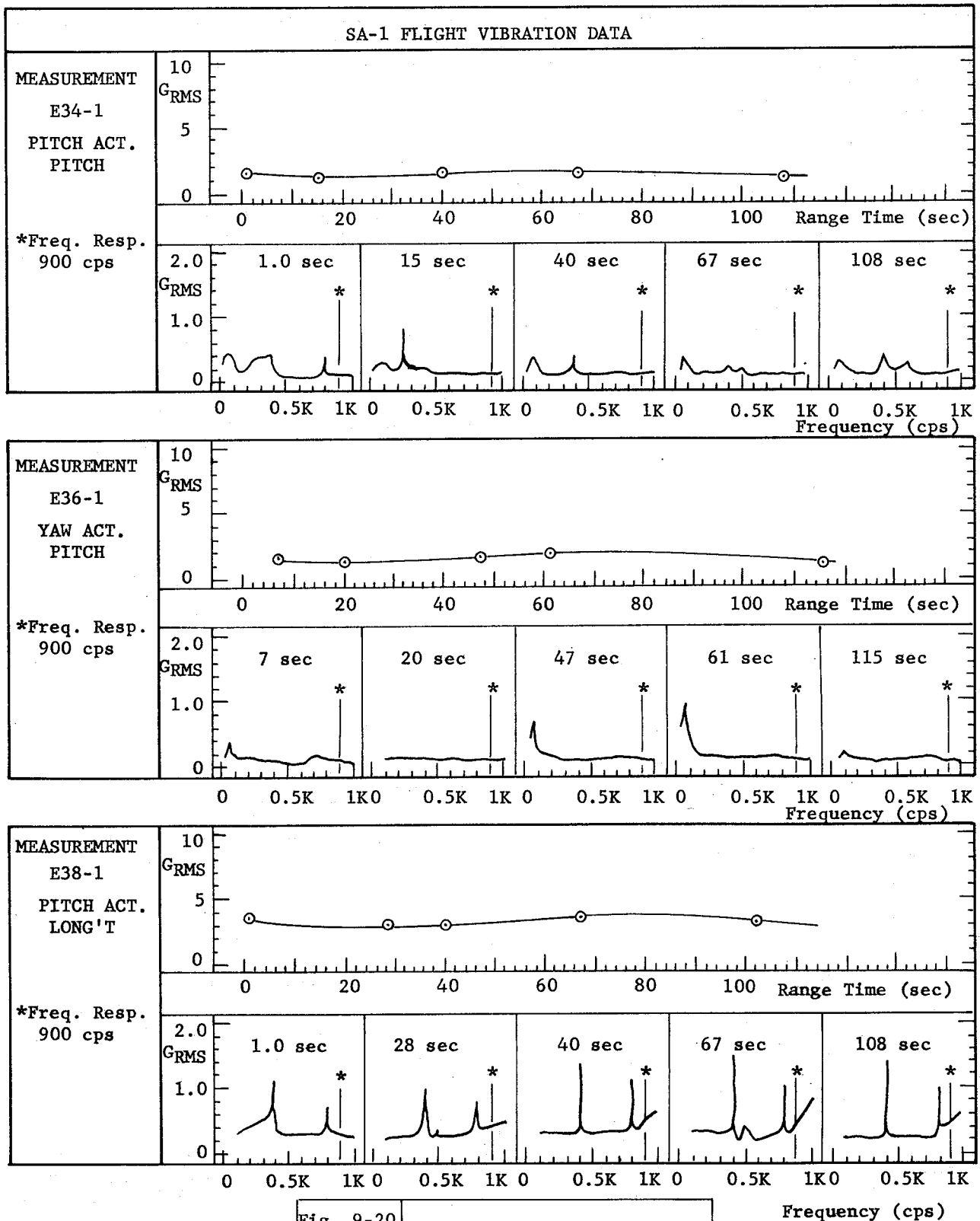

Fig. 9-20	INFLIGHT VIBRATIONS
SA-1	

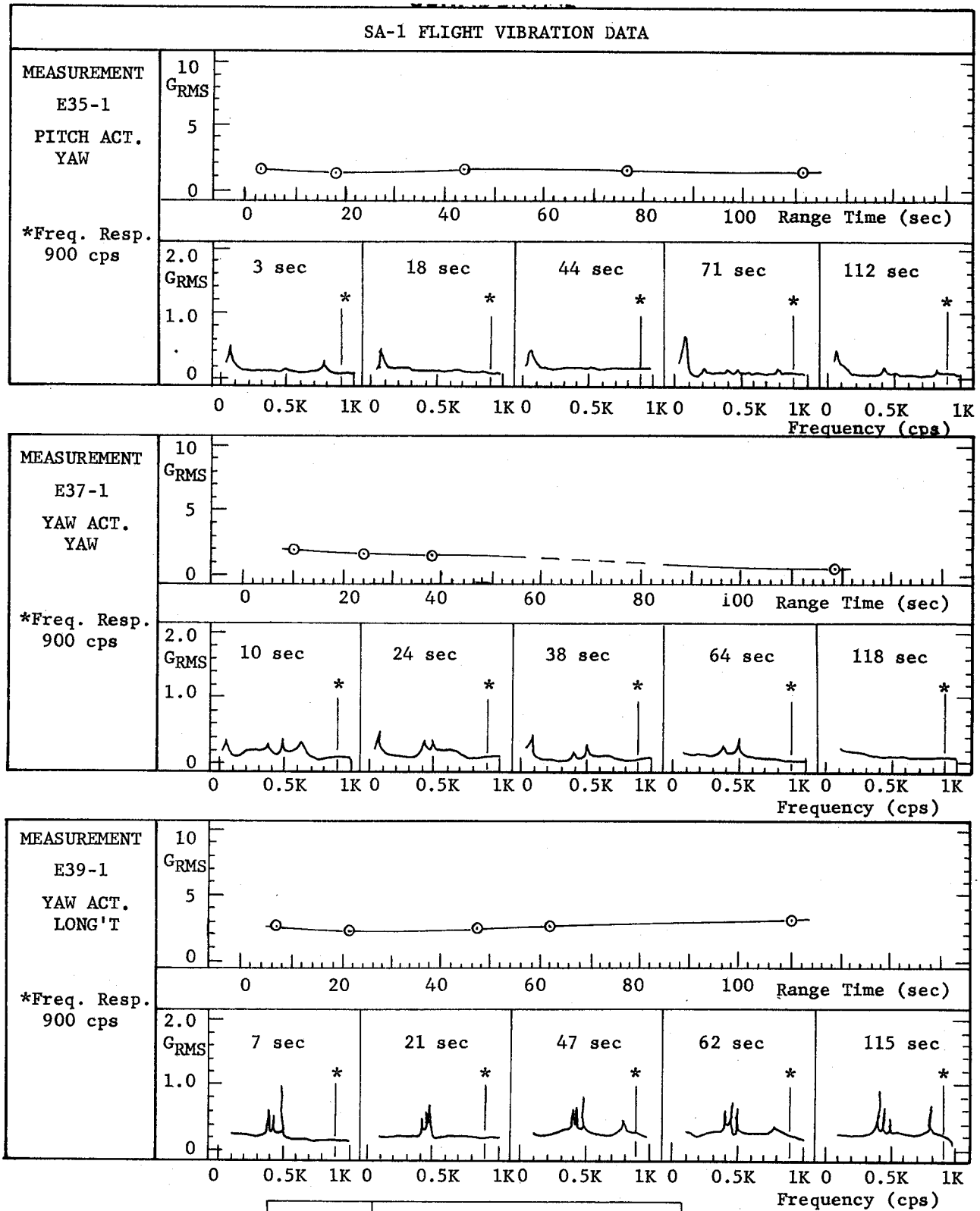

Fig. 9-21	INFLIGHT VIBRATIONS
SA-1	

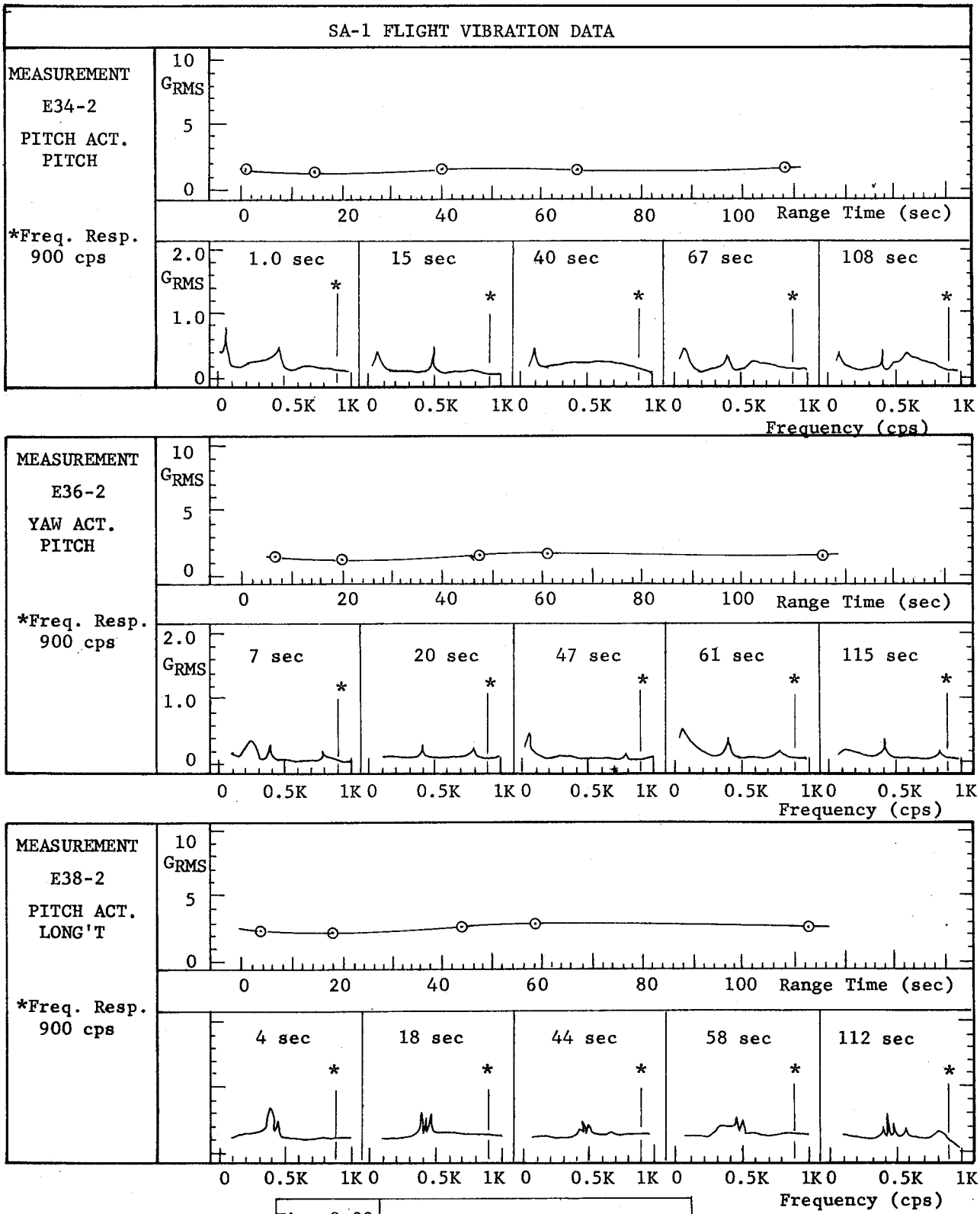

Fig. 9-22	INFLIGHT VIBRATIONS
SA-1	

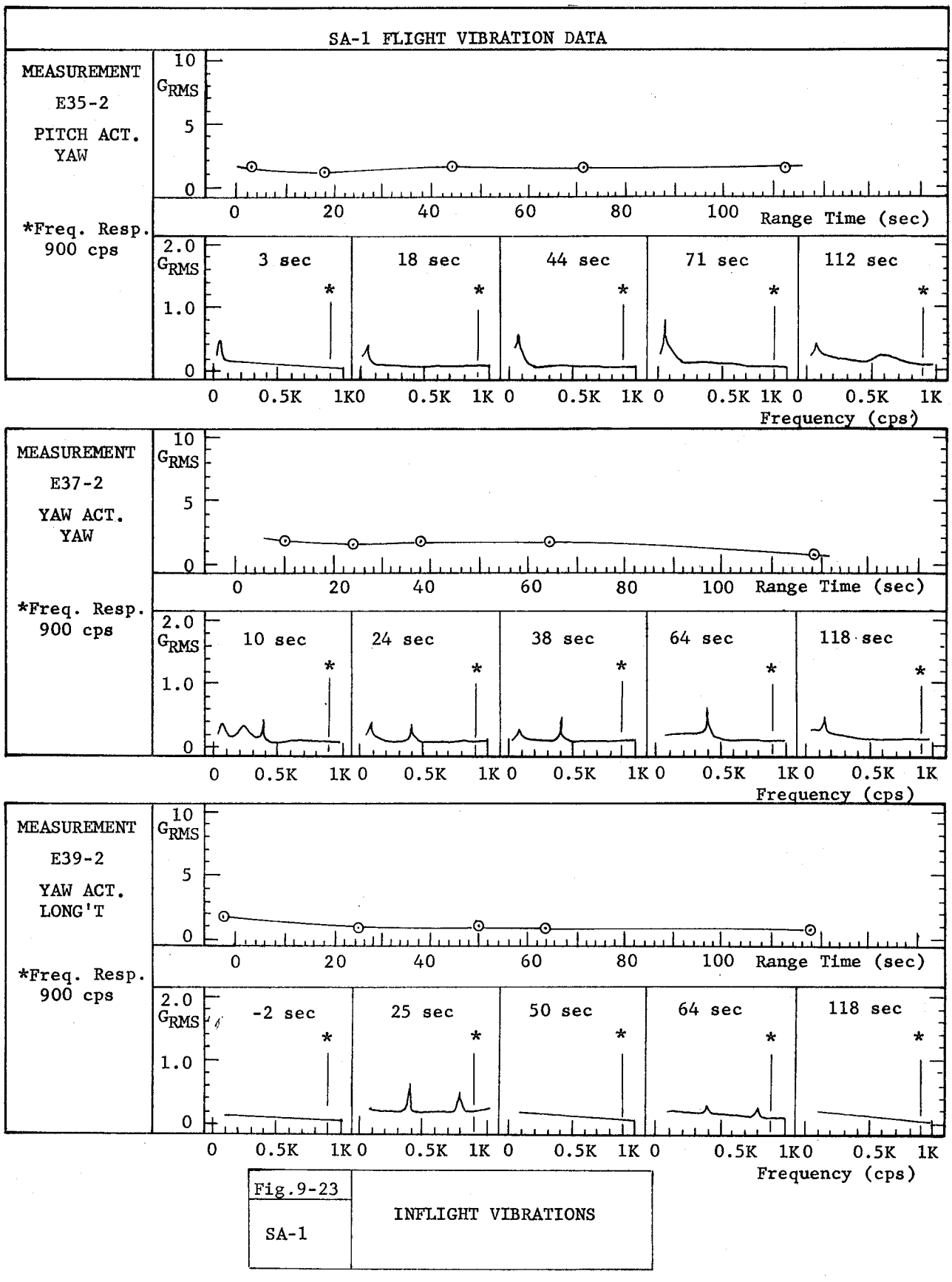

Fig.9-23	INFLIGHT VIBRATIONS
SA-1	

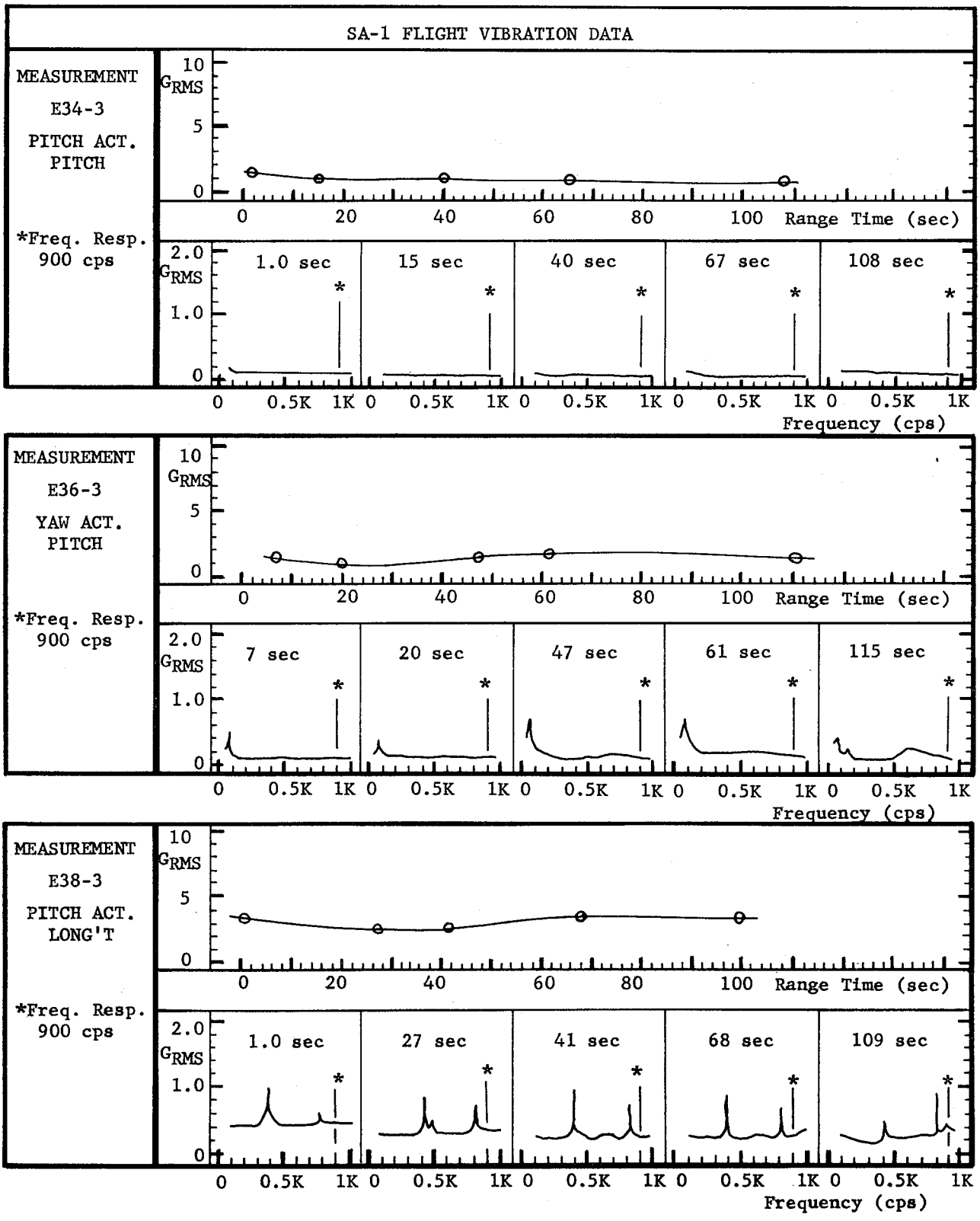

Fig. 9-24	INFLIGHT VIBRATIONS
SA-1	

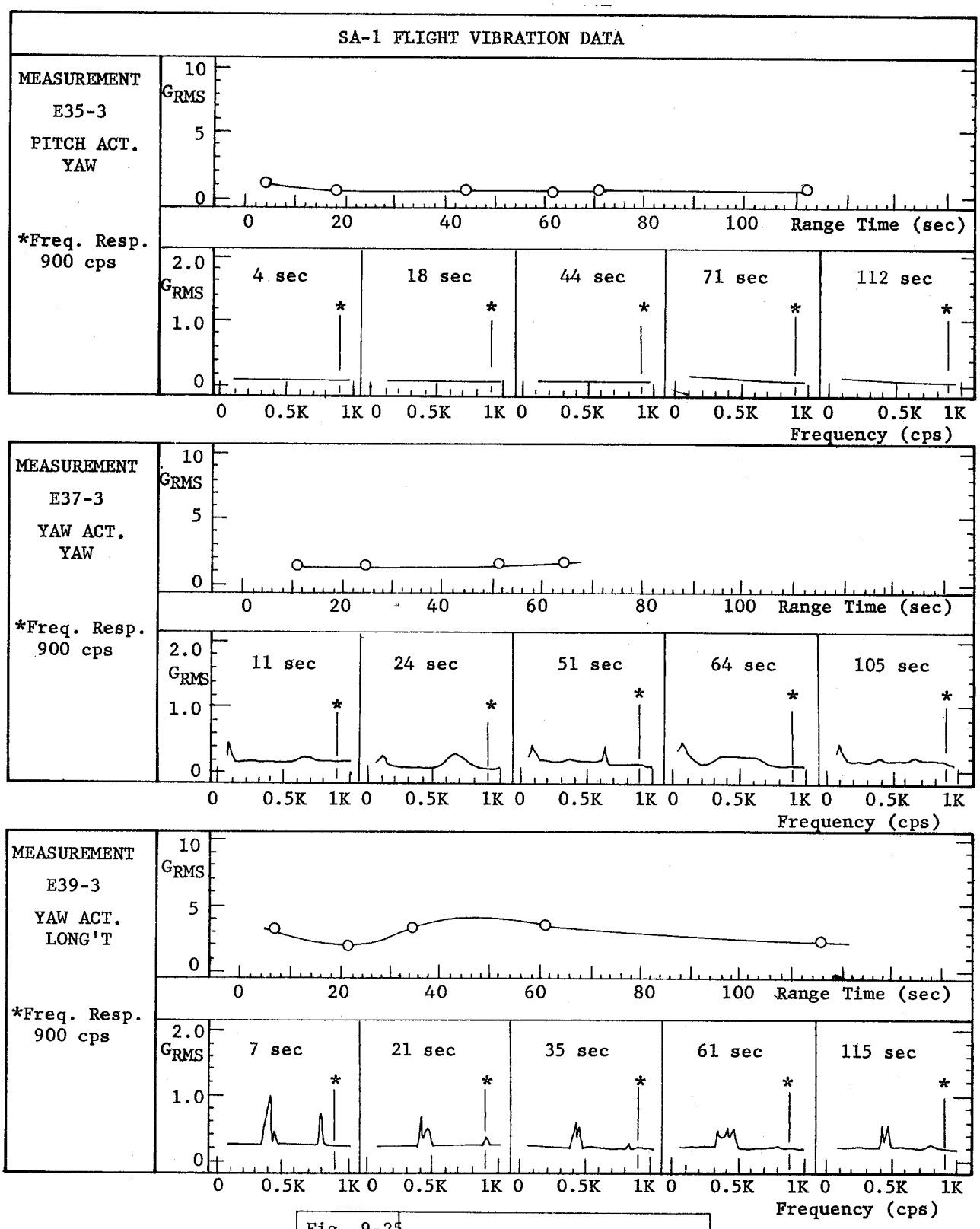

Fig. 9-25	INFLIGHT VIBRATIONS
SA-1	

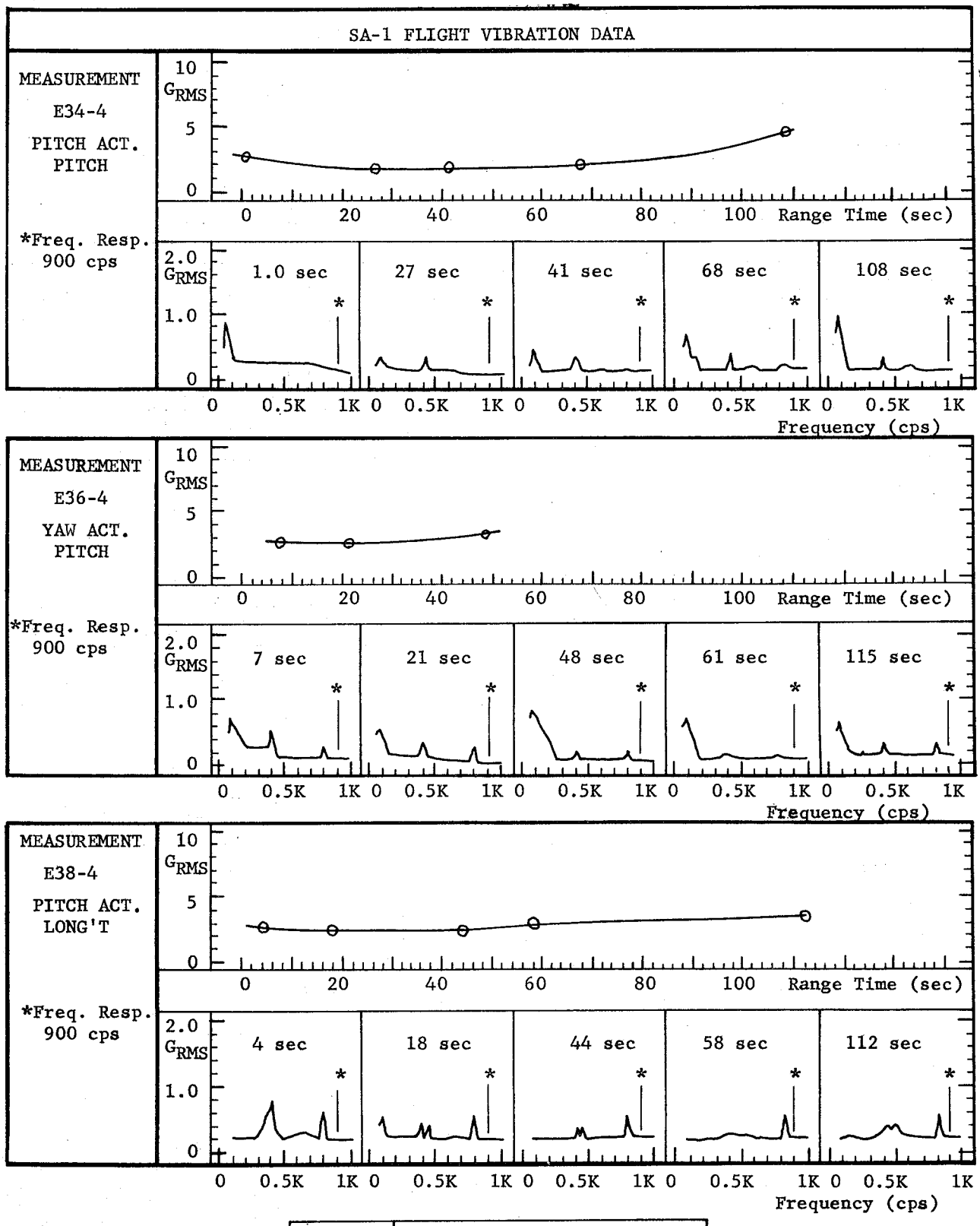

Fig. 9-26	INFLIGHT VIBRATIONS
SA-1	

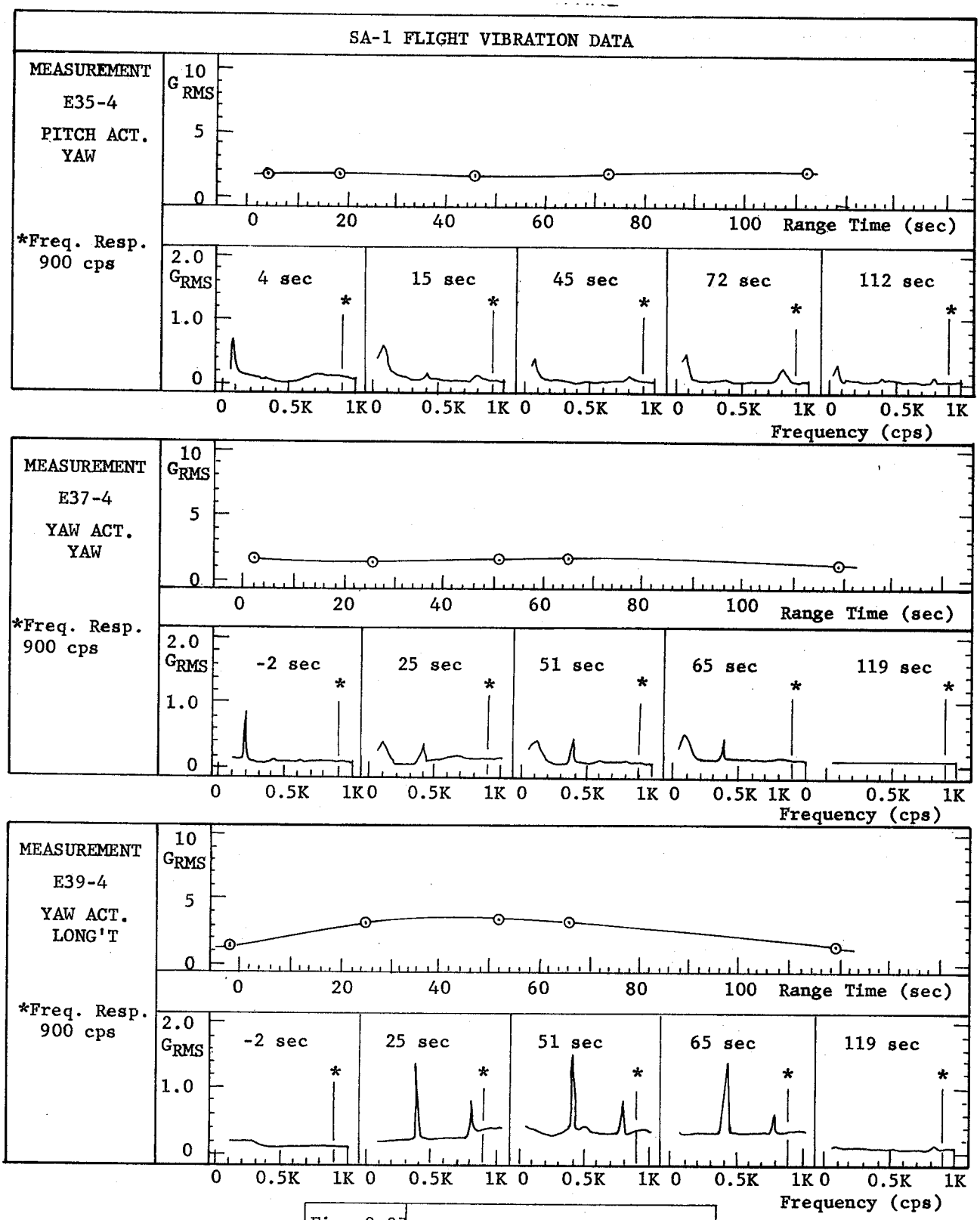

Fig. 9-27	INFLIGHT VIBRATIONS
SA-1	

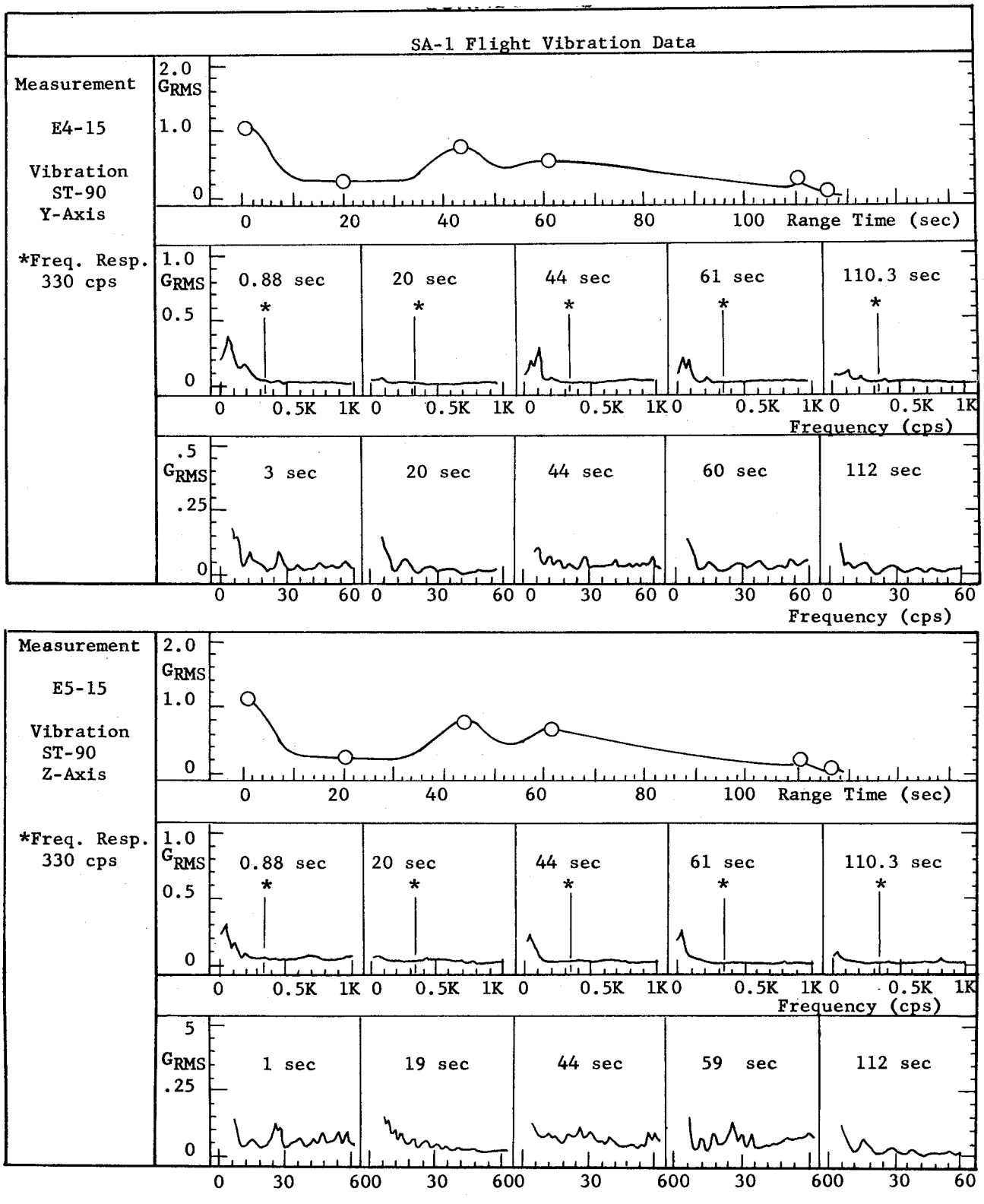

Fig. 9-28	
SA-1	INFLIGHT VIBRATIONS

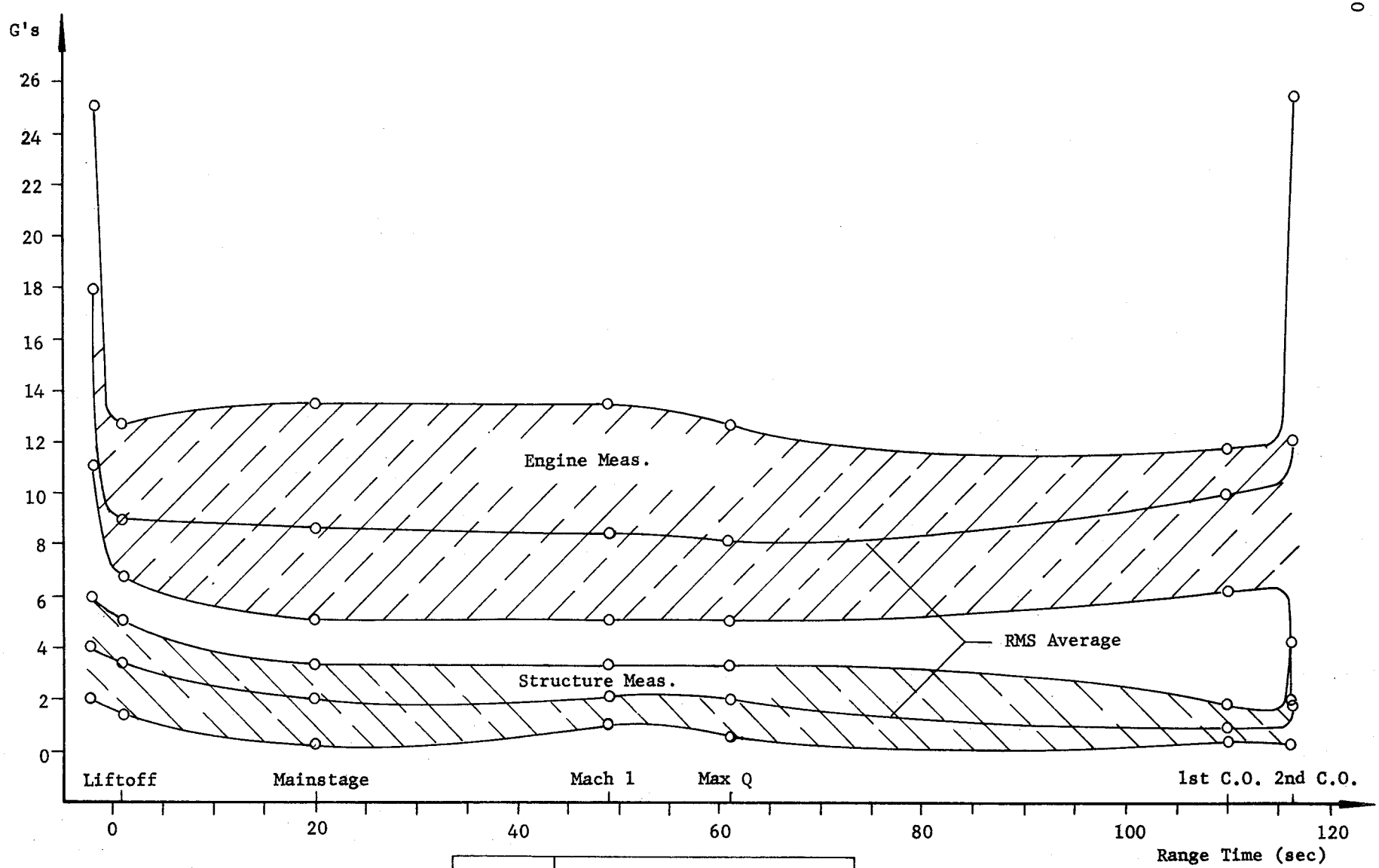

Fig. 9-29	VIBRATION ENVELOPE OF ENGINE AND STRUCTURE MEASUREMENTS
SA-1	

CONFIDENTIAL

9.7 ANALYSIS OF GROUND ACCOUSTIC MEASUREMENTS

9.7.1 SUMMARY

To investigate the dynamic environments created during the launch of SA-1, a large scale acoustic measurement program was established to evaluate the characteristics of these environments.

In general the over-all acoustic levels resulting from the launch were approximately of the magnitude expected.

9.7.2 NEAR-FIELD DATA

The results of the near-field acoustic measurement program are shown below. These values were recorded between ignition and liftoff within a hundred feet of the vehicle, and they give an indication of the magnitude of the sound pressures at some critical points on the complex.

NEAR-FIELD ACOUSTIC DATA

Measurement	Max. OA RMS SPL*
24' Horiz. From Station 54	153 db
" " " 167	152 db
" " " 216	153 db
" " " 860	148 db
Umb. Base, 'C' Platform	147 db
Umb. Base, B Platform	141 db
Large Utility Room	120 db
Instrument Room in Large Utility Rm.	114 db

9.7.3 MID-FIELD DATA

The measurements between 150 and 1500 feet, considered to be the acoustic mid-field, are given on the next page. While these measurements were made to evaluate the sound source subsequent to liftoff, detailed analysis must await the release of engine performance data and environment effect. A spectrum analysis of the acoustic data is shown in Figure 9-30 for two mid-field locations.

Note:

* The data represents over-all levels between ignition and liftoff. Reference .0002 microbar. (SPL = Sound pressure level.)

FAR FIELD ACOUSTIC DATA

Station	Range Feet	Titan (24 Oct 61) OA SPL RMS DB*	SA-1 (27 Oct 61) OA SPL RMS DB*
A	86,750	Unmanned	94 db
B	33,250	90 db	102 db
C	5,000	114 db	122 db
D	14,780	118 db	122 db
E	51,750	- - -	102 db
F	70,200	88 db	93 db
G	81,300	84 db	86 db
H	91,800	Unmanned	84 db
I	71,250	89 db	- - -
J	54,300	100 db	105 db

* Maximum RMS SPL recorded in decibels. Ref. 0.0002 microbar.

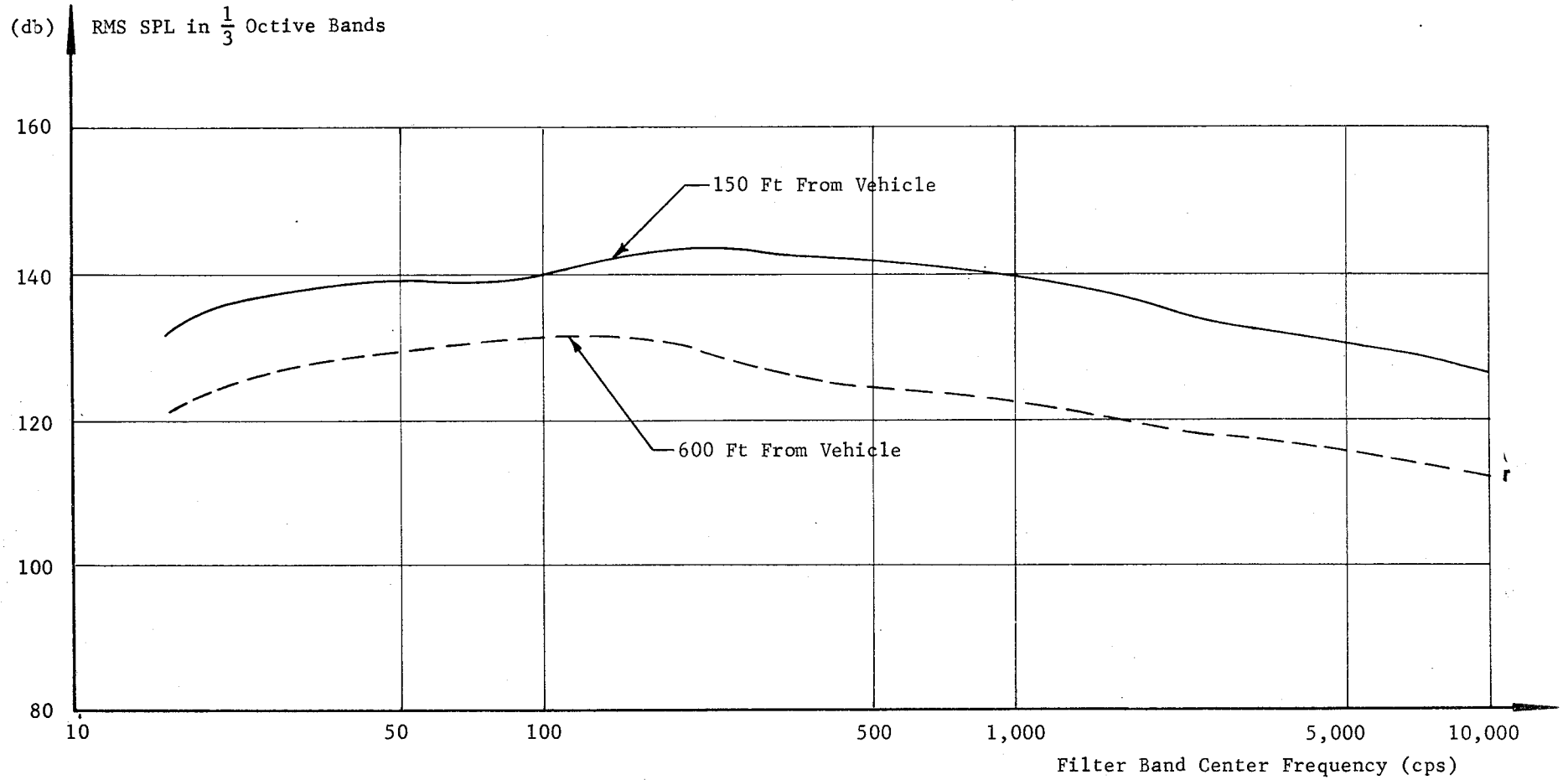

Fig. 9-30	
SA-1	SPECTRA ANALYSIS OF MIDFIELD ACOUSTIC DATA

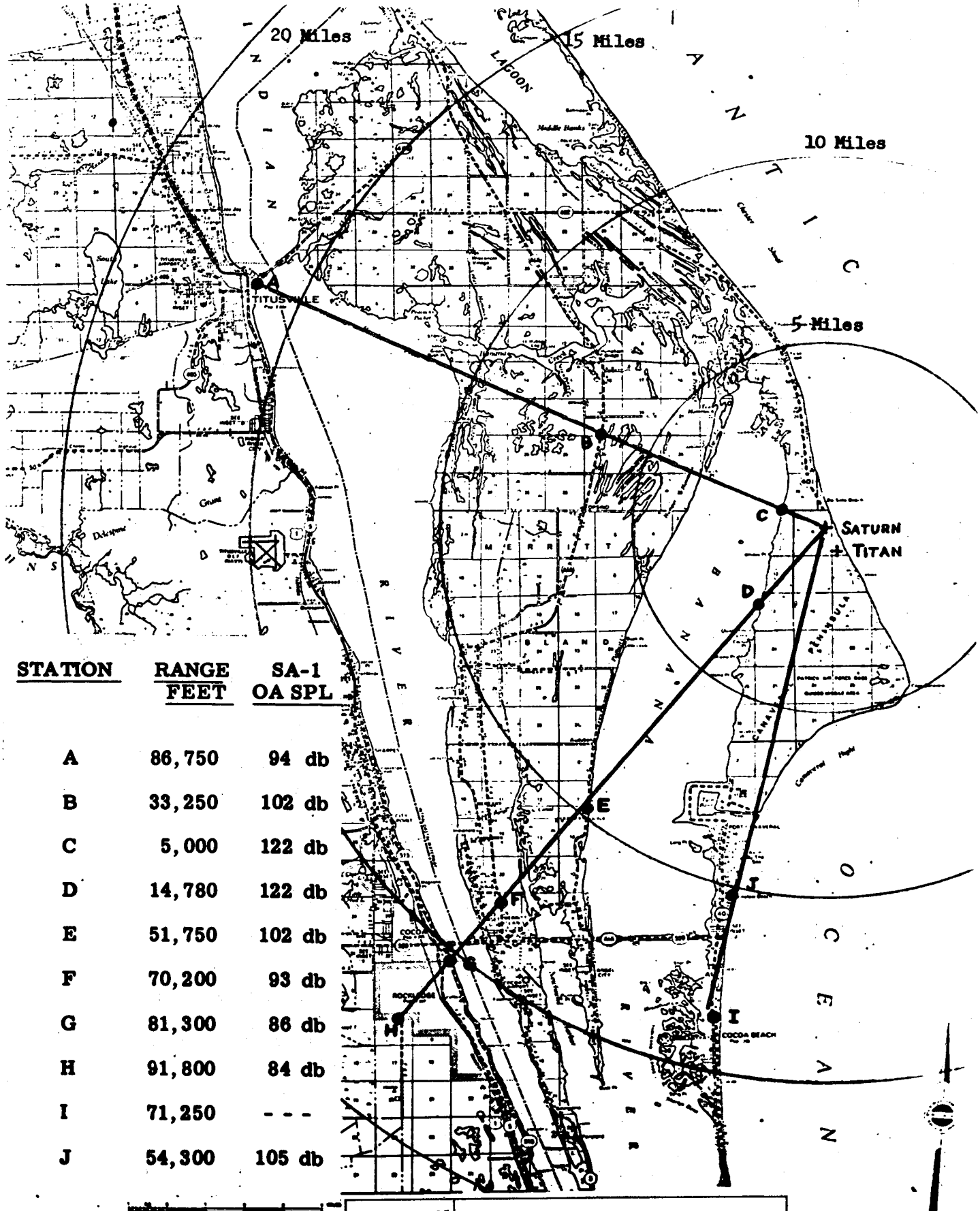

STATION	RANGE FEET	SA-1 OA SPL
A	86,750	94 db
B	33,250	102 db
C	5,000	122 db
D	14,780	122 db
E	51,750	102 db
F	70,200	93 db
G	81,300	86 db
H	91,800	84 db
I	71,250	- - -
J	54,300	105 db

Fig. 9-31	FAR FIELD ACOUSTIC MEASURING POINTS
SA-1	

10.0 (U) ENVIRONMENTAL TEMPERATURES AND PRESSURES

10.1 SUMMARY

The thermal environment of SA-1 was not detrimental to vehicle performance. Total heat flux to both the flame and heat shields was less than predicted; however, thermal radiation to the heat shield was close to that predicted. No fires or other abnormal heat sources occurred in the engine compartment.

Base pressure of the vehicle as telemetered from four measurements was as expected, showing close agreement with wind tunnel results.

Pressure in the canisters was maintained at the expected level (10-17 psia) during the flight. This pressure level was achieved by controlling the rate of gas venting.

10.2 TAIL SECTION

10.2.1 ENGINE COMPARTMENT

The engine compartment experienced no extreme temperature environments. Generally, temperatures varied between 24 to -46 °C for all measurements.

Ambient air temperature within each engine area was measured with thermocouples (measurements C61-1 to C61-8), and no ambient air temperatures above +10°C or below -46 °C were experienced, indicative that no fires or major LOX leaks existed (Fig. 10-1). However, the ambient temperature experienced a gradual 6° to 14°C drop after 90 seconds of flight time. This phenomenon could have been due to any one or more of three mechanisms:

1. Cooling due to low ambient air temperature at altitude
2. Vaporization of frost at low ambient pressures
3. A small LOX leak

The first mechanism could definitely be a contributing factor as atmospheric temperature was -34°C at the altitude the SA-1 vehicle reached at 90 seconds. However, this mechanism does not explain why the temperature drop generally started at 90 seconds flight time and not before, as the vehicle moved through colder portions of the atmosphere before this time.

The second mechanism, frost vaporization, is possible, but the

degree to which this mechanism would affect interior temperatures is not known due to lack of data as to the amount of circulation of ambient air inside the engine compartment.

The third mechanism, a small LOX leak, is not resolvable with the limited accuracy of the LOX flowmeters.

Thirty-two thermocouples are located on the fire wall to indicate the existence of fire in one or more engine compartments prior to lift-off. These thermocouples are divided into four loops of eight each, with each thermocouple connected in series, within the loop. Prior to lift-off these thermocouples (denoted by prefix X) are monitored in the block-house so the engines may be cut off if a fire is indicated by an unusual rise in temperature.

These measurements are not telemetered during flight. No unusual temperature rise occurred between ignition and liftoff of SA-1.

Nine thermocouples measured bulk temperatures of various structural members within the engine compartment (Fig. 10-1). All these measurements remained between -18°C and +20°C except measurement C60-2 (Temperature of the Tail Shroud) which reached 66°C at the end of powered flight. The rise in temperature of the tail shroud was probably due to heat influx from the burning turbine exhaust gases or aerodynamic heating, as the temperature of the stringer at this same location (measurement C13-2) showed no rise. If the heat source had been within the engine compartment or below the heat shield, the stringer would have experienced a comparable or even greater temperature rise.

Generally, all these measurements (with the exception mentioned above) experienced a temperature drop after 90 seconds corresponding to the similar drop in ambient air temperature.

One measurement monitoring air temperature near the thrust frame (C62-9) was mounted above the firewall. The ambient temperature in this area steadily decayed from -18 to -73°C at 110 seconds (approximate inboard engine cutoff) and then rapidly rose to -29°C by 116 seconds (see Fig. 10-1). As this measurement is near an inboard LOX suction line, the flow of LOX through the suction line may have cooled circulating ambient air. Upon inboard engine cutoff, heat transfer from ambient air to the suction line would be greatly reduced and the thermocouple would sense an ambient temperature slightly lower than atmospheric.

Locations of temperature measurements in the engine compartment are shown in Figure 10-2.

10.2.2 BASE ENVIRONMENT

SA-1 carried four base pressure measurements on the S-I stage. Three of these measurements (D25-4, D25-7, D38-4) were mounted on the heat shield at station 54 and measured the ambient pressure aft of the heat shield. The other measurement, D38-7, was mounted on the flame shield between the four inboard engines and sensed the ambient pressure aft of the flame shield. D38-7 was located 3.5 inches from the vehicle center line toward fin position I. Measurement D25-4 was located 62 inches from the center line, 30 deg off fin position IV toward I. Measurement D25-7 was located 66 inches from the center line, 2 deg from fin position III toward IV. Measurement D38-4 was located 140 inches from the center line, 45 deg between fin positions I and IV. A schematic of the pressure and temperature measurement locations is shown in Figure 10-3.

Two radiation calorimeters, measurements C79-2 and C64-4, and three total heating calorimeters, measurements C63-1, C77-5, and C76-3, were mounted on and in the vicinity of the heat shield to measure the base heating in this region. In addition, shielded gas temperature probes, projected several inches below and aft of the heat shield measured the temperature of the gas circulating in the vicinity of the heat shield (measurements C10-2, C10-4, C65-3). One calorimeter was mounted in the flame shield to measure the incoming flame thermal radiation and hot exhaust gas convective heating (measurement C78-8).

The thermocouples on the cold side (forward side) of the heat shield were C68-3, C69-5, C70-7, C71-4, C72-1 and C73-2. Two thermocouples (C20-5 and C21-5) were used to measure structural temperature of the back side of the flame shield and the flame shield struts.

Base Pressures

Differences between the individual base pressure measurements and ambient are shown in Figure 10-4. The pressure on the flame shield (D38-7) between the inboard engines experienced the largest magnitude pressure variations. A maximum difference of 3.5 psia between this pressure and ambient occurred at 102 seconds of flight. The pressure differences on the heat shield compared to ambient were generally less than 0.5 psia.

At 50 seconds, corresponding to the time the vehicle reaches Mach 1, measurements D25-7 and D38-4 showed a sharp drop while measurement D25-4 continued steady. The predominant angle of attack during this time was in the pitch plane (see Fig. 6-14). Possibly this rapid change in base pressure was a consequence of a transonic flow effect

through an angle of attack influence. The effect may have been more shielded from measurement D25-4 by jets from the engines.

Ratios of base pressure to ambient are shown as a function of Mach number in Figure 10-5. The average of the three measurements on the heat shield are shown in the upper portion. The flame shield measurement is shown in the lower portion. These are compared with the average results obtained from model tests in the Rocket Test Facility, AEDC. The flight test results have an error margin indicated which is based on a possible 2% measurement error (0.4 psia). Flight test measurements were in satisfactory agreement with the model test results.

Deviations between the base pressures measured in-flight and those obtained from model tests may possibly be attributed to a number of factors. The angle of attack, engine deflections, and Reynolds number differences may have caused most of the differences.

The average curve of the base pressure measurements on the heat shield was converted to a pressure coefficient curve and is shown as a function of time in Figure 10-6. The dashed line shown for comparison was obtained from model test results.

Base Temperatures

The heat shield thermal insulation material scheme consists of an outer layer of aluminum reflective tape adhered to the thin layer of low temperature subliner which was sprayed on the X-258 asbestos - plastic layer which is bonded to the thin metallic portion of the heat shield. Critical engine components were protected by wire reinforced asbestos cloth covered by reflective tape, or X-258 asbestos - plastic mixture with an outer layer of reflective aluminum tape. Other items in the base region, such as aerodynamic shrouding around outboard engines, support struts, etc., were thermally insulated from base heating by the X-258 asbestos - plastic mixture covered by reflective tape. The flexible curtain material around the four outboard engines was protected from base heating by an external layer of "Refrasil" cloth which in turn was covered by a layer of reflective aluminum tape.

The flame shield, located between the four inboard engines close to the nozzle exit plane, utilizes approximately 1.5 inches of high temperature asbestos - phenolic material for thermal protection requirements. Locations of the various temperature measurements on the heat and flame shields are shown in Figure 10-3.

The inflight gas temperature data measured on the SA-1 heat shield is shown in Figure 10-7. This flight data was measured by thermocouples enclosed in a double walled perforated radiation shield since the

protective shields were not removed. This shield caused the thermocouples to have a lag. This has been demonstrated in experimental tests. A shielded thermocouple (similar to the ones used on the SA-1 heat shield) and a bare thermocouple were exposed simultaneously to a hot gas source. The thermocouple with the shield demonstrated a much slower response in measuring gas temperature than the bare thermocouple.

The lower curves in Figure 10-7 (measurements C10-2 and C10-4) were made by shielded thermocouples in an area near the shroud scoops. They are the coolest, as would be expected, since the shroud scoops keep this area well flushed. Measurement C10-7 indicates somewhat higher temperatures and is expected for the area flushed by the valley scoops. The area between the two fixed inboard engines and an outboard engine (measurement C65-3) is least affected by flushing action of the scoop and indicates the highest temperatures. The decrease in temperature after 90 seconds is at least to some degree a measuring effect associated with low pressure.

The SA-1 measured radiative heat data is higher during the first 5 or 6 seconds of engine burning time than at any other time, reaching a peak of 27 BTU/ft^2 sec. This peak is caused by the deflecting and spreading exhaust plumes which increases the amount of flame and radiative heating. Several seconds after liftoff and when the plumes are no longer deflected by the ground equipment, the measured radiative heating (21.5 BTU/ft^2 sec) compares favorably with predicted. The predicted was based on single engine measurements of Jupiter flight tests which had been converted to the multi-engine Saturn configuration. An unexpected deviation between measured and predicted radiative heating occurs over the flight time interval of 45 to 85 seconds, with the maximum deviation occurring when the aerodynamic pressure and forces are the highest. The measured radiant heat flux first decreases and then increases over the time interval of 45 to 85 seconds. During this same period maximum dynamic pressure occurs and probably faces the opague turbine exhaust gases (from the inboard engines) to circulate in the base region. In this way the turbine exhaust gages partially shield the base from the plumes of the main jets and cause the radiation calorimeters to indicate lower results.

Convective heating and cooling rates to the SA-1 heat shield region are shown in Figure 10-9 for measurements C63-1, C76-3 and C77-5. The predicted data presented in Figure 10-9 was obtained by utilizing free-stream recovery temperature, wind tunnel convective film coefficients scaled to SA-1, and the calorimeter measured in-flight temperature-time history. The measured results of Figure 10-9 indicate the temperature of the reflective aluminum tape covering the heat shield would be less than 316°C prior to 60 seconds flight time. The measured in-flight heat shield thermal environment reveals the heat shield thermal protection is more than sufficient.

The asbestos - phenolic plastic flame shield is located between the four inboard engines close to the nozzle exit plane. Total heating calorimeter C78-8 was installed close to the center of the flame shield with the exposed surface of the calorimeter flush with the surface of the flame shield.

Heat influx to the flame shield was also a maximum at liftoff (approximately 90 BTU/ft^2-sec) due primarily to radiation (see Fig. 10-10). By 80 seconds flight time the heat flux had decreased to approximately 10 BTU/ft^2-sec and remained at this level until cutoff. The constant heating rate during the last 30 seconds was due to "choking" of the exhaust gases recirculating between the inboard engines. "Choking" occurs when the pressure ratio between the flame shield area and ambient is high enough to cause sonic gas velocity between the gaps of the inboard engines. Upstream pressure, velocity, and temperature conditions (on the flame shield) were constant during the remaining interval of inboard engine burning time and heat influx rate remained basically constant.

Two thermocouples were used to measure structural temperature on the back side of the flame shield and the flame shield struts. These measurements, C20 and C21, experienced an almost instantaneous temperature rise from 38° to 274°C, occurring from 87 to 116 seconds and from 95 to 116 seconds respectively (see Fig. 10-11). The exact reason for this sudden rise is unknown but may have been due to instrumentation malfunction.

The thermocouples on the cold side of the heat shield showed no temperature rise (Fig. 10-11) indicating adequate heat shield insulation.

10.3 SKIN

Skin temperature measurements (see Fig. 10-12) were taken at various locations along the propellant tanks of SA-1 to ascertain the magnitude of aerodynamic heating associated with the tank geometry. The ten measurements were located such that both longitudinal and circumferential heating profiles could be established. The measurements were generally within an average of 12% deviation from the predicted values. A re-evaluation of the heating estimates was based on the SA-1 pressurant gas temperature, (Fig. 10-13) which was higher than that used for the original estimate (SAT-13 data). The re-evaluated predictions were generally within 5% deviation from the measurements. Figures 10-14 through 10-18 indicate sufficient accuracy with respect to aerodynamic heating calculations and that secondary effects account for the majority of the deviations between measured and predicted values.

Discoloring of the lower sections of the fuel and LOX tanks was observed in the engineering sequential camera coverage analysis. The composition of the paint used on the tanks was zinc chromate primer covered with a paint meeting specification number MIL-E-5556. Analysis of this phenomenon indicates that the discoloration was not caused by high temperatures.

Skin temperatures on the LOX tanks are dependent upon the LOX level in the tank and the temperature of the pressurizing gas. Predictions were made for the skin temperature using the pressurizing gas temperature history observed on SA-T static tests. This gas temperature during the flight of SA-1 was generally 50°C above that observed during SA-T static tests, and therefore skin temperatures were correspondingly higher.

When the theoretical skin temperatures are corrected for the higher temperature of the pressurizing gas, good agreement results.

10.4 INSTRUMENT CANISTERS

10.4.1 CANISTER PRESSURE

Instrumentation and guidance components located in the canisters required the canister pressure to be maintained between 10 and 17 psia during flight. Pressure was maintained within this range by controlling the rate of venting gases.

A change was made in the original pressurization system which utilized an absolute pressure regulator to control the canister pressure at 16.5 ± 0.5 psia. This regulator was removed from canister 15 and located in the return duct of the cooler package where it would regulate the canister pressure until the cooler package was retracted from the vehicle. The pressure of this regulator was changed to 16.2 ± 0.5 psia.

An orifice plate (0.3754 inches in diameter) was installed on canister #15 where the regulator had previously been mounted. This orifice was installed to allow gases to vent from the canisters during flight to prevent a pressure buildup in the canisters. It was sized to permit a slight drop in pressure but assure that the pressure would be within allowable limits during flight.

The canisters were equipped with an auxiliary pressurization system which was provided to prevent the canister pressure from dropping below the minimum pressure should a malfunction or structural leak have occurred during flight. The system was designed to energize if the canister pressure dropped to 12 psia. This would have allowed gases (GN_2) to flow from the fuel tank pressurization high pressure spheres into the

canisters and would have built up the canister pressure to 14 psia where the system would de-energize. The original orifice in this system was replaced by a larger orifice (0.1018 inch diameter).

The pressure in two canisters (canisters #14 and #15) was measured during flight. Figure 10-19 shows close agreement between the flight data and predicted. Since the canister pressure did not drop to 12 psia during flight, the auxiliary pressurization system was never operative.

10.4.2 CANISTER TEMPERATURE

Temperature in the four canisters was controlled by an external cooler package which was mounted on top of the long cable mast. As programmed, the mast retracted from the vehicle during the countdown at T-25 seconds before ignition. There was no canister cooling during flight. Prior to T-25 seconds the cooler package was to maintain the temperature in each of the canisters at approximately 25°C. The acceptable range of temperature is 10° to 40°C. A temperature rise of approximately 9°C was predicted for the 120 seconds flight.

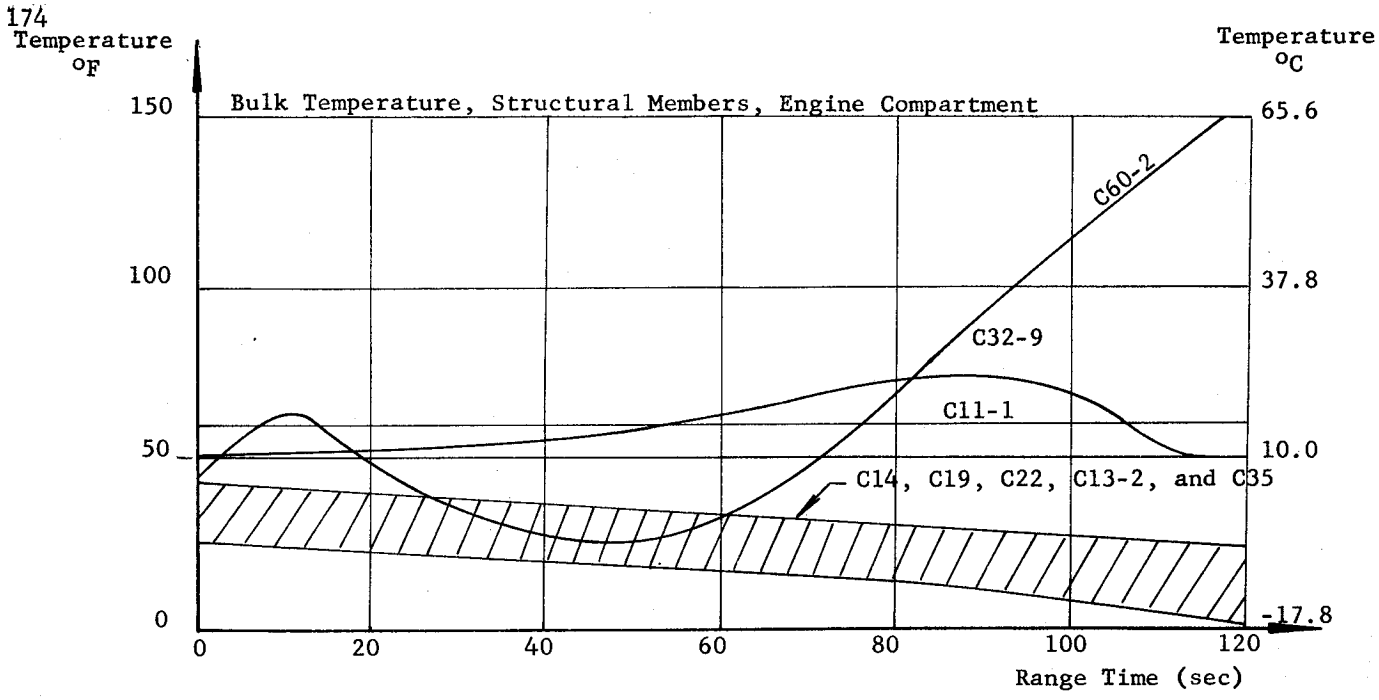

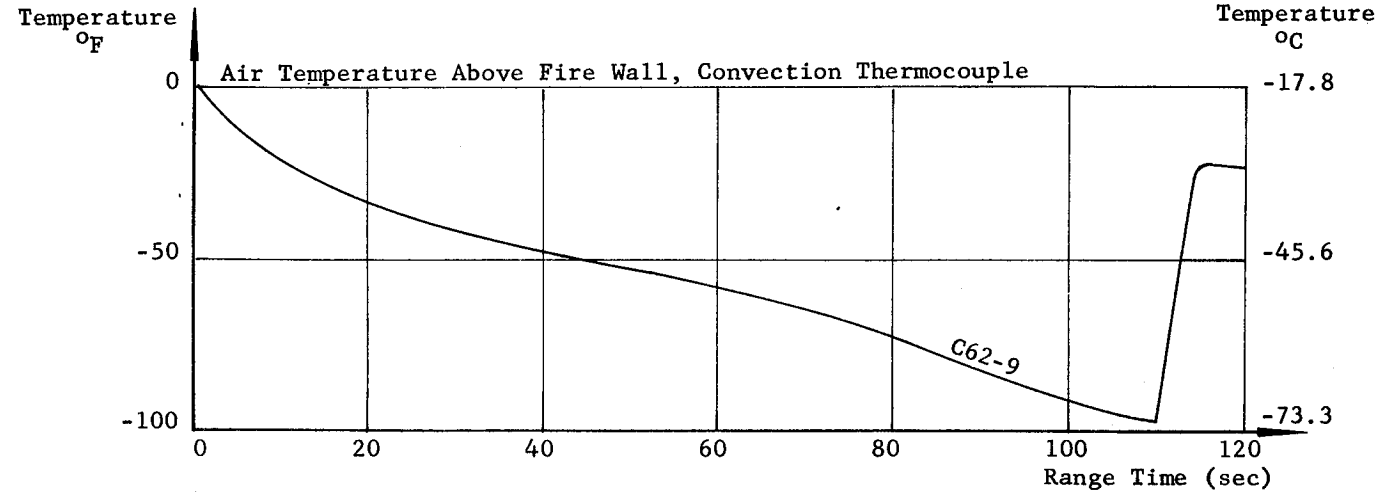

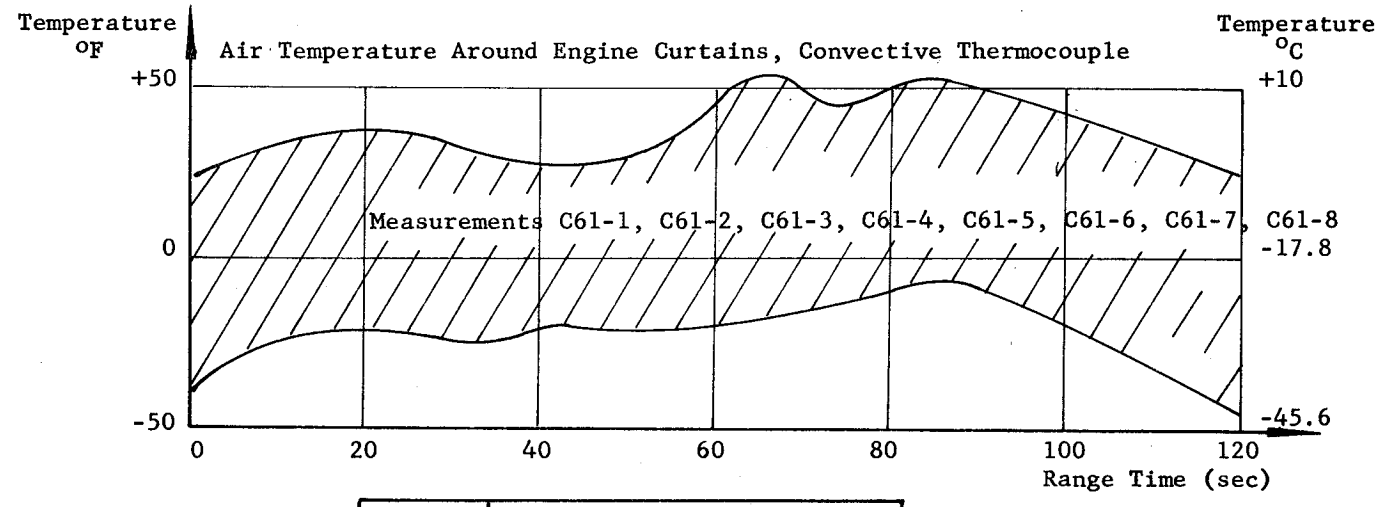

Fig. 10-1	TEMPERATURE VERSUS RANGE TIME
SA-1	

SATURN VEHICLE
SA-1

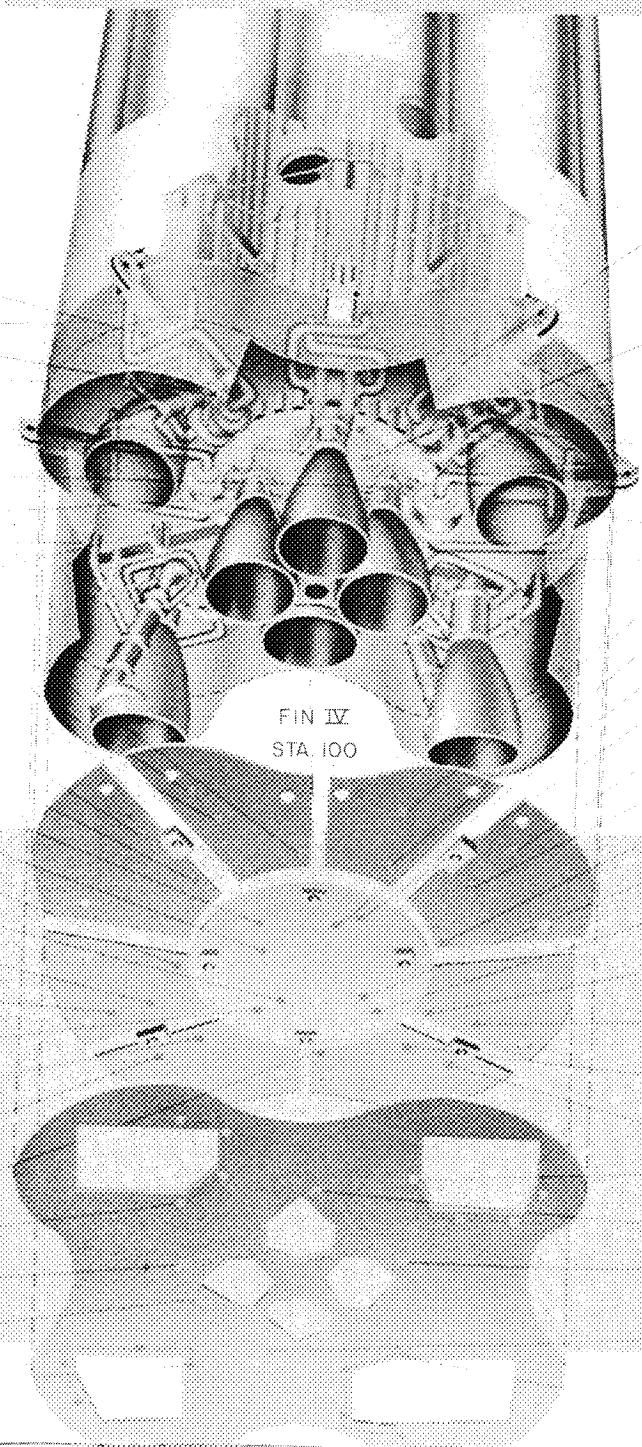

Fig. 10-2	
SA-1	TAIL TEMPERATURES AND PRESSURES

SATURN VEHICLE SA-1

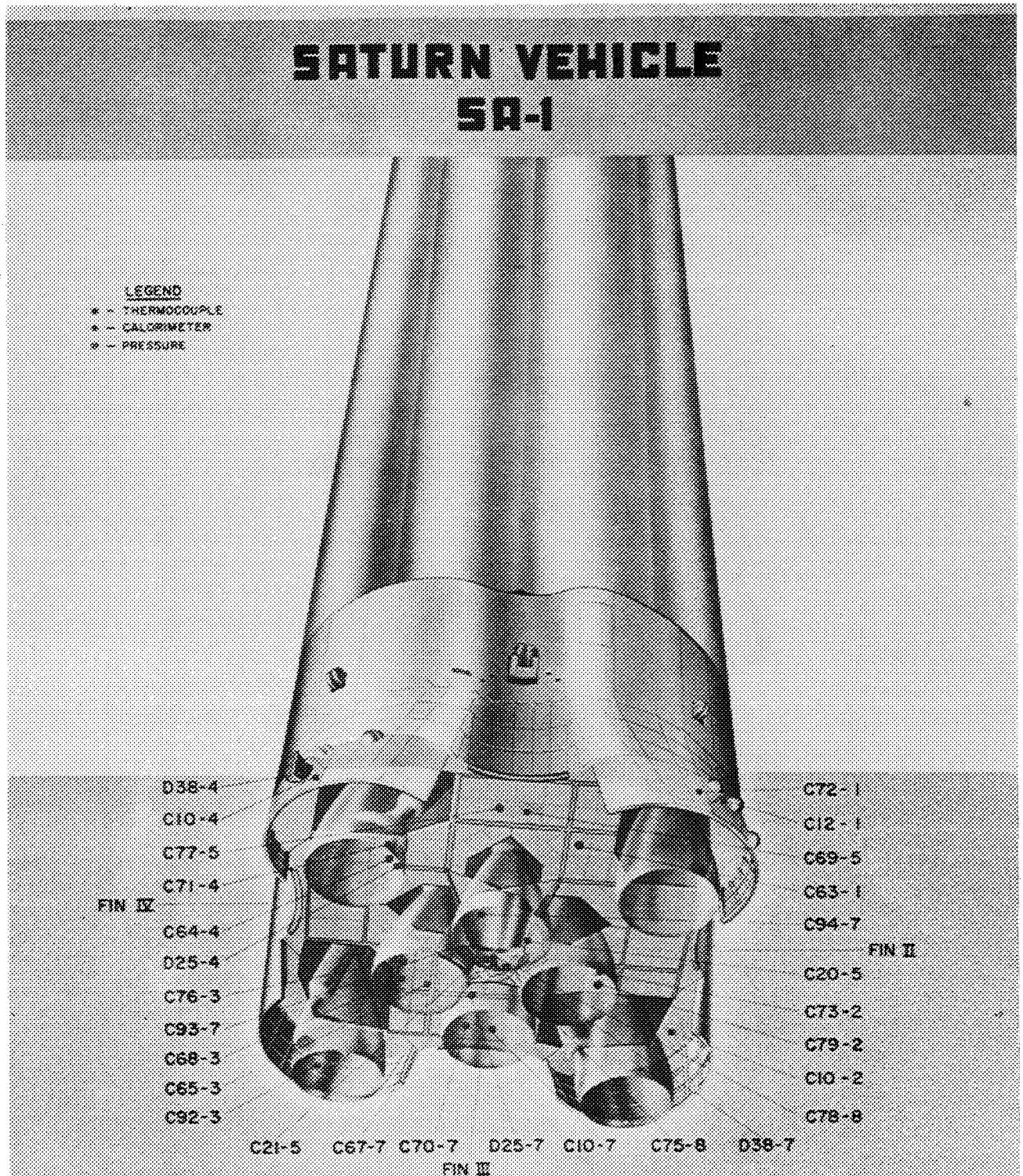

Fig. 10-3	S-1 STAGE FLIGHT MEASUREMENTS
SA-1	

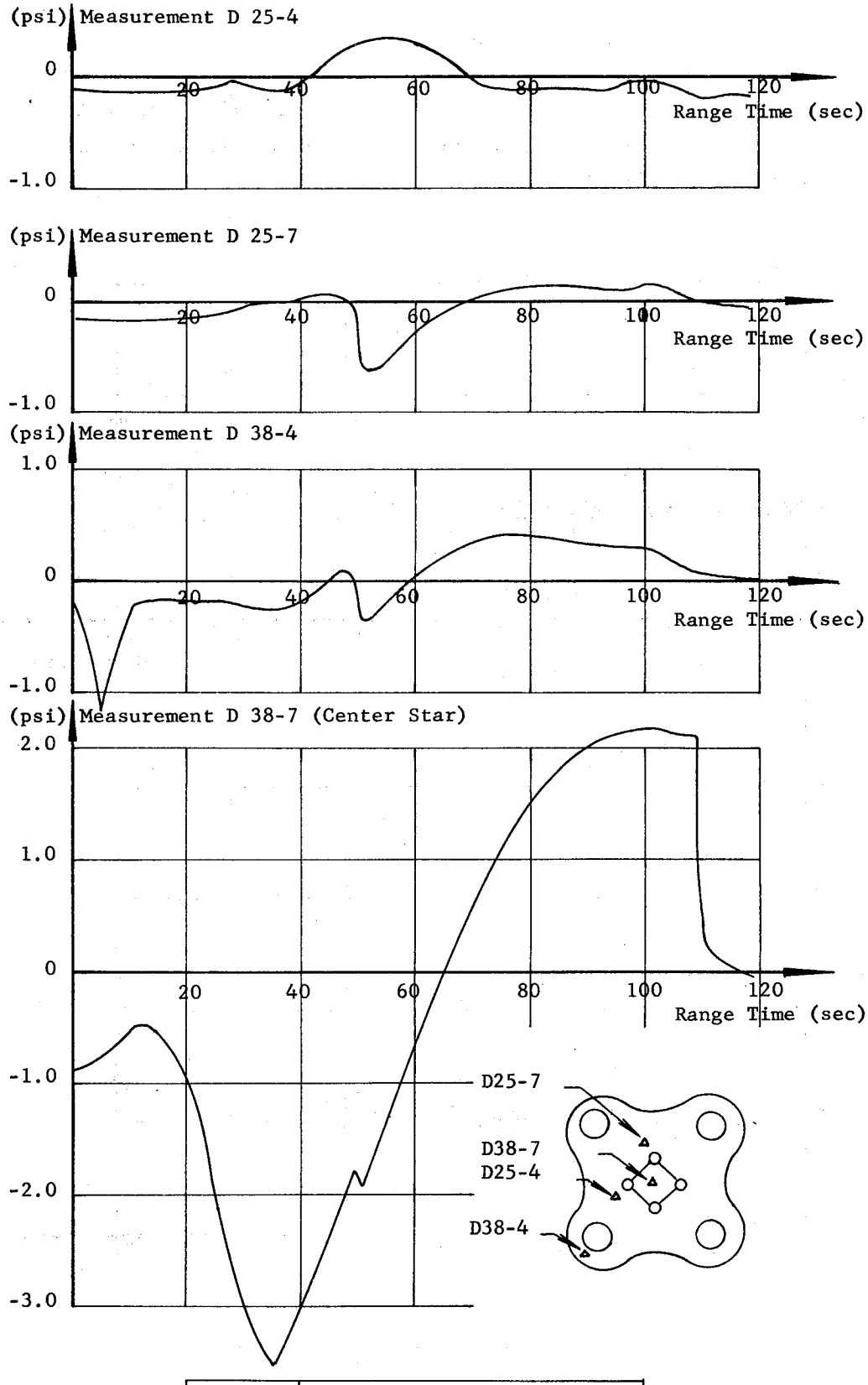

Fig. 10-4	BASE PRESSURE MINUS AMBIENT PRESSURE VERSUS TIME
SA-1	

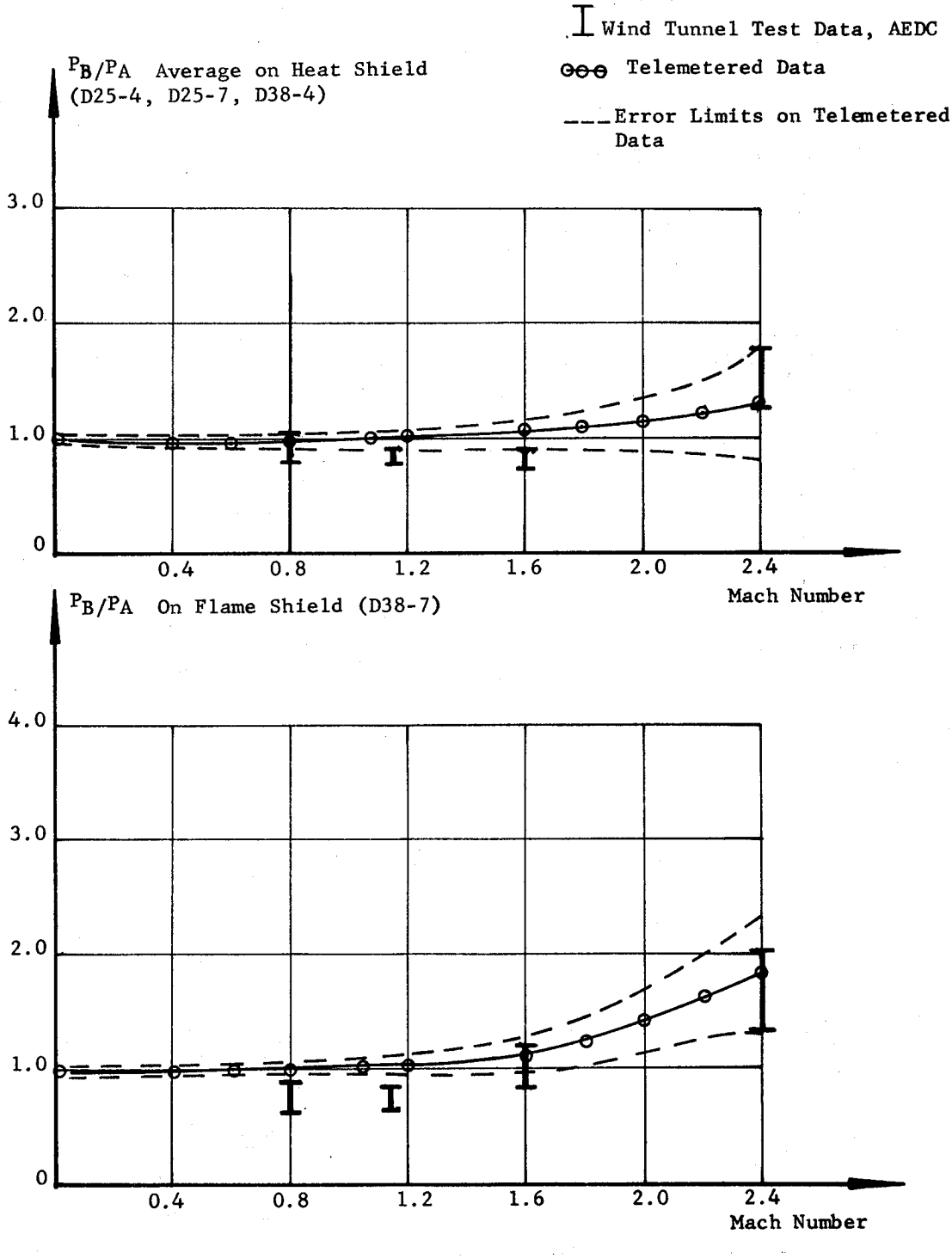

Fig. 10-5	
SA-1	RATIOS OF BASE PRESSURE TO AMBIENT PRESSURE VERSUS MACH NUMBER

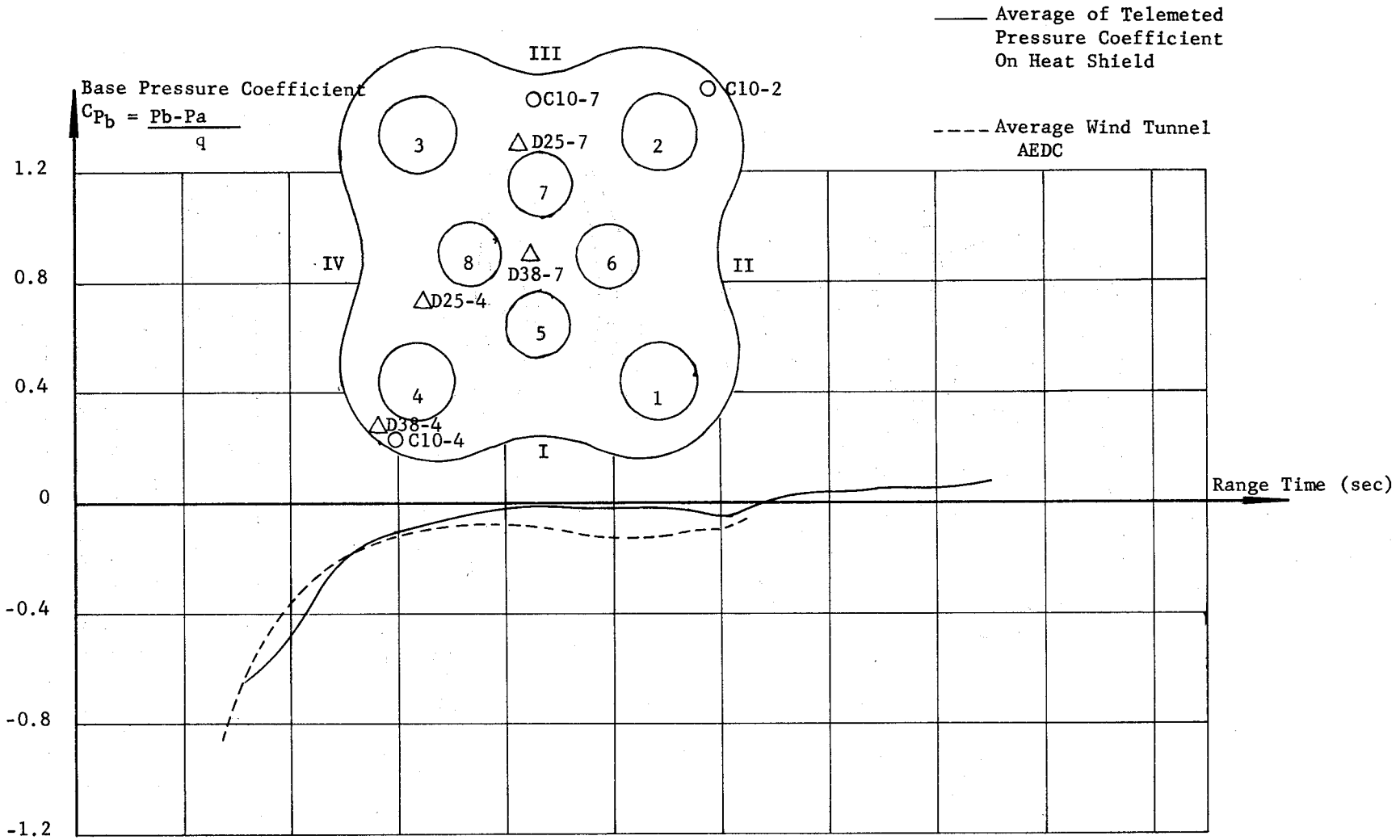

Fig. 10-6	BASE PRESSURE COEFFICIENT VERSUS TIME
SA-1	

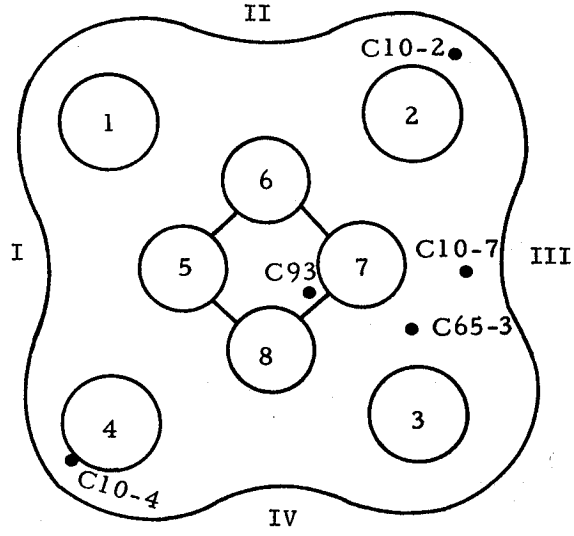

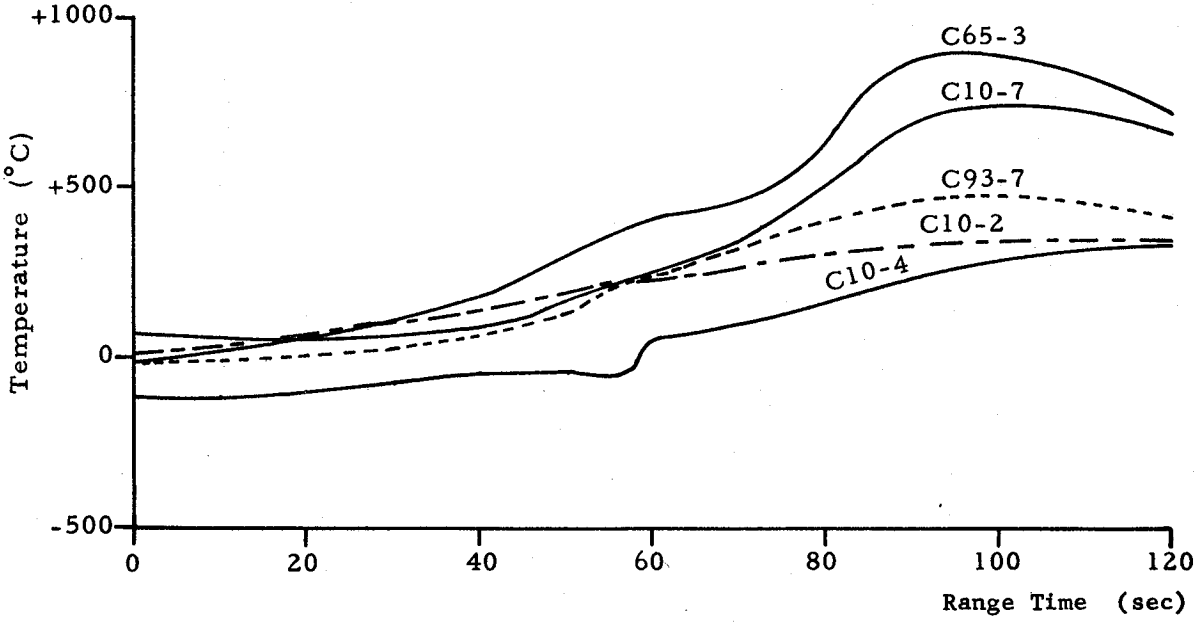

Fig. 10-7 SA-1	CONVECTION THERMOCOUPLES MOUNTED BELOW HEAT SHIELD

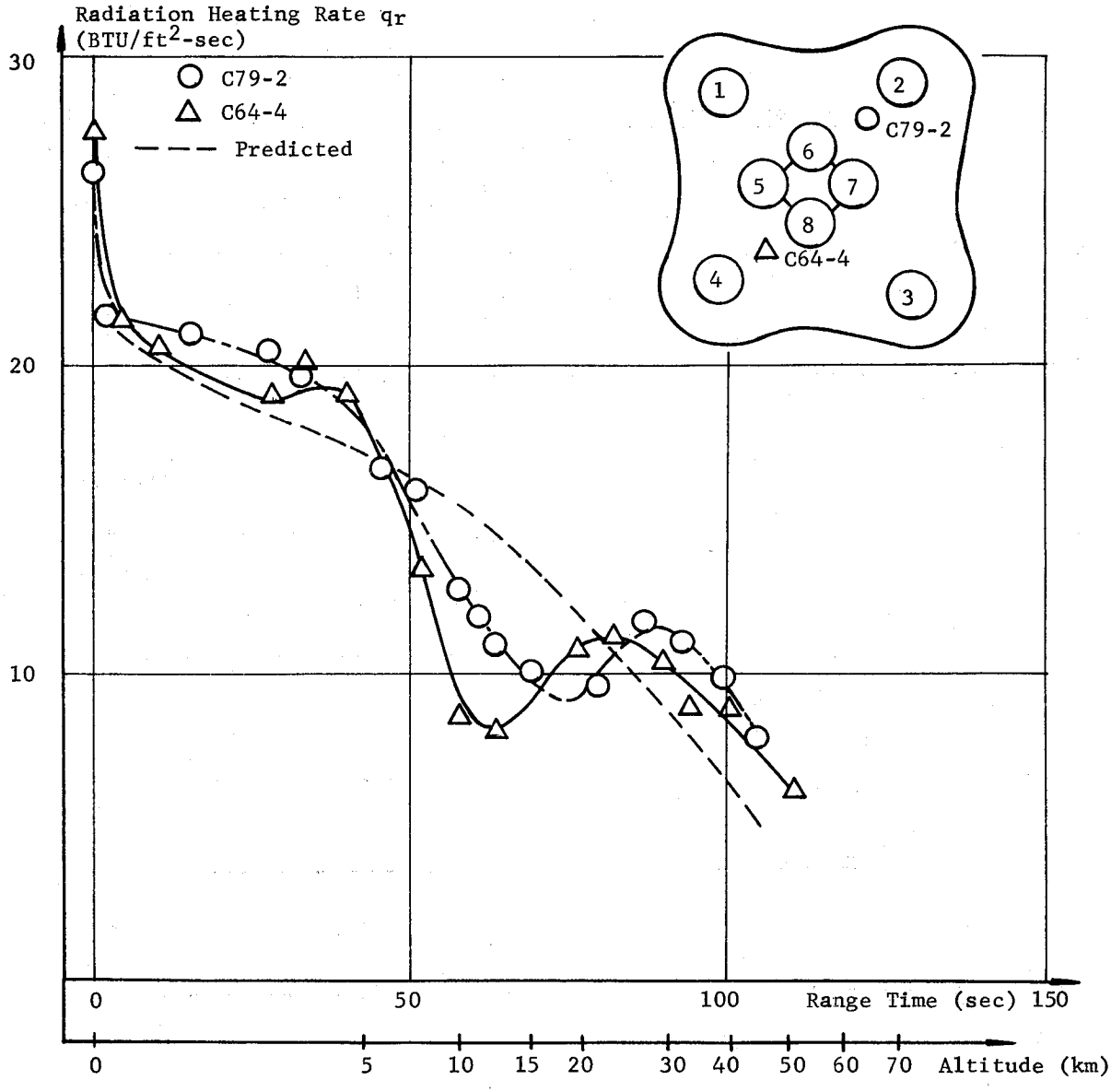

Fig. 10-8	RADIATION Q_R TO A PLANE 9 INCHES BELOW HEAT SHIELD
SA-1	

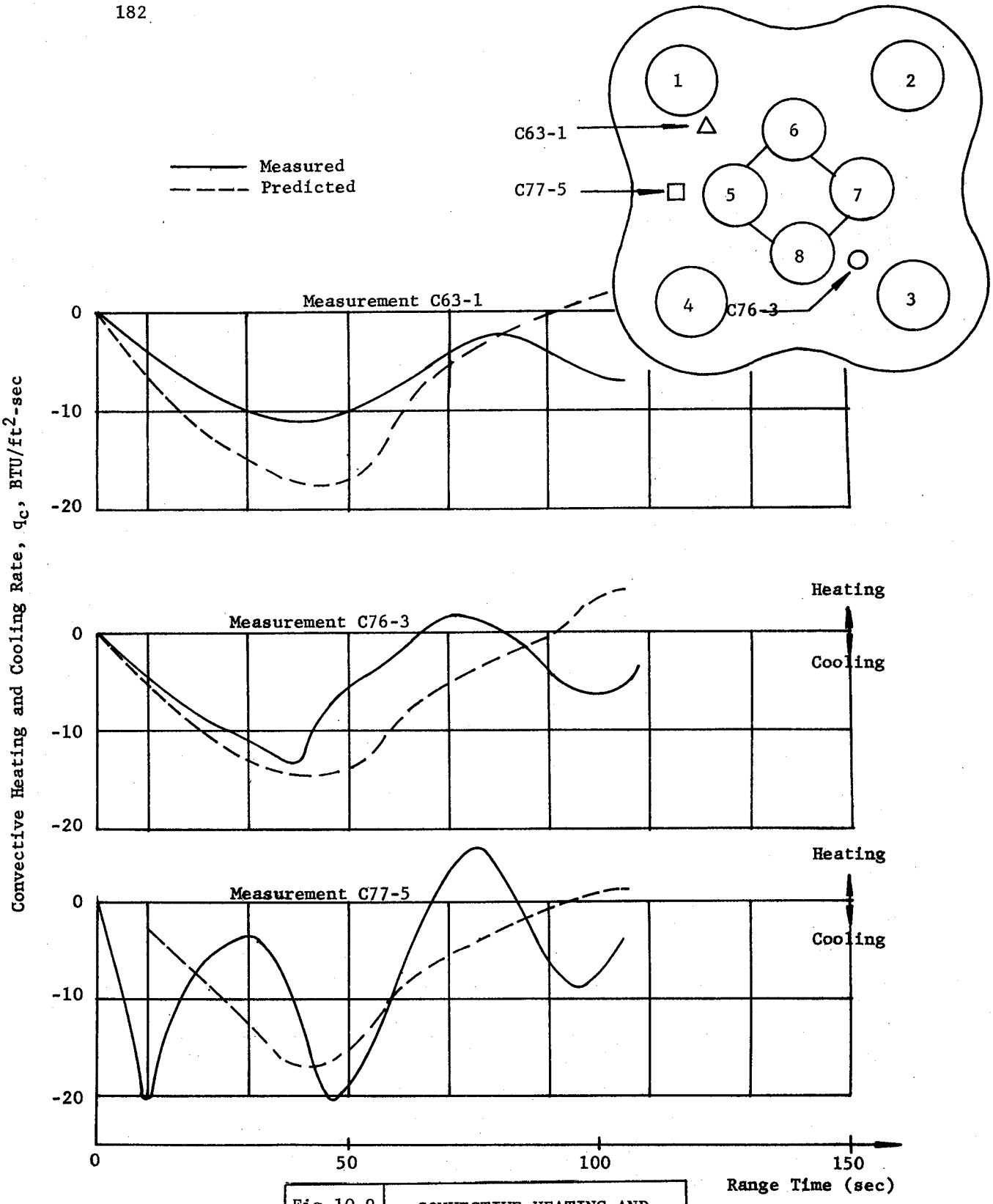

Fig. 10-9	CONVECTIVE HEATING AND COOLING RATE, q_c, IN SATURN HEAT SHIELD AREA VERSUS RANGE TIME
SA-1	

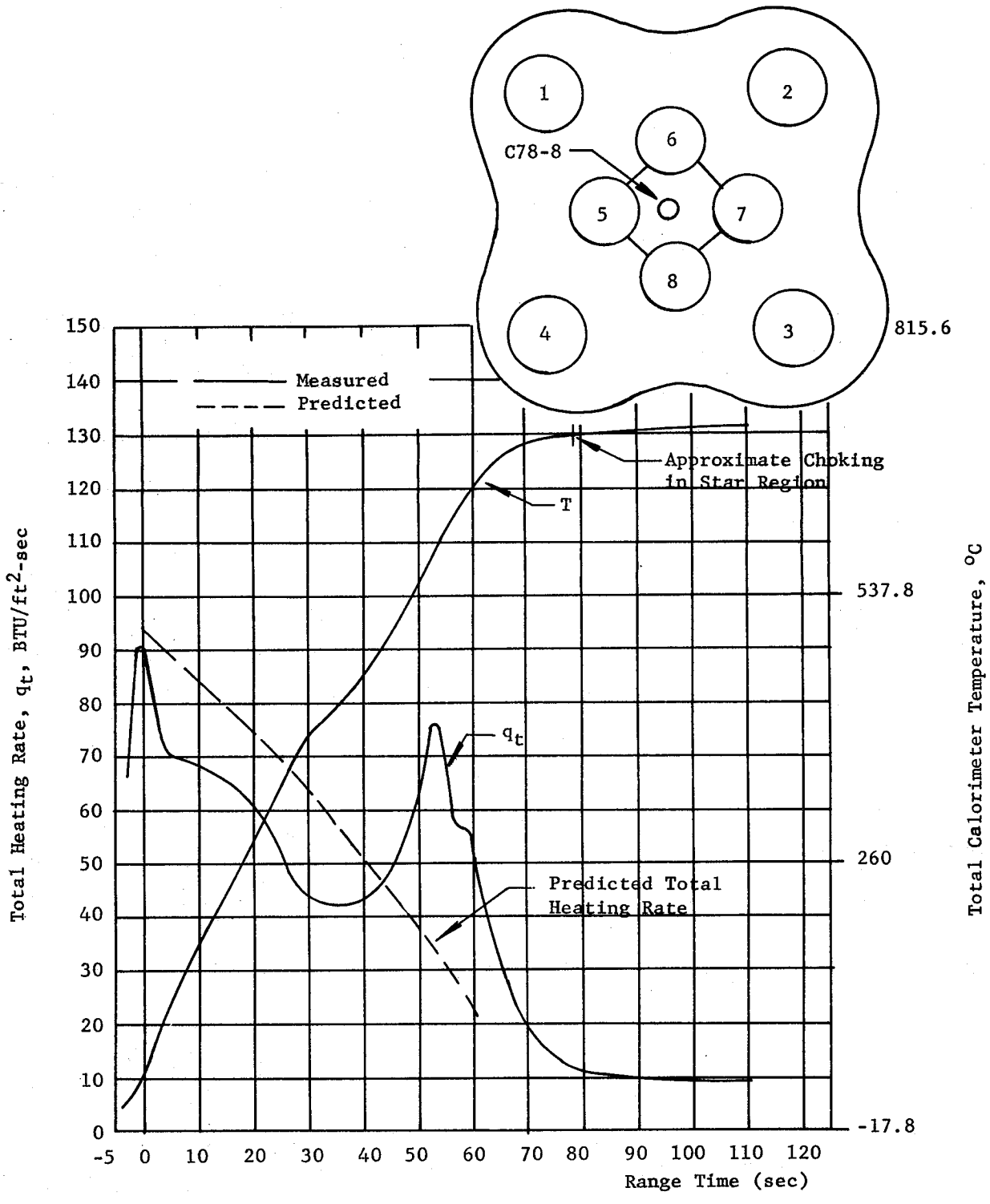

Fig.10-10 SA-1	MEASURED FLAME SHIELD HEATING RATE, q_t AND TOTAL CALORIMETER TEMPERATURE, T, VERSUS RANGE TIME

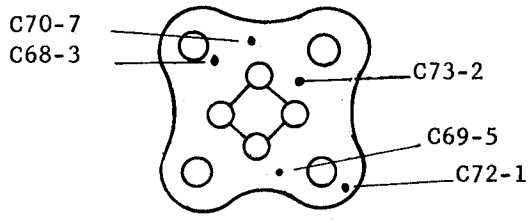

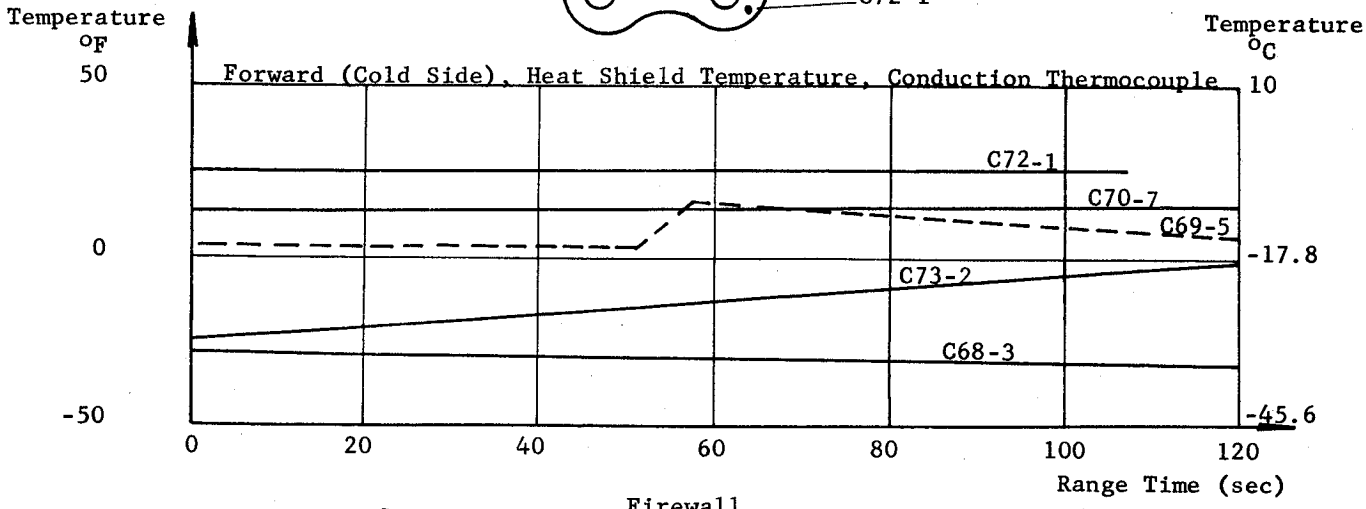

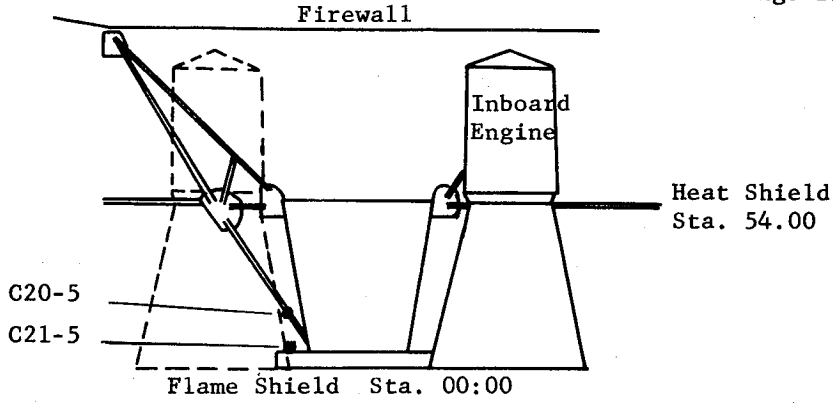

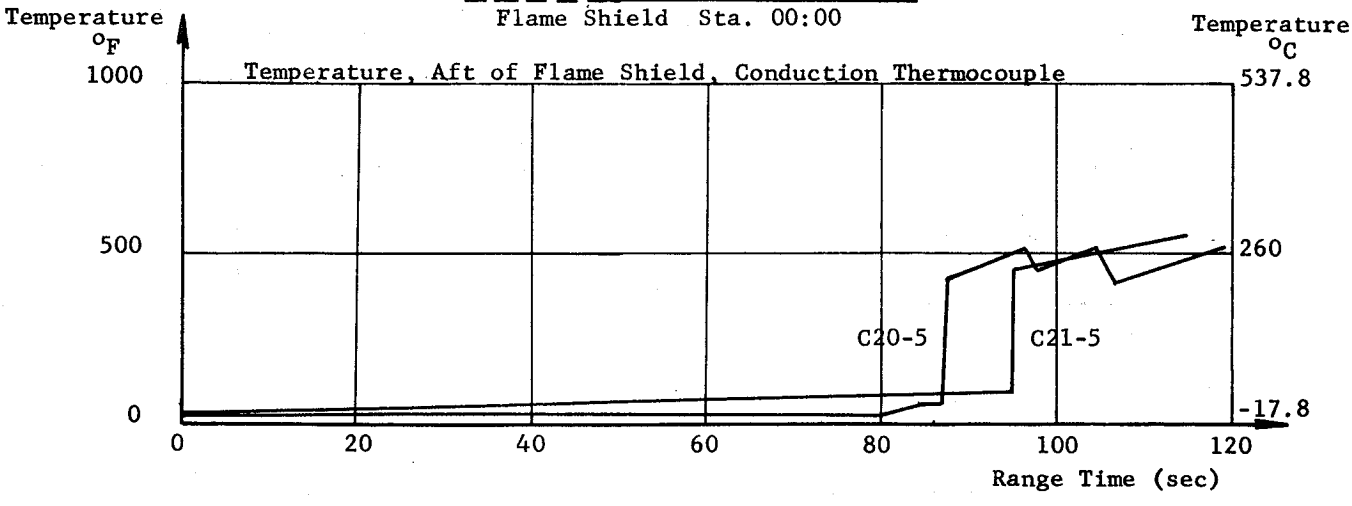

Fig. 10-11 SA-1	TEMPERATURE VERSUS RANGE TIME

SATURN VEHICLE
SA-1

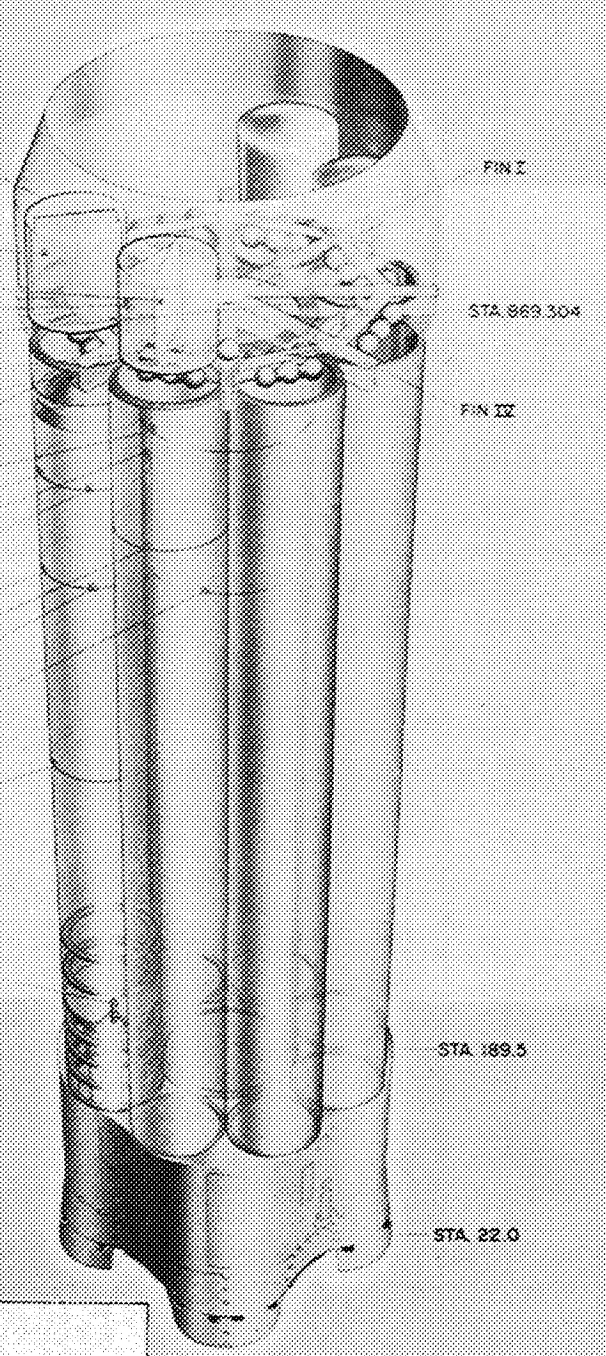

- D26-14 STA. 99
- D26-15 STA. 936
- D24-11 STA. 875
- C52-11 STA. 879
- C51-11 STA. 879
- C37-03
- C30-03 STA. 835
- C30-0C STA. 823
- C43-03 STA. 745
- C48-03 STA. 745
- C46-03 STA. 745
- C44-03 STA. 650
- C50-F3 STA. 741
- C47-03 STA. 590
- C39-0C STA. 641
- C45-03 STA. 485
- C53-03 STA. 382

Fig. 10-12	
SA-1	SA-1 SKIN TEMPERATURES

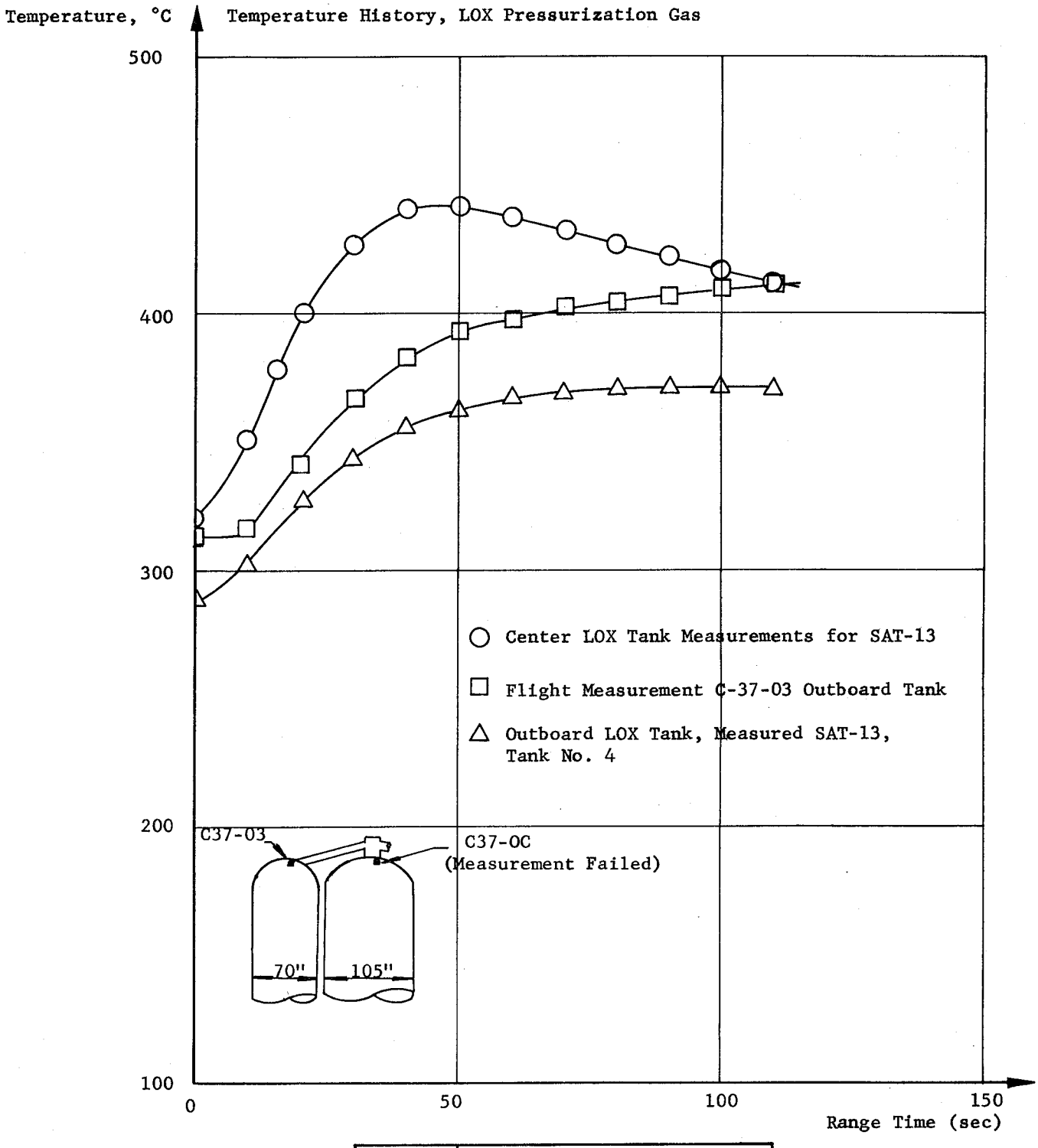

Fig. 10-13 SA-1	SA-1, AND SAT-13 DATA USED FOR LOX TANK SKIN TEMP. PREDICTIONS VERSUS RANGE TIME

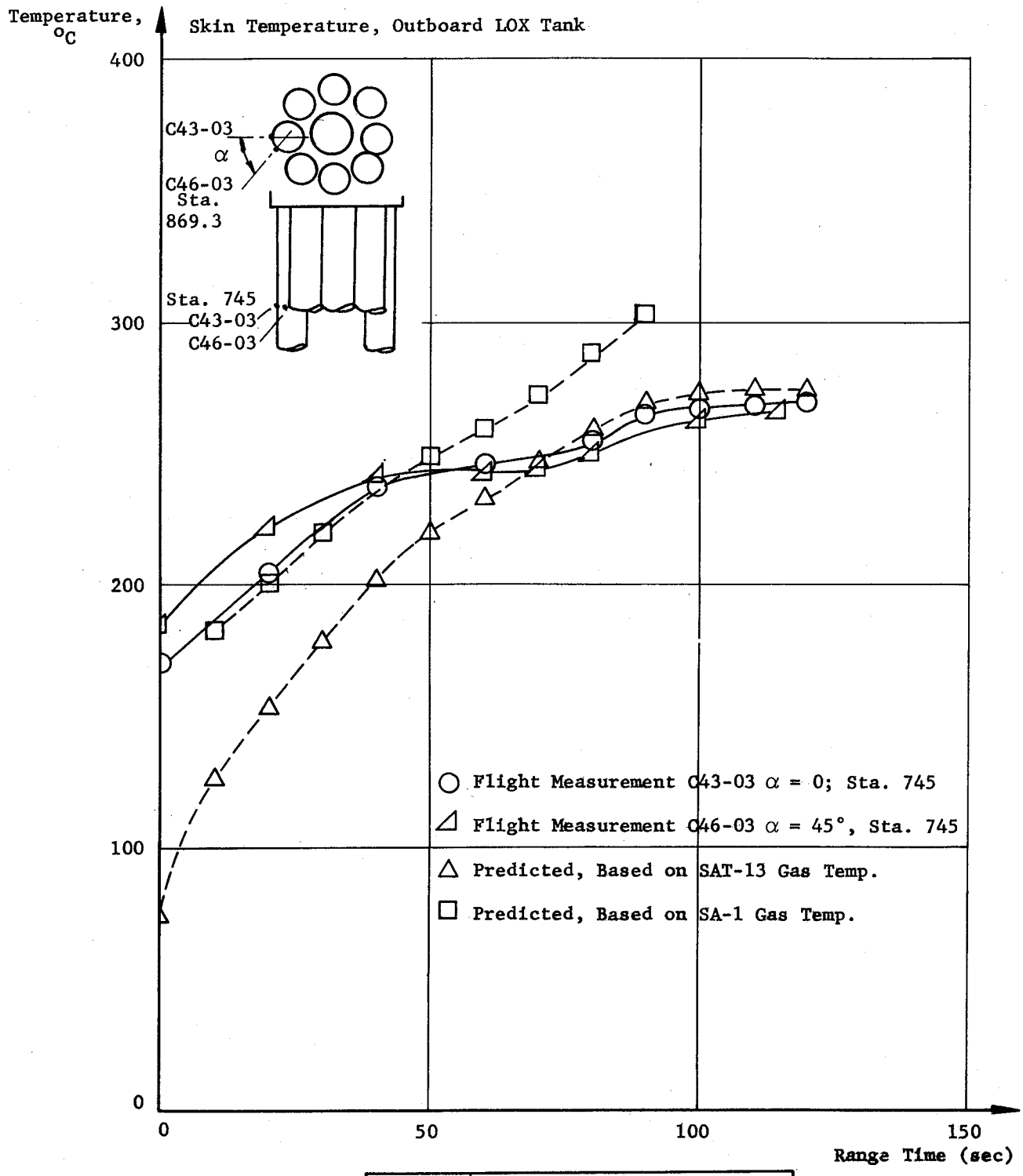

Fig. 10-14	SKIN TEMPERATURE VERSUS RANGE TIME
SA-1	

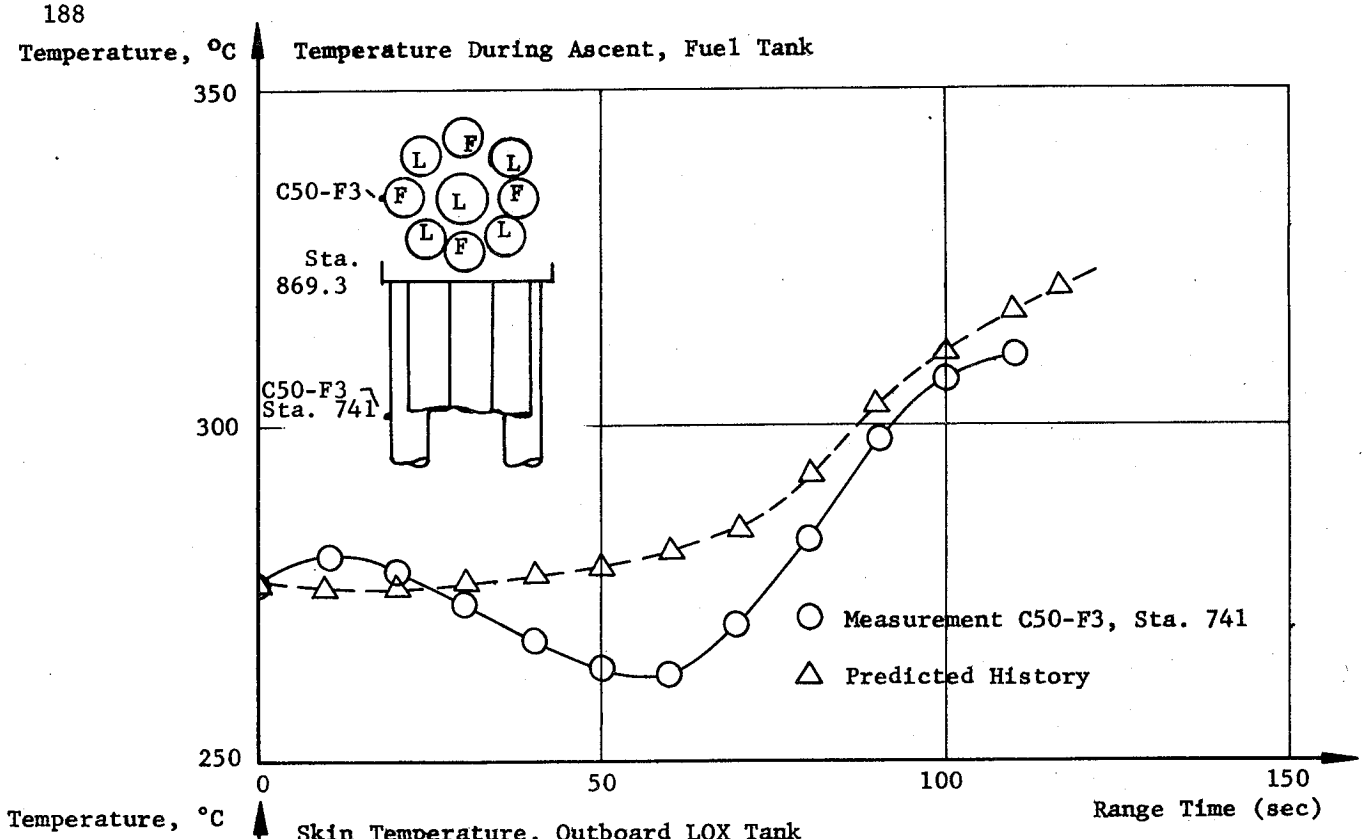

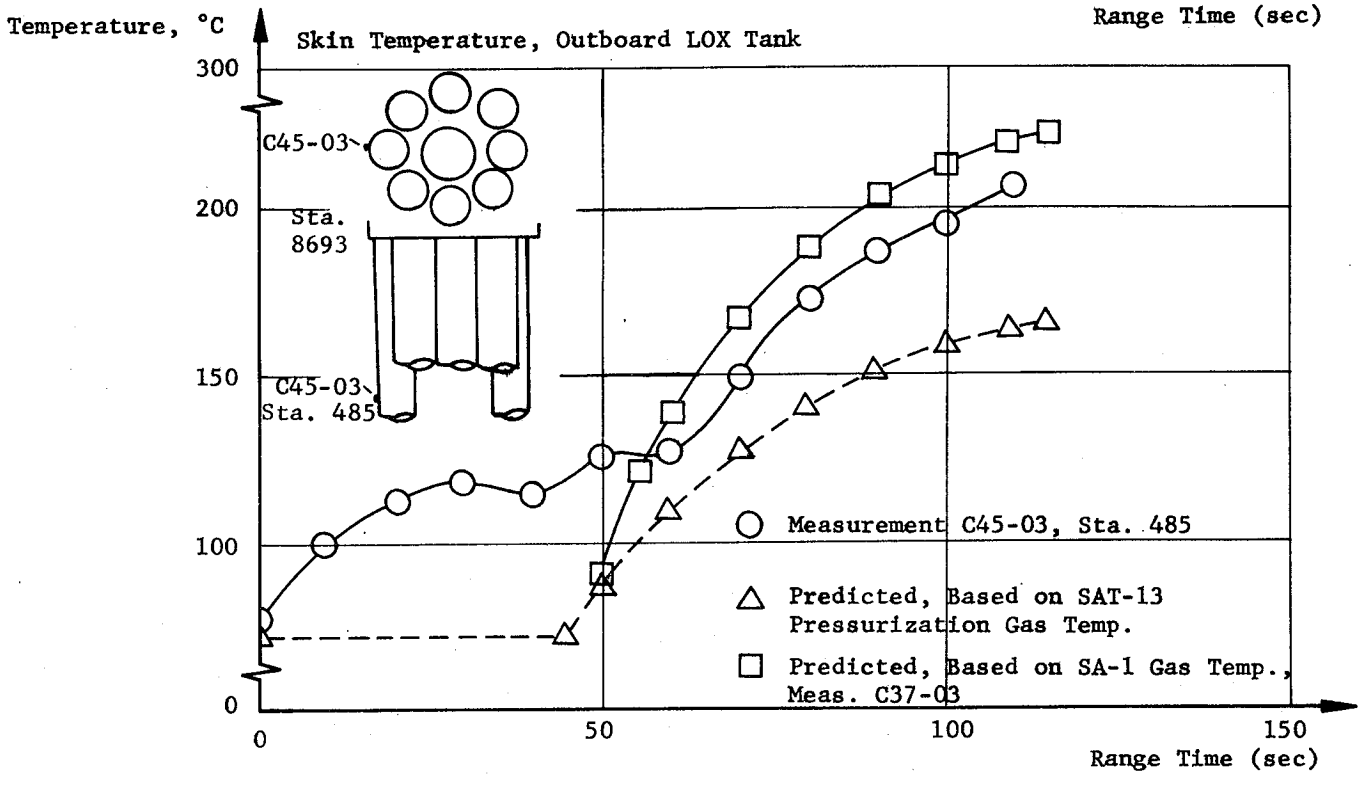

Fig. 10-15	SKIN TEMPERATURE VERSUS RANGE TIME
SA-1	

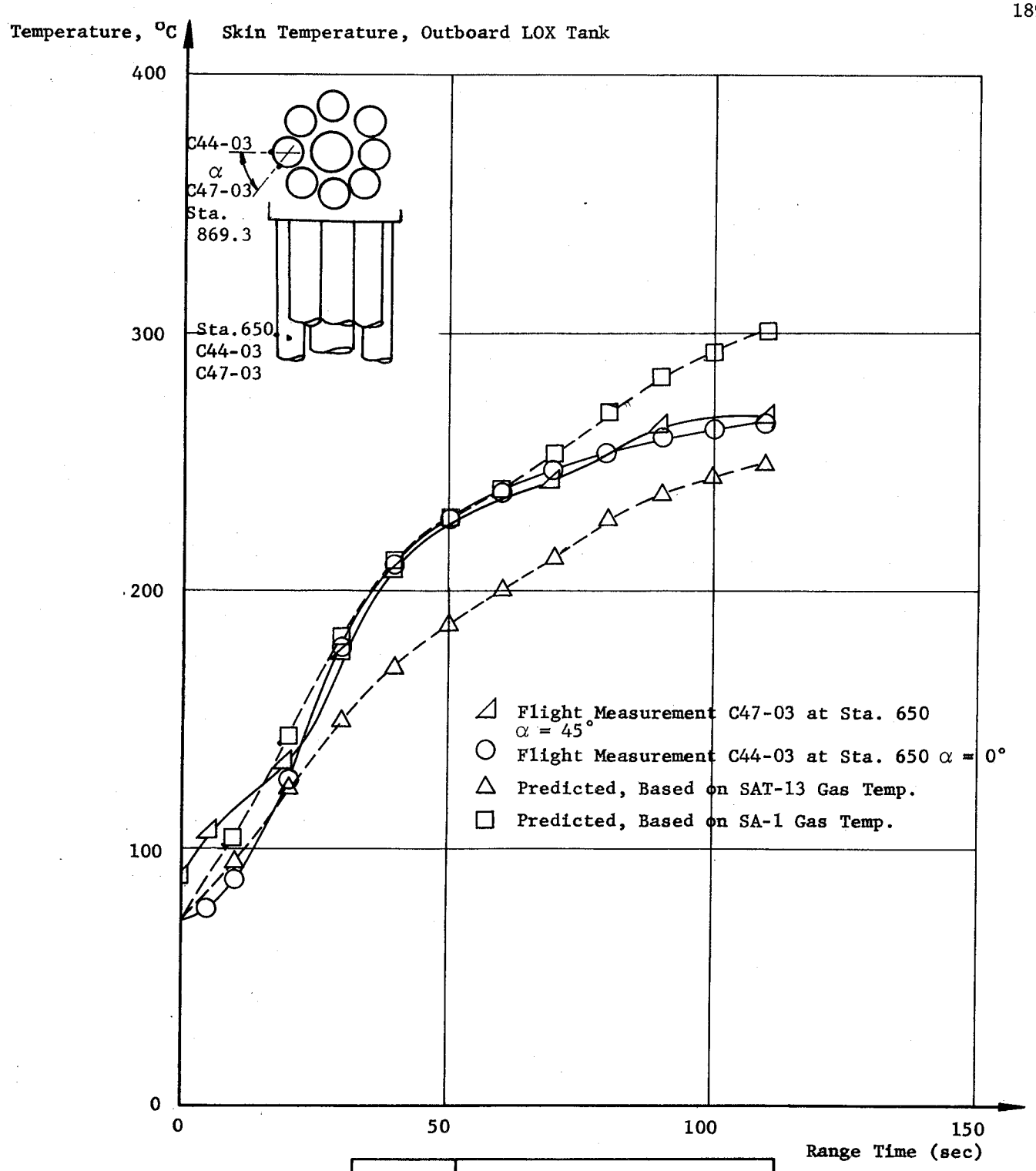

Fig.10-16	
SA-1	SKIN TEMPERATURE VERSUS RANGE TIME

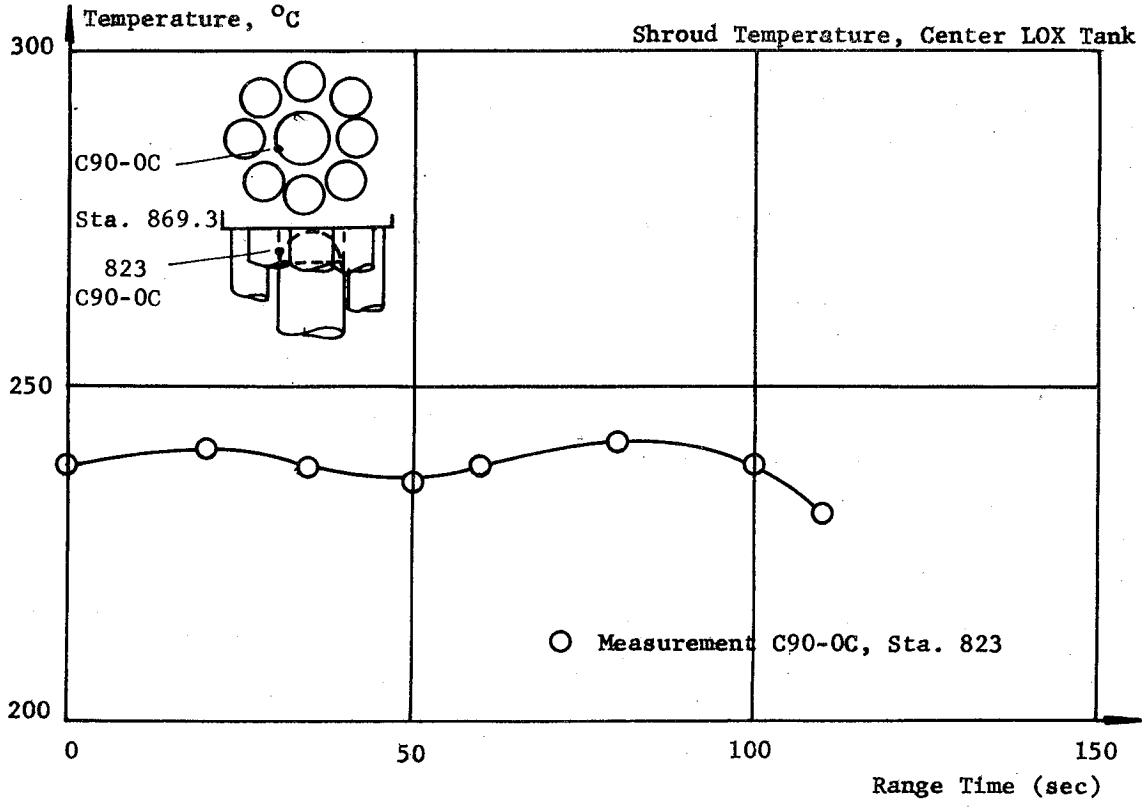

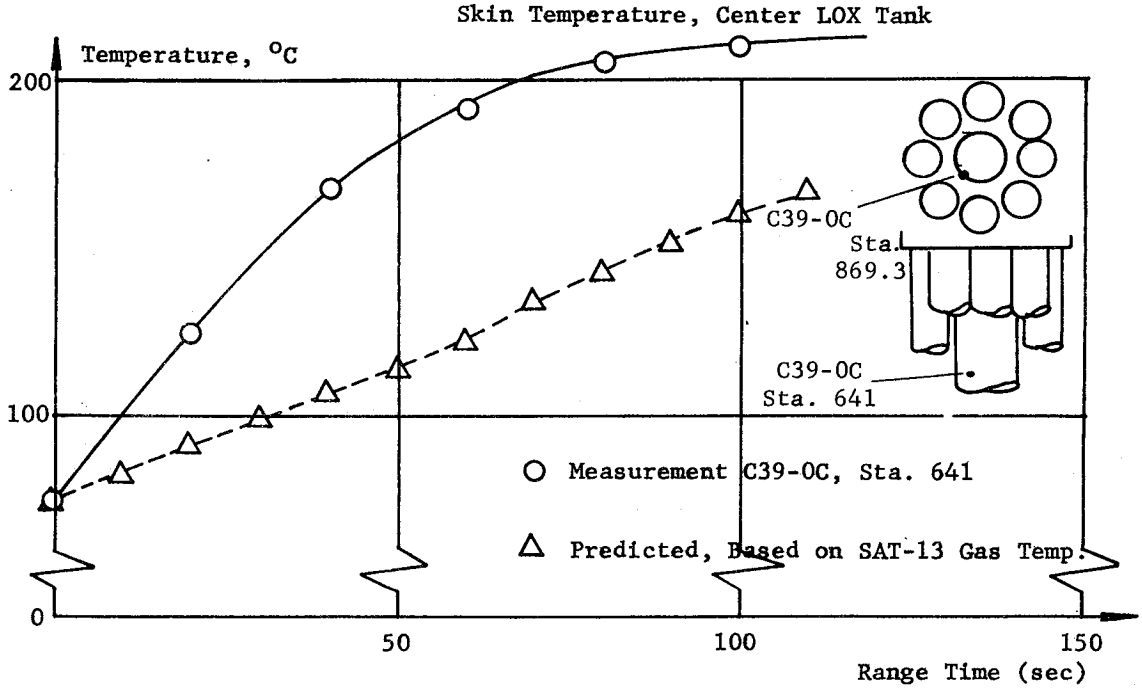

Fig.10-17	SKIN TEMPERATURE HISTORY VERSUS RANGE TIME
SA-1	

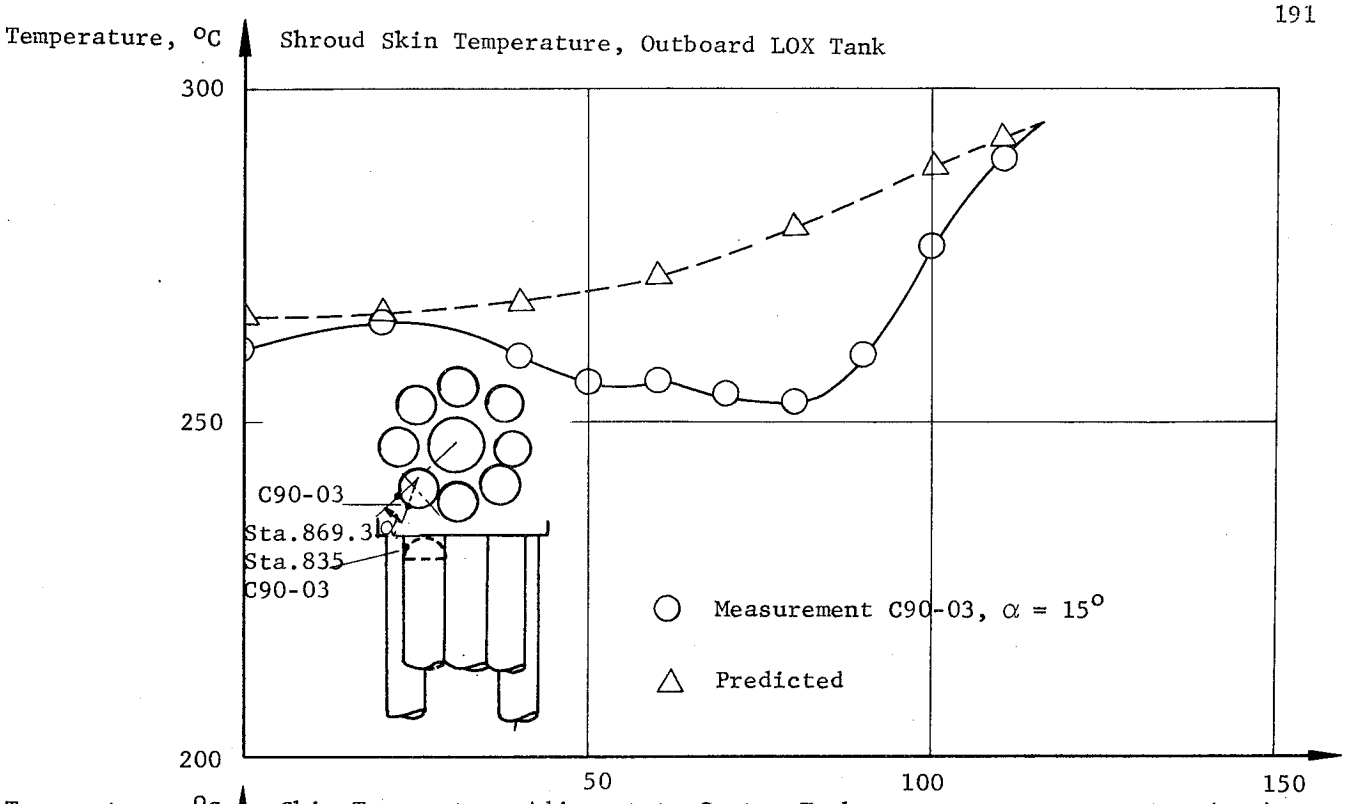

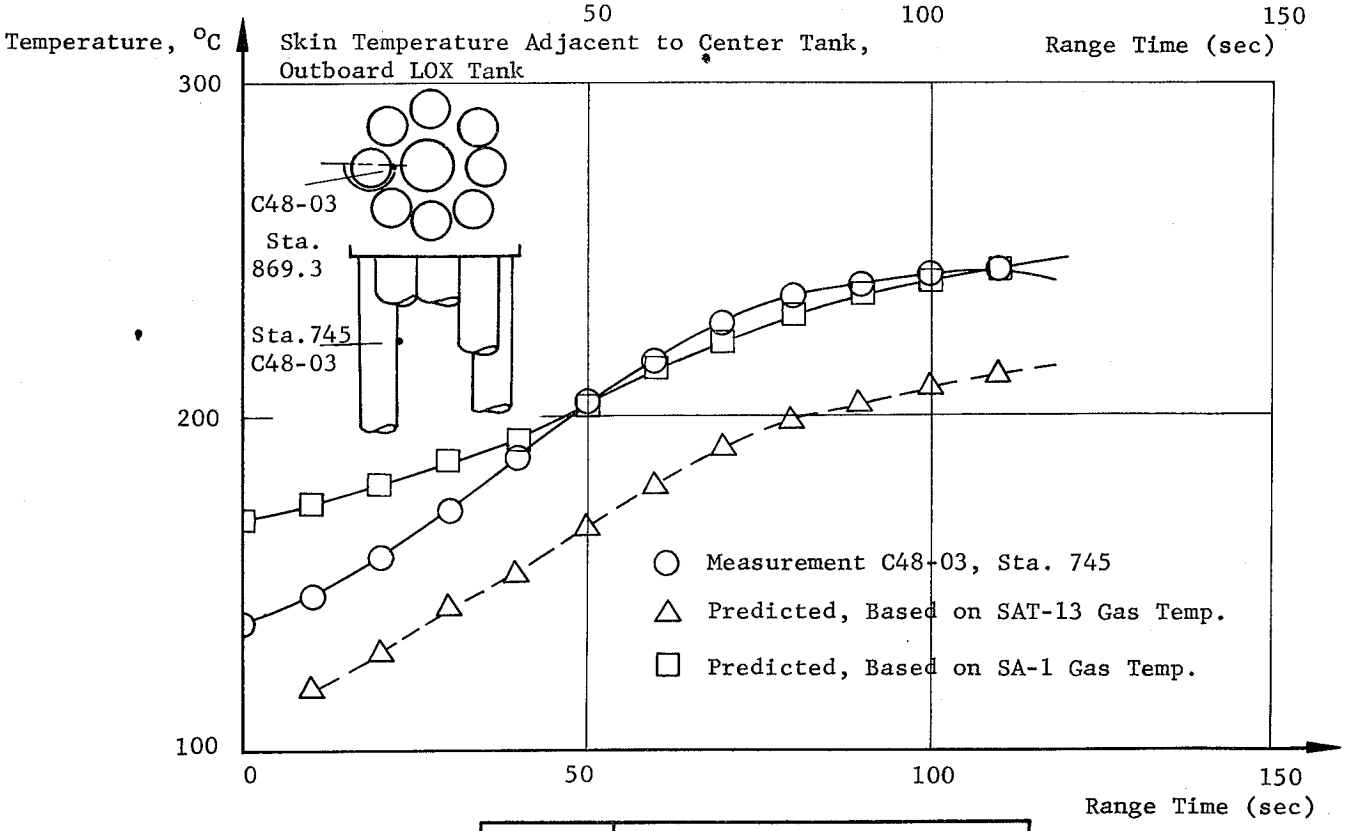

Fig.10-18	SKIN TEMPERATURE HISTORY VERSUS RANGE TIME
SA-1	

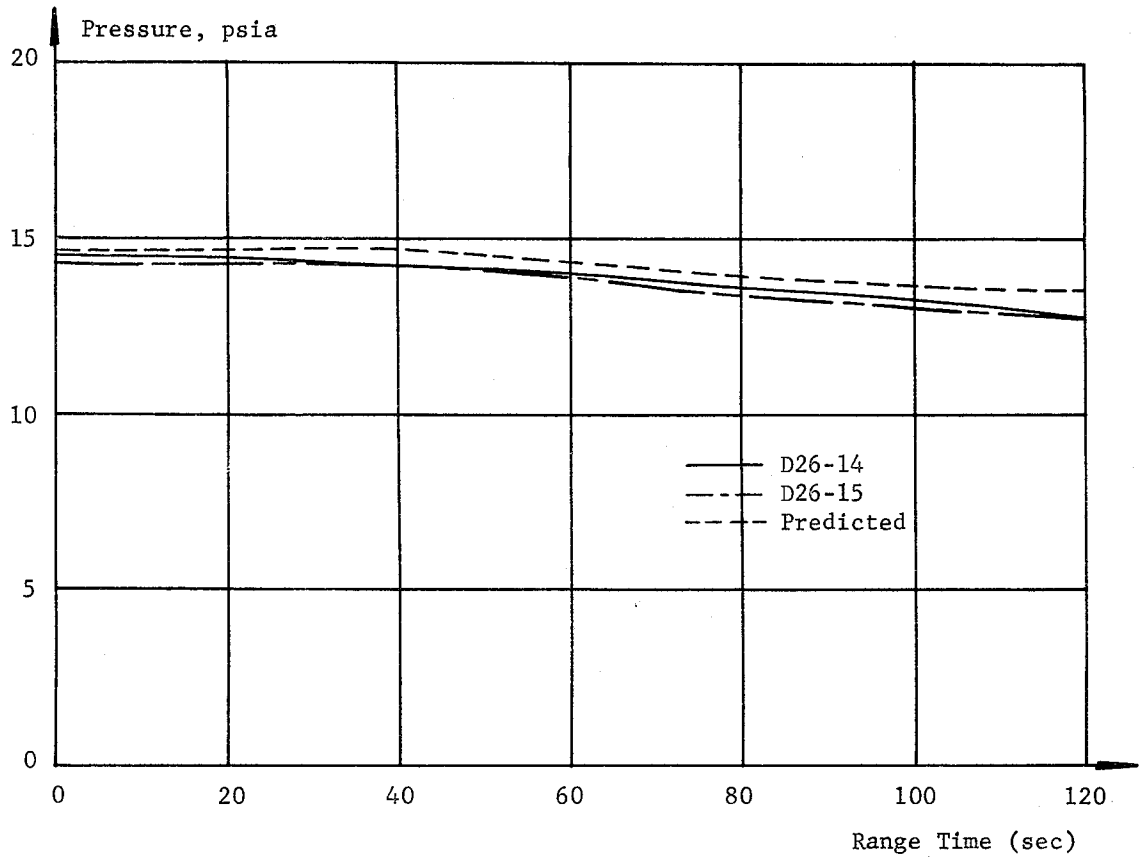

Fig. 10-19	
SA-1	INSTRUMENT COMPARTMENT PRESSURE VERSUS RANGE TIME

11.0 (C) AERODYNAMICS

11.1 SUMMARY

An analysis was made of the SA-1 telemetered data to determine the gradient of the normal force coefficient and center of pressure location for the powered flight phase. These results showed excellent agreement with the predicted parameters.

No attempt was made with the SA-1 data to determine the base drag coefficient. The measurements indicated some unsymmetrical pressure distributions, and it was decided to obtain another set of data from SA-2 to see if any angle of attack effect may be deduced. Generally, it appears that the actual base drag will be somewhat lower than predicted.

11.2 NORMAL FORCE AND CENTER OF PRESSURE LOCATION

Vehicle aerodynamic parameters as determined from SA-1 flight data are very close to predicted. The ratio of the gradients of angular acceleration was determined from the average pitch plane engine deflections and the free-stream angle of attack.

$$\frac{C_1}{B^o} = -\frac{\beta}{\alpha}$$

Where

C_1 = angular acceleration due to unit angle of attack

B^o = angular acceleration due to outboard engine deflection

These values were obtained by plotting the average engine deflections (β) versus the angle of attack (α) at 5 second intervals from 30 to 90 seconds and taking the average slope. A comparison of the flight results and predicted values is shown in Figure 11-1.

The gradient of the normal force coefficient was obtained from the telemetered angle of attack, average engine deflections, and telemetered normal acceleration from the pitch plane by the following relationship

$$C_Z' = \frac{ma_p - F\beta_p}{qS\alpha_p}$$

where:

C_Z' = gradient of normal force coefficient

m = mass of vehicle

a_p = normal acceleration pitch

F = measured thrust of outboard engines corrected for the cant angle of the engines

β_p = average engine deflection in the pitch plane

q = dynamic pressure

S = cross sectional area

α_p = free-stream angle of attack in pitch

The observed gradients of normal force coefficient are shown as circled points and the predicted values as a dashed line in Figure 11-2. Observed values below Mach 1 and above Mach 2.8 are not considered too reliable due to low dynamic pressure and normal accelerations.

The center of pressure location of the vehicle was determined by using smoothed values of the gradients of normal force coefficient (C_Z') and the observed ratio $(-\beta/\alpha)$ from the following relationship

$$CP/D = CG/D \left[1 + \frac{F \frac{\beta}{\alpha}}{C_Z' qS} \right]$$

where:

CP/D = center of pressure location from station 100 (calibers)

CG/D = center of gravity location from station 100 (calibers)

F = thrust of outboard engines corrected for the cant angle

Shown in Figure 11-2, as a solid line is the observed center of pressure location. The predicted center of pressure location is shown as a dashed line.

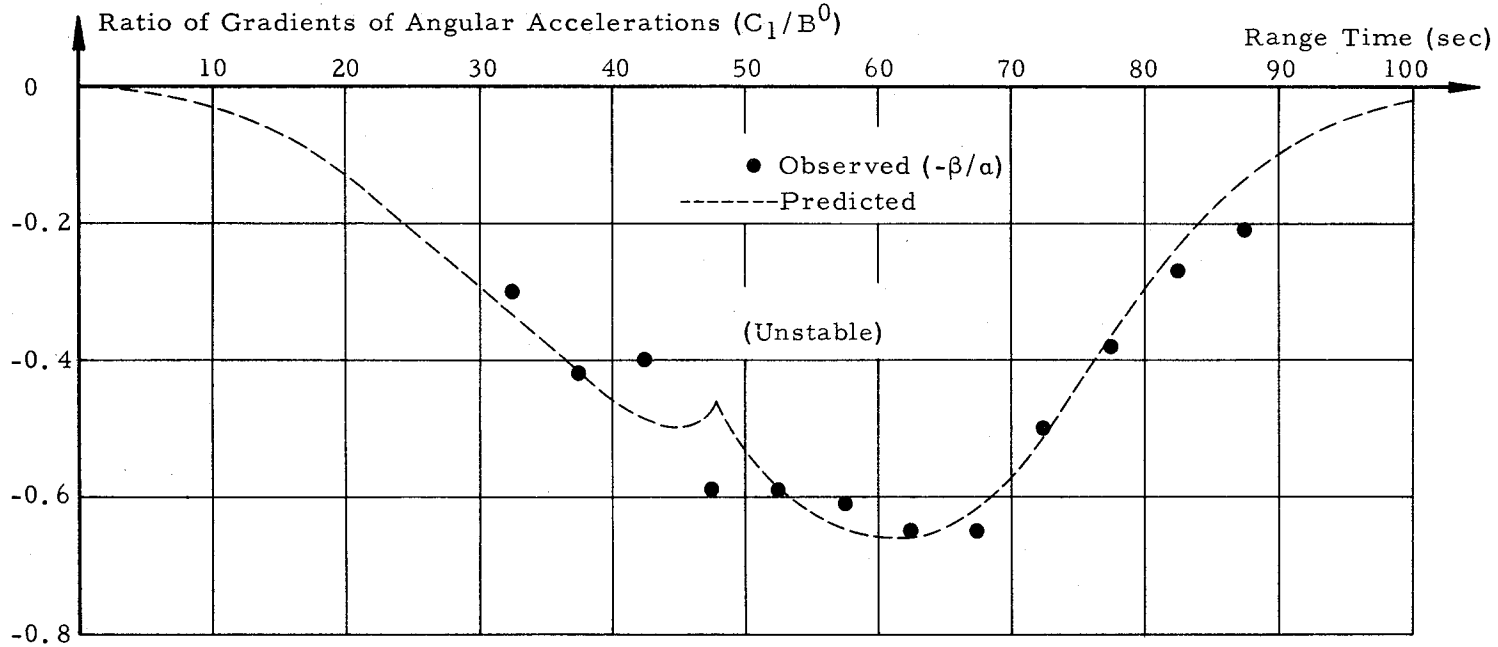

Fig. 11-1	Ratio of Gradients of Angular Accelerations Versus Time
SA-1	

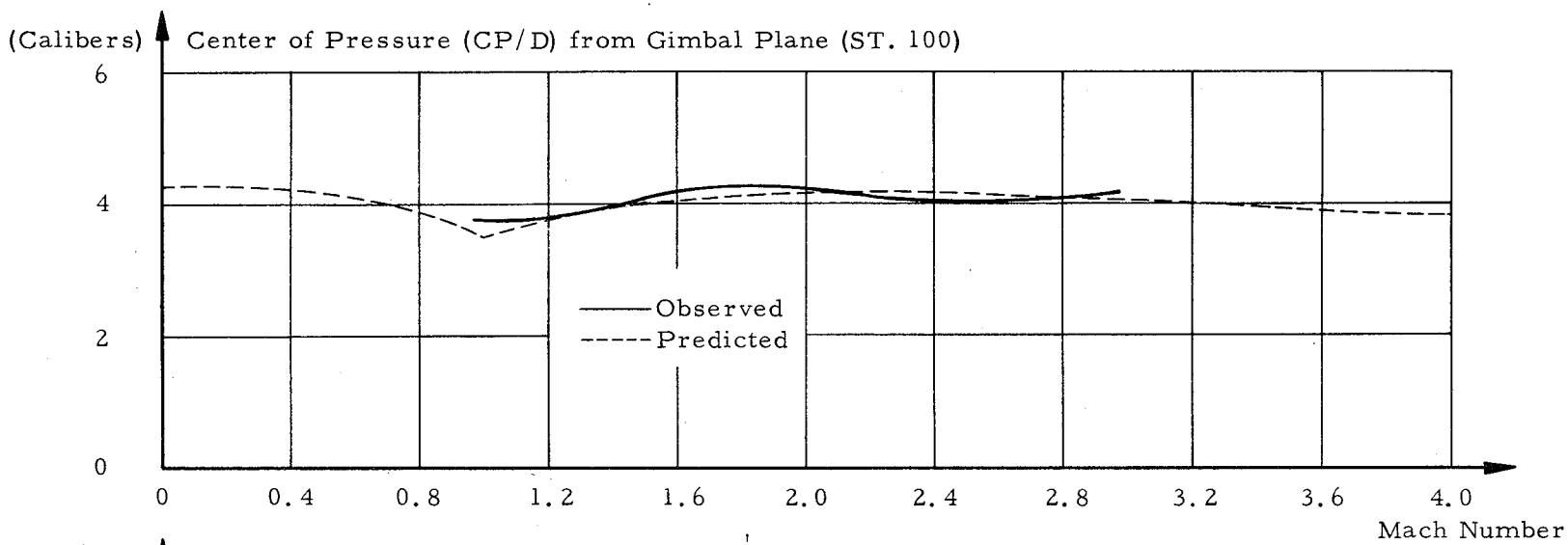

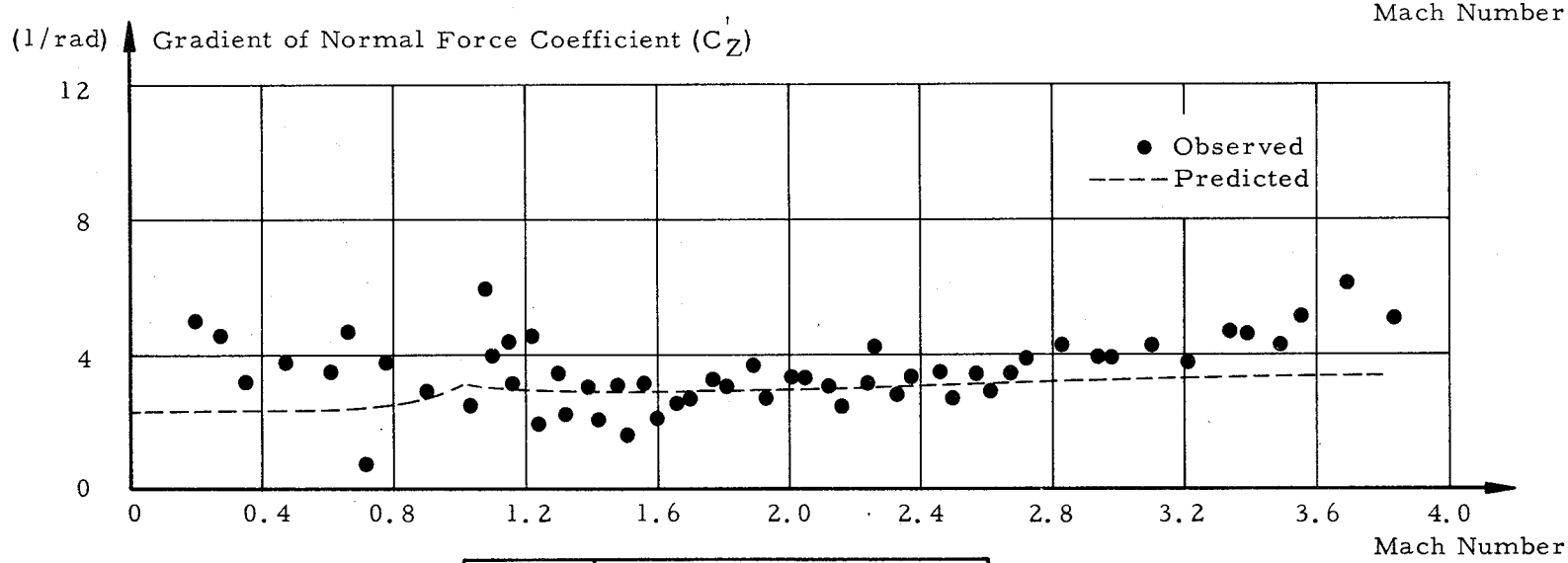

Fig. 11-2	Center of Pressure Location and Gradient of Normal Force Coefficient Versus Time
SA-1	

12.0 (U) INSTRUMENTATION

12.1 SUMMARY

The over-all reliability of the measuring components flown on this flight would be approximately 98 percent, giving half credit to eleven of the nineteen measurements which malfunctioned but are partially usable.

Performance of all mechanical and electronic commutating devices was excellent with no deviation from normal operation.

Preflight calibration from the on-board preflight calibrator was normal and satisfactory.

An in-flight calibrator for link 3 malfunctioned during prelaunch countdown. This was considered to be of small significance since valid prelaunch calibration was available. In-flight calibration on all other links was satisfactory.

Telemetry signals were considered good with only minor deviations being noted at some receiver sites. Hangar D telemetry did show noise before and during the time of cutoff which is believed to be due to flame attenuation. Satisfactory signals were received by all tracking stations.

12.2 MEASURING ANALYSIS

Measurement Malfunctions

SA-1 was instrumented with 505 telemetered flight measurements. Of these, 486 are considered reliable for the entire flight period. Of the nineteen (19) considered unusable for the entire flight, eleven (11) can be used for some periods during flight (Table 12-I).

Temperature measurement C7-4, Temperature Turbine Exhaust, did not respond normally and gave a noisy signal. This is a chromel/alumel type thermocouple having a small output which would rule out a failure of the thermocouple. Probable trouble areas are an intermittent connection between the thermocouple and amplifier or commutator noise.

Measurement C6-5, Temperature Turbine Shaft Brg. #8, had a noisy output. This measurement responded normally in respect to amplitude. If a mean reading of the noise oscillations is made, the output appears normal for this measurement. Noise level was ± 12.5 percent of full scale.

In the engine system number 6, measurement C3-6, Temperature H.S. Pinion Brg. #5, gave a short period of response then decayed to zero output. This is an iron/constantan thermocouple, which is supplied by Rocketdyne. Thermocouple damage is indicated.

The DC flowmeter converter A8-6 in this engine system did not operate. There was a preliminary reading, but the output decayed to zero. The AC counterpart of this flowmeter functioned properly.

Temperature measurement C67-7, Temperature Radiation Shield, whose output dropped to zero after engine ignition appears to have had an open thermocouple. This particular thermocouple is a platinum/platinum-rhodium type, which has been discontinued in favor of a faster response gage.

Temperature Gas Top LOX Tank, C37-0C, has an intermittent output from 18 seconds to 93 seconds after ignition. Though this measurement has this intermittent period, all preceeding and following data are reliable. An extrapolated curve connecting these reliable data zones should give an indication of the temperature performance in this time zone.

Measurement C53-03, Temperature LOX Tank, measured more than 100 percent before ignition and during flight and does not appear reliable. This is a resistance thermometer, and an open circuit would produce a reading of more than 100 percent. The two other LOX temperature measurements read normally.

Two of the discrete liquid level probes, A2-0C and A2-F2, did not function. The two respective probes, A3-0C and A3-F2, which are located below these measurements, functioned normally, indicating that the liquid level had passed them. The remaining probes will be discussed later in this report.

Data from the six ΔP sloshing pressure measurements (D4-F2, D5-F2, D6-0C, D7-0C, D6-04, D7-04) are unusable for a portion of the powered flight. From 60 seconds after ignition to cutoff they can be used and are considered reliable. On measurements D6-04 and D7-04 the range was exceeded at 109 seconds. These measurements will also be discussed in the sloshing analysis of this report.

Measurement E39-2, Vibration Yaw Actuator, Longitudinal, did not respond. Trouble could be in cabling or AC amplifier.

Measurements E33-1, E33-3, and E33-7, Vibration Thrust Chamber Dome, Longitudinal, became noisy 45, 25, and 29 seconds respectively

after ignition. Data previous to these times are reliable. Vibration data following these stated times is also reliable if the readings are made between the intermittent low frequency pulse trains. The exact cause of these low frequency pulses has not been exactly determined, though it is believed to be caused by shock vibrations within the vehicle. Studies are under way to determine the exact cause of these vibrations and to improve this measurement.

Measurement E5-15, Vibration ST-90, Z Azis, had a series of spikes before ignition and throughout the flight. This is caused by a turning on and off of the air bearing air heater. The noise is transmitted to these measurements because of a particular arrangement of shields associated with heater wiring. This was noted during the simulated flight test, but it was decided that it would not be corrected for the flight. Wiring will be corrected on future vehicles.

Liquid Level Measurements

Two liquid level probes are located in each of the nine tanks to sense the liquid level at predetermined points. Three different components, the liquid sensing probe, the discrete input and the pulse measuring unit, constitute one measuring signal. The probes operate on the principle that they sense the presence or absence of liquid. A high impedance is seen when the probe is submerged in liquid, and a low impedance when it is in an atmosphere of gas or vapor. These impedances are converted into voltage pulses. The upper probe produces a 1.0 ± 0.1 volt pulse; whereas the lower probe will produce a 0.5 ± 0.1 volt pulse. In the seventy inch LOX tanks, the bottom probes were 11.000 ± 0.016 inches from the bottom of the tank and the top probes were placed 19.00 inches above the bottom probes. In the center LOX tank the bottom probe was set 11.215 inches from the bottom of the tank and the upper probe was located 19 inches above this. In the fuel tanks the bottom probes were 8 inches above the bottom of the tank and the upper probes were 15.5 inches above these.

After the probes were originally installed in the outer LOX tanks, a baffling plate (hat plate) was added at the inlet of the tank to redirect the flow of LOX from the center tank to the outer tanks. This change made it necessary to move the probes laterally in the tank.

As the tanks empty and the liquid level reaches the level of the probe, the liquid being transferred into the outer LOX tanks appears to be splashing off this baffle plate and thereby continually tripping the probe or giving an indication of a level change. This would give a series of signals on the same probe as was seen in the case of measurements A2-04 and A2-01 which gave a series of pulses at the same level for over ten seconds. This phenomena can be eliminated by the addition of a shield around the probe. All other liquid level probes appeared to function properly.

The appearance of no signal on probes A2-02, A3-02, A2-03, and A3-03, which would indicate that the LOX level never reached the probes, is validated by the fact that the LOX level at cutoff was higher than predicted (Ref. para 5.5.1). These cutoff signals are located about one inch below the discrete level probes.

Sloshing Measurements

The ΔP sloshing measurements use potentiometer type differential transducers - D4-F2 and D5-F2 having a range of ± 0.3 psid and D6-0C, D7-0C, D6-04, and D7-04 having a range ± 0.5 psid.

These measurements have a bias voltage of plus 2.5 vdc which represents zero psid. Positive pressure would range from 2.5 vdc to 5 vdc, negative pressure 2.5 vdc to zero vdc.

Measurements D4-F2 and D5-F2 had a correct bias voltage before ignition. Four seconds after ignition they were indicating maximum negative range as were all the other ΔP measurements at this time. The fuel sloshing measurements read correctly 15 seconds after ignition. Measurements D6-0C and D7-0C are reliable 51 seconds after ignition. Measurements D6-04 and D7-04 are usable 60 and 64 seconds respectively after ignition. The range on both of these measurements was exceeded 109 seconds after ignition, indicating more than ± 0.5 psid. Bias levels on all six ΔP sloshing measurements were correct after cutoff. Slosh cycling data is good.

In an effort to correct these ΔP sloshing measurements in future vehicles, this type of transducer will be replaced by an unbonded strain gage type differential pressure transducer. This transducer will give a better response, and full scale adjustment will be better attained as will equal volume on both sides of the diaphragm. Calibration valves will be eliminated and 1/4 inch tubing can be used, thereby eliminating the 1/8 inch tubing in the system. This type of transducer can be hard mounted; whereas the potentiometer type had to be shockmounted.

12.3 TELEMETRY SYSTEMS ANALYSIS

Telemetry System Description

In the SA-1 flight test, eight telemetry links were utilized to obtain in-flight information. These eight links were composed of two basic telemetry systems. Seven of the eight links were the XO-4, XO-4B type system, previously flight proven in the Jupiter program. One link was an XO-6B type system recently developed in-house at Astrionics Division for the Saturn program. This was the first flight test in which the XO-6B system has participated. A tabulation of the telemeter systems used on SA-1 is shown in Table 12-II.

Mechanical Commutation

Mechanical commutation was used for commutators A and B on link 2, and commutator A on links 4, 6, 7, and 8. Performance analysis of all mechanical commutation indicates satisfactory performance with no failures or deviations from normal operation.

Electronic Commutation

Electronic commutation was used for all time shared vibration measurements and also for all time shared flow rate measurements. Link 5, commutator A, was an electronic commutator, 30x10. Link 1 was a high capacity electronic commutation system.

Performance analysis of all electronic commutating devices indicates satisfactory performance. No failures or deviation from normal operation were noted.

Calibrations

All preflight calibration steps were supplied from preflight calibrator located in the TM auxiliary equipment assembly. Preflight calibration performance was normal and satisfactory.

Malfunction of an in-flight calibrator supplying link 3 occurred during prelaunch countdown at T-6 minutes and continued malfunction was in evidence during all in-flight calibrations. The malfunction of this calibrator was known to LOD during prelaunch countdown, but since valid preflight calibration was available, the failure was considered to be of little significance. The failure of a gate transistor in the calibrator is suspected to be the most probable cause of malfunction. In-flight calibration on all other links was satisfactory.

Because of electrical leakage problems, link 3 telemeter assembly was replaced by a link 3 spare telemeter assembly prior to launch. The electrical leakage was found between two terminals on a terminal board in the mixer amplifier, which is a plug-in module part of the telemeter assembly. A white residue was found between the two terminals and the residue constituted an electrical leakage path. White residue was in evidence at other points on the telemeter assembly. This residue was apparently due to moisture condensation as a result of canister cooling.

Dropouts

Transmitted power from all telemeter links was sufficient to produce good records to approximately +409.4 seconds. No signal fades or dropouts were in evidence simultaneously on all receiving

station records during flight periods to approximately +409.4 seconds. At about this time all signals ceased.

12.4 R. F. SYSTEMS ANALYSIS

Telemetry

The telemetry records received were good with the exception of Cape Telemetry No. 3 (Mercury Control Center). This record showed fluctuation due to ground antenna scanning.

In the Hangar D record, link 8 measured about 20 db lower than the remaining links. This was probably due to faulty calibration since it did not appear in any of the other records. In the calibration of links 6, 7, 8, and 1 there was a break which was smoothed before tabulating data. In the Hangar D record a drop in signal strength accompanied by noise showed up from about 50 to 60 seconds. There was no apparent correlation between the two groups of links (1, 3, 5, 7, and 2, 4, 6, 8) which are on the different sets of antennas. However, links 2, 3, 4, 5, and links 6, 7, 8, and 1 showed a similarity which would indicate recorder trouble. Again in the Hangar D record, the period from 68.2 to 72.6 seconds showed noise and a signal drop in links 2, 4, 6, and 8. From about 70 to 77 seconds links 1, 2, 5, and 7 exhibited a decrease in signal and some noise, most pronounced in links 1 and 7. In this case there was definite correlation between the links on the separate sets of antennas. Noise before and during the time of cutoff appeared in all eight links and is presumed to be due to flame attentuation.

The reduction in signal also apparent during this period begins at about 94 seconds. A noise fluctuation seems to be superimposed on the regular antenna pattern during the attenuation period. This fluctuation varies directly as the amount of drop in signal and continues until second cutoff, disappears for about 1.5 seconds, flares again for about 1.5 second, then disappears completely. After the attenuation period, the signal averages about 5.3 db lower than before. This drop is to be expected with the increase in range. At maximum attenuation the signal varies rapidly from 15 to 30 db below normalized signal strength. At first cutoff the signal from one group of links increased, while that from the other remained unchanged. At second cutoff the signal for all links increased to normal.

In the record from Cape Telemetry No. 2, the noise between 50 and 60 seconds as shown in the Hangar D record did not appear. However, links 2, 4, 6, and 8 showed a decrease in signal of approximately 15 db from about 60 to 67 seconds. This decrease was accompanied by noise and did not appear in the other links. Links 1, 3, 5, and 7 showed a brief drop in signal of about 15 db between 36 and 40 seconds. Again

this did not show up in the other links. None of the irregularities showed in the GBI records. Figure 12-1 shows the maximum and minimum signal strength recorded at Cape Telemetry No. 2 and GBI along with the predicted values.

UDOP

The UDOP system performed sufficiently well to allow a continuous solution for position data from liftoff to 408.9 seconds independent of other tracking system tie-in points. All of the Doppler data exhibited slight intermittent jitter for a period of approximately 10 seconds near cutoff. Data from one down range receiver was characterized by excessive jitter throughout flight. The signal strength from Site C was about 5 db below predicted and showed considerable fluctuation.

Azusa

Azusa tracking was good from launch to 398.5 seconds except for a short dropout from 381.35 to 390.25 seconds and was used as the major data source in establishing the vehicle trajectory (see para 4.2.2).

Radar

Good track was obtained by radar from launch to 412 seconds. The C-Band radar signal strength from the Cape station 1.16 was good and followed the expected trend. There was a low of about 10 db between about 60 and 100 seconds. The GBI 3.16 (XN-2) record was good but dropped considerably after 300 seconds. Both these stations tracked beacon all the way.

12.5 PHOTOGRAPHIC COVERAGE

Fixed tracking cameras obtained good data from launch to approximately 20 seconds. Theodolite coverage was good from launch to 105.5 seconds.

Engineering Sequential Optics had only two failures out of the 65 cameras operated. All but 3 of the 50 Range User Optics obtained valid data.

TABLE 12-I

Measurement Malfunctions

Item No.	Meas. No.	Measurement	Remarks
Unusable			
1	A2-0C	Liquid Level, Discrete A	No Signal
2	A2-F2	Liquid Level, Discrete A	No Signal
3	A8-6	Flowrate Main LOX, DC	Zero Output, AC Flowrate Performed OK
4	C3-6	H.S. Pinion Brg. #5	Zero Output
5	C7-4	Temp. Turbine Exhaust	Abnormal Response and Noisy Signal
6	C53-03	Temp. LOX Tank	100 Percent + Output
7	C67-7	Temp. Radiation Shield	Zero Output After Ignition
8	E39-2	Vib. Yaw Actuator, Long't	No Response
Partially Usable			
9	C6-5	Temp. Turbine Shaft Brg.#8	Noisy Output, Mean of Noise Appears Valid
10	C37-0C	Temp. Gas Top LOX Tank	Intermittent Output From 18 to 93 sec
11	D4-F2	ΔP Fuel Sloshing, Pitch	Not Usable Until 15 sec
12	D5-F2	ΔP Fuel Sloshing, Yaw	Not Usable Until 15 sec
13	D6-0C	ΔP LOX Sloshing, Pitch	Not Usable Until 51 sec
14	D7-0C	ΔP LOX Sloshing, Yaw	Not Usable Until 51 sec
15	D6-04	ΔP LOX Sloshing, Pitch	Not Usable Until 60 sec
16	D7-04	ΔP LOX Sloshing, Yaw	Not Usable Until 64 sec
17	E33-1	Vib. Thrust Ch. Dome, Long't	Noisy After 45 sec
18	E33-3	Vib. Thrust Ch. Dome, Long't	Noisy After 25 sec
19	E33-7	Vib. Thrust Ch. Dome, Long't	Noisy After 29 sec

TABLE 12-II

SA-1 TELEMETRY SYSTEM

Telemeter Link No.	Freq. In Megacycles	System Type	Channel Capacity		REMARKS
			Straight	Commutated	
1	242.0	XO-6B	0	216	
2	246.3	XO-4	15	29	Commutator D, a vibration commutator located in the FM Auxiliary equipment assembly was connected to Channel 16.
3	248.6	XO-4B	13	60	Commutator C, a flowrate commutator was connected to Channel 13.
4	249.9	XO-4	14	37	Commutator D, a vibration commutator located in the TM auxiliary equipment assembly was connected to Channel 16. Commutator C, a flowrate commutator was connected to Channel 13.
5	252.4	XO-4	14	37	Commutator D, a vibration commutator located in the TM auxiliary equipment assembly was connected to Channel 16. Commutator C, a flowrate commutator was connected to Channel 13. Commutator A on this link was an electronic commutator.
6	253.8	XO-4	15	29	Commutator D, a vibration commutator located in the FM auxiliary equipment assembly was connected to Channel 16.
7	256.2	XO-4	15	29	Commutator D, a vibration commutator located in the FM auxiliary equipment assembly was connected to Channel 16.
8	259.7	XO-4	15	29	Commutator D, a vibration equipment located in the FM auxiliary equipment assembly was connected to Channel 16.
					Total Straight Channels = 101 Total Commutated Channels = 466

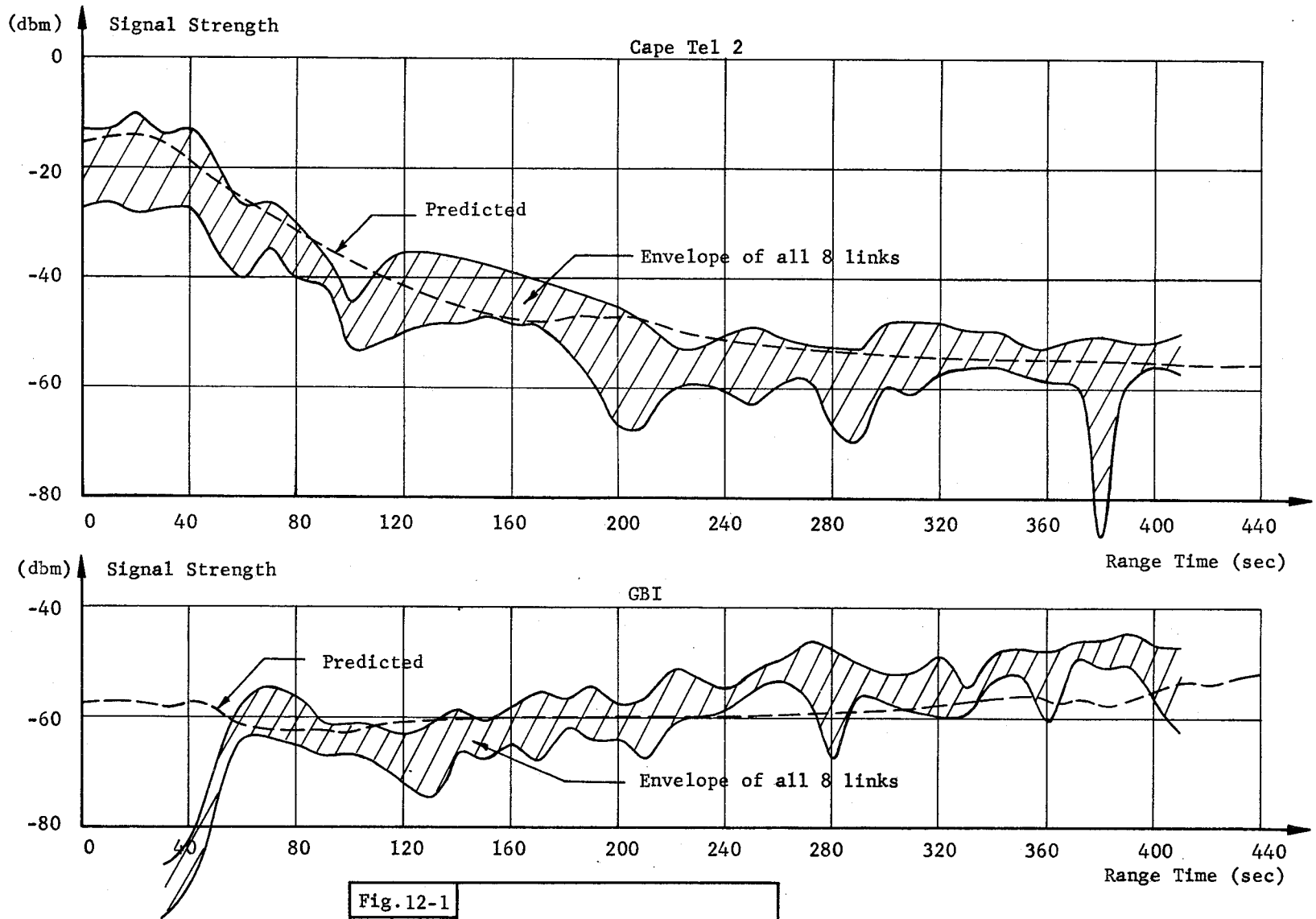

Fig. 12-1	CAPE TEL 2 AND GBI TELEMETRY SIGNAL STRENGTH
SA-1	

13.0 (C) SUMMARY OF MALFUNCTIONS AND DEVIATIONS

The flight test of SA-1 did not reveal any malfunctions or deviations which could be considered a serious system failure or design deficiency. However, a number of minor malfunctions and deviations did occur and are summarized here primarily for documentary purposes.

Corrective measures were recommended by the Divisions for some of the items listed. They are marked with an asterisk. In each case, reference is made to that section of the report where the occurrence is explained in detail. Malfunctions and deviations are each grouped approximately in the sequence of their relative importance.

Malfunctions

1. A sloshing instability became apparent after 90 seconds of flight (para. 6.1)*.

2. The fuel level manometer transformer burned out (para. 3.2.1)*.

3. The LOX vaporizer blower for the main tank pressurizing system cut off (para 3.2.1)*.

4. The LOX replenish vaporizer blower cut off (para. 3.2.1)*.

5. The main tank vaporizer heat exchanger developed three LOX leaks (para. 3.2.1)*.

6. A small amount of fuel overflowed from the air removal valve during adjust level drain (para. 3.2.1).

7. Fuel mast vacuum breaker leaked during leak check (para 3.2.1).

8. The in-flight calibrator for link 3 failed and was inoperative during flight (para. 12.3).

9. Erroneous level indication occurred in two outer LOX tanks (para. 12.2)*.

10. Sloshing measurements (ΔP) were out of range and therefore not valid during the first part of flight (para. 12.2)*.

11. Eight telemetry measurements failed to yield reliable data any time during flight (para. 12.2).

12. Eleven telemetry measurements were invalid during portions of flight (para. 12.2).

13. Two blockhouse sequence indications failed. (para. 3.2.2)

Deviations

1. Inboard engine cutoff occurred 1.61 seconds earlier than predicted (para. 5.5).

2. A deviation of approximately 0.4% was observed in the fuel density sensing of the tanking system (para. 3.2.1)*.

3. Hydraulic source pressure measurement indicated 500 psi lower than expected. Other information shows this measurement to be in error (para. 5.2).

4. A 22 to 25 cps oscillation of unexplained origin appeared in canister 15. (para. 7.3.2)

5. The fuel tanks filled unevenly (para. 3.2.1).

6. LOX tank pressure was 3 to 4 psi higher than predicted (para. 5.4.2).

7. Cutoff impulse for engine No. 5 was higher than expected (Table 5-II).

8. Engine No. 5 thrust was high by 3.9% (para. 5.2).

9. Low pressure to air bearing was one psi below the lower limit (para. 5.4.3).

10. Cycling of the pressure "OK" switches was observed on three hydraulic systems during engine transition (para. 3.2.3).

11. A sudden, unexplained temperature rise occurred in the area of the structure behind the flame shield at approximately 87-95 seconds (para. 10.2.2).

12. One of the strain measurements yielded high levels causing magnitude of some load information to be questionable (para. 9.2.2).

13. The ΔP ratio measurement from P.U. Computer saturated measuring range at approximately 93 seconds (para. 5.5.1)*.

14. Attitude motion after cutoff indicates the presence of a small unexplained moment (para. 6.2.4).

(U) APPROVAL

SATURN SA-1 FLIGHT EVALUATION

Fridtjof A. Speer
Chairman, Saturn Flight Evaluation Working Group

Oswald H. Lange
Director, Saturn Systems Office

Wernher von Braun
Director, Marshall Space Flight Center

SA-1 FLIGHT EVALUATION REPORT

(U) DISTRIBUTION

M-DIR
M-DEP-R&D
M-DEP-ADM

M-AERO
M-AERO-DIR
M-AERO-PS, O.C. Jean (3)
M-AERO-A (2)
M-AERO-G (3)
M-AERO-D
M-AERO-E
M-AERO-F (16)
M-AERO-P

M-L&M
M-L&M-DIR (2)

M-COMP
M-COMP-DIR
M-COMP-A
M-COMP-R
M-COMP-S

M-ME
M-ME-DIR
M-ME-TS (4)

M-FPO
M-FPO-DIR (2)
M-FPO, Mr. Weaver

M-ASTR
M-ASTR-DIR
M-ASTR-TSJ (4)
M-ASTR-A
M-ASTR-R
M-ASTR-E
M-ASTR-M
M-ASTR-F
M-ASTR-G
M-ASTR-I
M-ASTR-I, Mr. Bell
M-ASTR-N
M-ASTR-NT

M-LOD
M-LOD-DIR
M-LOD-TS (4)
M-LOD-G
M-LOD-E
M-LOD-EP, Mr. Collins
M-LOD-D
M-LOD-GE
M-LOD-P
M-LOD-M

M-REL (3)

M-QUAL
M-QUAL-DIR
M-QUAL-TS, Mr. Klauss
M-QUAL-E
M-QUAL-M
M-QUAL-P
M-QUAL-PS, Mr. Peck
M-QUAL-Q

M-RP
M-RP-DIR
M-RP-R
M-RP-N
M-RP-P
M-RP-T
M-RP-I

M-SAT
M-SAT-DIR
M-SAT (6)

M-P&VE
M-P&VE-DIR, Mr. Mrazek
Mr. Weidner
M-P&VE-TSC
M-P&VE-TSM
M-P&VE-TSR

M-P&VE-TSS
M-P&VE-TSV
M-P&VE-PP (2)
M-P&VE-E (3)
M-P&VE-ES
M-P&VE-F
M-P&VE-M
M-P&VE-ME
M-P&VE-NP
M-P&VE-P (2)
M-P&VE-EA, Mr. Hurber
M-P&VE-PL
M-P&VE-PM
M-P&VE-PT
M-P&VE-PV (3)
M-P&VE-S
M-P&VE-SD
M-P&VE-SS

M-TPC

M-TEST
M-TEST-DIR
M-TEST-E
M-TEST-M
M-TEST-MC, Mr. Thornton
M-TEST-T

M-MS
M-MS-IPL (8)
M-MS-IP

M-PAT

M-H

DISTRIBUTION (cont')

EXTERNAL

Headquarters, National Aeronautics & Space Administration
Washington 25, D.C.
- Administrator, Attn: Div Research Information (5)
- Director, Technical Information Division
- Secretary, Civilian-Military Liaison Committee
- Mr. Franklyn W. Phillips, Nation Aeronautics & Space Council
- Director of Space Flight Development
- Asst. Director for Space Sciences
- Asst. Director for Advanced Technology
- Asst. Director for Propulsion
- Asst. Director for Space Flight Operations
- Asst. Director for Applications & Manned Space Programs
- Asst. Director for Vehicles
- Asst. Director for Launch Operations
- Director for Aeronautical & Space Research
- Mr. Morton J. Stoller

Goddard Space Flight Center
4555 Overlook Avenue
Washington 25, D.C.
Attn: Mr. Herman LaGow

Director, Ames Research Center
National Aeronautics & Space Administration
Moffett Field, California

Director, Manned Space Flight Center
Houston, Texas

Director, Langley Research Center
National Aeronautics & Space Administration
Langley Field, Virginia

Director, Lewis Research Center
National Aeronautics & Space Administration
21000 Brookpark Road
Cleveland 35, Ohio

Director, Western Operations Office
National Aeronautics & Space Administration
150 Pico Blvd., Santa Monica, California

Director, High Speed Flight Station
National Aeronautics & Space Administration
Edwards, California

Engineer in Charge, Wallops Station
National Aeronautics & Space Administration
Wallops Island, Virginia

Officer-in-Charge, Jet Propulsion Lab
4800 Oak Grove Drive
Pasadena 2, California
Attn: Mr. Irl Newlan, Reports Group

Jet Propulsion Laboratories, CCMTA
Attn: Mr. H. Levy (4)

Office of the Asst. Sec. of Defense For Research & Engineering
Room 3E1065
The Pentagon
Washington 25, D.C.
Attn: Tech Library

Director of Guided Missiles
Office of the Secretary of Defense
Room 3E131
The Pentagon
Washington 25, D.C.

Commander, Armed Services Tech Info Agency (5)
Arlington Hall Station
Arlington 12, Va.
Attn: TIPCR (Transmittal per cognizant Act. Security Instruction)

U.S. Atomic Energy Commission, Sandia Corp.
University of California Radiation Lab
Tech Info Div
P.O. Box 808
Livermore, California
Attn: Clovis Craig

U.S. Atomic Energy Commission, Sandia Corp.
Livermore Br, P.O. Box 969
Livermore, California
Attn: James McMinn, Document Control Sec.

Central Intelligence Agency (2)
2430 E Street, N. W
Washington 25, D.C.
Attn: Liaison Div, OCD

Director, National Security Agency
Washington 25, D.C.
Attn: CREF-22

Commanding General (3)
White Sands Proving Ground
New Mexico
Attn: ORDBS-OMTIO-TL

Commander, AF Missile Test Center (3)
Patrick AFB, Florida
Attn: Tech Info & Intelligence Office, MTGRY

Chief of Staff, U.S. Air Force (2)
The Pentagon
Washington 25, D.C.
1 Cpy marked for DCS/D AFDRD
1 Cpy marked for DCS/D AFDRD-EX

Commander (5)
Wright Air Development Center
Wright-Patterson Air Force Base, Ohio
Attn: WCOSI-3

Commander
Air Force Flight Test Center
Edwards AFB, California
Attn: FTOTL

Commander
Air Force Ballistic Missile Div
Hdqrs, ARDC, Air Force Unit Post Office
Los Angeles 45, California
Attn: WDSOT

Commander-in-Chief
Strategic Air Command
Offutt AFB, Nebraska
Attn: Dir of Opns, Missile Division

Commander
Air Force Missile Development Center
Holloman Air Force Base
New Mexico
Attn: Tech Library (SRLT)

Commander
U.S. Naval Air Missile Test Center
Point Mugu, California

Chief, Bureau of Weapons (4)
Dept. of Navy
Washington 25, D.C.
1 Cpy to RESI, 1 Cpy to SP, 1 Cpy to AD3
1 Cpy to REW3

Chief of Naval Research
Department of Navy
Washington 25, D.C.
Code 463

Director (2)
U.S. Naval Research Lab
Washington 25, D.C.
Attn: Code 2027

Douglas Aircraft
Attn: Mr. German (6)

CCMD, Huntsville Industrial Center
Attn: Frank Stewart

ORDAB-HT Technical Library, ABMA (5)
ORDAB-C Control Office, ABMA

Aerospace Corporation
2400 East El Segundo
El Segundo, California
Attn: D.C. Bakeman

APPENDIX A

(C) SYSTEM DESCRIPTION

A.1.0 LAUNCH CHARACTERISTICS

Saturn vehicle SA-1 was launched October 27, 1961, at 1006:3.89 EST from Launch Complex 34, Cape Canaveral, Florida, with a firing azimuth of 100 degrees east of North.

The geographical coordinates of Complex 34 are:

Geodetic Latitude	28.521529 degrees
Longitude	80.561357 degrees

A.2.0 SA-1 VEHICLE DESCRIPTION

Saturn SA-1, the first of the C-1 series of Saturn launch vehicles, represents the first United States launch vehicle in the 1.5 million pound thrust class to be flight tested. With a total length of approximately 163 feet and measuring more than 21 feet in diameter at the base, SA-1 was powered by eight Rocketdyne H-1 liquid propellant rocket engines developing a total sea level thrust of more than 1.3 million pounds. The total vehicle weight was approximately 930,000 lbs at liftoff with approximately 608,000 lbs of propellant consumed during the S-I powered phase of flight.

The vehicle consisted of a live S-I stage, a dummy S-IV stage, a dummy S-V stage, and a dummy payload. A diagram of the overall Saturn configuration including some of the more important vehicle dimensions is presented in Figure A-1. SA-1 mass characteristics are presented in Appendix D.

A.2.1 S-I STAGE

The S-I stage was the only active stage of the SA-1 Saturn vehicle. Propulsion was provided by a unique arrangement of eight clustered H-1 rocket engines. Propellants were supplied to the engines from a cluster of nine propellant tanks. Most of the SA-1 instrumentation, including guidance and control components, were located in the S-I stage.

Propulsion

The S-I or booster stage of the SA-1 vehicle was powered by eight clustered H-1 liquid propellant engines. Engines 1 through 4 are designated outboard while engines 5 through 8 are designated inboard. The four inboard engines are fixed mounted on a 64 inch diameter with

a 3° cant angle. The four outboard engines are gimbal mounted to provide pitch, yaw, and roll control with a null position cant angle of 6°. The outboard engines have a maximum gimbal angle of 7° in the pitch and yaw planes.

The H-1 engine is a fixed thrust, single start type, bi-propellant rocket engine. It is a derivative of the Thor-Jupiter-Atlas family of rocket engines manufactured by Rocketdyne Division of North American Aviation. The SA-1 version of the engine produces a nominal 165,000 pounds of thrust and has a nominal sea level specific impulse of 252.7 lb sec/lb.

Liquid oxygen (LOX) and RP-1 fuel are the propellants used as the main power source. A hypergolic fuel mixture is used for combustion chamber ignition, and a solid propellant charge provides initial gas to spin the turbine.

Major components of the H-1 engine are a thrust chamber assembly, turbopump assembly, gas generator assembly, hydraulic system (outboard engines only), and a hypergolic ignition system. The H-1 engine has no thrust or chamber pressure control.

The exhaust gases from the turbine are handled differently in the outboard and inboard engines. In the case of the outboard engines the exhaust is routed rearward through the heat exchanger and into an aspirator. The aspirator is welded around the periphery of the expansion nozzle exit to form an integral part of the thrust chamber. Use of the aspirator on the gimballed engines allows removal of the hot gases from the engine compartment without the need for flexible joints in the turbine exhaust ducts. The exhaust gas from the inboard engine turbine is routed laterally from the heat exchanger through the outer vehicle skin, then ejected rearward.

Propellants were supplied to the engines by use of suction lines from an arrangement of nine propellant tanks. These tanks consist of four 70" LOX tanks, four 70" fuel tanks, and one 105" LOX tank. The 70" fuel and LOX tanks are mounted alternately around the circumference of the center LOX tank. Each outboard tank (LOX and fuel) supplies propellant to one inboard and one outboard engine. The center LOX tank is used to supply the outboard tanks through the LOX interchange system and does not supply LOX directly to any engine.

LOX tank pressurization is provided by gaseous oxygen (GOX). The GOX is obtained by passing LOX through a heat exchanger (one for each engine). Pressurization of the fuel tanks is provided by gaseous nitrogen (GN_2) supplied from 48 storage spheres located atop the propellant tanks.

Eight outriggers and a spider beam assembly support the outer propellant tanks. The LOX tanks form the basic structure with the fuel tanks mounted to allow for thermal contraction of the S-I stage structural elements. All four fuel tanks are interconnected at the base through the fuel interchange system. Baffles used to prevent propellant sloshing in the tanks may be seen on page

A propellant utilization (PU) system was flown as a passenger on this flight to obtain flight data for performance evaluation of the system. The system utilized two (one for LOX and one for fuel) differential pressure transducers for propellant weight information. Signals from the transducers were sent to a computer for mass ratio determinations.

Guidance and Control

Active inertial guidance was not incorporated in SA-1. However, in anticipation of future guided flights, partially active guidance components were carried as passengers only. Several components (i.e., ST-90 stabilized platform, program device, angle of attack transducers, etc.,) from the Jupiter Missile Program were utilized with relatively minor modifications for control and sequencing.

The ST-90 stabilized platform was used to provide the attitude reference signals for control of the four gimbal engines. Angular rate information for vehicle damping was obtained by electrical differentiation of the attitude signal in the Flight Control Computer. First and second bending mode influences on the control system were suppressed by phase shaping and/or attenuation of those frequencies in the computer. Angle of attack information* is derived from four local type transducers (see Fig. A-4 for location) and fed into the Flight Control Computer. The computer filters, amplifies and/or attenuates, shapes, sums these signals, and issues commands to the eight hydraulic actuators for proper positioning of the control engines. This gives vehicle control in pitch, yaw, and roll.

Structure

The booster structure consists basically of a thrust frame on which the eight engines are mounted, five LOX containers (designed as load carrying members), four fuel containers (flexible mounted to allow for shrinkage), and at the top of the containers a transitional structure extending to the base of the second stage.

* For artificial stabilization

Heat and Flame Protection

(1) Firewall

Location: Lower end of thrust frame (see Figure A-5)

Function: Prevents fires originating in engine compartment from spreading into propellant tank area

(2) Heat Shield

Location: Station 54, (46" from engine gimbal point) covers entire area within shrouds (see Figure A-5)

Function: Provides (1) lateral support for shrouding and (2) protection to all equipment forward of Station 54 (structures, engines, etc.,) from flames and heat flux of engines.

(3) Flame Shield (Star or Base Plate)

Location: Exit of inner engine nozzles (see Figure A-5)

Function: Provides heat and flame protection for engine compartment principally by recirculating hot exhaust gases in base region.

Instrumentation

SA-1 carried a telemetry system composed of eight separate R-F links. The telemetry units and antenna's were located in the Adapter Section at the top of the S-I stage. The instrumentation program for the S-I stage was as follows:

Type Measurement	Total Number
Propulsion	84
Temperature	158
Pressure	115
Strain and Vibration	69
Flight Mechanics	13
Steering Control	21
Stabilized Platform	5
Guidance	3
Signals	15
Volt, Current and Frequency	17
Total Measurements (S-I)	500

A.2.2 S-IV DUMMY STAGE (FIGURE A-2)

The S-IV dummy second stage for Saturn SA-1 carried water ballast (89,525 lb) to simulate the weight and aerodynamic characteristics of the live S-IV stage. Dimensions of the S-IV stage are given in Figures A-1 and A-2.

A.2.3 S-V DUMMY STAGE (FIGURE A-3)

The S-V dummy third stage was basically a Centaur cruiser tank modified by increased skin gages. The tank carried water ballast (102,000 lb) to simulate upper stage weight. Dimensions of the S-V stage are given in Figures A-1 and A-3. The only in-flight measurement on this stage was the pressure of the S-V dummy ballast.

A.2.4 DUMMY PAYLOAD (FIGURE A-4)

SA-1 carried a Jupiter type nose cone and aft unit as dummy payload. An adapter section was required to mate the aft unit to the S-V stage. Four local angle of attack meters and two bending accelerometers were mounted on the aft unit as instrumentation. Three ΔP nose cap measurements were also located on the dummy payload.

A.3.0 GROUND SUPPORT EQUIPMENT (FIGURE A-6)

A.3.1 SHORT CABLE MAST ASSEMBLY

Number : 2

Location: Fin II and Fin IV

Function: Provides (1) means of routing electrical cables and pneumatic lines from launcher to vehicle, (2) quick disconnect of these cables and lines 0.3 seconds before liftoff, and (3) successful release to initiate support arm retraction.

A.3.2 LONG CABLE MAST ASSEMBLY

Number : 1

Location: 30° from Fin II toward Fin I

Function: Provides (1) means for mounting equipment; routing and connecting electrical cables, pneumatic lines, LN_2 line, and two air conditioning ducts to the vehicle booster instrument compartment; and (2) rapid disconnect prior to liftoff.

Operation: Automatically retracted prior to liftoff.

A.3.3 SUPPORT ARMS

Number : 4

Location: 45° off fin lines

Function: Support the vehicle on the launch table. After thrust buildup is complete, support is no longer needed; therefore, on release of the short masts, the support arms begin to retract. During the retraction period, combustion instability and low thrust are monitored continuously. Any malfunctioning engine is cut off immediately. A malfunction stops the sequence and initiates support arm return. The remaining engines are cut off when the supports have returned. Successful retraction of the support arms initiates launch commit and vehicle holddown arm release.

A.3.4 HOLDDOWN ARMS

Number : 4

Location: On fin lines

Function: Secure vehicle to launch table during the holddown period. Release vehicle after monitoring systems show "go" position and launch commit is given.

A.3.5 FUEL AND LOX FILLING MAST ASSEMBLIES

Position: Fuel fill 30° from Fin I toward Fin II: LOX fill 30° from Fin III toward Fin II.

Function: Supply the final links in the fuel and LOX filling systems to the vehicle storage tanks.

A.3.6 BOATTAIL CONDITIONING SYSTEM

The purpose of the boattail conditioning system is to provide a controlled atmosphere in the vehicle boattail area during various periods while the vehicle is on the launch pad. A controlled atmosphere is necessary for personnel safety and vehicle protection. The function of the system is threefold:

(1) Air Purge - with LOX tanks empty, supply oil-free air at 10° - 21° C at rate of 1900 SCFM for personnel. With LOX tanks full, air temperature is at 21° C.

(2) Gaseous Nitrogen Normal Purge - At T-5 sec gaseous nitrogen is supplied at 1800 SCFM.

(3) Gaseous Nitrogen Deluge Purge - Used for vehicle malfunction requiring shutdown. Rate of supply is 5400 SCFM at -46° C.

A.3.7 HIGH PRESSURE BATTERY

Function: Source of all GN_2 and H_e used for checkout, servicing, and launching.

A.3.8 LOX REPLENISHING SYSTEM

Function: Provides LOX topping for booster tanking system.

A.3.9 LIFTOFF SWITCH INSTALLATION

Number : 4

Location: Mounted on forward portion of each holddown arm

Function: Provides means of completing electrical circuit to recorder located in blockhouse for recording time of vehicle liftoff from launch pedestal.

A.3.10 WATER QUENCH SYSTEM

Function: (1) Conveys water to tail section spray nozzle system for combating fires in boattail section.

(2) Supplies conditioned air to tail section spray nozzle system.

A.4.0 GROUND INSTRUMENTATION

Three ground instrumentation systems were utilized during the flight. These were telemetry receivers, optical systems, and tracking systems.

A.4.1 TELEMETRY RECEIVERS

Telemetry stations used to record signals received from the onboard telemetry transmitters were as follows:

NASA Stations

Hangar D
Blockhouse 34

RCA Stations

Station Location	Station Number
Cape	Tel 2
Cape	Tel 3
GBI	3.0

Each receiver station contains a minimum of one receiver, one panadapter, and two 7-channel recorders.

A.4.2 OPTICAL SYSTEMS

Documentary Cameras

A documentary history of significant events and vehicle activities was recorded on film. These cameras were located in appropriate positions to record the desired activities.

Engineering Sequential Cameras

Fixed and tracking engineering sequential cameras were used to monitor significant vehicle events and to provide information for vehicle performance evaluation. Wide camera coverage was obtained on the launch table. Four cameras were used to view the four retractable support arms; four cameras viewed the two short cable masts, and five cameras, located on the torus ring, covered ignition of the eight engines. Other cameras were used to view the complete vehicle, launcher, and a portion of the pad area during ignition and liftoff, and to record vehicle motion, structural integrity, and flame effects. In addition to the fixed and tracking cameras, long focal length tracking telescopes were used as follows:

Type	Locations
Recording Optical Tracking Instrument (ROTI)	Melbourne Beach and Vero Beach
Intercept Ground Optical Recorders (IGOR)	False Cape, Williams Point, Cocoa Beach, and Patrick AFB
Metric Cameras	False Cape, East Cape, West Cape, South Cape, Cocoa Beach, PAFB

A.4.3 TRACKING

The following tracking systems were used for the SA-1 test flight:

a. UDOP
b. Azusa
c. S-Band Radar
d. C-Band Radar

All SA-1 tracking beacons were located in Instrument Canister No. 14. The antennas for this equipment were located in the vehicle skin as follows:

a. UDOP (2) Station 919	7° off Fin II toward Fin I 7° off Fin IV toward Fin III
b. Azusa (1) Station 911.3	29° 30' off Fin IV toward Fin I
c. S-Band Radar (2) Station 911.3	20° 40' off Fin IV toward Fin I 25° 5' off Fin IV toward Fin I
d. C-Band Radar (1) Station 911.3	33° 45' off Fin IV toward Fin I

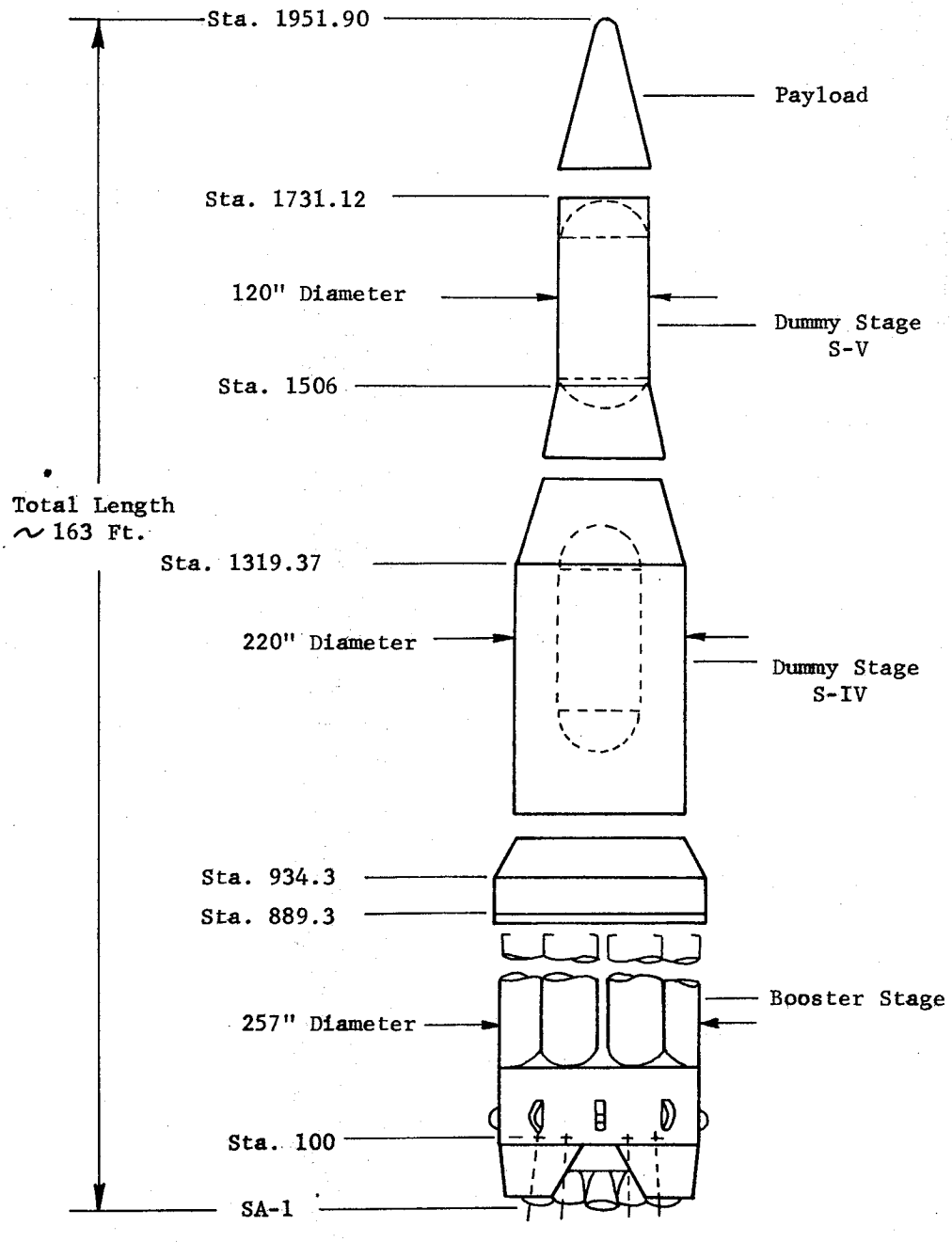

Fig. A-1	SATURN CONFIGURATION
SA-1	

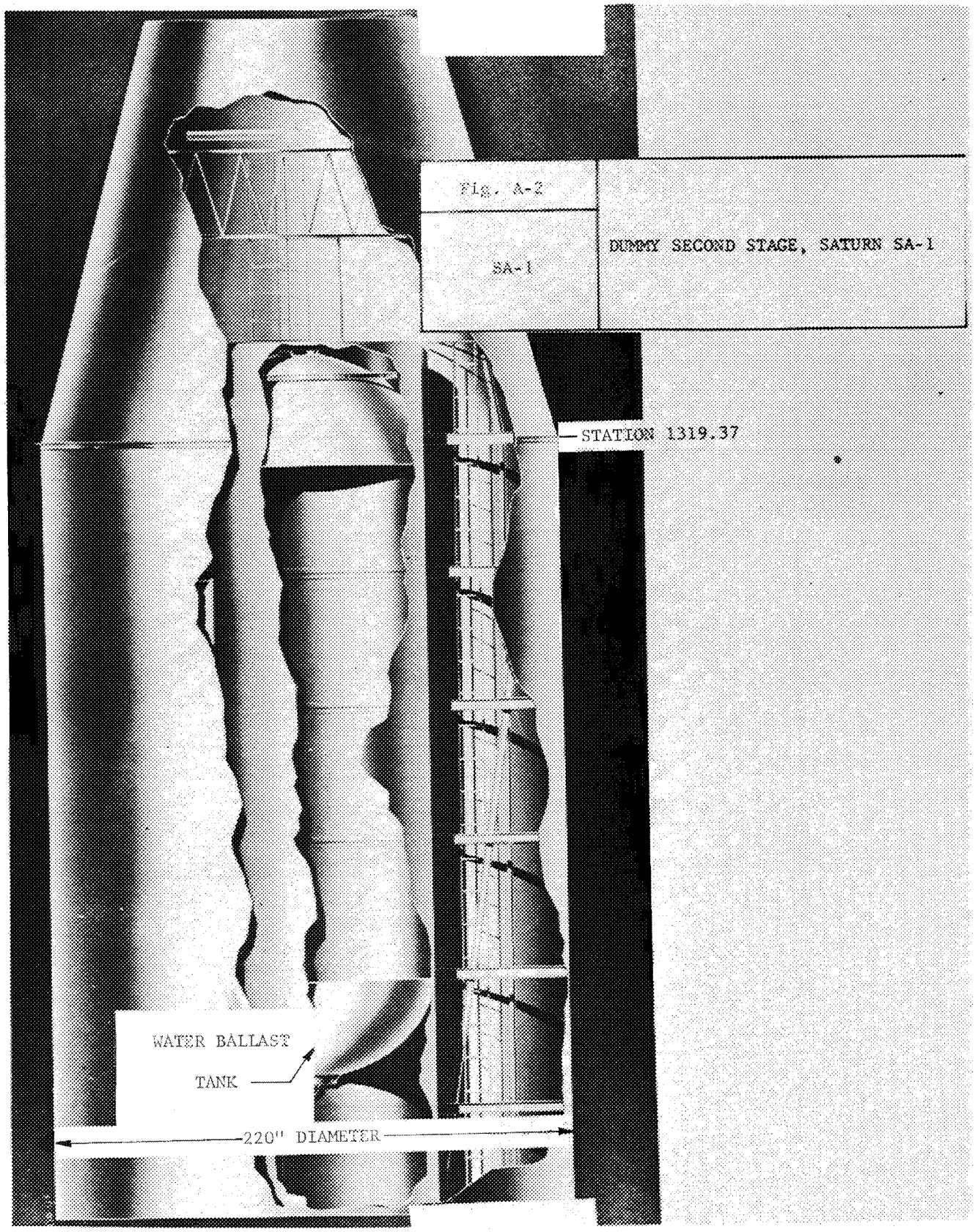
Fig. A-2
SA-1
DUMMY SECOND STAGE, SATURN SA-1
STATION 1319.37
WATER BALLAST
TANK
220" DIAMETER

Fig. A-3	DUMMY THIRD STAGE, SATURN SA-1
SA-1	

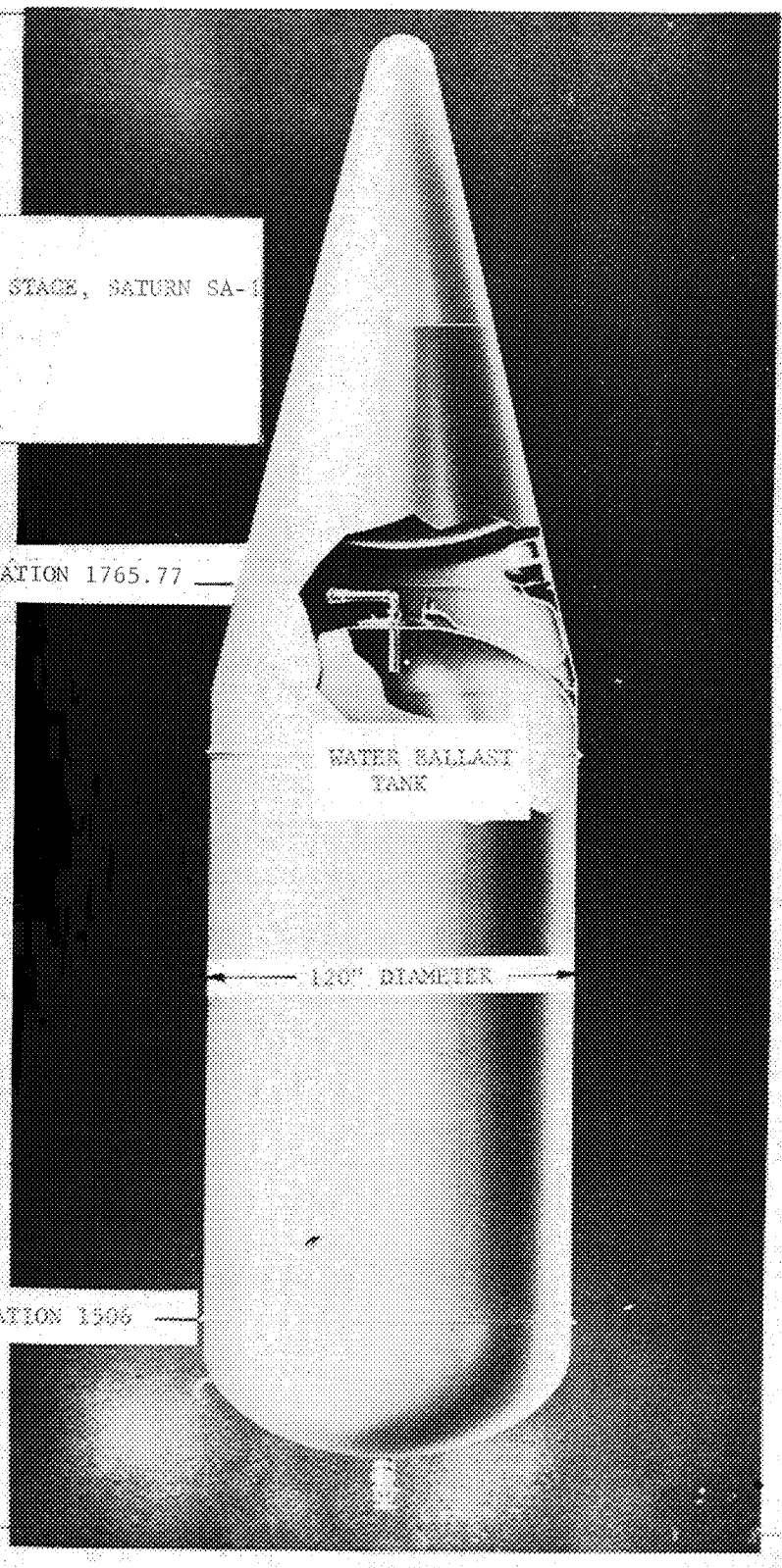

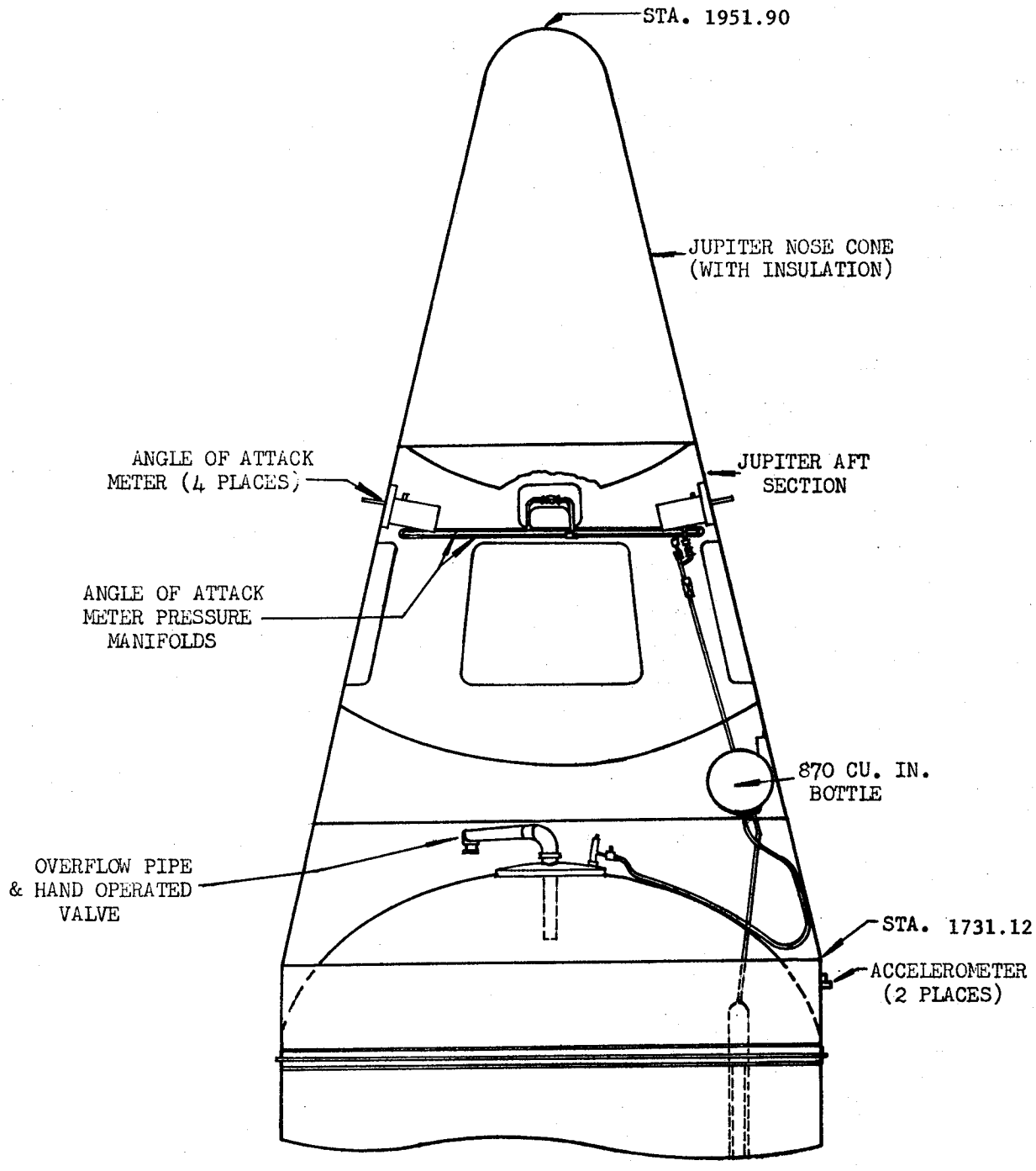

Fig. A-4	
SA-1	PAYLOAD

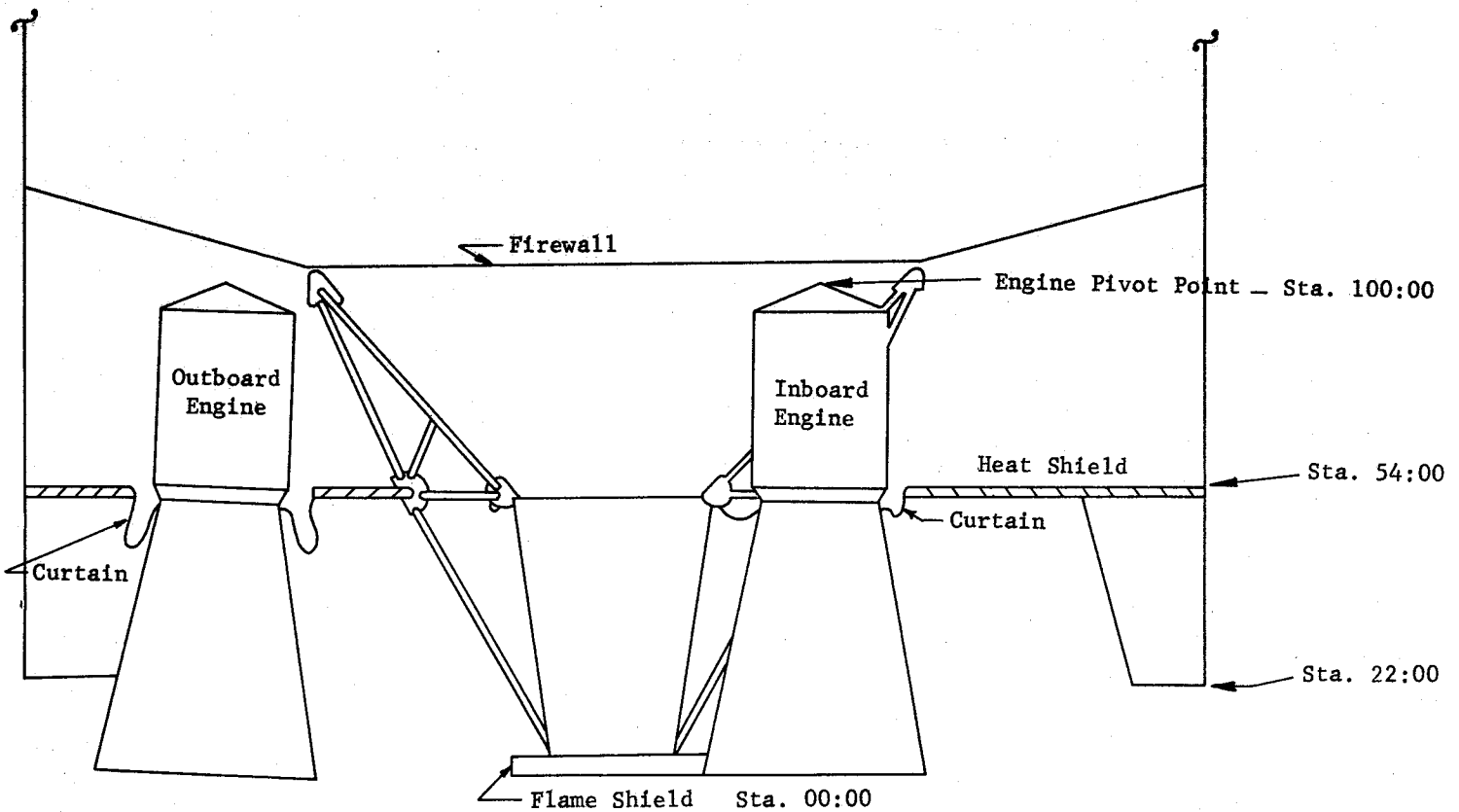

Fig. A-5	ENGINE COMPARTMENT LAYOUT
SA-1	

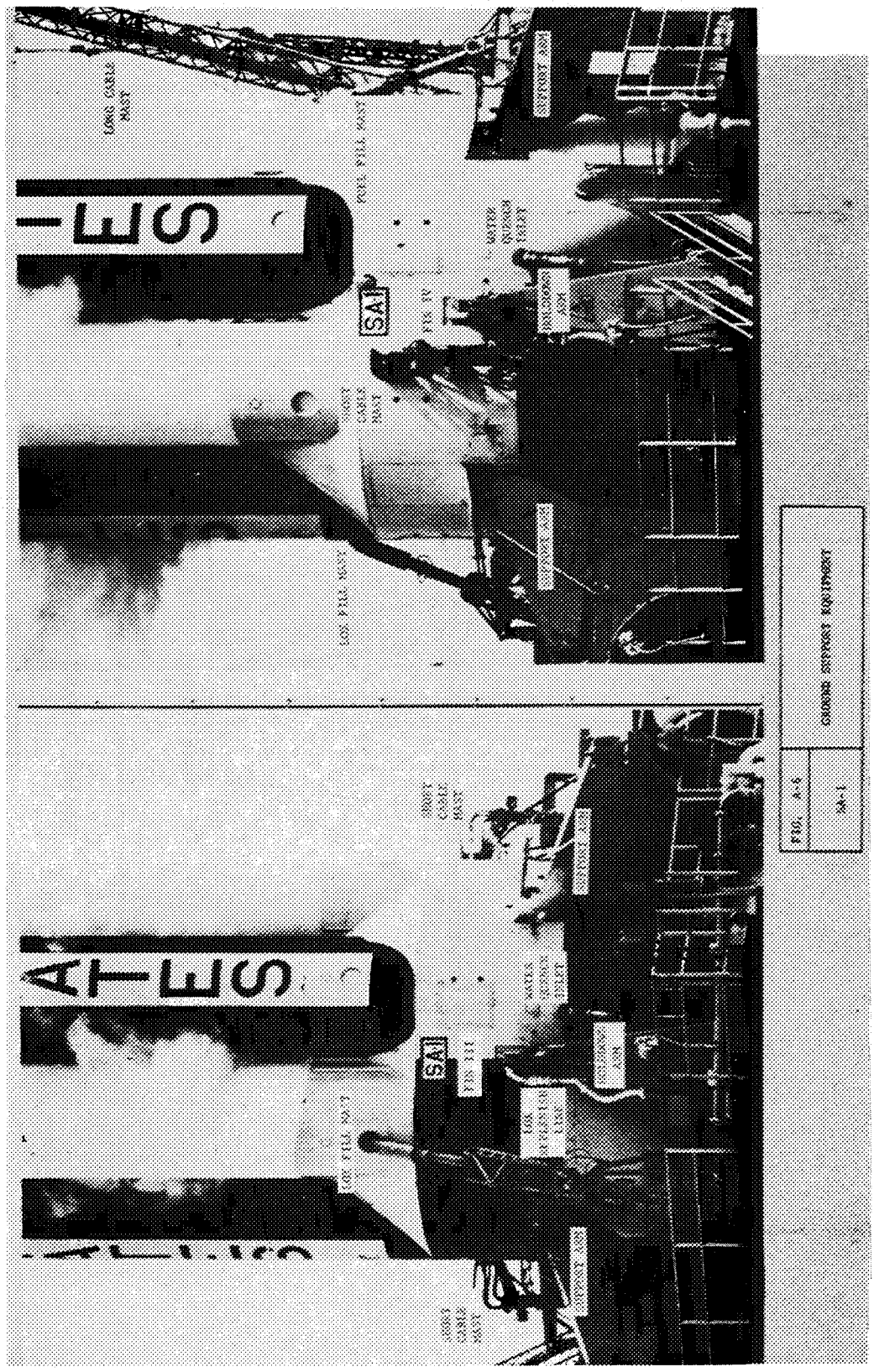

TABLE B-I

(C) APPENDIX B. REDLINE VALUES

Meas. No.	Parameter	Redline Values		Actual Values	
		Min.	Max.	Min.	Max.
XC1-(1 thru 8)	Temp LOX Pump Bearing No. 1 (°F)	0	N/A	108.1	-
XC54-(1 thru 8)	Temp LOX Pump Inlet (°F) (at Ignition Command)	-290	-280	-287.3	-281.9
XC59-(1 thru 4)	Temp Hydraulic Oil (°F) (at Liftoff)	N/A	210	-	103.1
XC89-(1 thru 8)	Temp Gear Case Lubricant (°F)	105	145	107.8	125.4
XC113-(1 thru 8)	Temp Turbine Spinner Case (°F)	40	75	54.9	61.7
XD2-F3	Press Gas in Fuel Tank (psig)	N/A	23	N/A	16.7
XD2-OC	Press Gas in LOX Tank (psig)	N/A	50	N/A	44.2
XD24-11	Press Gas in H.P. Spheres (psig) (at Liftoff)	2600	3200	3010	3010
XD39-11	Press Air Bearing Supply (psig)	2600	3200	3098	3110
XD40-9	Press Control Equipt, Supply (psig)	2600	3200	2920	3005
XD56-30	Press S-V Dummy Ballast (psig)	N/A	23	N/A	19.8
XG8-(1 thru 4)	Level Hydraulic Oil (% reservoir) (at Liftoff)	18	68	31.3	46

N/A - Not applicable

TABLE C-I

APPENDIX C

(C) GROUND SEQUENCE EVENTS

Event	Predicted Time Nominal (sec)	Actual Time* (sec)
Firing Command	-364	-361.34
Fuel Vent No. 1 Closed	-362	-360.80
Fuel Vent No. 2 Closed	-362	-360.84
Fuel Pressurizing Command	-362	-360.80
Fuel Pressurizing Valve No. 1 Open	-362	-360.75
Fuel Pressurizing Valve No. 2 Open	-362	-360.75
Fuel Pressurizing Valve No. 3 Open	-362	-360.75
Fuel Pressurizing Valve No. 4 Open	-362	-360.75
Fuel Pressurized	-349	-341.52
Open LOX Vent and Relief No. 1	-115	-112.66
Open LOX Relief No. 2	-115	-112.66
LOX Relief No. 1 Closed	-115	Switch Failed
LOX Relief No. 2 Closed	-115	-111.12
LOX Vent Open	-115	-112.38
LOX Vent Closed	-115	Switch Failed
LOX Pressurizing Valve Open	-115	-112.03
LOX Pressurized	-35	-35.23
Power Transfer Command	-35	-35.23
Power Transfer Complete	-35	-35.14
Long Mast Eject Command	-25	-25.58
Long Mast Retracted	-2	-8.24
Ignition Start Timer	0	0
Ignition Command	0	0
Eng. No. 5 Igniter No. 1 Energized	0	+.03
Eng. No. 5 Igniter No. 2 Energized	0	+.03
Eng. No. 7 Igniter No. 1 Energized	0	+.03
Eng. No. 7 Igniter No. 2 Energized	0	+.03
Eng. No. 6 Igniter No. 1 Energized	+.10	+0.14
Eng. No. 6 Igniter No. 2 Energized	+.10	+0.14
Eng. No. 8 Igniter No. 1 Energized	+.10	+0.14
Eng. No. 8 Igniter No. 2 Energized	+.10	+0.14
Eng. No. 2 Igniter No. 1 Energized	+.20	+0.24
Eng. No. 2 Igniter No. 2 Energized	+.20	+0.24
Eng. No. 4 Igniter No. 1 Energized	+.20	+0.24
Eng. No. 4 Igniter No. 2 Energized	+.20	+0.24
Eng. No. 1 Igniter No. 1 Energized	+.30	+0.33
Eng. No. 1 Igniter No. 2 Energized	+.30	+0.33
Eng. No. 3 Igniter No. 1 Energized	+.30	+0.34
Eng. No. 3 Igniter No. 2 Energized	+.30	+0.35

* Times referenced to ignition command

(C) GROUND SEQUENCE EVENTS (CONT)

All Igniters Energized	+.30	+0.35
All Engines Running	+2.15	+1.29
Thrust OK Timer	+3.30	+3.23
Thrust Commit	+3.31	+3.27
Retract Support Timer	+3.32	No Operation
Short Mast No. 2 Valve No. 1 Open	+3.32	+3.32
Short Mast No. 2 Valve No. 2 Open	+3.32	+3.32
Short Mast No. 4 Valve No. 1 Open	+3.32	+3.33
Short Mast No. 4 Valve No. 2 Open	+3.32	+3.33
Retract Support Command	+3.40	+3.36
Retract Valve No. 1 Open	+3.40	+3.54
Retract Valve No. 2 Open	+3.40	+3.54
Retract Valve No. 3 Open	+3.40	+3.52
Retract Valve No. 4 Open	+3.40	+3.55
Support No. 1 Not Supporting	-	+3.61
Support No. 2 Not Supporting	-	+3.61
Support No. 3 Not Supporting	-	+3.60
Support No. 4 Not Supporting	-	+3.61
Launch Commit	+3.67	+3.63
H.D. Release Valve No. 1 Open	+3.67	+3.68
H.D. Release Valve No. 2 Open	+3.67	+3.68
H.D. Release Valve No. 3 Open	+3.67	+3.68
H.D. Release Valve No. 4 Open	+3.67	+3.68
Holddown No. 1 Released	+3.77	+3.69
Holddown No. 2 Released	+3.77	+3.70
Holddown No. 3 Released	+3.77	+3.70
Holddown No. 4 Released	+3.77	+3.70
Liftoff No. 1	+3.77	+3.81
Liftoff No. 2	+3.77	+3.81
Liftoff No. 3	+3.77	+3.81
Liftoff No. 4	+3.77	+3.81
Liftoff	+3.77	+3.93

TABLE D-I

APPENDIX D

MASS CHARACTERISTICS COMPARISON (Ref. para. 5.6)

Event		Range Time Seconds	Weight Pounds	% Dev	Longitudinal C.G. (X-Sta) Inches	Dev	Radial C.G. Inches	Dev	Pitch Moment of Inertia Kg-M-Sec^2	%Dev	Roll Moment of Inertia Kg-M-Sec^2	%Dev
*Dry Vehicle	Act	N/A	309,635	0.7	1,108	0	0.15	0	2,489,925	0	26,435	0
	Pred	N/A	307,635		1,108		0.15		2,489,925		26,435	
Ignition Command	Act	-3.03	946,551	0.4	673	0	0.05	0	5,505,629	0.5	151,695	0.4
	Pred	-3.03	942,617		673		0.05		5,479,037		151,129	
Liftoff	Act	.89	928,725	0.3	673	0	0.05	0	5,501,649	0.5	148,475	0.2
	Pred	.89	926,229		673		0.05		5,475,364		148,165	
Max "q"	Act	61.00	613,894	1.0	729	2 in.	0.08	0	5,257,825	0.6	90,581	2.7
	Pred	60.89	607,605		731		0.08		5,225,569		88,218	
Inboard Engine Cutoff	Act	110.10	356,051	4.9	994	24 in.	0.14	0	3,430,742	9.0	38,136	12.1
	Pred	111.71	339,223		1,018		0.14		3,146,495		34,004	
Outboard Engine Cutoff	Act	116.08	339,543	4.8	1,029	37 in.	0.15	0	3,161,744	11.1	33,904	13.7
	Pred	117.71	323,791		1,066		0.15		2,845,913		29,811	
End Thrust Decay	Act	119.00	338,236	5.0	1,033	35 in.	0.15	0	3,137,643	10.9	33,650	13.7
	Pred	120.26	322,060		1,068		0.15		2,827,384		29,593	

* Includes 191,525 pounds water ballast

Notes:
1. GOX vented not included
2. No gas vented from fuel containers
3. Fuel weight includes ½ lb/sec lube fuel flow per engine
4. Ice accumulation (approximately 1000 pounds at liftoff) not included
5. % Dev = $\frac{\text{Act-Pred}}{\text{Pred}}$

TABLE D-II

VEHICLE WEIGHTS

Event		Ignition Command	Lift-off	Max Q	Inboard Cutoff	Outboard Cutoff	End Of Thrust Decay
Range Time (sec)	Pred	-3.03	.89	60.89	111.71	117.71	120.26
	Act	-3.03	.89	61.00	110.10	116.08	119.00
Dry Vehicle (lb)	Pred	307,635	307,635	307,635	307,635	307,635	307,635
	Act	309,635	309,635	309,635	309,635	309,635	309,635
LOX (lb)	Pred	438,002	426,049	204,067	17,169	6,743	5,682
	Act	442,762	429,887	210,580	30,874	19,820	19,307
Fuel (lb)	Pred	194,766	190,275	92,796	10,473	5,350	4,680
	Act	192,566	187,548	90,726	11,602	6,058	5,264
Gas in LOX Containers (lb)	Pred	1,252	1,308	2,145	2,984	3,101	3,101
	Act	630	697	1,995	2,982	3,072	3,072
GN_2 (lb)	Pred	902	902	902	902	902	902
	Act	898	898	898	898	898	898
Hydraulic Oil (lb)	Pred	60	60	60	60	60	60
	Act	60	60	60	60	60	60
TOTAL (lb)	Pred	942,617	926,229	607,605	339,223	323,791	322,060
	Act	946,551	928,725	613,894	356,051	339,543	338,236

NOTE:
1. Gox not included
2. No gas vented from fuel containers
3. Fuel includes 1/2 lb/sec lube flow per engine
4. Ice accumulation (approximately 1000 pounds at lift-off) not included

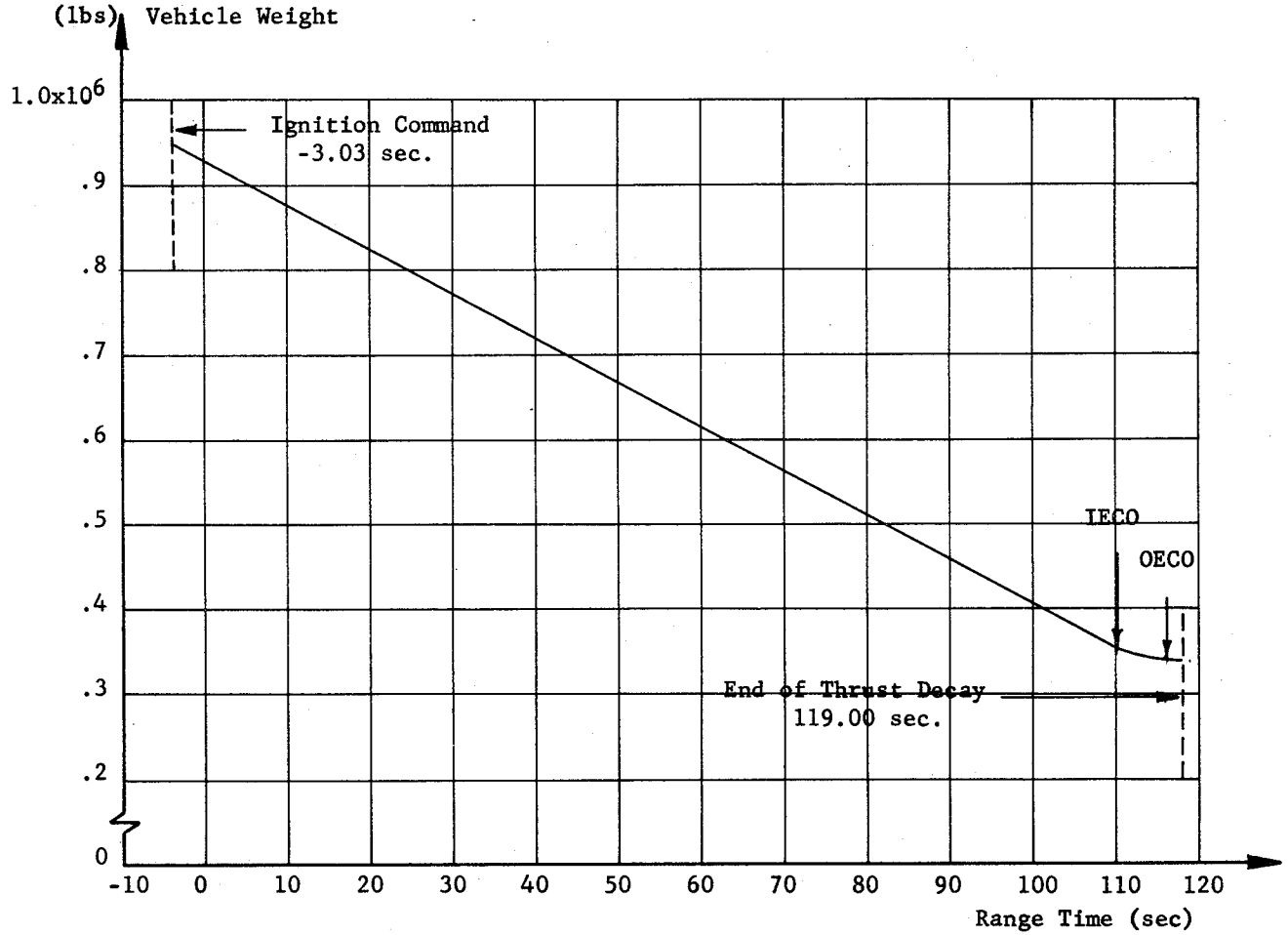

Fig. D-1	VEHICLE WEIGHT VERSUS RANGE TIME
SA-1	

CONFIDENTIAL

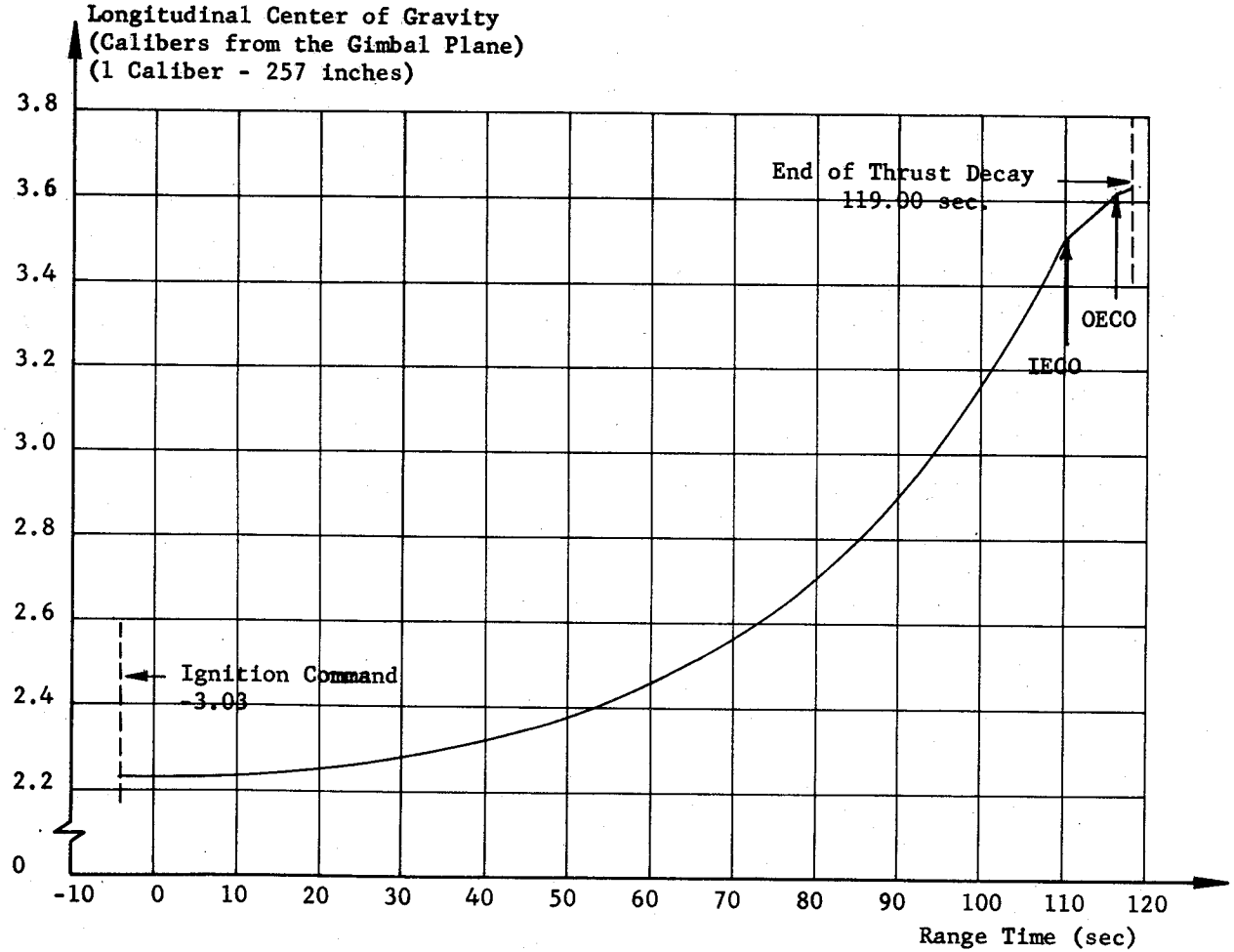

Fig. D-2	LONGITUDINAL CENTER OF GRAVITY VS. RANGE TIME
SA-1	

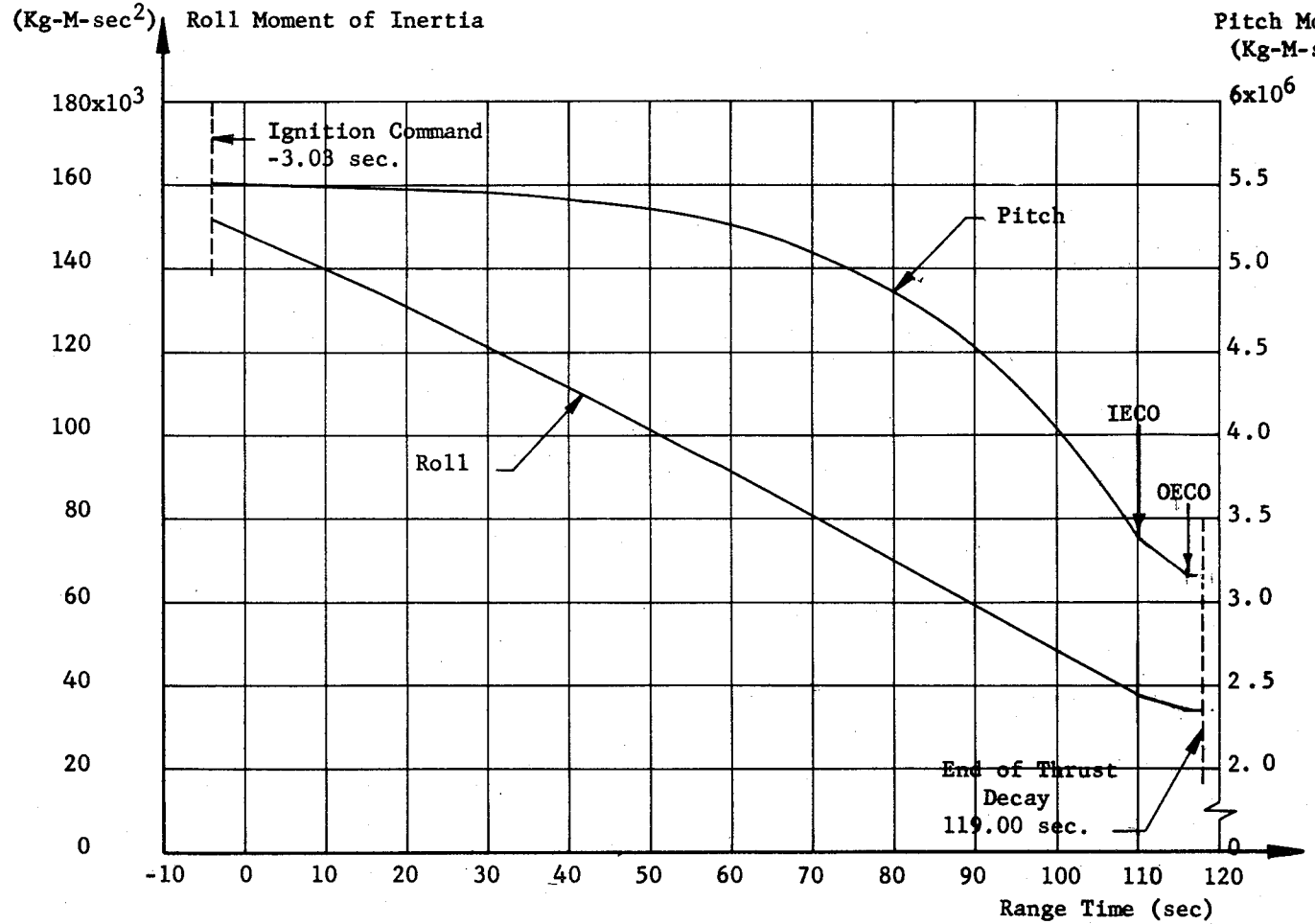

Fig. D-3	PITCH AND ROLL MOMENT OF INERTIA VS. RANGE TIME
SA-1	

APPENDIX E

(U) ATMOSPHERIC DATA

E.1 INTRODUCTION

This appendix presents the more important portions of the atmospheric environment for the flight of SA-1 - the general weather situation for the flight area, surface observations at launch time, and upper-air conditions as measured by rawinsonde and rocketsonde observations soon after flight time. These data are given in a form which will permit comparison with other space vehicle flights at the Atlantic Missile Range. Winds and thermodynamic data are presented in graphic form as a function of altitude and range time.

E.2 GENERAL SYNOPTIC SITUATION AT LAUNCH TIME

Pressure Distribution and Fronts. A large, but rather shallow, continental Polar air mass covered most of the eastern United States at launch time, with a central pressure of 1029 mb centered over eastern Kentucky. From a trough of low pressure some 600 km off the East Coast, a broad, weak, and diffuse cold front extended east-west along the southern edge of the continental Polar high pressure area. This diffuse cold front was moving southward across central Florida at launch time.

The core of the high pressure area tilted southward with increasing altitude and was centered over the Gulf Coast at the 700 mb level (3 km altitude). At the 200 mb level (12 km altitude) the high pressure area was replaced by a trough of low pressure which extended southward over the Gulf of Mexico causing strong southwesterly winds in the jet stream zone.

Associated Weather and Jet Streams. The frontal passage caused considerable cloudiness and scattered light rain showers in the launch area. An Air Force reconnaissance plane reported cumulus activity up to approximately 4 km altitude; scattered to broken cloudiness also prevailed south and east of the launch area. Surface winds in the Cape Canaveral area were mostly 5 to 9 m/sec from the east-northeast. A jet stream crossed Florida from west-southwest to east-northeast about midway between Miami and Cape Canaveral with winds near 50 m/sec in the 12 km region.

E.3 SURFACE OBSERVATIONS AT LAUNCH TIME

Blockhouse Observations. Recording instruments at the blockhouse showed the surface pressure to be 14.805 psi and the relative humidity 51 percent. Temperature was not recorded.

Cape Canaveral Observations. Surface observations were made at launch time 5 km south of the launch pad at the Cape Canaveral Weather Station. These observations showed the surface pressure to be 14.825 psi, temperature 26.2°C, dewpoint 18.9°C, relative humidity 64 percent, and the wind (8.2 m above ground level) 6.7 m/sec from the east-northeast. Eight-tenths of the sky was obscured by cumulus clouds based 1200 m above the ground, and towering cumulus could be seen in all quadrants; however SA-1 was launched through a break in the clouds. Although rain showers were noted south of the station, visibility was better than 16 km.

Launch Pad Observations. A recording anemometer on the launch pad, 13.4 m above ground level and 38 m north of the launch pedestal, showed the winds to be 6.4 m/sec from 65 degrees just prior to launching (Fig. E-1). The launch blast caused the wind to veer to 101 degrees at 14.4 m/sec about 17 seconds after the first wind fluctuations caused by the space vehicle motors. The wind then backed to 20 degrees at 6.7 m/sec about 24 seconds after the first fluctuations. The wind returned to prelaunch conditions within 30 seconds after the first fluctuations began.

Service Structure Observations. A recording anemometer on the service structure, 95 m above ground level and 207 m southwest of the Saturn launch pedestal (see Fig. E-1), showed the wind to be blowing at 9.2 m/sec from 71 degrees just prior to launch time. The launch blast created a circulation pattern near the surface which caused the wind speed atop the service structure to drop to 4.1 m/sec, 10 seconds after the first wind fluctuations. Wind direction fluctuated rapidly, backing to 353 degrees eight seconds after the first fluctuations and then veering to 98 degrees in the next five seconds. The wind returned to prelaunch conditions about 30 seconds after the first fluctuations began. Times of the various wind measurements were not synchronized, so exact comparisons cannot be made. Recording instruments 13.4 m above ground level on the service structure showed the temperature to be 24.5°C just prior to launching with an abrupt rise to 25.5°C during the launching. Relative humidity fell sharply from 76 percent prior to launching to 61 percent during the launching. The abrupt temperature and humidity changes were caused by engine heat, and they quickly returned to prelaunch values after liftoff.

E.4 TIME AND SPACE VARIATION BETWEEN MISSILE FLIGHT PATH AND UPPER AIR MEASUREMENTS BY RAWINSONDE AND ROCKETSONDE

Rawinsonde Path. A rawinsonde was released 5 km south of the Saturn pedestal seven minutes after SA-1 liftoff. The light northeasterly winds in the first 6 km above the surface carried the rawinsonde balloon about 18 km south-southwest of the launch pad. West and south-westerly winds at higher altitudes then carried the rawinsonde balloon about 58 km east-northeast of the launch pad where it burst one hour and 43 minutes after SA-1 liftoff, ending the rawinsonde observation. At that time the rawinsonde was about 46 km east-northeast of the position reached by SA-1 at the same altitude.

Rocketsonde Path. A LOKI II Rocket was fired and the chaff target was acquired by radar at an altitude of 57 km and about 35 km east of the SA-1 launch pad, one hour and 57 minutes after SA-1 liftoff. The chaff target was then 6 km northeast of the position reached by SA-1 at the same altitude. Strong westerly winds aloft carried the chaff target rapidly eastward as it fell. The target was lost at an altitude of 47.5 km, when it was 60 km east of the SA-1 launch pad, two hours and four minutes after SA-1 liftoff. At that time the chaff target was 38 km east-northeast of SA-1's position at the same altitude.

E.5 WIND DATA

Wind Speed and Direction. Rawinsonde wind measurements are unreliable from 2 to 7 km altitude because of equipment malfunction. Based on available rawinsonde data and the angle of attack wind measurements, the winds were light (10 m/sec or less) and mostly east to northeast up to about 6 km altitude (Fig. E-2). It should be noted that the anemometers on the launch pad and the service structure showed east-northeast winds at launch time (Fig. E-1). Above 7 km altitude, the winds shifted to westerly and increased with altitude to reach a peak speed of 47 m/sec from the west-southwest at 12 km altitude, about 64 seconds range time. Winds continued mostly westerly above this level but dropped to about 5 m/sec between 18 and 25 km altitude. The rawinsonde observation ended at 33 km altitude. Rocketsonde observation (Fig. E-6) shows westerly winds between 47 and 57 km altitude which reached a speed of 86 m/sec at 53 km.

Wind Components. Wind components (Fig. E-3) were less than 10 m/sec up to 7 km altitude. The strongest cross-range component in the high dynamic pressure region was 29 m/sec from the right at 12 km altitude, about 64 seconds flight time (angle of attack measurement showed 37 m/s). This was accompanied by a rawinsonde tail wind component of 36 m/sec. Wind components were generally less than

10 m/sec from 18 to 26 km but increased above this altitude. The rocketsonde observation shows a cross-wind component of 81 m/sec from the left at 54 km altitude (Fig. E-7). Rawinsonde and angle-of-attack measured winds were in rather good agreement to about 20 km altitude. Above this altitude, the range component winds began to diverge due to time-space variation or measuring system differences, or a combination of these two.

Wind Shear. Pitch component wind shear is shown in Figure E-4, and yaw component wind shear in Figure E-5. These values as illustrated are for the modulus of the shear, ie., the absolute shear values. The strongest rawinsonde wind shear observed (computed over a 250 m layer) was 0.0415 sec^{-1} in the pitch plane, which occurred at 15 km altitude or about 69 seconds range time. The strongest rawinsonde shear in the yaw plane was 0.035 sec^{-1} which occurred at 16 km altitude or about 71 seconds range time. Pitch plane shears slightly exceeded the 99 percent envelope at 26 km altitude. The yaw plane shears exceeded the 99 percent envelope at 21 km altitude. These shear values occurred in the altitude region where wind speed and shears are usually relatively low. Wind shear over 250 m layers is difficult to measure with rawinsonde equipment, and the shear values that exceed the 99 percent shear envelope are due in part to measurement errors. Rocketsonde shears, computed over 1000 m altitude layers, are shown in Figure E-6. They are not excessive despite the high wind speeds encountered here.

E.6 THERMODYNAMIC DATA

Thermodynamic quantities were near normal at launch time. Temperature, pressure, and density did not vary from the Patrick Air Force Base Reference Atmosphere (defined as the normal condition) by as much as two percent from the surface to 14 km altitude. The greatest deviations of temperature and density occurred at 19 km altitude. Here the temperature was 3.2 percent above normal and the density 2.4 percent below normal.

The greatest deviation of the refractive index from the Patrick Air Force Base Reference Atmosphere was plus $23(n-1)10^6$ units at 2 ½ km altitude. This sharp increase in the refractive index was caused by an over-running layer of extremely dry air. Above 5 km altitude the index of refraction was near normal.

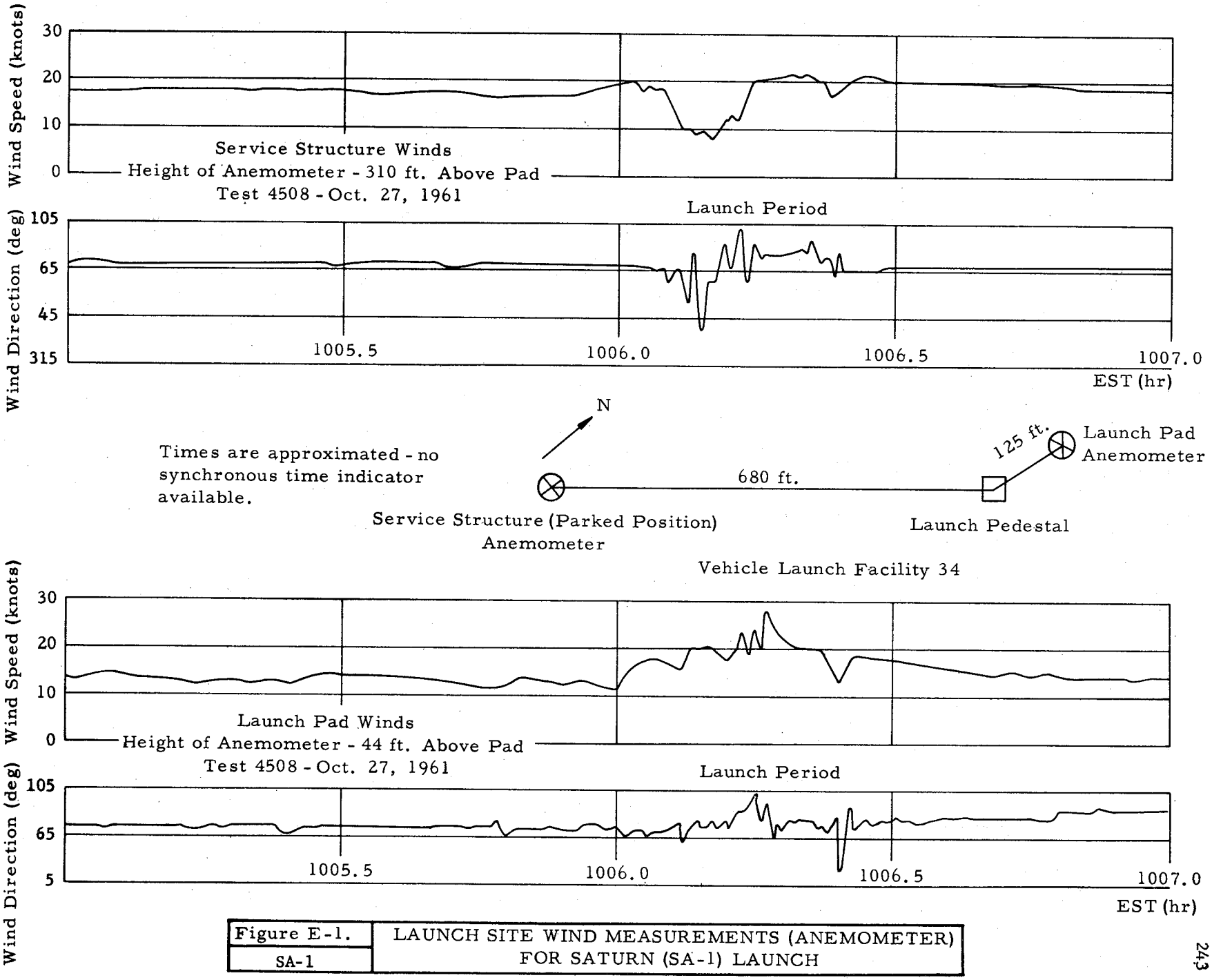

Figure E-1.	LAUNCH SITE WIND MEASUREMENTS (ANEMOMETER) FOR SATURN (SA-1) LAUNCH
SA-1	

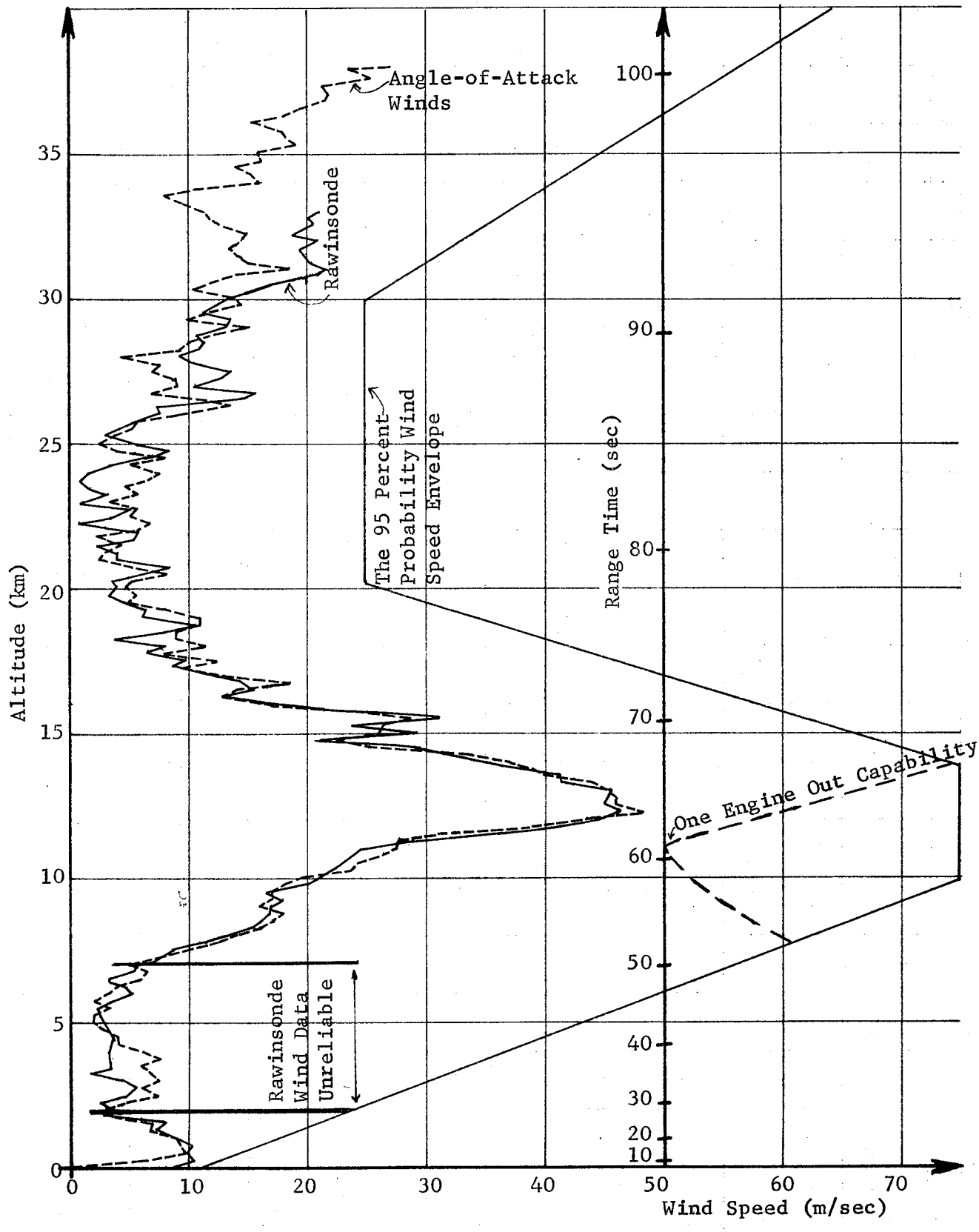

Figure E-2	WIND SPEED BY RAWINSONDE AND ANGLE-OF-ATTACK MEASUREMENT
SA-1	

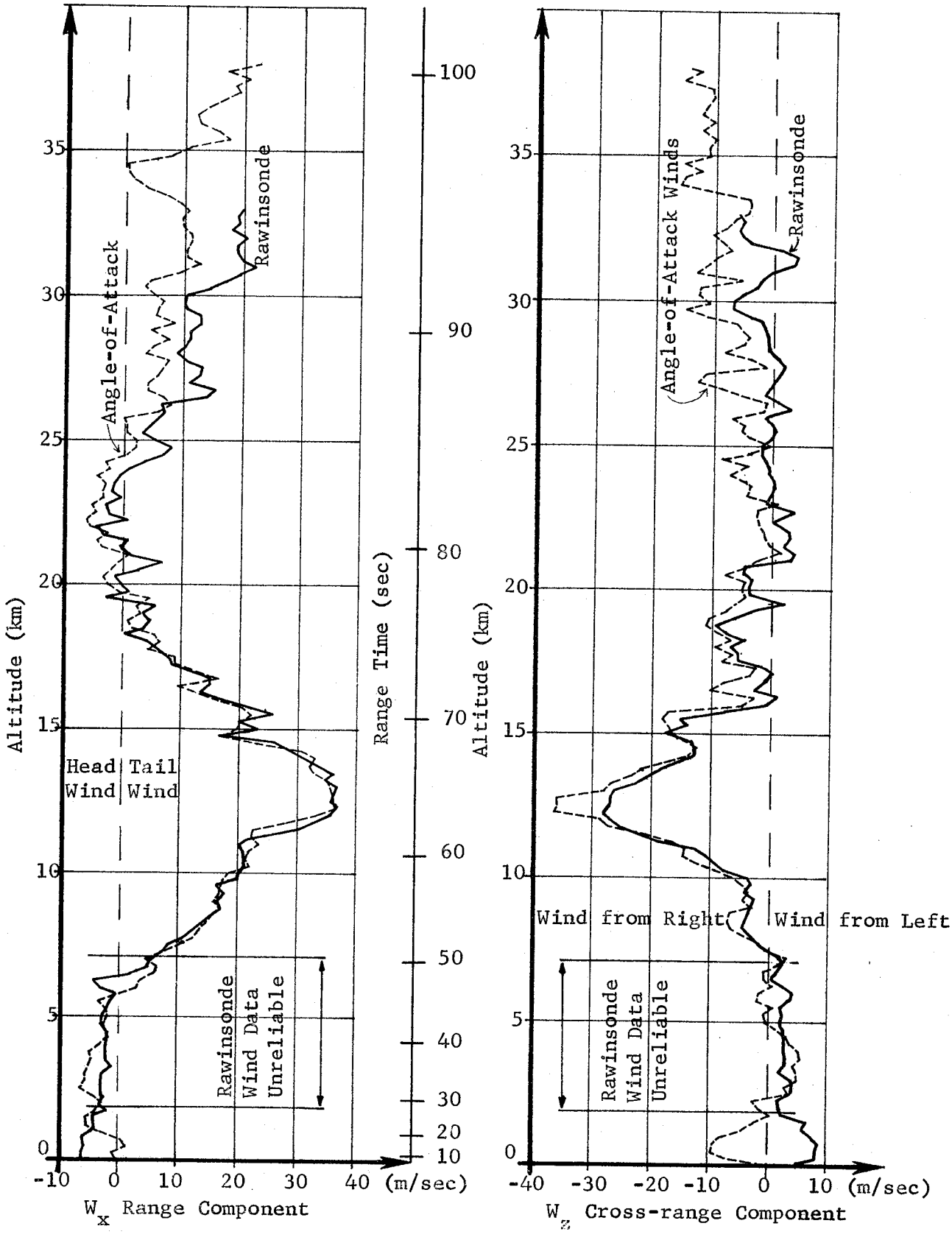

Figure E-3	WIND COMPONENTS BY RAWINSONDE AND ANGLE-OF-ATTACK MEASUREMENT
SA-1	

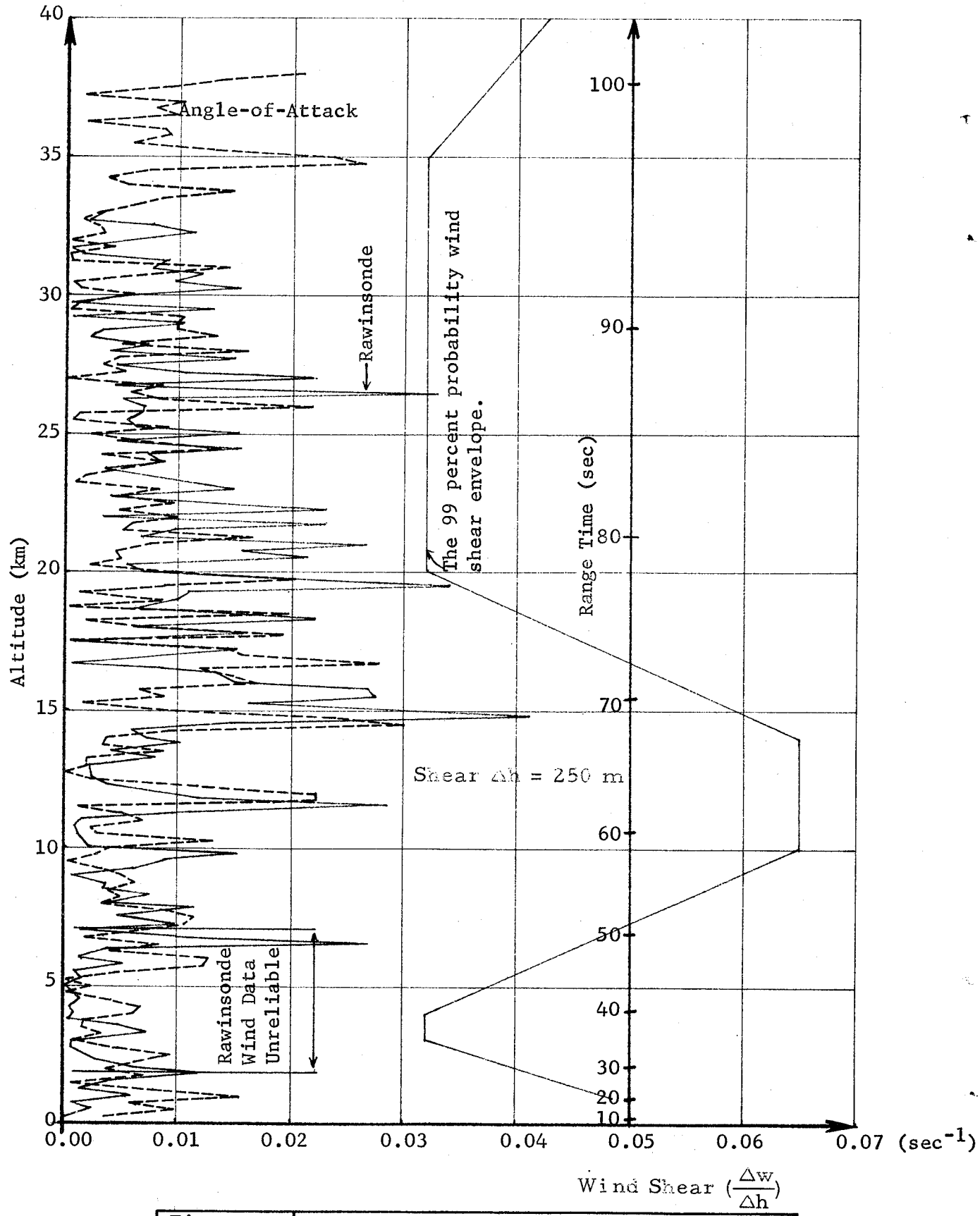

Figure E-4	PITCH COMPONENT WIND SHEAR BY RAWINSONDE AND ANGLE-OF-ATTACK MEASUREMENT
SA-1	

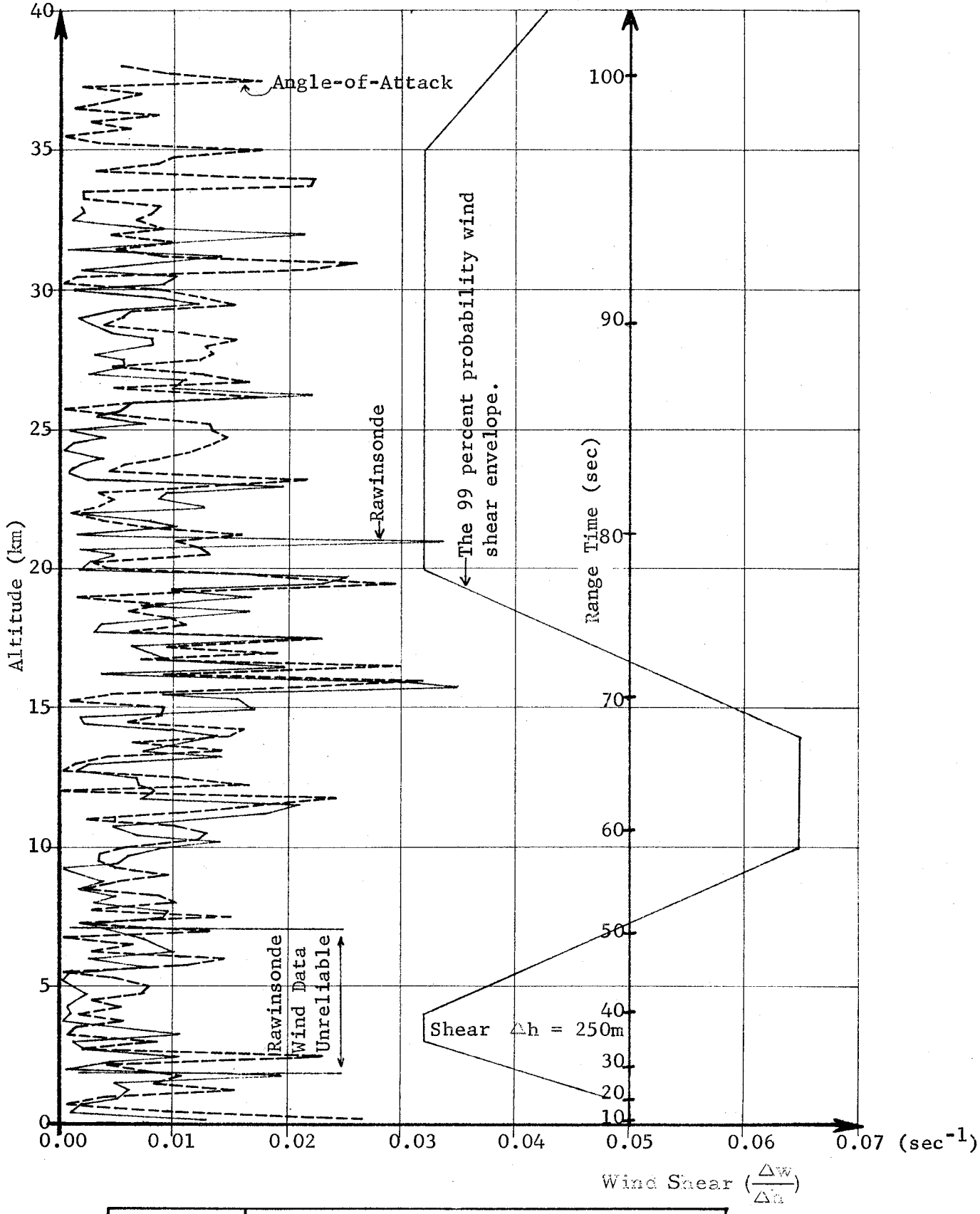

Figure E-5	YAW COMPONENT WIND SHEAR BY RAWINSONDE AND ANGLE-OF-ATTACK MEASUREMENT
SA-1	

Rocketsonde target acquired one hour and 57 minutes after lift-off; lost two hours and four minutes after SA-1 lift-off.

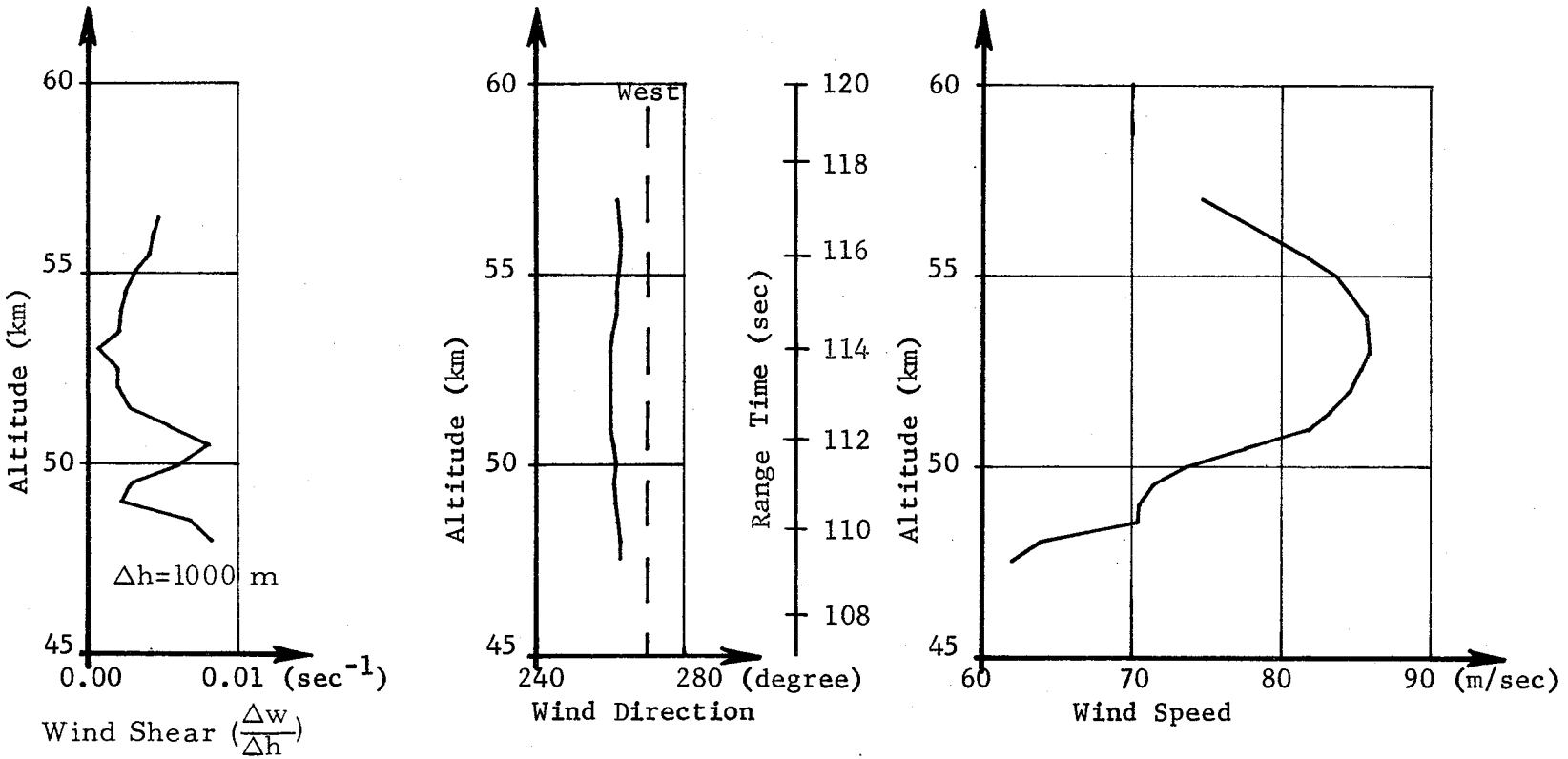

Fig. E-6	ROCKETSONDE WIND SHEAR, DIRECTION AND SPEED
SA-1	FOR SA-1 LAUNCH, CAPE CANAVERAL, FLORIDA

Rocketsonde target acquired one hour and 57 minutes after lift-off; lost two hours and four minutes after SA-1 lift-off.

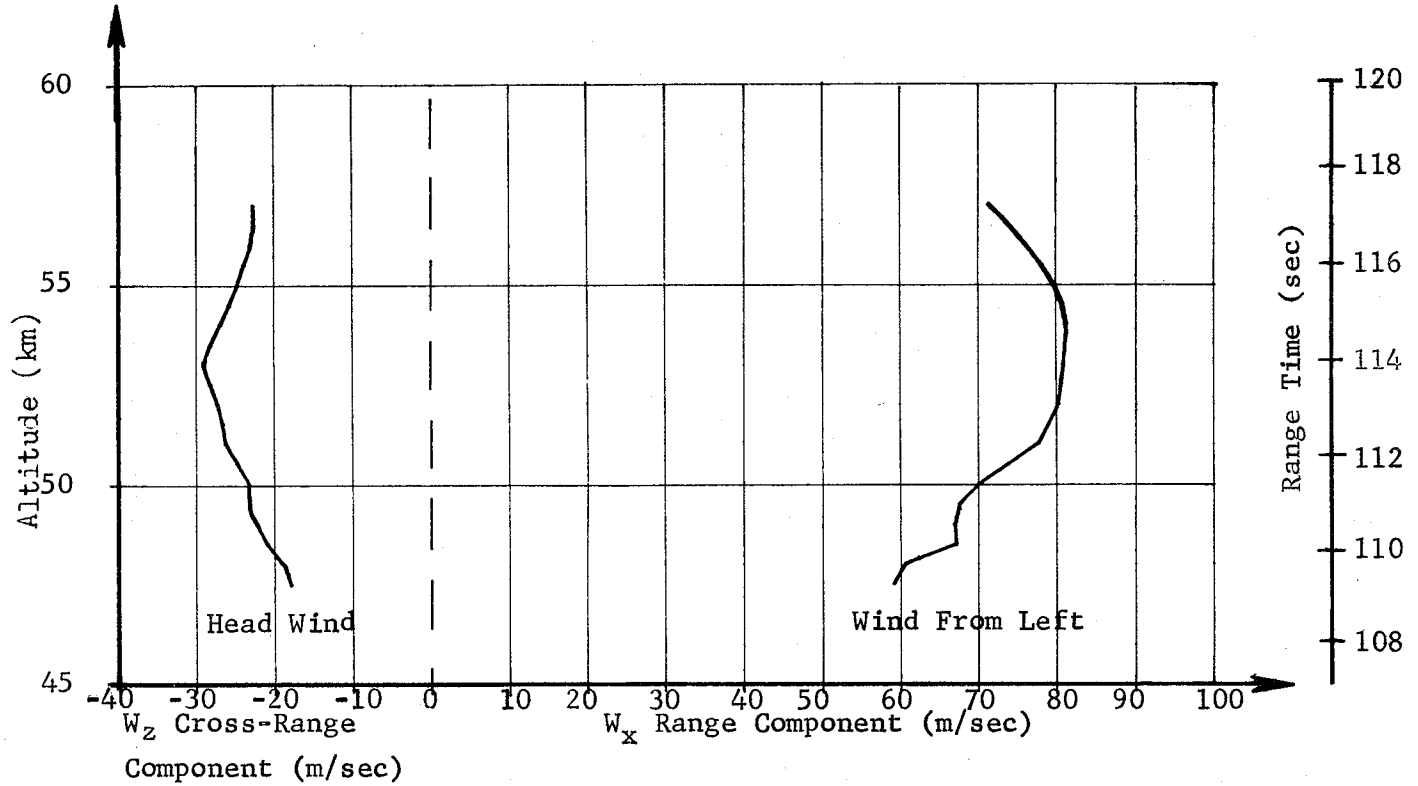

Fig. E-7	WIND COMPONENTS (ROCKETSONDE) AT LAUNCH TIME
SA-1	FOR SATURN-1, CAPE CANAVERAL, FLORIDA

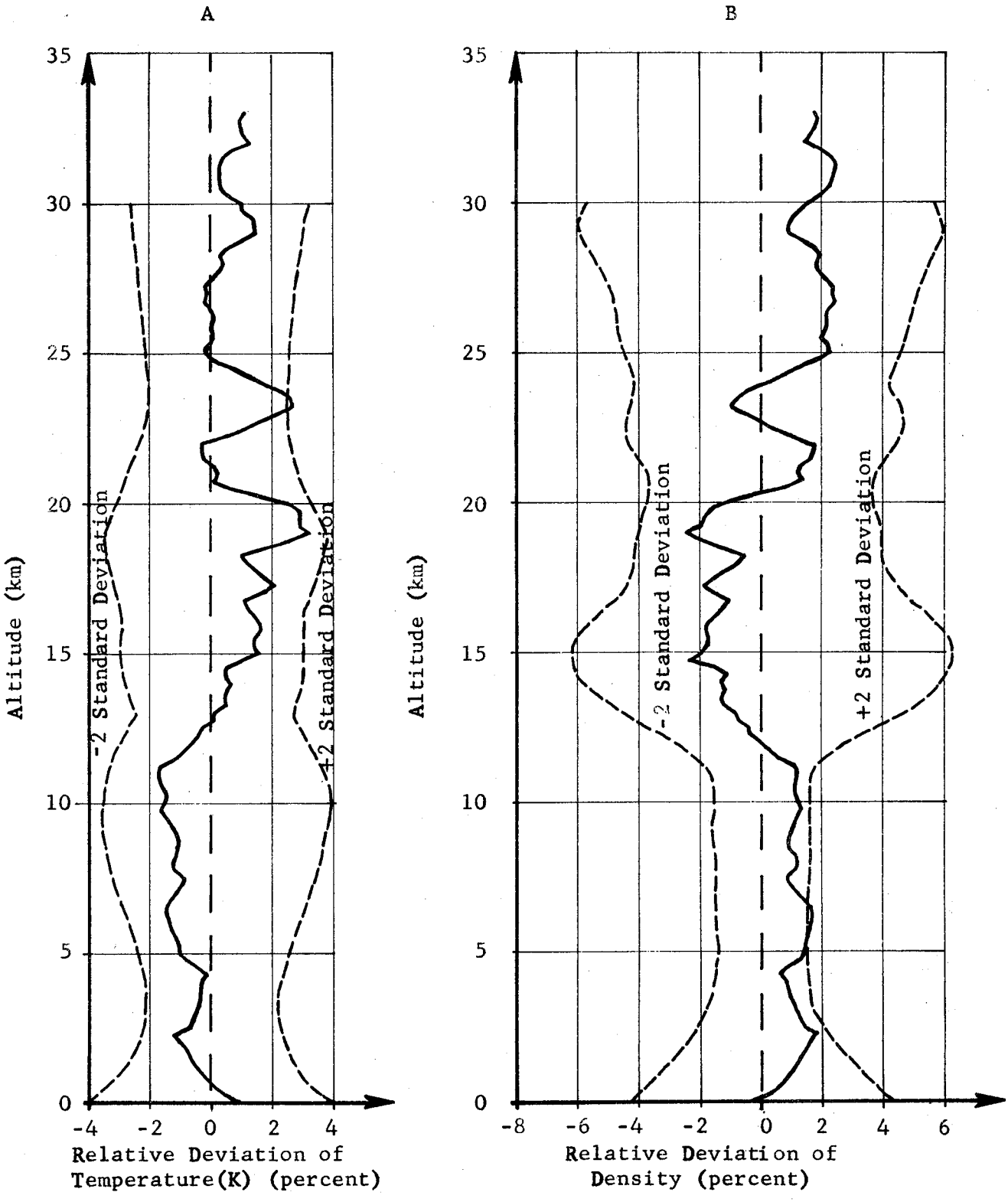

Figure E-8	RELATIVE DEVIATION OF THE LAUNCH SITE TEMPERATURE AND DENSITY FROM PAFB REFERENCE ATMOSPHERE FOR SA-1
SA-1	

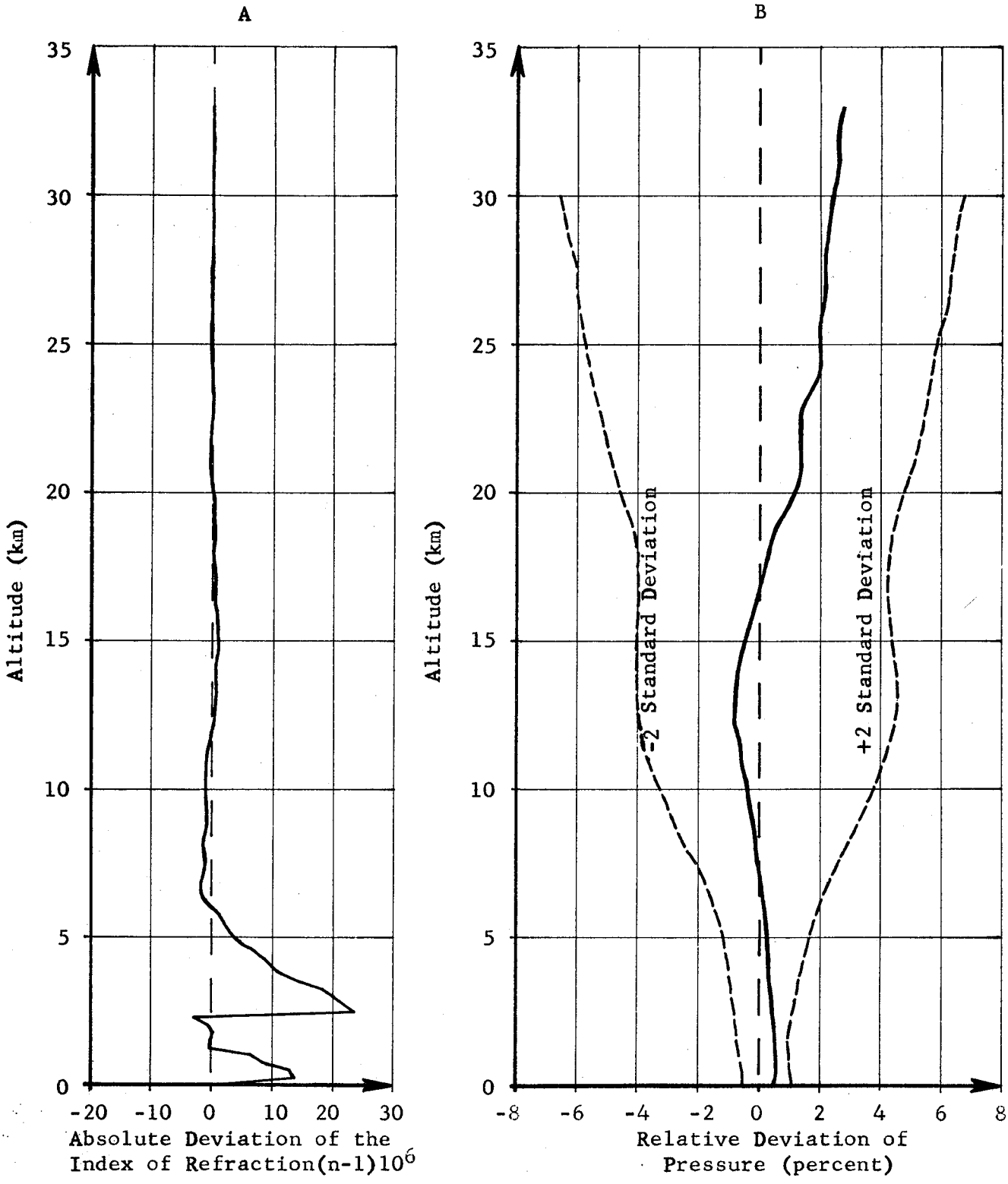

Figure E-9	ABSOLUTE DEVIATION OF THE INDEX OF REFRACTION AND RELATIVE DEVIATION OF PRESSURE FROM PAFB REFERENCE ATMOSPHERE
SA-1	